

# BULLETIN OF RUSSIAN STATE MEDICAL UNIVERSITY

BIOMEDICAL JOURNAL OF PIROGOV RUSSIAN NATIONAL  
RESEARCH MEDICAL UNIVERSITY

**EDITOR-IN-CHIEF** Denis Rebrikov, DSc, professor

**DEPUTY EDITOR-IN-CHIEF** Alexander Oettinger, DSc, professor

**EDITORS** Valentina Geidebrekht, PhD; Nadezda Tikhomirova

**TECHNICAL EDITOR** Evgeny Lukyanov

**TRANSLATORS** Nadezda Tikhomirova, Vyacheslav Vityuk

**DESIGN AND LAYOUT** Marina Doronina

## EDITORIAL BOARD

**Averin VI**, DSc, professor (Minsk, Belarus)  
**Alipov NN**, DSc, professor (Moscow, Russia)  
**Belousov VV**, DSc, professor (Moscow, Russia)  
**Bogomilskiy MR**, corr. member of RAS, DSc, professor (Moscow, Russia)  
**Bozhenko VK**, DSc, CSc, professor (Moscow, Russia)  
**Bylova NA**, CSc, docent (Moscow, Russia)  
**Gainetdinov RR**, CSc (Saint-Petersburg, Russia)  
**Gendlin GYe**, DSc, professor (Moscow, Russia)  
**Ginter EK**, member of RAS, DSc (Moscow, Russia)  
**Gorbacheva LR**, DSc, professor (Moscow, Russia)  
**Gordeev IG**, DSc, professor (Moscow, Russia)  
**Gudkov AV**, PhD, DSc (Buffalo, USA)  
**Gulyaeva NV**, DSc, professor (Moscow, Russia)  
**Gusev EI**, member of RAS, DSc, professor (Moscow, Russia)  
**Danilenko VN**, DSc, professor (Moscow, Russia)  
**Zarubina TV**, DSc, professor (Moscow, Russia)  
**Zatevakhin II**, member of RAS, DSc, professor (Moscow, Russia)  
**Kagan VE**, professor (Pittsburgh, USA)  
**Kzyzhkowska YuG**, DSc, professor (Heidelberg, Germany)  
**Kobriniskii BA**, DSc, professor (Moscow, Russia)  
**Kozlov AV**, MD PhD (Vienna, Austria)  
**Kotelevtsev YuV**, CSc (Moscow, Russia)  
**Lebedev MA**, PhD (Darem, USA)  
**Manturova NE**, DSc (Moscow, Russia)  
**Milushkina OYu**, DSc, professor (Moscow, Russia)  
**Mitupov ZB**, DSc, professor (Moscow, Russia)  
**Moshkovskii SA**, DSc, professor (Moscow, Russia)  
**Munblit DB**, MSc, PhD (London, Great Britain)

**Negrebetsky VV**, DSc, professor (Moscow, Russia)  
**Novikov AA**, DSc (Moscow, Russia)  
**Pivovarov YuP**, member of RAS, DSc, professor (Moscow, Russia)  
**Polunina NV**, corr. member of RAS, DSc, professor (Moscow, Russia)  
**Poryadin GV**, corr. member of RAS, DSc, professor (Moscow, Russia)  
**Razumovskii AYU**, corr. member of RAS, DSc, professor (Moscow, Russia)  
**Rebrova OYu**, DSc (Moscow, Russia)  
**Rudoy AS**, DSc, professor (Minsk, Belarus)  
**Rylova AK**, DSc, professor (Moscow, Russia)  
**Savelieva GM**, member of RAS, DSc, professor (Moscow, Russia)  
**Semiglazov VF**, corr. member of RAS, DSc, professor (Saint-Petersburg, Russia)  
**Skoblina NA**, DSc, professor (Moscow, Russia)  
**Slavyanskaya TA**, DSc, professor (Moscow, Russia)  
**Smirnov VM**, DSc, professor (Moscow, Russia)  
**Spallone A**, DSc, professor (Rome, Italy)  
**Starodubov VI**, member of RAS, DSc, professor (Moscow, Russia)  
**Stepanov VA**, corr. member of RAS, DSc, professor (Tomsk, Russia)  
**Suchkov SV**, DSc, professor (Moscow, Russia)  
**Takhchidi KhP**, member of RAS, DSc, professor (Moscow, Russia)  
**Trufanov GE**, DSc, professor (Saint-Petersburg, Russia)  
**Favorova OO**, DSc, professor (Moscow, Russia)  
**Filipenko ML**, CSc, leading researcher (Novosibirsk, Russia)  
**Khazipov RN**, DSc (Marsel, France)  
**Chundukova MA**, DSc, professor (Moscow, Russia)  
**Shimanovskii NL**, corr. member of RAS, DSc, professor (Moscow, Russia)  
**Shishkina LN**, DSc, senior researcher (Novosibirsk, Russia)  
**Yakubovskaya RI**, DSc, professor (Moscow, Russia)

**SUBMISSION** <http://vestnikrgmu.ru/login?lang=en>

**CORRESPONDENCE** [editor@vestnikrgmu.ru](mailto:editor@vestnikrgmu.ru)

**COLLABORATION** [manager@vestnikrgmu.ru](mailto:manager@vestnikrgmu.ru)

**ADDRESS** ul. Ostrovityanova, d. 1, Moscow, Russia, 117997

Indexed in Scopus. CiteScore 2022: 0.6

**Scopus**<sup>®</sup>

SCImago Journal & Country Rank 2020: 0.14

**SJR**

Scimago Journal & Country Rank

Indexed in WoS. JCR 2021: 0.5

**WEB OF SCIENCE**<sup>™</sup>

Listed in HAC 31.01.2020 (№ 507)



ВЫСШАЯ  
АТТЕСТАЦИОННАЯ  
КОМИССИЯ (ВАК)

Five-year h-index is 8

**Google**  
scholar

Open access to archive

**CYBERLENINKA**

Issue DOI: 10.24075/brsmu.2024-04

The mass media registration certificate № 012769 issued on July 29, 1994

Founder and publisher is Pirogov Russian National Research Medical University (Moscow, Russia)

The journal is distributed under the terms of Creative Commons Attribution 4.0 International License [www.creativecommons.org](http://www.creativecommons.org)



Approved for print 31.08.2024  
Circulation: 100 copies. Printed by Print.Formula  
[www.print-formula.ru](http://www.print-formula.ru)

# ВЕСТНИК РОССИЙСКОГО ГОСУДАРСТВЕННОГО МЕДИЦИНСКОГО УНИВЕРСИТЕТА

НАУЧНЫЙ МЕДИЦИНСКИЙ ЖУРНАЛ РНИМУ ИМ. Н. И. ПИРОГОВА

**ГЛАВНЫЙ РЕДАКТОР** Денис Ребриков, д. б. н., профессор

**ЗАМЕСТИТЕЛЬ ГЛАВНОГО РЕДАКТОРА** Александр Эттингер, д. м. н., профессор

**РЕДАКТОРЫ** Валентина Гейдебрехт, к. б. н.; Надежда Тихомирова

**ТЕХНИЧЕСКИЙ РЕДАКТОР** Евгений Лукьянов

**ПЕРЕВОДЧИКИ** Надежда Тихомирова, Вячеслав Витюк

**ДИЗАЙН И ВЕРСТКА** Марины Дорониной

## РЕДАКЦИОННАЯ КОЛЛЕГИЯ

В. И. Аверин, д. м. н., профессор (Минск, Белоруссия)  
Н. Н. Алипов, д. м. н., профессор (Москва, Россия)  
В. В. Белоусов, д. б. н., профессор (Москва, Россия)  
М. Р. Богомилский, член-корр. РАН, д. м. н., профессор (Москва, Россия)  
В. К. Боженко, д. м. н., к. б. н., профессор (Москва, Россия)  
Н. А. Былова, к. м. н., доцент (Москва, Россия)  
Р. Р. Гайнетдинов, к. м. н. (Санкт-Петербург, Россия)  
Г. Е. Гендлин, д. м. н., профессор (Москва, Россия)  
Е. К. Гинтер, академик РАН, д. б. н. (Москва, Россия)  
Л. Р. Горбачева, д. б. н., профессор (Москва, Россия)  
И. Г. Гордеев, д. м. н., профессор (Москва, Россия)  
А. В. Гудков, PhD, DSc (Буффало, США)  
Н. В. Гуляева, д. б. н., профессор (Москва, Россия)  
Е. И. Гусев, академик РАН, д. м. н., профессор (Москва, Россия)  
В. Н. Даниленко, д. б. н., профессор (Москва, Россия)  
Т. В. Зарубина, д. м. н., профессор (Москва, Россия)  
И. И. Затевахин, академик РАН, д. м. н., профессор (Москва, Россия)  
В. Е. Каган, профессор (Питтсбург, США)  
Ю. Г. Кжышковска, д. б. н., профессор (Гейдельберг, Германия)  
Б. А. Кобринский, д. м. н., профессор (Москва, Россия)  
А. В. Козлов, MD PhD (Вена, Австрия)  
Ю. В. Котелевцев, к. х. н. (Москва, Россия)  
М. А. Лебедев, PhD (Дарем, США)  
Н. Е. Мантурова, д. м. н. (Москва, Россия)  
О. Ю. Милушкина, д. м. н., доцент (Москва, Россия)  
З. Б. Митупов, д. м. н., профессор (Москва, Россия)  
С. А. Мошковский, д. б. н., профессор (Москва, Россия)  
Д. Б. Мунблит, MSc, PhD (Лондон, Великобритания)

В. В. Негребцкий, д. х. н., профессор (Москва, Россия)  
А. А. Новиков, д. б. н. (Москва, Россия)  
Ю. П. Пивоваров, д. м. н., академик РАН, профессор (Москва, Россия)  
Н. В. Полунина, член-корр. РАН, д. м. н., профессор (Москва, Россия)  
Г. В. Порядин, член-корр. РАН, д. м. н., профессор (Москва, Россия)  
А. Ю. Разумовский, член-корр., профессор (Москва, Россия)  
О. Ю. Реброва, д. м. н. (Москва, Россия)  
А. С. Рудой, д. м. н., профессор (Минск, Белоруссия)  
А. К. Рылова, д. м. н., профессор (Москва, Россия)  
Г. М. Савельева, академик РАН, д. м. н., профессор (Москва, Россия)  
В. Ф. Семиглазов, член-корр. РАН, д. м. н., профессор (Санкт-Петербург, Россия)  
Н. А. Скоблина, д. м. н., профессор (Москва, Россия)  
Т. А. Славянская, д. м. н., профессор (Москва, Россия)  
В. М. Смирнов, д. б. н., профессор (Москва, Россия)  
А. Спаллоне, д. м. н., профессор (Рим, Италия)  
В. И. Стародубов, академик РАН, д. м. н., профессор (Москва, Россия)  
В. А. Степанов, член-корр. РАН, д. б. н., профессор (Томск, Россия)  
С. В. Сучков, д. м. н., профессор (Москва, Россия)  
Х. П. Тахчиди, академик РАН, д. м. н., профессор (Москва, Россия)  
Г. Е. Труфанов, д. м. н., профессор (Санкт-Петербург, Россия)  
О. О. Фаворова, д. б. н., профессор (Москва, Россия)  
М. Л. Филипенко, к. б. н. (Новосибирск, Россия)  
Р. Н. Хазипов, д. м. н. (Марсель, Франция)  
М. А. Чундокова, д. м. н., профессор (Москва, Россия)  
Н. Л. Шимановский, член-корр. РАН, д. м. н., профессор (Москва, Россия)  
Л. Н. Шишкина, д. б. н. (Новосибирск, Россия)  
Р. И. Якубовская, д. б. н., профессор (Москва, Россия)

**ПОДАЧА РУКОПИСЕЙ** <http://vestnikrgmu.ru/login>

**ПЕРЕПИСКА С РЕДАКЦИЕЙ** [editor@vestnikrgmu.ru](mailto:editor@vestnikrgmu.ru)

**СОТРУДНИЧЕСТВО** [manager@vestnikrgmu.ru](mailto:manager@vestnikrgmu.ru)

**АДРЕС РЕДАКЦИИ** ул. Островитянова, д. 1, г. Москва, 117997

Журнал включен в Scopus. CiteScore 2022: 0,6

Журнал включен в WoS. JCR 2021: 0,5

Индекс Хирша (h<sup>2</sup>) журнала по оценке Google Scholar: 8

Scopus<sup>®</sup>

SCImago Journal & Country Rank 2020: 0,14

SJR  
Scimago Journal & Country Rank

WEB OF SCIENCE™

Журнал включен в Перечень 31.01.2020 (№ 507)



ВЫСШАЯ  
АТТЕСТАЦИОННАЯ  
КОМИССИЯ (ВАК)

Google  
scholar

Здесь находится открытый архив журнала

CYBERLENINKA

DOI выпуска: 10.24075/vrgmu.2024-04

Свидетельство о регистрации средства массовой информации № 012769 от 29 июля 1994 г.

Учредитель и издатель — Российский национальный исследовательский медицинский университет имени Н. И. Пирогова (Москва, Россия)

Журнал распространяется по лицензии Creative Commons Attribution 4.0 International [www.creativecommons.org](http://www.creativecommons.org)



Подписано в печать 31.08.2024

Тираж 100 экз. Отпечатано в типографии Print.Formula  
[www.print-formula.ru](http://www.print-formula.ru)

**REVIEW**

4

**Photopolymerizable materials for biocompatible implantable matrices**

Rudik IS, Mironov AV, Kuznetsova VS, Vasiliev AV

**Фотополимеризуемые материалы для биосовместимых имплантируемых матриц**

И. С. Рудик, А. В. Миронов, В. С. Кузнецова, А. В. Васильев

**OPINION**

12

**Prospects for the use of long-living printed temporary orthopedic structures**

Proskokova SV, Enikeev AM, Pirogov AE, Kuliev RM

**Перспективы применения принтованных временных ортопедических конструкций при длительной эксплуатации**

С. В. Просскова, А. М. Еникеев, А. Е. Пирогов, Р. М. Кулиев

**ORIGINAL RESEARCH**

17

**Effects of biocompatible piezoelectric membranes on the development of fibrosis associated with the oral mucosal wound regeneration**

Koniaeva AD, Varakuta EYu, Leiman AE, Kormashov GM, Fedosova MV, Bolbasov EN, Stankevich KS

**Влияние биосовместимых пьезоэлектрических мембран на развитие фиброза при регенерации ран слизистой оболочки полости рта**

А. Д. Коняева, Е. Ю. Варакута, А. Е. Лейман, Г. М. Кормашов, М. В. Федосова, Е. Н. Больбасов, К. С. Станкевич

**ORIGINAL RESEARCH**

24

**Disclosing adolescents' gynecological concerns: exploring trends in adolescent gynecology visits and complaints**

Uyaniklar OO, Rahimli Ocakoglu S, Atak Z, Suer E

**Гинекологические проблемы у подростков: тенденции обращений к гинекологам и жалоб**

О. О. Уйяныклар, С. Рахимлы Очакоглу, З. Атак, Э. Суэр

**ORIGINAL RESEARCH**

30

**Assessment of blood amino acid and polyamine levels in placenta-associated pregnancy complications**

Gasanbekova AP, Frankevich NA, Chagovets VV, Dolgoplova EL, Novoselova AV, Karapetyan TE, Mamedova GE, Frankevich VE

**Изучение уровня аминокислот и полиаминов крови при ассоциированных с плацентой осложнениях беременности**

А. П. Гасанбекова, Н. А. Франкевич, В. В. Чаговец, Е. Л. Дербенцева, А. В. Новоселова, Т. Э. Карапетян, Г. Э. Мамедова, В. Е. Франкевич

**ORIGINAL RESEARCH**

38

**Discriminatory power of multiplex PCR for detection of mycobacterial co-infection**

Smirnova TG, Andreevskaya SN, Ustinova VV, Larionova EE, Kiseleva EA, Chernousova LN, Ergeshov A

**Дискриминирующая способность метода мультиплексной ПЦР при выявлении микобактериальной коинфекции**

Т. Г. Смирнова, С. Н. Андреевская, В. В. Устинова, Е. Е. Ларионова, Е. А. Киселева, Л. Н. Черноусова, А. Эргешов

**ORIGINAL RESEARCH**

44

**Effectiveness of enriching drug treatment with systemic ozone therapy in patients with post-COVID asthenic syndrome**

Soldatenko AA, Gumenyuk LN, Berdieva DM, Ponomarchuk EI

**Эффективность добавления системной озонотерапии к фармакологическому лечению у пациентов с постковидным астеническим синдромом**

А. А. Солдатенко, Л. Н. Гуменюк, Д. М. Бердиева, Э. И. Пономарчук

**ORIGINAL RESEARCH**

52

**Association of local bioimpedance analysis of the abdominal region with morphological and biochemical traits**

Bondareva EA, Leonov GE, Parfenteva OI, Arutiunian AA, Bevziuk NA, Kovaleva ON, Gadziakhmedova AN, Shemyakov SE, Kulemin NA

**Связь локальной биоимпедансометрии в абдоминальной области с ее морфологическими и биохимическими признаками**

Э. А. Бондарева, Г. Е. Леонов, О. И. Парфентьева, А. А. Арутюнян, Н. А. Бевзюк, О. Н. Ковалева, А. Н. Гаджихмедова, С. Е. Шемяков, Н. А. Кулемин

**ORIGINAL RESEARCH**

60

**Structure of time perspective in combatants with amputated limbs**

Nikishina VB, Petrash EA, Yunina-Pakulova NYu, Lukyanov ES

**Структура временной перспективы участников боевых действий с ампутацией конечностей**

В. Б. Никишина, Е. А. Петраш, Н. Ю. Юнина-Пакулова, Е. С. Лукьянов

**ORIGINAL RESEARCH**

67

**Estimation of diffusion chamber biocompatibility in the experimental model of implantation in the neurovascular bundle**

Marzol EA, Dvornichenko MV, Mityaikin NS, Aparshev NA

**Оценка биосовместимости диффузионных камер в экспериментальной модели имплантации на сосудисто-нервном пучке**

Е. А. Марзоль, М. В. Дворниченко, Н. С. Митрайкин, Н. А. Апаршев

## PHOTOPOLYMERIZABLE MATERIALS FOR BIOCOMPATIBLE IMPLANTABLE MATRICES

Rudik IS<sup>1</sup>✉, Mironov AV<sup>1,2</sup>, Kuznetsova VS<sup>1</sup>, Vasiliev AV<sup>1,3</sup><sup>1</sup> Central Research Institute of Dentistry and Maxillofacial Surgery, Moscow, Russia<sup>2</sup> Federal Scientific Research Center "Crystallography and Photonics", Russian Academy of Sciences, Moscow, Russia<sup>3</sup> Sechenov First Moscow State Medical University, Moscow, Russia

The review considers photopolymerizable compositions based on biocompatible polymers for regenerative medicine. Assessment of the physical-mechanical and biological properties of photopolymerizable polymeric matrices, polyethyleneglycol, lactic acid, collagen, and hyaluronic acid, as well as of the effectiveness and toxicity of various photoinitiator supplements has been performed. Mechanical properties and degradation rate of the photopolymerizable matrices are ensured by selection of proportions of methacrylated mono-, oligo-, and polymers these consist of, while their toxicity largely depends on the photoinitiator systems used. It has been concluded that it is necessary to search for and develop the methods to obtain photopolymerizable polymeric matrices by using the compounds capable of initiating radical polymerization with lower toxic effect.

**Keywords:** biocompatible polymers, photoinitiators, matrices**Author contribution:** Rudik IS — literature data acquisition, analysis, systematization, review planning and writing; Mironov AV — literature data acquisition, editing, writing the conclusion; Kuznetsova VS — peer review; Vasiliev AV — review planning, structurization, peer review.✉ **Correspondence should be addressed:** Irina S. Rudik  
Timura Frunze, 16/1, k. 112, Moscow, 119021, Russia; rudik\_is@cniis.ru**Received:** 15.07.2024 **Accepted:** 12.08.2024 **Published online:** 31.08.2024**DOI:** 10.24075/brsmu.2024.036

## ФОТОПОЛИМЕРИЗУЕМЫЕ МАТЕРИАЛЫ ДЛЯ БИОСОВМЕСТИМЫХ ИМПЛАНТИРУЕМЫХ МАТРИКСОВ

И. С. Рудик<sup>1</sup>✉, А. В. Миронов<sup>1,2</sup>, В. С. Кузнецова<sup>1</sup>, А. В. Васильев<sup>1,3</sup><sup>1</sup> Центральный научно-исследовательский институт стоматологии и челюстно-лицевой хирургии, Москва, Россия<sup>2</sup> Федеральный научно-исследовательский центр «Кристаллография и фотоника», Москва, Россия<sup>3</sup> Первый Московский государственный медицинский университет имени И. М. Сеченова, Москва, Россия

В обзоре рассмотрены фотополимеризуемые композиции на основе биосовместимых полимеров для регенеративной медицины. Проведена оценка физико-механических и биологических свойств фотополимеризуемых полимерных матриц полиэтиленгликоля, молочной кислоты, коллагена и гиалуроновой кислоты, а также эффективности и токсичности различных фотоиницирующих добавок. Механические свойства и скорость деградации фотополимеризуемых матриц обеспечиваются подбором пропорций метакрилованных моно-, олиго- и полимеров в его составе, тогда как их токсичность в большей степени зависит от используемых фотоиницирующих систем. Сделан вывод о необходимости поиска и развития способов получения фотополимеризуемых полимерных матриц с применением соединений способных инициировать радикальную полимеризацию при меньшем токсическом эффекте.

**Ключевые слова:** биосовместимые полимеры, фотоинициаторы, матрицы**Вклад авторов:** И. С. Рудик — сбор, анализ, систематизация литературных данных, планирование и написание обзора; А. В. Миронов — сбор литературных данных, редактирование, написание заключения; В. С. Кузнецова — рецензирование; А. В. Васильев — планирование, структурирование обзора, рецензирование.✉ **Для корреспонденции:** Ирина Сергеевна Рудик  
ул. Тимура Фрунзе, д. 16/1, к. 112, г. Москва, 119021, Россия; rudik\_is@cniis.ru**Статья получена:** 15.07.2024 **Статья принята к печати:** 12.08.2024 **Опубликована онлайн:** 31.08.2024**DOI:** 10.24075/vrgmu.2024.036

The set of unique properties, specifically moisture resistance and resistance to biological media, fast transition between liquid and solid states, the possibility of adjusting physical and mechanical properties without altering chemical composition allow biocompatible photopolymerizable compositions to become popular materials not only in dentistry and orthopedics, but also in regenerative medicine and tissue engineering [1]. Thus, with development of additive manufacturing, biocompatible photopolymerizable compositions have become widely used as the stereolithography materials when manufacturing implantable devices [2, 3]. According to the Google Scholar statistics, more than 10,000 research papers focused on photopolymerizable polymer matrices for biomedical applications have been published since 2020, and the number of such paper increases by an average of 15% every year (Fig. 1).

Despite the large number of new studies, modification of polymers with acrylate groups is still the main method to produce biocompatible photocurable materials. Today, the

number of photopolymerizable systems suitable for biomedical applications is limited, since ions or radicals formed when photopolymerization is initiated make a considerable number of such materials toxic [4, 5]. Furthermore, the living tissues can be exposed to toxic effects of the components that have not fully reacted during the polymerization process [6, 7].

In terms of effects on the living tissues, radical transfer and intermolecular crosslinking at the functional acrylate groups represent the most secure photopolymerization method. Furthermore, it is important to select appropriate initiator or initiator-co-initiator pair, the main requirement for which is low toxicity in both inactive and radical form. Currently, no more than 10 various biocompatible photoinitiators are used in practice, among which camphorquinone (CQ) and diphenyl(2,4,6-trimethylbenzoyl)phosphine oxide (TPO) are the most common [8].

The review was aimed to systematize the literature data describing the types of photopolymerizable materials and certain components of such materials for biomedical applications. Keyword search in the PubMed, Google Scholar,

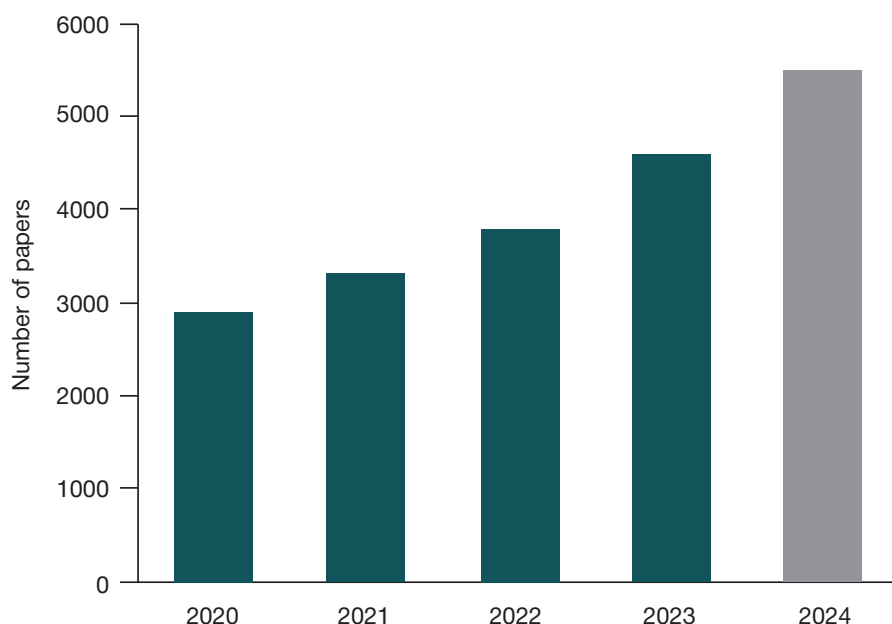


Fig. 1. Number of papers focused on photopolymerizable compositions in biomedical research published between 2020 and 2024 according to Google Scholar

and Elibrary databases was performed. The number of studies published in 2020–2024 was assessed based on the following requests: photopolymerization, photocurable biomaterials, photo-crosslinkable hydrogels, tissue engineering, degradable biomaterials, 3D-printing, photoinitiator.

PHOTOCURABLE MATERIALS FOR PRODUCTION OF MATRICES

Polymer matrices are produced by crosslinking of modified oligomeric or polymeric chains containing two or more active groups. Each active group can be chemically integrated either in the growing polymer chain, or in the crosslink between two chains due to radical formation. Transfer of radicals from initiators to the polymerized compound results in macroradical formation. Further attachment of the parent substance molecules to the growing macroradical ensures molecular weight increase, while interaction of two macroradicals results in the polymerization reaction termination (Fig. 2) [9]. The presence of competing mechanisms makes it possible to control supramolecular structure and molecular weight of the compound produced, which, in turn, helps control its physical and mechanical properties [10].

The use of photocurable materials as polymer matrices is of great interest in terms of solving the problems of biomedical materials science due to their capability of crosslinking at physiological temperatures in the absence of aggressive chemicals and good biocompatibility [3].

Photocurable polymer systems can be conditionally divided into synthetic and natural (biopolymers) based on their components. Among synthetic systems, polymer matrices based on polyethylene glycol, polylactide and their derivatives are actively studied, while the actively studied natural polymers are collagen and hyaluronic acid.

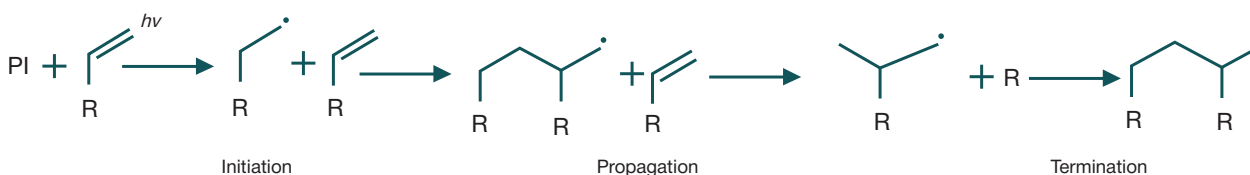


Fig. 2. Free radical polymerization reaction mechanism

Polyethylene glycol

Polyethylene glycol is a water-soluble, biocompatible ether that is widely used in tissue engineering and for drug delivery [11]. Polyethylene glycol-acetal-dimethylacrylate was used to produce biodegradable polymers potentially applicable for bone tissue regeneration. Nanoparticles made of calcium carbonate possessing enough reactivity for conversion to hydroxyapatite were used as an additive [12]. The resulting matrices were implanted in the subcutaneous pockets of mice for 15 and 30 days. Histological examination showed comparable moderate tissue response involving primarily macrophages, which showed biocompatibility of the photocurable polymer system. To solve the problem of infections following prosthetics, a specific technology of covering implants with a photocurable polymer based on polyethylene glycol and polyallyl-mercaptan was developed [13]. The technology demonstrates the possibility of mixing various antibiotics with the photopolymer solutions ensuring the necessary antimicrobial compatibility.

Polyester-based polymers

Such polymers are widely used in medicine as surgical threads, orthopedic implants, as well as for production of personalized scaffolds in tissue engineering. The personalized tissue scaffolds, 3D printed of the polycaprolactone-polyurethane photopolymers, are characterized by high cytocompatibility and survival rate of murine fibroblasts (above 85%), as well as by rapid biodegradation (2–6 h) [14]. Of interest is the example of producing the polylactide and polyethylene glycol-based polymer matrices for cartilage tissue restoration. Thus, the poly-D,L-lactic acid–poly(ethylene glycol)–poly-D,L-lactic acid co-polymer was developed [15]. The chondrocyte culture-based *in vivo* tests showed that the composition showed the capability

Table 1. Photocurable polymer matrix composition and production conditions

Composition	Photoinitiator	Photocuring conditions	Area of application	Literature
Methacrylated polyethylene glycol-acetal	Lithium phenyl(2,4,6-trimethylbenzoyl) phosphinate (LAP) 0.1% w/v	UV radiation 365 nm 30 s	Connective and soft tissue regeneration	[11]
Methacrylated polyethylene glycol-acetal	2-hydroxy-4'-(2-hydroxyethoxy)-2-methylpropiophenone 0.2% w/v	UV radiation 365 nm 15 min	Injectable bone substitutes	[12]
Acrylated derivatives of polyethylene glycol and polyallyl mercaptan	2,2-dimethoxy-2-phenylacetophenone	UV radiation 365 nm 20 mW/cm <sup>2</sup> 5 min	Antimicrobial coating for implants	[13]
Acrylated polycaprolactone Polyethylene glycol diacrylate	TPO 3% w/v	LED light 405 nm 30 s	3D printing for personalized tissue engineering	[14]
Acrylated derivatives of poly-D,L-lactic acid and polyethylene glycol	LAP	UV radiation 395 nm	Implant fixation	[15]
Methacrylated type I collagen Genipin	VA-086 1% w/v	UV radiation 365 nm 17 mW/cm <sup>2</sup> 1 min	3D printing of tissue scaffolds	[17]
Methacrylated type I collagen	LAP	UV radiation 365 nm 5 mW/cm <sup>2</sup> 30 min	Circulatory system repair	[18]
Chitosan-azide Keratin	–	UV radiation 365 nm 100 mW/cm <sup>2</sup> 15 min	Connective and soft tissue regeneration	[20]
Methacrylated chitosan Oxidized hyaluronic acid	LAP 0.1% w/v	UV radiation 405 nm 10 mW/cm <sup>2</sup> 120 s	Drug delivery	[21]
Methacrylated chitosan Methacrylated gelatin Polyethylene glycol diacrylate	2-hydroxy-2-methylpropiophenone 0.5% w/v	UV radiation 320 nm 180 mW/cm <sup>2</sup> 120 s	Drug delivery	[22]
Methacrylated hyaluronic acid Methacrylated gelatin	LAP 0.1% w/v	UV radiation 405 nm 25 mW/cm <sup>2</sup> 60 s	Tissue engineering	[23]
Oxalated hyaluronic acid Polyethylene glycol dimaleimide	LAP	UV radiation 365 nm 30 mW/cm <sup>2</sup>	Injectable cartilage substitutes	[24]
Hyaluronic acid Methacrylated chitosan	LAP 0.01–0.05% w/v	UV radiation 385 nm 19 mW/cm <sup>2</sup>	Extracellular matrix for tissue regeneration or drug delivery	[25]

of forming high-strength bonds with the host cartilage tissue under conditions of photopolymerization without affecting cell viability and tissue phenotype.

### Collagen

This is one of the basic biopolymers used in tissue engineering and regenerative medicine, since it accounts for about 33% of all body's proteins and forms the skin, tendons, cartilage and bone tissues, blood vessel walls [16]. Low mechanical resistance represents one collagen's disadvantage, however, polymer constructs with improved properties can be produced due to dual crosslinking. The study results have shown that dual crosslinking positively affects the elastic modulus and degradation degree, increasing them 2-fold relative to the non-crosslinked hydrogels [17]. The methacrylamide-modified collagen hydrogel developed for vascular tissue engineering compared to modified gelatin was characterized by high degree of polymerization (83–88% vs. 74–84%), adjustable mechanical properties (elastic modulus 4.8–9.4 kPa vs. 3.9–8.4 kPa), and higher cytocompatibility [18].

### Chitosan

Chitosan is a linear aminopolysaccharide consisting of glucosamine elements with free amino groups ensuring high reactivity and solubility. It differs from other biopolymers with good cell adhesion [19]. The process of chitosan chemical modification by the photopolymerizable 4-azidobenzoic acid groups is described in detail [20]. The study was aimed to produce a photocurable polymer membrane based on chitosan-azide and keratin. It is noteworthy that photopolymerization of the keratin-chitosan membranes occurred without adding a photoinitiator. The results of in vitro tests have shown that the keratin concentration increase positively affects the cell survival rate and adhesion. In the similar study, methacrylic anhydride-modified chitosan was used to produce a novel photopolymerizable composition characterized by rapid polymerization and high injectability [21]. It was reported that survival rate of mesenchymal stem cells exceeded 92%. The method to produce the chitosan and gelatin-based photopolymerizable hydrogel containing the albumin particles was reported [22]. Incubation tests in the model physiological

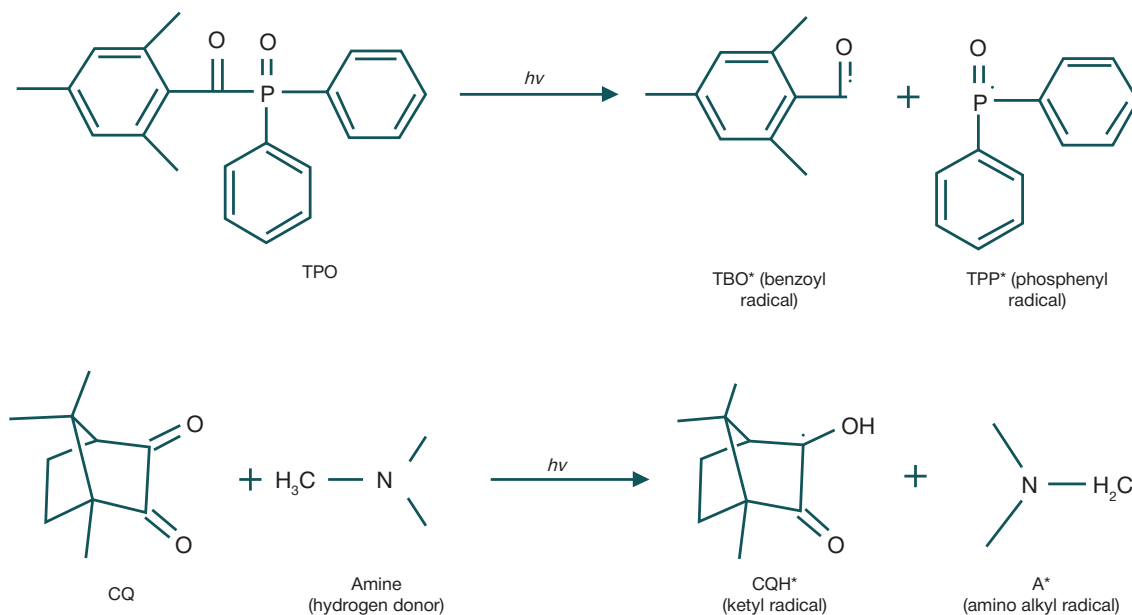


Fig. 3. Free radical production by type I and II photoinitiators under exposure of radiation on the example of TPO and CQ

fluids showed stability and no degradation of hydrogel. The murine fibroblast viability was 92.73%.

### Hyaluronic acid

This natural polysaccharide contained primarily in the animal tissue extracellular matrix is highly hydrophilic and biodegradable [23]. The possibility of producing photocurable matrices based on hyaluronic acid and polyethylene glycol through dual crosslinking has been reported [24]. The cell survival rate and strength characteristics of the resulting polymer suggested the prospects of its use for the connective tissue repair. The combination of chitosan and hyaluronic acid is of special interest. Polymerization degree and rate, mechanical and rheological properties of the photo-crosslinkable polymers based on methacrylated chitosan and hyaluronic acid depending on their ratio were studied [25]. When the photoinitiator content was 0.04% w/v, the polymerization degree exceeded 90% within 3 s. All the polymer compositions were completely degraded within the first 20–24 days in hydrolytic environment and 5–10 days in enzymatic environment, which makes the use of such compositions for prolonged drug delivery or tissue engineering promising. The decrease in cell viability with increasing concentrations of photoinitiator and hyaluronic acid in the original mixture were demonstrated in the embryonic fibroblast culture. The cell survival rate reported for all the studied compositions was within the range of 85–96%.

The photocurable polymer matrix composition and production conditions are provided in Table 1.

The data provided suggest that synthesis of the biocompatible polymer methacrylated derivatives represents the main approach to production of biomedical photopolymerizable compositions.

### PHOTOINITIATORS

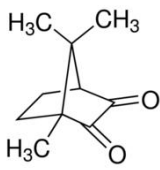
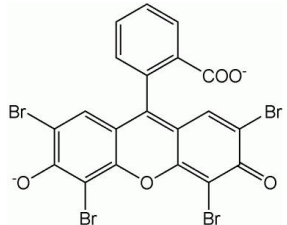
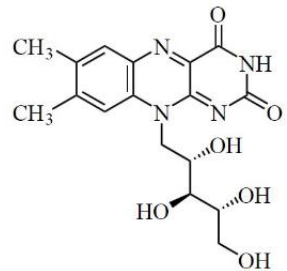
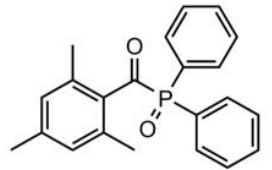
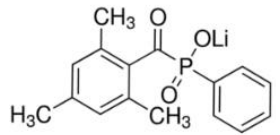
Photoinitiators are essential to initiate the free radical polymerization reaction. These are divided into two types. Type I photoinitiators undergo their own breakdown yielding free radicals after the light excitation. Type II photoinitiators produce radicals through hydrogen atom abstraction or electron/proton transfer from the co-initiator (Fig. 3) [26].

Camphorquinone is one of the first and still most commonly used photoinitiators. It belongs to the group of type II photoinitiators being less toxic compared to type I. However, the CQ lower chemical activity demands involvement of the tertiary amine as a photopolymerization reaction co-initiator. Polymerization rate is the main factor limiting the use of camphorquinone [7]. Special additives, representing the pyrrole derivatives that competitively absorb the initiating radiation, thereby preventing undesired formation of the initiator active form, have been proposed in order to increase resistance of the camphorquinone-based photocurable materials to sunlight [27]. Special attention is also paid to the camphorquinone toxicity. By the example of fibroblast lines it has been shown that the camphorquinone concentration increase from 50 mg/L to 100 mg/L in the photoinitiator system results in the cell viability decrease from 80% to 60% [28]. It has been proposed to use the compounds increasing the content of active groups (tetramethacrylate and tetraacrylate monomers) as co-initiators in photopolymerizable materials in order to ensure effective polymerization at the biologically acceptable camphorquinone concentrations [29].

Camphorquinone is poorly soluble in water, which considerably limits its use. In a number of studies, riboflavin and eosin were suggested as alternative water-soluble photoinitiators ensuring comparable photo-crosslinking characteristics. Eosin is non-toxic, cell viability exceeds 96% even when its concentration in the photopolymerizable material is 69 mg/L, and the survival rate exceeded 90% at the riboflavin concentration of 188 mg/L [30–32].

Type I photoinitiators include the aromatic ketone compounds, along with the phosphine and phosphine oxide derivatives (Table 2). TPO is one of the best studied and most commonly used in practice photoinitiators. The study focused on comparing the efficacy of type I and II photoinitiators showed that the monomer polymerization degree observed when using TPO was 13% higher, than that observed when using the camphorquinone–amine system. Furthermore, the radiation dose necessary for polymerization of the composition with CQ 4-fold exceeded the dose necessary for the same composition with TPO [33]. However, according to the TPO cytotoxicity assessment results, viability of various cell lines did not exceed 75% at the photoinitiator concentration of

Table 2. Photoinitiator efficacy and toxicity

Photoinitiator name	Type	Structural formula	Polymerization efficiency*	Cell viability*	Literature
Camphorquinone	II		★★★★☆☆	★★★★☆☆	[7, 28]
Eosin Y	II		★★★★★☆☆	★★★★★★★	[30]
Riboflavin	II		★★★★★☆☆	★★★★★☆☆	[31, 32]
TPO	I		★★★★★☆☆	★★★★★☆☆	[26, 33]
LAP	I		★★★★★☆☆	★★★★★★★	[34, 35]

Note: ★★★★★ — no more than 70%; ★★★★★★ — 70%–90%; ★★★★★★★ — more than 90%.

17.4 mg/L [26]. Significantly lower toxicity was demonstrated by the water-soluble lithium ion-modified LAP photoinitiator: the murine renal collecting duct cell viability was 95%. Thus, despite the fact that lithium is nephrotoxic, the lithium ions have not been identified as an important cytotoxic component [34].

The literature data analysis suggests that photoinitiators have a significant impact on cytotoxicity of the material produced. That is why photoinitiator selection becomes one of the defining challenges when designing the photopolymerizable composition. In terms of biocompatibility, it is preferable to use type II photoinitiators. Assessment of the efficacy and toxicity of the discussed photoinitiators is provided in Table 2.

## CONCLUSION

The growing body of research on photopolymerizable compositions that are promising for tissue engineering suggests the increased need for such materials. The approaches to production of novel photopolymerizable materials are conservative, and there is still a trend towards predominant use of the method to produce such materials by methacrylation of various biocompatible oligo- and polymers.

Thus, the main areas of material development are selecting and combining the proportions of methacrylated mono-, oligo- and polymers aimed to obtain the required physical and mechanical properties of the material with preserved biocompatibility.

In recent years, water-insoluble camphorquinone and diphenyl(2,4,6-trimethylbenzoyl)phosphine oxide showing considerable cytotoxicity are still most commonly used as photoinitiator additives for radical polymerization. Currently, the compounds retaining the ability to effectively initiate radical polymerization with the relatively lower toxic effects, such as endogenous photoinitiator riboflavin, synthetic photoinitiators eosin and lithium phenyl(2,4,6-trimethylbenzoyl)phosphinate, have been found and tested.

The vast majority of the studies of photopolymerizable compositions for biomedical applications reported in modern scientific papers are not complex; these describe a limited range of properties of the material produced and involve a small number of cell types (usually only one type). That is why the studies focused on the development, assessment of physical and mechanical properties, biological and clinical testing of such materials are relevant.



## References

- Shi H, Li Y, Xu K, Yin J. Advantages of photo-curable collagen-based cell-laden bioinks compared to methacrylated gelatin (GelMA) in digital light processing (DLP) and extrusion bioprinting. *Materials Today Bio*. 2023; 23: 100799. Available from: <https://doi.org/10.1016/j.mtbio.2023.100799>.
- Zhang Q, Zhou J, Zhi P, Liu L, Liu C, Fang A, et al. 3D printing method for bone tissue engineering scaffold. *Medicine in Novel Technology and Devices*. 2023; 17:100205. Available from: <https://doi.org/10.1016/j.medntd.2022.100205>.
- Mohammadpour Z, Kharazima M, Zarabi A. 3D-printing of silk nanofibrils reinforced alginate for soft tissue engineering. *Pharmaceutics*. 2023; 15: 763. Available from: <https://doi.org/10.3390/pharmaceutics15030763>.
- Li C, Zheng Z, Jia J, Zhang W, Qin L, Zhang Wei, et al. Preparation and characterization of photocurable composite extracellular matrix-methacrylated hyaluronic acid bioink. *J Mater Chem B*. 2022; 10: 4242–53. Available from: <https://doi.org/10.1039/D2TB00548D>.
- Ceylan G, Emik S, Yalcinyuva T, Sunbuloglu E, Bozdog E, Unalan F. The effects of cross-linking agents on the mechanical properties of poly (methyl methacrylate) resin. *Polymers*. 2023; 15: 2387. Available from: <https://doi.org/10.3390/polym15102387>.
- Voet V, Strating T, Schnelting G, Dijkstra P, Tietema M, Xu J, et al. Biobased acrylate photocurable resin formulation for stereolithography 3D printing. *ACS Omega*. 2018; 3: 1403–8. Available from: <https://doi.org/10.1021/acsomega.7b01648>.
- Tapety C, Carneiro Y, Chagas Y, Souza L, de O Souza N, Valadas L. Degree of conversion and mechanical properties of a commercial composite with an advanced polymerization system. *Acta Odontol Latinoam*. 2023; 36 (2): 112–9. Available from: <https://doi.org/10.54589/aol.36/2/112>.
- Kowalska A, Sokolowski J, Gozdek T, Krasowski M, Kopacz K, Bociong K. The influence of various photoinitiators on the properties of commercial dental composites. *Polymers*. 2021; 13: 3972. Available from: <https://doi.org/10.3390/polym13223972>.
- Fouassier JP, Lalevee J. Photoinitiators: Structures, reactivity and applications in polymerization. Weinheim, Germany: Wiley-VCH; 2021. Available from: <https://doi.org/10.1002/9783527821297>.
- Anusavice KJ, Shen C, Rawls HR. Phillips' science of dental materials. 12th ed. USA: Elsevier Inc., 2013.
- Shen C, Li Y, Meng Q. Adhesive polyethylene glycol-based hydrogel patch for tissue repair. *Colloids and Surfaces B: Biointerfaces*. 2022; 218: 112751. Available from: <https://doi.org/10.1016/j.colsurfb.2022.112751>.
- Unger RE, Stojanovic S, Besch L, Alkildani S, Schröder R, Jung O, et al. In vivo biocompatibility investigation of an injectable calcium carbonate (vaterite) as a bone substitute including compositional analysis via SEM-EDX technology. *Int J Mol Sci*. 2022; 23: 1196. Available from: <https://doi.org/10.3390/ijms23031196>.
- Xi W, Hegde V, Zoller SD, Park HY, Hart CM, Kondo T, et al. Point-of-care antimicrobial coating protects orthopaedic implants from bacterial challenge. *Nature Communications*. 2021; 12: 5473. Available from: <https://doi.org/10.1038/s41467-021-25383-z>.
- Chen H, Lee SY, Lin YM. Synthesis and formulation of PCL-based urethane acrylates for DLP 3D printers. *Polymers*. 2020; 12: 1500. Available from: <https://doi.org/10.3390/polym12071500>.
- Kuang B, Yang Y, Lin H. Infiltration and in-tissue polymerization of photocross-linked hydrogel for effective fixation of implants into cartilage-an in vitro study. *ACS Omega*. 2019; 4: 18540–4. Available from: <https://doi.org/10.1021/acsomega.9b02270>.
- Hulmes D, P. Fratzl P, editors. Collagen: structure and mechanics. 2th ed. Boston: Springer; 2008: 15–47.
- Kajave NS, Schmitt T, NguyenTU, Kishore V. Dual crosslinking strategy to generate mechanically viable cellladen printable constructs using methacrylated collagen bioinks. *Mater Sci Eng C Mater Biol Appl*. 2020; 107: 110290. Available from: <https://doi.org/10.1016/j.msec.2019.110290>.
- Pien N, Pezzoli D, Van Hoorick J, Copes F, Vansteenland M, Albu M, et al. Development of photo-crosslinkable collagen hydrogel building blocks for vascular tissue engineering applications: A superior alternative to methacrylated gelatin. *Materials Science Engineering C*. 2021; 130: 112460. Available from: <https://doi.org/10.1016/j.msec.2021.112460>.
- Valentino C, Vigani B, Zucca G, Ruggeri M, Boselli C, Cornaglia AI, et al. Formulation development of collagen/chitosan-based porous scaffolds for skin wounds repair and regeneration. *International Journal of Biological Macromolecules*. 2023; 242: 125000. Available from: <https://doi.org/10.1016/j.ijbiomac.2023.125000>.
- Lin CW, Chen YK, Lu M, Lou KL, Yu J. Photo-crosslinked keratin/chitosan membranes as potential wound dressing materials. *Polymers*. 2018; 10: 987. Available from: <https://doi.org/10.3390/polym10090987>.
- Han C, Zhang H, Wu Y, He X, Chen X. Dual-crosslinked hyaluronan hydrogels with rapid gelation and high injectability for stem cell protection. *Scientific Reports*. 2020; 10: 14997. Available from: <https://doi.org/10.1038/s41598-020-71462-4>.
- Bankosz, M. Development of chitosan/gelatin-based hydrogels incorporated with albumin particles. *International Journal of Molecular Sciences*. 2022; 23: 14136. Available from: <https://doi.org/10.3390/ijms232214136>.
- Xiao X, Huang Z, Jiang X, Yang Y, Yang L, Yang S, et al. Facile synthesise of norbornene-hyaluronic acid to form hydrogel via thiol-norbornene reaction for biomedical application. *Polymer*. 2022; 245: 124696. Available from: <https://doi.org/10.1016/j.polymer.2022.124696>.
- Wang G, Cao X, Dong H, Zeng L, Yu C, Chen X. A hyaluronic acid based injectable hydrogel formed via photo-crosslinking reaction and thermal-induced Diels-Alder reaction for cartilage tissue engineering. *Polymers*. 2018; 10: 949. Available from: <https://doi.org/10.3390/polym10090949>.
- Maiz-Fernandez S, Perez-Alvarez L, Silvan U, Vilas-Vilela JL, Lanceros-Mendez S. Photocrosslinkable and self-healable hydrogels of chitosan and hyaluronic acid. *International Journal of Biological Macromolecules*. 2022; 216: 291–302. Available from: <https://doi.org/10.1016/j.ijbiomac.2022.07.004>.
- Zeng B, Cai Z, Lalevee J, Yang Q, Lai H, Xiao P, et al. Cytotoxic and cytocompatible comparison among seven photoinitiators-triggered polymers in different tissue cells. *Toxicology in Vitro*. 2021; 72: 105103. Available from: <https://doi.org/10.1016/j.tiv.2021.105103>.
- Li J, Wu H, Chen Y, Cao K, Li Y, Ding Q, et al. Improvement in the storage stability of camphorquinone-based photocurable materials in sunlight via Z-E photoisomerization of photomask agent. *Progress Organic Coatings*. 2023; 178: 107455. Available from: <https://doi.org/10.1016/j.porgcoat.2023.107455>.
- Cuevas-Suarez CE, Da Silva AF, Dallegrave A, Petzhold CL, De Pereira CM, Oliveira Da Rosa WL, et al. The role of camphorquinone in the cytotoxicity of universal dental adhesives. *International Journal of Adhesion Adhesives*. 2023; 127: 103519. Available from: <https://doi.org/10.1016/j.ijadhadh.2023.103519>.
- Perez-Mondragon AA, Cuevas-Suarez CE, Gonzalez-Lopez JA, Trejo-Carbajal N, Herrera-Gonzalez AM. Evaluation of new coinitiators of camphorquinone useful in the radical photopolymerization of dental monomers. *Journal Photochemistry Photobiology, A: Chemistry*. 2020; 403: 112844. Available from: <https://doi.org/10.1016/j.jphotochem.2020.112844>.
- Petta D, Grijpma D.W, Alini M, Eglin D, D'Este M. Three-dimensional printing of a tyramine hyaluronan derivative with double gelation mechanism for independent tuning of shear thinning and postprinting curing. *ACS Biomater Sci Eng*. 2018; 4: 3088–98. Available from: <https://doi.org/10.1021/acsbmaterials.8b00416>.
- Kang Y, Kim JH, Kim SY, Koh W-G, Lee HJ. Blue light-activated riboflavin phosphate promotes collagen crosslinking to modify the properties of connective tissues. *Materials*. 2021; 14: 5788. Available from: <https://doi.org/10.3390/ma14195788>.
- Goto R, Nishida E, Kobayashi S, Aino M, Ohno T, Iwamura Y, et al. Gelatin methacryloyl-riboflavin (GelMA-RF) hydrogels for bone regeneration. *Int J Mol Sci*. 2021; 22: 1635. Available from: <https://doi.org/10.3390/ijms22041635>.
- Vaidyanathan TK, Vaidyanathan J, Lizymol PP, Ariya S, Krishnan KV. Study of visible light activated polymerization in BisGMA-TEGDMA monomers with Type 1 and Type 2 photoinitiators using Raman spectroscopy. *Dental Materials*. 2017; 33: 1–11. Available from: <https://doi.org/10.3390/ijms22041635>.
- Nguyen AK, Goering PL, Elespuru RK, Das SS, Narayan RJ. The photoinitiator lithium phenyl (2,4,6-trimethylbenzoyl) phosphinate

- with exposure to 405 nm light is cytotoxic to mammalian cells but not mutagenic in bacterial reverse mutation assays. *Polymers*. 2020; 12: 1489. Available from: <https://doi.org/10.3390/polym12071489>.
35. Xu H, Casillas J, Krishnamoorthy S, Xu C. Effects of Irgacure 2959

and lithium phenyl-2,4,6-trimethylbenzoylphosphinate on cell viability, physical properties, and microstructure in 3D bioprinting of vascular-like constructs. *Biomed Mater*. 2020; 15: 055021. Available from: <https://doi.org/10.1088/1748-605X/ab954e>.

## Литература

- Shi H, Li Y, Xu K, Yin J. Advantages of photo-curable collagen-based cell-laden bioinks compared to methacrylated gelatin (GelMA) in digital light processing (DLP) and extrusion bioprinting. *Materials Today Bio*. 2023; 23: 100799. Available from: <https://doi.org/10.1016/j.mtbio.2023.100799>.
- Zhang Q, Zhou J, Zhi P, Liu L, Liu C, Fang A, et al. 3D printing method for bone tissue engineering scaffold. *Medicine in Novel Technology and Devices*. 2023; 17:100205. Available from: <https://doi.org/10.1016/j.medntd.2022.100205>.
- Mohammadpour Z, Kharaziha M, Zarrabi A. 3D-printing of silk nanofibrils reinforced alginate for soft tissue engineering. *Pharmaceutics*. 2023; 15: 763. Available from: <https://doi.org/10.3390/pharmaceutics15030763>.
- Li C, Zheng Z, Jia J, Zhang W, Qin L, Zhang Wei, et al. Preparation and characterization of photocurable composite extracellular matrix-methacrylated hyaluronic acid bioink. *J Mater Chem B*. 2022; 10: 4242–53. Available from: <https://doi.org/10.1039/D2TB00548D>.
- Ceylan G, Emik S, Yalcinyuva T, Sunbuloglu E, Bozdogan E, Unalan F. The effects of cross-linking agents on the mechanical properties of poly (methyl methacrylate) resin. *Polymers*. 2023; 15: 2387. Available from: <https://doi.org/10.3390/polym15102387>.
- Voet V, Strating T, Schnelting G, Dijkstra P, Tietema M, Xu J, et al. Biobased acrylate photocurable resin formulation for stereolithography 3D printing. *ACS Omega*. 2018; 3: 1403–8. Available from: <https://doi.org/10.1021/acsomega.7b01648>.
- Tapety C, Carneiro Y, Chagas Y, Souza L, de O Souza N, Valadas L. Degree of conversion and mechanical properties of a commercial composite with an advanced polymerization system. *Acta Odontol Latinoam*. 2023; 36 (2): 112–9. Available from: <https://doi.org/10.54589/aol.36/2/112>.
- Kowalska A, Sokolowski J, Gozdek T, Krasowski M, Kopacz K, Bociong K. The influence of various photoinitiators on the properties of commercial dental composites. *Polymers*. 2021; 13: 3972. Available from: <https://doi.org/10.3390/polym13223972>.
- Fouassier JP, Lalevee J. Photoinitiators: Structures, reactivity and applications in polymerization. Weinheim, Germany: Wiley-VCH; 2021. Available from: <https://doi.org/10.1002/9783527821297>.
- Anusavice KJ, Shen C, Rawls HR. Phillips' science of dental materials. 12th ed. USA: Elsevier Inc., 2013.
- Shen C, Li Y, Meng Q. Adhesive polyethylene glycol-based hydrogel patch for tissue repair. *Colloids and Surfaces B: Biointerfaces*. 2022; 218: 112751. Available from: <https://doi.org/10.1016/j.colsurfb.2022.112751>.
- Unger RE, Stojanovic S, Besch L, Alkildani S, Schröder R, Jung O, et al. In vivo biocompatibility investigation of an injectable calcium carbonate (vaterite) as a bone substitute including compositional analysis via SEM-EDX technology. *Int J Mol Sci*. 2022; 23: 1196. Available from: <https://doi.org/10.3390/ijms23031196>.
- Xi W, Hegde V, Zoller SD, Park HY, Hart CM, Kondo T, et al. Point-of-care antimicrobial coating protects orthopaedic implants from bacterial challenge. *Nature Communications*. 2021; 12: 5473. Available from: <https://doi.org/10.1038/s41467-021-25383-z>.
- Chen H, Lee SY, Lin YM. Synthesis and formulation of PCL-based urethane acrylates for DLP 3D printers. *Polymers*. 2020; 12: 1500. Available from: <https://doi.org/10.3390/polym12071500>.
- Kuang B, Yang Y, Lin H. Infiltration and in-tissue polymerization of photocross-linked hydrogel for effective fixation of implants into cartilage-an in vitro study. *ACS Omega*. 2019; 4: 18540–4. Available from: <https://doi.org/10.1021/acsomega.9b02270>.
- Hulmes D, P. Fratzl P, editors. Collagen: structure and mechanics. 2th ed. Boston: Springer, 2008; 15–47.
- Kajave NS, Schmitt T, Nguyen TU, Kishore V. Dual crosslinking strategy to generate mechanically viable cellladen printable constructs using methacrylated collagen bioinks. *Mater Sci Eng C Mater Biol Appl*. 2020; 107: 110290. Available from: <https://doi.org/10.1016/j.msec.2019.110290>.
- Plen N, Pezzoli D, Van Hoorick J, Copes F, Vansteenland M, Albu M, et al. Development of photo-crosslinkable collagen hydrogel building blocks for vascular tissue engineering applications: A superior alternative to methacrylated gelatin. *Materials Science Engineering C*. 2021; 130: 112460. Available from: <https://doi.org/10.1016/j.msec.2021.112460>.
- Valentino C, Vigani B, Zucca G, Ruggeri M, Boselli C, Cornaglia AI, et al. Formulation development of collagen/chitosan-based porous scaffolds for skin wounds repair and regeneration. *International Journal of Biological Macromolecules*. 2023; 242: 125000. Available from: <https://doi.org/10.1016/j.ijbiomac.2023.125000>.
- Lin CW, Chen YK, Lu M, Lou KL, Yu J. Photo-crosslinked keratin/chitosan membranes as potential wound dressing materials. *Polymers*. 2018; 10: 987. Available from: <https://doi.org/10.3390/polym10090987>.
- Han C, Zhang H, Wu Y, He X, Chen X. Dual-crosslinked hyaluronan hydrogels with rapid gelation and high injectability for stem cell protection. *Scientific Reports*. 2020; 10: 14997. Available from: <https://doi.org/10.1038/s41598-020-71462-4>.
- Bankosz, M. Development of chitosan/gelatin-based hydrogels incorporated with albumin particles. *International Journal of Molecular Sciences*. 2022; 23: 14136. Available from: <https://doi.org/10.3390/ijms232214136>.
- Xiao X, Huang Z, Jiang X, Yang Y, Yang L, Yang S, et al. Facile synthesis of norbornene-hyaluronic acid to form hydrogel via thiol-norbornene reaction for biomedical application. *Polymer*. 2022; 245: 124696. Available from: <https://doi.org/10.1016/j.polymer.2022.124696>.
- Wang G, Cao X, Dong H, Zeng L, Yu C, Chen X. A hyaluronic acid based injectable hydrogel formed via photo-crosslinking reaction and thermal-induced Diels-Alder reaction for cartilage tissue engineering. *Polymers*. 2018; 10: 949. Available from: <https://doi.org/10.3390/polym10090949>.
- Maiz-Fernandez S, Perez-Alvarez L, Silvan U, Vilas-Vilela JL, Lancers-Mendez S. Photocrosslinkable and self-healable hydrogels of chitosan and hyaluronic acid. *International Journal of Biological Macromolecules*. 2022; 216: 291–302. Available from: <https://doi.org/10.1016/j.ijbiomac.2022.07.004>.
- Zeng B, Cai Z, Lalevee J, Yang Q, Lai H, Xiao P, et al. Cytotoxic and cytocompatible comparison among seven photoinitiators-triggered polymers in different tissue cells. *Toxicology in Vitro*. 2021; 72: 105103. Available from: <https://doi.org/10.1016/j.tiv.2021.105103>.
- Li J, Wu H, Chen Y, Cao K, Li Y, Ding Q, et al. Improvement in the storage stability of camphorquinone-based photocurable materials in sunlight via Z–E photoisomerization of photomask agent. *Progress Organic Coatings*. 2023; 178: 107455. Available from: <https://doi.org/10.1016/j.porgcoat.2023.107455>.
- Cuevas-Suarez CE, Da Silva AF, Dallegre A, Petzhold CL, De Pereira CM, Oliveira Da Rosa WL, et al. The role of camphorquinone in the cytotoxicity of universal dental adhesives. *International Journal of Adhesion Adhesives*. 2023; 127: 103519. Available from: <https://doi.org/10.1016/j.ijadhadh.2023.103519>.
- Perez-Mondragon AA, Cuevas-Suarez CE, Gonzalez-Lopez JA, Trejo-Carbajal N, Herrera-Gonzalez AM. Evaluation of new coinitiators of camphorquinone useful in the radical photopolymerization of dental monomers. *Journal Photochemistry Photobiology, A: Chemistry*. 2020; 403: 112844. Available from: <https://doi.org/10.1016/j.jphotochem.2020.112844>.
- Petta D, Grijpma D.W, Alini M, Eglin D, D'Este M. Three-dimensional printing of a tyramine hyaluronan derivative with double gelation mechanism for independent tuning of shear thinning and postprinting curing. *ACS Biomater Sci Eng*. 2018; 4: 3088–98. Available from: <https://doi.org/10.1021/acsbomaterials.8b00416>.
- Kang Y, Kim JH, Kim SY, Koh W-G, Lee HJ. Blue light-activated

- riboflavin phosphate promotes collagen crosslinking to modify the properties of connective tissues. *Materials*. 2021; 14: 5788. Available from: <https://doi.org/10.3390/ma14195788>.
32. Goto R, Nishida E, Kobayashi S, Aino M, Ohno T, Iwamura Y, et al. Gelatin methacryloyl-riboflavin (GelMA-RF) hydrogels for bone regeneration. *Int J Mol Sci*. 2021; 22: 1635. Available from: <https://doi.org/10.3390/ijms22041635>.
  33. Vaidyanathan TK, Vaidyanathan J, Lizymol PP, Ariya S, Krishnan KV. Study of visible light activated polymerization in BisGMA-TEGDMA monomers with Type 1 and Type 2 photoinitiators using Raman spectroscopy. *Dental Materials*. 2017; 33: 1–11. Available from: <https://doi.org/10.3390/ijms22041635>.
  34. Nguyen AK, Goering PL, Elespuru RK, Das SS, Narayan RJ. The photoinitiator lithium phenyl (2,4,6-trimethylbenzoyl) phosphinate with exposure to 405 nm light is cytotoxic to mammalian cells but not mutagenic in bacterial reverse mutation assays. *Polymers*. 2020; 12: 1489. Available from: <https://doi.org/10.3390/polym12071489>.
  35. Xu H, Casillas J, Krishnamoorthy S, Xu C. Effects of Irgacure 2959 and lithium phenyl-2,4,6-trimethylbenzoylphosphinate on cell viability, physical properties, and microstructure in 3D bioprinting of vascular-like constructs. *Biomed Mater*. 2020; 15: 055021. Available from: <https://doi.org/10.1088/1748-605X/ab954e>.

## PROSPECTS FOR THE USE OF LONG-LIVING PRINTED TEMPORARY ORTHOPEDIC STRUCTURES

Proskokova SV, Enikeev AM , Pirogov AE, Kuliev RM

Pirogov Russian National Research Medical University, Moscow, Russia

The non-removable temporary structures are used in orthopedic dentistry to provide high-quality treatment. The approaches in prosthetics are conditionally divided into conventional and digital. These approaches imply the use of both common materials for prosthetics and unique options. When the conventional approach is used, the quality of orthopedic dental treatment depends on the manual skill of the provider (dental technician). Unlike the conventional approach, the digital one uses a wide range of libraries with ready-made templates for various options for the dentoalveolar system aesthetic and functional characteristics. This fact allows the attending physician to do without any intermediary for the manufacture of dental prostheses, if the material and technical resources permit. The use of 3D printing in dentistry has only recently begun. From our point of view, the active use of photopolymer 3D resins can become a promising option in terms of economic and strength characteristics.

**Keywords:** 3D printing, photopolymers, digital dentistry, temporary prosthetics


**Author contribution:** Proskokova SV — project management, manuscript editing; Enikeev AM — literature search and analysis, manuscript writing; Pirogov AE, Kuliev RM — manuscript editing.

✉ **Correspondence should be addressed:** Amir M. Enikeev  
Ostrovityanova, 1, str. 9, Moscow, 117997, Russia; amir.stomat.art@gmail.com

**Received:** 16.07.2024 **Accepted:** 03.08.2024 **Published online:** 30.08.2024

**DOI:** 10.24075/brsmu.2024.037

## ПЕРСПЕКТИВЫ ПРИМЕНЕНИЯ ПРИНТОВАННЫХ ВРЕМЕННЫХ ОРТОПЕДИЧЕСКИХ КОНСТРУКЦИЙ ПРИ ДЛИТЕЛЬНОЙ ЭКСПЛУАТАЦИИ

С. В. Проскокова, А. М. Еникеев , А. Е. Пирогов, Р. М. Кулиев

Институт стоматологии, Российский национальный исследовательский медицинский университет имени Н. И. Пирогова, Москва, Россия

Для осуществления качественного лечения в ортопедической стоматологии применяют несъемные временные конструкции. Существует условное разделение подходов в протезировании на традиционный и цифровой. Эти подходы подразумевают использование как общих материалов для протезирования, так и уникальных вариантов. При традиционном подходе качество исполнения ортопедического стоматологического лечения зависит от мануального навыка исполнителя (зубного техника). В отличие от традиционного подхода, цифровой использует широкий набор библиотек с готовыми шаблонами под различные варианты эстетических и функциональных характеристик зубочелюстной системы. Данный факт позволяет лечащему врачу обходиться без посредника для изготовления зуботехнических протезов, если позволяет материально-техническая база. Использование 3D-печати в стоматологии появилось относительно недавно. С нашей точки зрения, активное применение фотополимерных 3D-смола может стать перспективным вариантом по экономическим и прочностным характеристикам.

**Ключевые слова:** 3D-печать, фотополимеры, цифровая стоматология, временное протезирование

**Вклад авторов:** С. В. Проскокова — руководство проектом, редактирование рукописи; А. М. Еникеев — поиск и анализ литературы, написание рукописи; А. Е. Пирогов, Р. М. Кулиев — редактирование рукописи.

✉ **Для корреспонденции:** Amir Maratovich Enikeev  
ул. Островитянова, д. 1, с. 9, г. Москва, 117997, Россия; amir.stomat.art@gmail.com

**Статья получена:** 16.07.2024 **Статья принята к печати:** 03.08.2024 **Опубликована онлайн:** 30.08.2024

**DOI:** 10.24075/vrgmu.2024.037

Treatment of partially edentulous patients is a pressing issue of prosthetic dentistry [1, 2]. The use of non-removable temporary structures in prosthetics proved to be not only important, but also uncontested stage of the effective high-quality treatment. During the period between the start of tooth preparation and permanent fixation of non-removable structures it is necessary to manufacture and use the temporary prostheses showing high mechanical stability and protecting the prepared teeth against bacterial infection and irritants of various types: thermal and chemical. The temporary prostheses ensure safety of the pulp, protection of the marginal periodontium, predictable shaping of the marginal gingiva, lack of negative effects on the components of the temporomandibular joint (TMJ) and the mastication muscles. Furthermore, temporary structures make it possible to preserve or reconstruct the lost occlusion and aesthetics. Currently, the arsenal of prosthetic dentists includes a large number of materials used for temporary structures.

The study was aimed to present the main temporary prosthetics methods and the advantages of 3D-printed structures.

The search for scientific papers on the issue was conducted in the catalogues of scientific electronic libraries (<https://www.elibrary.ru>, <https://pubmed.ncbi.nlm.nih.gov>) for the years 2017–2024.

The search in Elibrary involving the use of the “3D-печать” word phrase and the dentistry filter yielded 205 results (among them 195 for the years 2017–2024), the search performed using the “временные коронки” word phrase yielded 310 results (among them 150 for the years 2017–2024), the search in Pubmed involving the use of the “3d printed crowns” word phrase yielded 389 results (among them 362 for the years 2017–2024), and the search performed using the “Temporary crowns” word phrase yielded 1716 results (among them 344 for the years 2017–2024) (Fig. 1).

A total of 153 papers were selected by manual sorting.

When performing advanced search in the set prepared, we managed to obtain the following information about the paper types: dissertations — 2 (1.3%); books — 15 (9.8%); conference papers — 29 (18.9%); patents — 11 (7.1%) (Fig. 2).

**Conventional approach**

Conventional approach involves the use of the acrylic-based plastics and composites with various types of polymerization.

The methyl methacrylate-based acrylic plastics are most often used in the laboratory manufacture of temporary structures. The crowns and dental bridges made of plastics of this type are characterized by high strength and color stability and can be also used over a long recovery period.

Ethyl methacrylate is used in temporary prosthetics for short-term application in the oral cavity. Lower heat emission and the decreased shrinkage rate represent the advantages of this material.

The Bis-acrylate-based materials for temporary prosthetics are very popular. This two-component material is based on the methyl methacrylate-derived multifunctional acrylic esters. The Bis-acrylate-based materials are produced primarily in the form of cartridges for the 4 : 1 or 1 : 1 dispensing and mixing systems, which enables quick and easy manufacture of temporary systems when there is silicone index. Lower strength characteristics and the need to manufacture a silicone index represent disadvantages of such materials.

Composite materials with low-temperature polymerization are also produced in the form of cartridges for the 4 : 1 dispensing and mixing systems or in the form of syringes as fluid variants of dental filling composites. These materials are characterized by positive effects peculiar to modern dental materials: are easy to administer to the cavity due to their texture [3].

**Digital approach**

As for digital approach, the structures manufactured by CAD/CAM milling represent one option for temporary prosthetics.

CAD is the Computer Aided Design, i.e. creation of a virtual structure. CAM is the Computer Aided Manufacturing. CAD/CAM represents the advanced technology for production of scaffolds or complete dentures by computer aided design and milling on the numerically controlled machines (CNC).

The polymethyl methacrylate (PMMA) plastic is the main material for the temporary structure milling. PMMA is used for both short-term restorative care and the long-living structures. This material is flexible and very strong. Difficulty to achieve

enough strength of adhesion with the prepared tooth stump is a disadvantage.

The emergence of the 3D printing technology represents the next stage of development of the digital temporary prosthetic approach. Today, the technology makes it possible to manufacture full removable prostheses, crowns, suprastructures for implants, and navigation templates. The prototyping results obtained are superior to the equivalent use of conventional materials [4].

The photopolymer resin 3D printing belongs to the broad category of light polymerization in baths. The concept is based on the photosensitive resin capability of solidifying under exposure to light energy.

Currently, there are several 3D printing options: SLA, DLP, LCD. The SLA (laser stereolithography, stereolithography apparatus) technology is based on directing the UV laser beam onto the bath with polymer resin, which leads to polymerization at a certain point. Then the working surface is shifted downward by 0.025–0.300 mm, and the laser ensures polymerization of the next layer. The process continues until the model construction is over [5].

DLP is the Digital Light Processing. Radiation emitted by the digital projector selectively affects the liquid photopolymer resin contained in the special container through the print area. The resin is solidified layer-by-layer at the exposure sites, and the 3D model is steadily constructed. The distinctions of the technology are the relatively small working area, high printing speed, wide range of compatible expendables.

LCD technology is the youngest among photopolymer printers. Initially, LCD emerged as a more affordable analogue of the DLP technology, since the operation principles are similar. In LCD, the UV LEDs are used that light through the LCD screen to solidify the photopolymer resin. Despite the fact that the LCD screen also constructs the entire layers over the same time, as the DLP 3D printers, the quality of layers depends on the screen resolution. The higher is LCD screen resolution, the higher is printing quality.

Polymer materials are widely used for medical applications. Along with the common technical requirements (melting point, strength, wear resistance, etc.) for medical polymer materials, especially dental materials, there are additional sanitary and hygienic requirements: minimal interaction with bioactive environments, no toxic effects, low solubility, minimal sorption properties.

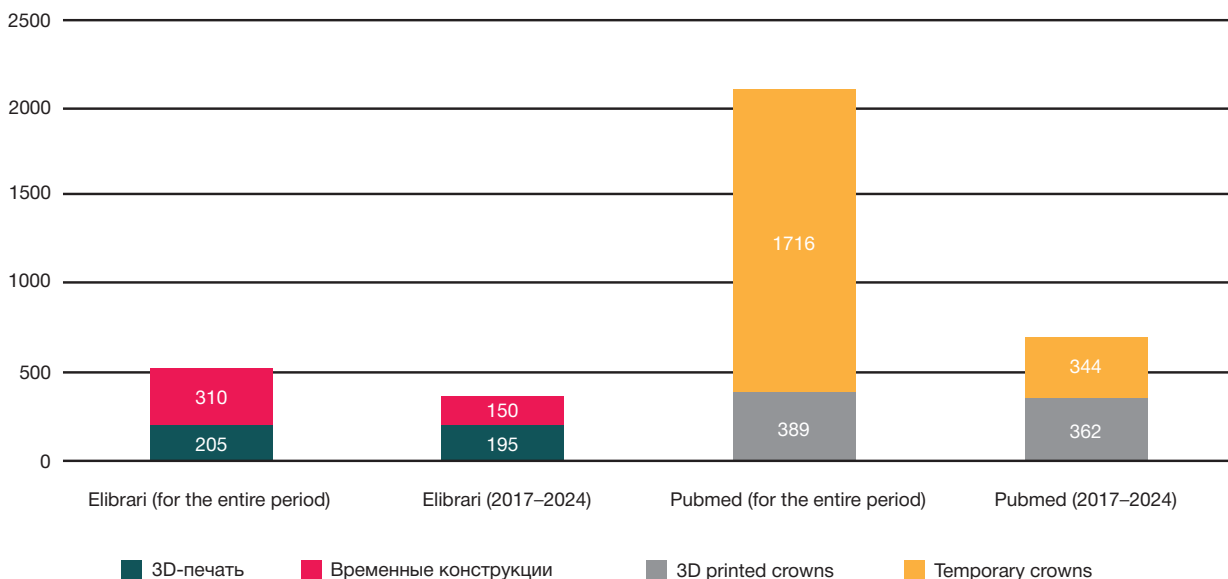


Fig. 1. Results for searchable word phrases

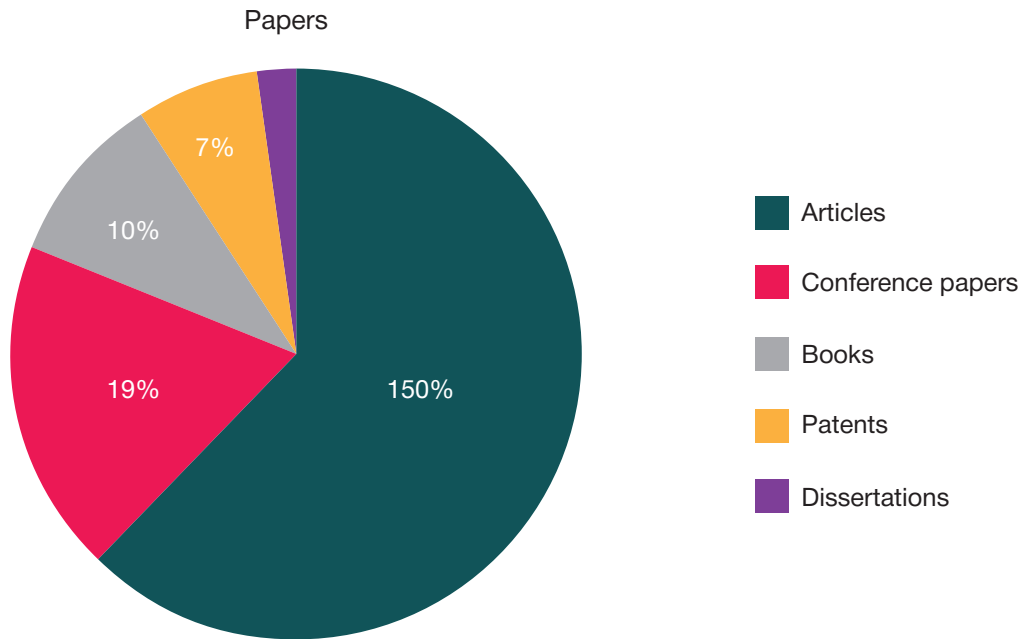


Fig. 2. Paper types

The following components are usually contained in photopolymer resins for temporary prostheses:

**Monomeric base.** Methacrylate-based monomers are commonly used, such as Bis-GMA (bisphenol A-glycidyl methacrylate) or UDMA (urethane dimethacrylate). These monomers ensure high strength and stability of the resin.

**Photoinitiators** are substances triggering the polymerization reaction due to light. Camphorquinone (CQ), benzophenone (BP) and 4-methylaminobenzoic acid phenylpropionate (MABBP) are the most common photoinitiators. These absorb light of a particular wavelength and generate free radicals that initiate the polymerization process.

**Fillers** are represented by particles added to the resin in order to improve its properties. These can be mineral (for example, silicon dioxide), organic (for example, barium sulfate) or synthetic (for example, microglass).

**Curative** is a substance that accelerates the polymerization process. Benzoyl peroxide or other organic peroxides are commonly used.

**Pigments** are substances that give the resin a certain color. These can be organic or inorganic.

**Additives** are supplementary substances that can be added to the resin in order to improve its properties. For example, antioxidants are added to prevent oxidation, plasticizers to improve flexibility, and moisturizing agents are added to prevent dehydration.

Dentistry is widely accepted as the field that can greatly benefit from the 3D printing technologies. In domestic literature, there are many review papers focused on the use of 3D printing. However, there are few papers considering parameters, characteristics, and properties of such materials in detail [6, 7].

The review of foreign literature has yielded much more data. Some studies claim that 3D-printed interim polymer materials show lower flexural strength (FS) compared to the milled interim restoration [8, 9]. However, the 3D-printed interim polymer materials show higher flexural strength compared to the temporary structures made of conventional materials [10, 11]. Multiple studies focused on comparing wear resistance of materials showed lower loss of volume associated with wear and smoother surfaces in the 3D-printed samples [12]. When

printing, printers are able to apply layers sized up to a tenth of a micromillimeter to yield a product with a smoother surface, and the time of polishing is reduced compared to milling [13].

Moreover, the 3D-printed materials usually have higher elastic modulus (EM) compared to conventional materials, but the EM does not exceed that of milled materials. As for surface roughness, the 3D-printed materials have a smoother surface compared to the milled and conventional interim materials.

Thus, the data of assessing physical and mechanical properties suggest that 3D resins show better results, than conventional materials. Milled structures are the favorites, except for the prosthesis smoothness.

However, we must not forget about the economic aspect. A number of papers consider the feasibility of photopolymer resin printing [14, 15]. The 3D printing method is cost-effective, and the possibility of manufacturing the necessary structure only without using the plaster model reduces the production time. The amount of photopolymer necessary to manufacture the structure is spent during printing, while about 30% of the block volume constitutes the cost when using milling. Digital approach and the 3D printer availability allow the attending physician to perform all the procedures necessary for treatment in the same clinic without involving third-party dental laboratories and dental technicians.

In our country, the domestically produced photopolymer resins that are cheaper compared to foreign analogues are mainly used. It should be noted that resins produced in Russia are not inferior in their properties to imported materials and are exported to other countries for dental applications. By contrast, manufacturers from China dominate almost completely in the market of the CAD/CAM preforms for temporary prosthetics, due to which the final product becomes more expensive.

The process of improving the printed polymer flexural strength still continues. There are polymer resin modifications, in which the zirconium oxide (ZrO<sub>2</sub>) nanoparticles are added to various concentrations. Mechanical properties superior to that of conventional printing resin have been revealed, which increase possible lifespan of such structures. These modifications are already available on the market, including modifications produced by the domestic 3D printing resin manufacturers.

## CONCLUSION

The use of dental 3D resins is a promising avenue for temporary prosthetics, including that for continuous exploitation. These

materials are not inferior to competitors in mechanical properties. The structures are cheaper compared to the CAD/CAM-milled analogues. This opens the door for the use of effective and affordable prosthetic options.

## References

1. Apresyan SV. Optimizaciya vremennyh zubnyh protezov iz poliuretana [dissertaciya]. M., 2012. Russian.
2. Babunashvili GB. Kliniko-laboratornoe obosnovanie primeneniye materiala «Akrodent» dlya vremennyh zubnyh protezov [dissertaciya]. M., 2007. Russian.
3. Luckaya IK, Novak NV, Ershov-Pavlov P E. Primeneniye vremennyh koronok na etape protezirovaniya zubov keramicheskimi konstrukciyami. *Sovremennaya stomatologiya*. 2017; 4 (69): 51–54. Russian.
4. YUmashev AV, Mihajlova MV, Kuderova IG, Kristal EA. Varianty ispol'zovaniya 3D skanirovaniya v ortopedicheskoy stomatologii. *Vestnik novyh medicinskih tekhnologij. Elektronnoe izdanie*. 2015; 1: 2–6. Russian.
5. Evsevev EN. Obzor tekhnologij 3D-pechati. *Science Time*. 2017; 10 (46): 11–15. Russian.
6. ZHulev EN. Sravnitel'naya ocenka razmernoj tochnosti iskusstvennyh koronok, izgotovlennyh s pomoshch'yu CAD/CAM sistemy i 3d PRINTERA po tekhnologii. *Vestnik novyh medicinskih tekhnologij. Elektronnoe izdanie*. 2020; 3: 40–45. Russian.
7. Shnajder SD, Nurieva NS, YUrasov AD. Issledovaniya prochnosti i uprugosti na trekhtochechnyj izgib materialov vremennyh konstrukcij pryamym sposobom i koronok metodom 3d-pechati. *Stomatologicheskaya vesna v Belgorode — 2022: Sbornik trudov Mezhdunarodnoj nauchno-prakticheskoy konferencii v ramkah mezhdunarodnogo stomatologicheskogo festivalya «Ploshchadka bezopasnosti stomatologicheskogo pacienta», posvyashchennogo 100-letiyu Moskovskogo gosudarstvennogo mediko-stomatologicheskogo universiteta im. A. I. Evdokimova, Belgorod, 09 iyunya 2022 goda. Belgorod: Belgorodskij gosudarstvennyj nacional'nyj issledovatel'skij universitet, 2022; s. 260–262. Russian.*
8. Tasin S, Ismatullaev A. Comparative evaluation of the effect of thermocycling on the mechanical properties of conventionally polymerized, CAD-CAM milled, and 3D-printed interim materials. *J Prosthet Dent*. 2022; 127: 173.e1–173.e8. PubMed PMID: 34756771.
9. Mayer J, Stawarczyk B, Vogt K, Hickel R, Edelhoff D, Reymus M. Influence of cleaning methods after 3D printing on two-body wear and fracture load of resin-based temporary crown and bridge material. *Clin Oral Investig*. 2021; 25 (10): 5987–96. PubMed PMID: 33811531.
10. Albahri R, Yoon HI, Lee JD, Yoon S, Lee SJ. Shear bond strength of provisional repair materials bonded to 3D printed resin. *J Dent Sci*. 2021; 16 (1): 261–7. PubMed PMID: 33384807.
11. Alzahrani SJ, Hajjaj MS, Azhari AA, Ahmed WM, Yeslam HE, Carvalho RM. Mechanical properties of three-dimensional printed provisional resin materials for crown and fixed dental prosthesis: a systematic review. *Bioengineering*. 2023; 10 (6): 663. PubMed PMID: 37370594.
12. Manjunath KS, Sridhar K, Gopinath V, Sankar K, Sundaram A, Gupta N, et al. Facile manufacturing of fused-deposition modeled composite scaffolds for tissue engineering—an embedding model with plasticity for incorporation of additives. *Biomed Mater*. 2020; 16 (1): 015028. PubMed PMID: 33331292.
13. Myagmar G, Lee JH, Ahn JS, Yeo IL, Yoon HI, Han JS. Wear of 3D printed and CAD/CAM milled interim resin materials after chewing simulation. *J Adv Prosthodont*. 2021; 13 (3): 144–51. PMID: 34234924.
14. Tahayeri A, Morgan M, Fugolin AP, Bompolaki D, Athirasala A, Pfeifer CS, et al. 3D printed versus conventionally cured provisional crown and bridge dental materials. *Dent Mater*. 2018; 34 (2): 192–200. PubMed PMID: 29110921.
15. Vokulova YU. A., ZHulev E. N. Sravnitel'naya ocenka ekonomicheskogo obosnovaniya izgotovleniya vremennyh iskusstvennyh koronok, poluchennyh s pomoshch'yu traditsionnyh i cifrovyyh tekhnologij. *The Scientific Heritage*. 2020; 47–2 (47): 3–6.

## Литература

1. Апресян С. В. Оптимизация временных зубных протезов из полиуретана [диссертация]. М., 2012.
2. Бабунашвили Г. Б. Клинико-лабораторное обоснование применения материала «Акродент» для временных зубных протезов [диссертация]. М., 2007.
3. Луцкая И. К., Новак Н. В., Ершов-Павлов П. Е. Применение временных коронок на этапе протезирования зубов керамическими конструкциями. *Современная стоматология*. 2017; 4 (69): 51–54.
4. Юмашев А. В., Михайлова М. В., Кудерова И. Г., Кристал Е. А. Варианты использования 3D сканирования в ортопедической стоматологии. *Вестник новых медицинских технологий. Электронное издание*. 2015; 1: 2–6.
5. Евсевьев Е. Н. Обзор технологий 3D-печати. *Science Time*. 2017; 10 (46): 11–15.
6. Жулев Е. Н. Сравнительная оценка размерной точности искусственных коронок, изготовленных с помощью CAD/CAM системы и 3d ПРИНТЕРА по технологии. *Вестник новых медицинских технологий. Электронное издание*. 2020; 3: 40–45.
7. Шнайдер С. Д., Нуриева Н. С., Юрасов А. Д. Исследования прочности и упругости на трехточечный изгиб материалов временных конструкций прямым способом и коронок методом 3d-печати. *Стоматологическая весна в Белгороде — 2022: Сборник трудов Международной научно-практической конференции в рамках международного стоматологического фестиваля «Площадка безопасности стоматологического пациента», посвященного 100-летию Московского государственного медико-стоматологического университета им. А. И. Евдокимова, Белгород, 09 июня 2022 года. Белгород: Белгородский государственный национальный исследовательский университет, 2022; с. 260–262.*
8. Tasin S, Ismatullaev A. Comparative evaluation of the effect of thermocycling on the mechanical properties of conventionally polymerized, CAD-CAM milled, and 3D-printed interim materials. *J Prosthet Dent*. 2022; 127: 173.e1–173.e8. PubMed PMID: 34756771.
9. Mayer J, Stawarczyk B, Vogt K, Hickel R, Edelhoff D, Reymus M. Influence of cleaning methods after 3D printing on two-body wear and fracture load of resin-based temporary crown and bridge material. *Clin Oral Investig*. 2021; 25 (10): 5987–96. PubMed PMID: 33811531.
10. Albahri R, Yoon HI, Lee JD, Yoon S, Lee SJ. Shear bond strength of provisional repair materials bonded to 3D printed resin. *J Dent Sci*. 2021; 16 (1): 261–7. PubMed PMID: 33384807.
11. Alzahrani SJ, Hajjaj MS, Azhari AA, Ahmed WM, Yeslam HE, Carvalho RM. Mechanical properties of three-dimensional printed provisional resin materials for crown and fixed dental prosthesis:

- a systematic review. *Bioengineering*. 2023; 10 (6): 663. PubMed PMID: 37370594.
12. Manjunath KS, Sridhar K, Gopinath V, Sankar K, Sundaram A, Gupta N, et al. Facile manufacturing of fused-deposition modeled composite scaffolds for tissue engineering-an embedding model with plasticity for incorporation of additives. *Biomed Mater*. 2020; 16 (1): 015028. PubMed PMID: 33331292.
  13. Myagmar G, Lee JH, Ahn JS, Yeo IL, Yoon HI, Han JS. Wear of 3D printed and CAD/CAM milled interim resin materials after chewing simulation. *J Adv Prosthodont*. 2021; 13 (3): 144–51. PMID: 34234924.
  14. Tahayeri A, Morgan M, Fugolin AP, Bompolaki D, Athirasala A, Pfeifer CS, et al. 3D printed versus conventionally cured provisional crown and bridge dental materials. *Dent Mater*. 2018; 34 (2): 192–200. PubMed PMID: 29110921.
  15. Вокулова Ю. А., Жулев Е. Н. Сравнительная оценка экономического обоснования изготовления временных искусственных коронок, полученных с помощью традиционных и цифровых технологий. *The Scientific Heritage*. 2020; 47–2 (47): 3–6.



## EFFECTS OF BIOCOMPATIBLE PIEZOELECTRIC MEMBRANES ON THE DEVELOPMENT OF FIBROSIS ASSOCIATED WITH THE ORAL MUCOSAL WOUND REGENERATION

Koniaeva AD<sup>1</sup>✉, Varakuta EYu<sup>1</sup>, Leiman AE<sup>1</sup>, Kormashov GM<sup>1</sup>, Fedosova MV<sup>1</sup>, Bolbasov EN<sup>2</sup>, Stankevich KS<sup>3</sup>

<sup>1</sup> Siberian State Medical University, Tomsk, Russia

<sup>2</sup> Tomsk Polytechnic University, Tomsk, Russia

<sup>3</sup> Montana State University, Bozeman, MT, USA

Prevention of fibrosis during the oral mucosal wound regeneration is a pressing issue of today's surgical dentistry. The study was aimed to perform morphological assessment of the effects of biocompatible piezoelectric membranes on fibrous tissue formation during regeneration of the oral mucosal wounds. We assessed cell-cell interactions of macrophages and fibroblasts, along with changes in the CD68 and TGFβ1 marker expression and their effects on the development of fibrosis under conditions of using biocompatible polymeric membranes with piezoelectric properties at various stages of the oral mucosal wound defect regeneration. Comparative morphological assessment of the oral mucosal structures was conducted in animals having intact mucosa ( $n = 15$ ), having open wound defects ( $n = 15$ ), and having wounds covered with biocompatible piezoelectric membranes ( $n = 15$ ). Biomaterial was collected from the wound defect site on days 3, 7, and 12 of the experiment; collection of biomaterial from intact animals was performed on the same days. In the group, where biocompatible membranes were used, signs of proliferation phase at the defect site were detected as early as on day 3 of the study; the faster shift from macrophage infiltration to fibroblast infiltration, the decline in inflammatory response were detected on day 7; restoration of the numerical density of macrophages and fibroblasts to the intact values was detected on day 12. The expression of CD68 and TGFβ1, the prognostic markers of fibrosis, was lower in the group, where no membranes were used. Reduction of the dense fibrous connective tissue specific area was observed at the microscopic level, severe soft tissue deformation was reported at the macroscopic level. In the group with no wound covering, extensive cell infiltration and increased CD68 and TGFβ1 expression persisted throughout the experiment, which resulted in the fact that specific area of dense fibrous connective tissue was larger, than that of loose connective tissue, on day 12 of the study, as well as in the cicatricial soft tissue deformities.

**Keywords:** regeneration, wound defect, fibrosis, piezoelectrics, oral mucosa, inflammation

**Funding:** the study was supported by the RSF (research project No. 23-25-00346)

**Author contribution:** Koniaeva AD, Varakuta EYu, Bolbasov EN, Stankevich KS — study concept and design; Koniaeva AD, Leiman AE, Kormashov GM, Fedosova MV — data acquisition and processing; Koniaeva AD, Varakuta EYu — manuscript writing; Koniaeva AD, Varakuta EYu, Bolbasov EN, Stankevich KS — manuscript editing.

**Compliance with ethical standards:** the study was approved by the IACUC of the Siberian State Medical University (protocol No. 11-1 dated 12 July 2022). Rats were handled in accordance with the Directive 2010/63/EU of the European Parliament and of the Council on the protection of animals used for scientific purposes dated 22 September 2010.

✉ **Correspondence should be addressed:** Anastasiia D. Koniaeva  
Moskovskij trakt, 2, Tomsk, 634034, Russia; asyakonya95@gmail.com

**Received:** 18.06.2024 **Accepted:** 06.08.2024 **Published online:** 26.08.2024

**DOI:** 10.24075/brsmu.2024.033

## ВЛИЯНИЕ БИОСОВМЕСТИМЫХ ПЬЕЗОЭЛЕКТРИЧЕСКИХ МЕМБРАН НА РАЗВИТИЕ ФИБРОЗА ПРИ РЕГЕНЕРАЦИИ РАН СЛИЗИСТОЙ ОБОЛОЧКИ ПОЛОСТИ РТА

А. Д. Коняева<sup>1</sup>✉, Е. Ю. Варакута<sup>1</sup>, А. Е. Лейман<sup>1</sup>, Г. М. Кормашов<sup>1</sup>, М. В. Федосова<sup>1</sup>, Е. Н. Большасов<sup>2</sup>, К. С. Станкевич<sup>3</sup>

<sup>1</sup> Сибирский государственный медицинский университет, Томск, Россия

<sup>2</sup> Томский политехнический университет, Томск, Россия

<sup>3</sup> Государственный университет штата Монтана, Бозмен, Монтана, США

Профилактика развития фиброза при регенерации раневых дефектов слизистой оболочки полости рта является актуальной проблемой в современной хирургической стоматологии. Целью исследования было провести морфологическую оценку влияния биосовместимых пьезоэлектрических мембран на формирование фиброзной ткани в процессе регенерации ран слизистой оболочки полости рта. Были проанализированы межклеточное взаимодействие макрофагов и фибробластов, а также изменения уровня экспрессии маркеров CD68 и TGFβ1 и их влияние на развитие фиброза в условиях использования биосовместимых полимерных мембран с пьезоэлектрическими свойствами на различных этапах регенерации раневого дефекта слизистой оболочки полости рта. Проведена сравнительная морфологическая оценка структур слизистой оболочки ротовой полости у животных с интактной слизистой оболочкой ( $n = 15$ ), с открытым раневым дефектом ( $n = 15$ ) и раной, перекрытой биосовместимой пьезоэлектрической мембраной ( $n = 15$ ). Забор материала из области раневого дефекта осуществляли на 3-и, 7-е и 12-е сутки эксперимента, в аналогичные сроки отбирали материал у интактных животных. В группе с использованием биосовместимой мембраны в области дефекта выявлены признаки стадии пролиферации уже на 3-и сутки исследования, более быстрая смена макрофагальной инфильтрации на фибробластическую, снижение воспалительной реакции — на 7-е сутки и восстановление численной плотности макрофагов и фибробластов до интактных значений — на 12-е сутки. Выраженность экспрессии маркеров, прогнозирующих развитие фиброза, CD68 и TGFβ1, была ниже, чем в группе без использования мембраны. Наблюдали уменьшение удельной площади плотной волокнистой соединительной ткани на микроскопическом уровне и выраженность деформации мягких тканей на макроскопическом уровне. В группе без раневого покрытия на всем протяжении эксперимента сохранялись обширная клеточная инфильтрация и усиленная экспрессия CD68 и TGFβ1, что приводило к преобладанию удельной площади плотной волокнистой соединительной ткани над рыхлой соединительной тканью на 12-е сутки исследования и рубцовой деформации мягких тканей.

**Ключевые слова:** регенерация, раневой дефект, фиброз, пьезоэлектрики, слизистая оболочка полости рта, воспаление

**Финансирование:** исследование выполнено при финансовой поддержке РНФ в рамках научного проекта №23-25-00346.

**Вклад авторов:** А. Д. Коняева, Е. Ю. Варакута, Е. Н. Большасов, К. С. Станкевич — концепция и дизайн исследования; А. Д. Коняева, А. Е. Лейман, Г. М. Кормашов, М. В. Федосова — сбор и обработка материала; А. Д. Коняева, Е. Ю. Варакута — написание текста; А. Д. Коняева, Е. Ю. Варакута, Е. Н. Большасов, К. С. Станкевич — редактирование текста.

**Соблюдение этических стандартов:** исследование одобрено комитетом IACUC Сибирского государственного медицинского университета (протокол № 11-1 от 12 июля 2022 г.). Все манипуляции с крысами проводили в соответствии с Директивой Европейского Парламента № 2010/63 ЕС от 22.09.2010 «О защите животных, используемых в научных целях».

✉ **Для корреспонденции:** Анастасия Денисовна Коняева  
Московский тракт, д. 2, г. Томск, 634034, Россия; asyakonya95@gmail.com

**Статья получена:** 18.06.2024 **Статья принята к печати:** 06.08.2024 **Опубликована онлайн:** 26.08.2024

**DOI:** 10.24075/vrgmu.2024.033

Fibrosis is one option for the oral mucosal wound defect repair [1]. However, the presence of fibrosis results in the soft tissue volume reduction, adversely affects the damaged area architecture and further dental treatment [2].

A number of predictors, the analysis of the severity of which can predict the risk of fibrosis, can be distinguished at the early stages of wound defect regeneration. It is noted that the fibroblast–macrophage reciprocal interactions change depending on the wound healing stage and probability of the risk of fibrosis [3].

The transforming growth factor — (TGF $\beta$ ) release by cell populations at the wound defect site also indicates the development of fibrosis. TGF $\beta$  is released by fibroblasts, macrophages, and other cells of the wound bed; granulation tissue formation, collagen synthesis, and angiogenesis are stimulated against the background of the TGF $\beta$  expression increase [4]. However, the TGF $\beta$  expression levels and effects on the development of dense fibrous connective tissue depend heavily on microenvironment and cellular context. TGF $\beta$  either stimulates, or inhibits cell proliferation. It acts as a chemoattractant for monocytes and fibroblasts; high TGF $\beta$  expression levels during the first phase of wound regeneration contribute to granulation tissue development. However, the increased TGF $\beta$  expression is accompanied by severe cell infiltration and reduced collagenolysis in the final phase of repair [5]. CD68, the macrophage activity marker, can be also assessed in order to predict the wound healing variant [6].

Efficacy of the use of various biocompatible materials for wound defect closure can be assessed based on the analysis of the above indicators.

There are no data on assessment of the efficacy of using wound coverings with similar physical and chemical properties for oral mucosal wound defect regeneration in the literature.

The study was aimed to perform morphological assessment of the effects of biocompatible piezoelectric membranes on the fibrous tissue formation during regeneration of the oral mucosal wounds.

## METHODS

The experiment represented a simple comparative study of two approaches to treatment of the oral mucosal wound defects (involving/not involving closure of the defect with a biocompatible covering).

A polymeric piezoelectric membrane assessed in our study represents the nonwoven fabric made of vinylidene fluoride/tetrafluoroethylene copolymer by electrospinning. The membrane consists of two layers: hydrophilic one facing the wound defect and hydrophobic external one. The membrane is not biodegradable: it is removed from the surface of the healed wound defect after the end of repair. The earlier studies have shown that the fact of piezoelectric properties in the membranes compared to dielectric membranes contributes to the accelerated formation of loose fibrous connective tissue with the smaller specific area of dense fibrous connective tissue. Coverings were also tested for biocompatibility and cytotoxicity using the 3T3L1 fibroblasts at the laboratory of biopolymers and biotechnology of the Tomsk State University [7].

The study involved 45 Wistar rats (4-month-old males with the body weight of 350  $\pm$  30 g), 15 animals per group. Group 1 ( $n = 15$ ) included animals with open wound defects, group 2 ( $n = 15$ ) included animals with the wound defects closed with polymeric piezoelectric membranes, group 3 ( $n = 15$ ) included animals with intact mucosa. Animals were divided into groups by block randomization. Rats were provided by the Goldberg

Research Institute of Pharmacology and Regenerative Medicine (Tomsk, Russia). The experiment was conducted after the two-week acclimatization of animals. All rats were kept under standard conditions: in the separate labeled cages, five animals per cage, with ad libitum access to food and water starting from day 2 of the study, at the temperature of +12 °C to +18 °C [8].

This animal species was selected as a research object due to a number of factors: high degree of the experimental modeling data translation relative to humans, genetic homogeneity (homozygosity) determining consistency of response to the exposure to physical and chemical, physiological, biopathogenic, and stress factors, well-known level of sensitivity to stimuli; specificity and levels of biochemical, immunological, functional, and morphological indicators [9].

The mucosal flap sized 7  $\times$  4 mm was excised from the animal's buccal area in order to simulate the oral mucosal wound defect. After that the membrane was secured to the wound edges with the loop sutures in animals of group 2. All surgical procedures were conducted after putting the animals under anesthesia using Zoletil 100 in a dose of 10 mg/kg (Virbac, Carros; France). The criteria for exclusion of animals from the study with subsequent euthanasia were as follows: general deterioration characterized by lethargy, apathy, refusal to eat, sleep disorder or the animal's premature death. None of the animals was excluded from the study.

The animals were withdrawn from the study on days 3, 7, and 12 (five animals per group) by inducing hypoxia in the CO<sub>2</sub> chamber.

Tissue specimens for histological assessment were collected from the wound defect site by seizing 1 mm of the tissue from the margins. The tissues collected during autopsy were fixed in the 10% neutral formalin solution (Biovitrum; Russia), washed with running water, dehydrated with ascending alcohol concentrations and isopropanol (Biovitrum; Russia), and embedded in paraffin (Biovitrum; Russia). The 5  $\mu$ m histological sections were cut using the MS-1 sliding microtome (Orion-Medic; Russia). Sections were stained with hematoxylin and eosin (ABRIS+; Russia) and van Gieson's picrofuchsin (Biovitrum; Russia). Semithin sections were toluidine blue stained.

We performed qualitative and quantitative histological assessment of the fibrous connective tissue specific area, macrophage and fibroblast numerical density in 1 mm<sup>2</sup> of the section. Histological sections were examined using the Axioskop 40 light microscope (Carl Zeiss AG; Germany) with the 40 $\times$  and 90 $\times$  lenses, 10 $\times$  eye lenses). A total of 50 fields of view from the wound defect site per group were examined.

Immunohistochemical staining involved the use of the recombinant rabbit polyclonal antibody CD68 and isotype I IgG TGF $\beta$  (Abcam; USA). The McCarthy immunohistochemical staining intensity was graded [10]: 0 — no detectable staining, 1 — weak staining, 2 — moderate staining, 3 — strong staining, 4 — very strong staining.

Formula:

$$\text{Histochemical scores} = \sum P(i) \times i,$$

where  $i$  — staining intensity graded on a scale of 0–4,

$P(i)$  — percentage of cells stained with different intensity.

Enumeration was performed in three cohorts of 100 cells in various fields of view (40 $\times$ , 90 $\times$  lens).

Images were processed using the Axio Vision 4.8.2 (Carl Zeiss AG; Germany) and ImageJ v.1.54u (National Institutes of Health, Maryland) tools.

To assess the macrophage and fibroblast fine structure, we prepared samples for electron microscopy by standard method: fixed tissues in the 2.5% glutaraldehyde solution and cacodylate buffer (0.2 M; 1 : 9), applied postfixation with 1% osmium tetroxide, dehydrated and embedded in the araldite M and epon mixture. Sections were cut with the LKB-5 ultramicrotome (BROMMA; Sweden); the uranyl acetate and lead citrate contrast enhancement was applied to the slides. Fine structure was assessed using the JEOL JEM -1400 CX electron microscope (Jeol; Japan).

### Statistical processing

The Statistica v. 10.0 software (StatSoft Inc.; USA) was used for in vivo analysis. The hypothesis of trait distribution was tested for normality using the Kolmogorov–Smirnov test. All the results were presented as the median and quartiles,  $M(Q_1; Q_3)$ . The nonparametric Kruskal–Wallis test with the median test was used to compare independent samples; the Wilcoxon test was used for pairwise comparison. The differences were considered significant at  $p < 0.05$ .

### RESULTS

On day 3 of the study, there was granulation tissue at the wound defect site in the experimental groups; sporadic bundles of connective tissue fibers were found in the group with covering. Cell infiltration represented mainly by neutrophils was visible at the wound defect site. Furthermore, macrophages and fibroblasts were detected, which were more often visualized in the group with covering (Fig. 1A). Thus, the fibroblast numerical density was significantly (1.4 times) higher in the group with the wound covering ( $p = 0.035$ ), than in the group with no covering, and significantly (14 times) higher ( $p = 0.012$ ), than in the intact mucosa (see Table). We can say that mostly small immature fibroblasts with the moderately developed organelles involved in synthesis were visualized during ultra-microscopic examination. Macrophage infiltration was also more prominent in the group with membranes, the numerical density of this cell population was significantly (2.3 and 10.7 times) higher, than in the group with open wound defects and the control group, respectively ( $p = 0.034$ ,  $p = 0.018$ ). At the ultra-microscopic level, macrophages showed signs of high phagocytic and synthetic activity, which affected the CD68 marker expression that was significantly (2.6- and 4.2-fold) increased in the group with no covering and the group with membranes, respectively, compared to the values for the intact mucosa ( $p = 0.022$ ,

$p = 0.031$ ). Higher expression of the TGF $\beta$ 1 marker was observed in the group with open wound defects: H-score of the group was significantly (1.4 times) higher ( $p = 0.045$ ), than that of the group with membranes, and significantly (6.3 times) higher, than that of intact mucosa ( $p = 0.022$ ) (see Table) (Fig. 1B).

On day 7 of the study, the newly-formed loose fibrous connective tissue, between the fibers of which clusters of macrophages and fibroblasts were found, was visualized in the experimental groups (Fig. 1C). In this phase of wound regeneration, macrophages and fibroblasts were most often found in all fields of view. The macrophage numerical density reached its maximum in the group with no covering and was significantly (1.6 and 11.3 times) higher compared to appropriate values reported for the group with polymeric membranes and the control group ( $p = 0.019$ ,  $p = 0.011$ ) (see Table). This correlated with the CD68 marker expression, the H-score of which in the group with no covering was significantly (1.2 and 6.5 times) higher, than in the group with covering and the group with intact mucosa ( $p = 0.048$ ,  $p = 0.024$ ). Furthermore, the fibroblast numerical density, in contrast, reached its maximum in the group with membranes and was significantly (1.35) higher compared to the group with no membranes ( $p = 0.041$ ) (see Table). Immature fibroblasts still prevailed in the group with no covering, while in the group, where membranes were used, the differentiated mature fibroblasts showing ultrastructural signs of increased synthetic activity were most often visualized (Fig. 1D). No foreign body reaction at the membrane implantation site was observed in any phase of the experiment. The TGF $\beta$ 1 marker expression was significantly (2.8 times) higher in the group with open wound defects, than in the group with membranes ( $p = 0.036$ ), and 8 times higher, than in the control group ( $p = 0.013$ ).

On day 12 of the study, large foci of dense fibrous connective tissue were found in the group with no wound covering (Fig. 1E). Its specific area was significantly (3.9 times) higher, than in the group with covering ( $p = 0.036$ ). At the macroscopic level, this was reflected in the buccal area deformities with soft tissue loss; the scar, 4.5 mm in length, was determined at the wound defect site (Fig. 1F). In the group with polymeric membranes, the scar length reached 1.5 mm, and soft tissue deformation was slight. In the group with membranes, the macrophage and fibroblast numerical density reached the control values. In the group with no wound covering, these values were significantly (6 and 7.2 times) higher compared to the values of the intact group ( $p = 0.032$ ,  $p = 0.021$ ). In the group with no wound covering, fibroblasts still showed ultrastructural signs of high synthetic activity, while functionally inactive fibrocytes prevailed

**Table 1.** Morphological indicators characterizing the degree of fibrosis in the oral mucosa during regeneration of a wound defect,  $M(Q_1:Q_3)$

	TGF $\beta$	CD68	Numerical density of fibroblasts. c.u.	Numerical density of macrophages. c.u.	Specific area of dense fibrous connective tissue. %
Control	45.0 (40.0; 48.75)	50.0 (45.0; 55.0)	380.0 (376.0; 391.7)	163.0 (158.0; 165.0)	–
Day 3					
Group 1	285.0 (276.25; 290.0)*	140.0 (135.0; 145.0)*	3782.0* (3721.0; 3849.5)	772.5* (750.2; 788.0)	–
Group 2	200.0 (190.0; 205.0)*#	210.0 (205.0; 215.0)*#	5378.5*# (5346.2; 5465.7)	1750.0*# (1735.2; 1785.5)	–
Day 7					
Group 1	367.5 (351.25; 375.0)*	325.0 (320.0; 330.0)*	4530.5* (4472.5; 4579.7)	1846.0* (1831.2; 1869.0)	–
Group 2	130.0 (125.0; 135.0)*#	280.0 (275.0; 285.0)*#	6136.0*# (6126.0; 6145.0)	1128.0*# (1118.5; 1145.7)	–
Day 12					
Group 1	230.0 (225.0; 235.0)*	170.0 (165.0; 175.0)*	2746.5* (2639.0; 2906.0)	971.0* (947.0; 1138.2)	23.0 (14.3; 27.8)*
Group 2	85.0 (80.0; 90.0)*#	85.0 (80.0; 90.0)*#	397.5# (395.0; 402.0)	147.5# (143.0; 149.7)	5.9 (5.5; 6.3)*#

**Note:** \* — significant differences compared to the control group ( $p < 0.05$ ); # — significant differences compared to group 1 ( $p < 0.05$ ).

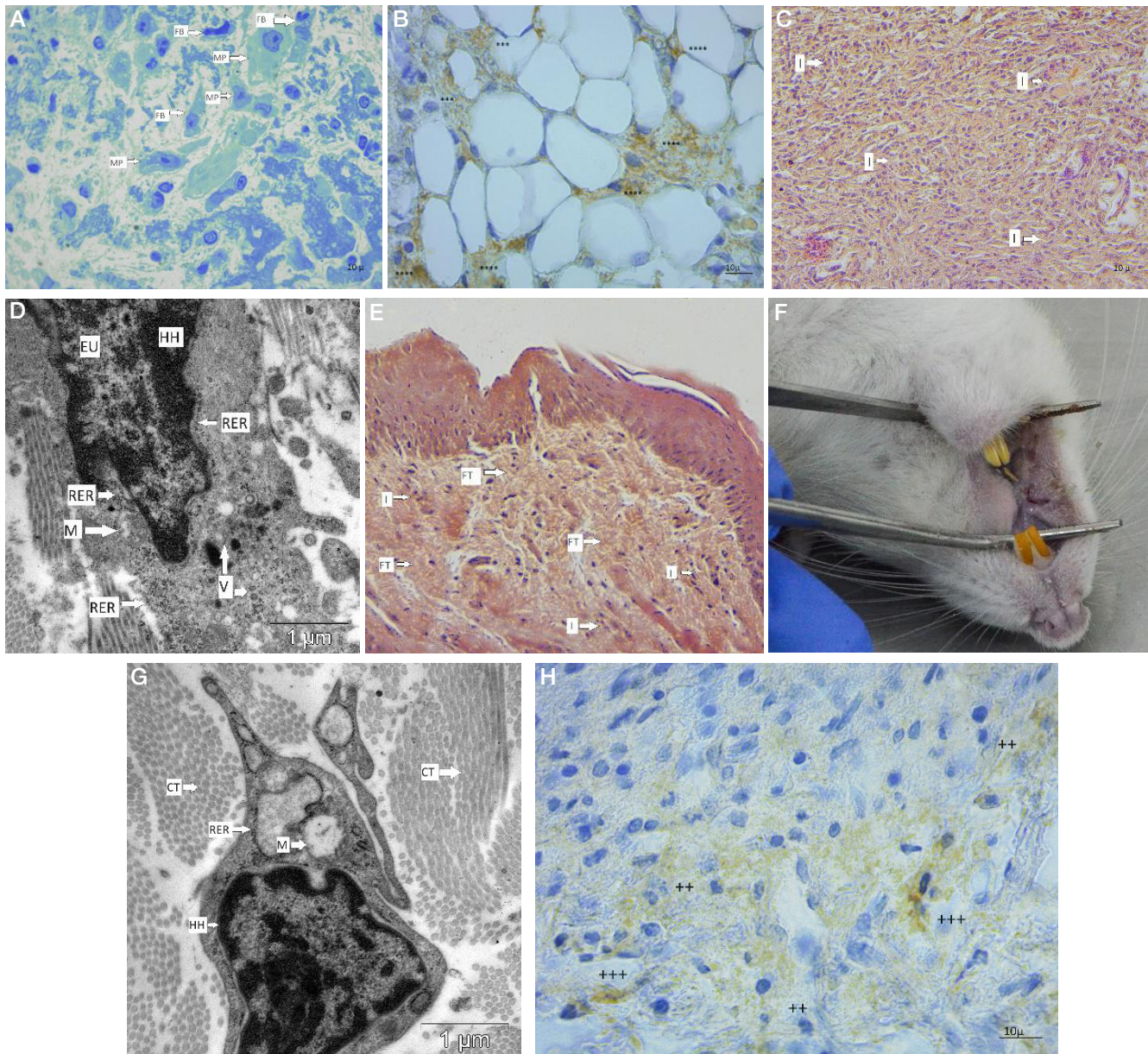


**Fig. 1.** Phases of the oral mucosal wound defect regeneration. **A.** Granulation tissue containing macrophages and fibroblasts at the wound defect site (day 3, group 2;  $\times 900$ ; stain: toluidine blue). **B.** TGF $\beta$ 1 expression by the granulation tissue cells at the wound defect site, hematoxylin staining of nuclei (day 3, group 1;  $900\times$ ). **C.** Loose fibrous connective tissue at the wound defect site showing extensive cell infiltration (day 7, group 1; stain: hematoxylin and eosin;  $400\times$ ). **D.** Differentiated fibroblast (day 7, group 2; TEM,  $5000\times$ ). **E.** Dense fibrous connective tissue showing cell infiltration (day 12, group 1; stain: hematoxylin and eosin;  $400\times$ ). **F.** Macroscopic features after the wound defect regeneration. Scar, 4.5 mm in length. **G.** Fibrocyte showing no synthetic activity (day 12, group 2; TEM,  $5000\times$ ). **H.** CD68 expression by the connective tissue cells, hematoxylin staining of nuclei (day 12, group 2;  $400\times$ ). FT — dense fibrous connective tissue, I — cell infiltration, EU — euchromatin, HH — heterochromatin, RER — rough endoplasmic reticulum, M — mitochondrion, V — vesicles, MP — macrophage, FB — fibroblast; ++++ — very strong staining; +++ — strong staining; ++ — moderate staining; + — weak staining; — no detectable staining

in the group with covering (Fig. 1G). At the ultrastructural level, the well-developed rough endoplasmic reticulum, Golgi apparatus, and mitochondria were visible in macrophages, which indicated high synthetic activity. The CD68 and TGF $\beta$ 1 expression was significantly higher in the group with open wound defects, than in the groups with coverings and intact mucosa: 2 and 3 times higher, respectively ( $p = 0.019$ ,  $p = 0.025$ ) (see Table) (Fig. 1H).

## DISCUSSION

During this study we assessed the major predictors of fibrous tissue development at the oral mucosal wound defect site. The following scheme of pathomorphogenesis can be drawn based on the study results and the literature review (Fig. 2).

According to the scheme, extensive cell infiltration in the healing area was observed at the first stage of wound defect regeneration, in the inflammatory phase. A large cluster of macrophages, the numerical density of which was significantly higher, than in the group with open wound defects, was revealed in the group, where biocompatible membranes were used. This indicator correlated with the increased macrophage CD68 marker expression in the group with polymeric membranes. At the ultra-microscopic level, the signs of increased synthetic activity could be noted in the group with covering. The well-developed synthetic apparatus was essential for the release of bioactive substances, which were also attractants for migration of fibroblasts to the wounded area [11]. We interpreted the data obtained as the fact of the inflammatory phase transition to the proliferative phase, since it is macrophages that are responsible

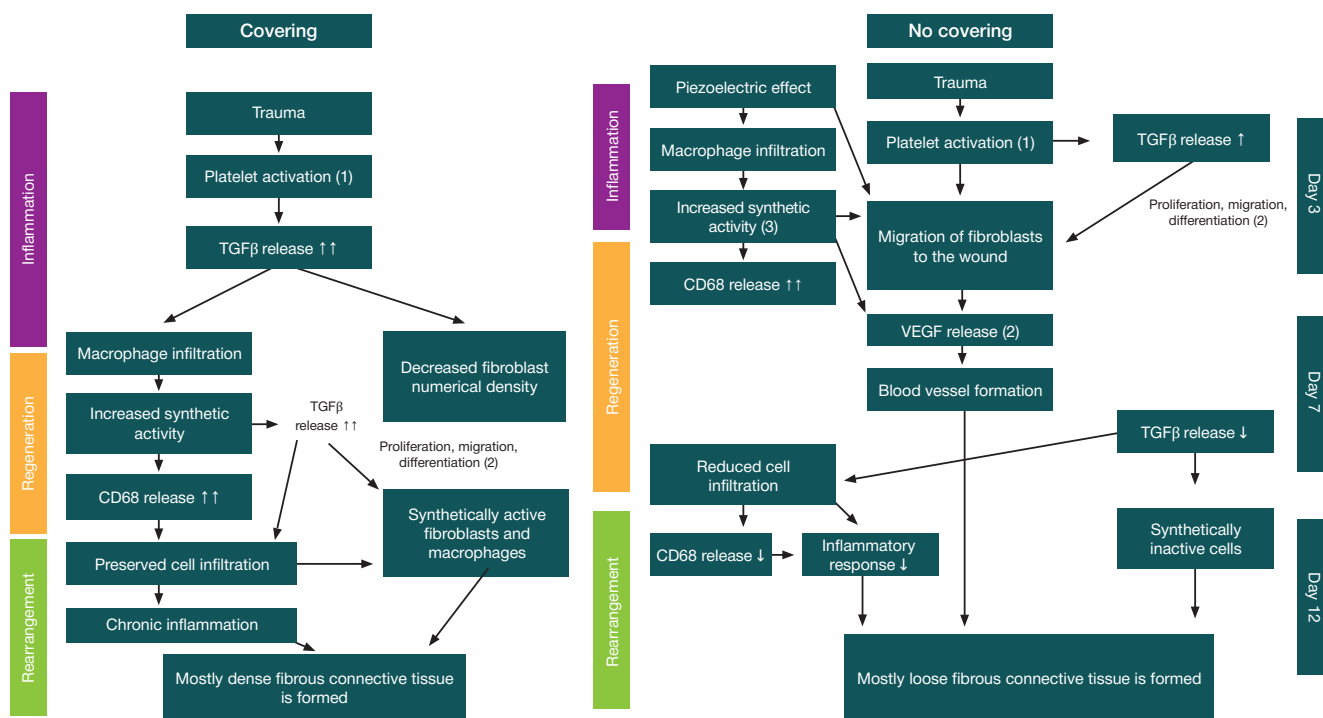


**Fig. 2.** Scheme of the oral mucosal wound defect regeneration pathomorphogenesis in cases of using/not using a polymeric piezoelectric membrane. ↑ — slightly increased expression; ↑↑ — moderately increased expression; ↑↑↑ — markedly increased expression; ↓ — decreased expression. 1 — according to Morikawa M, Derynck R, et al. [5]; 2 — according to Xu X, Gu SY, et al. [11]; 3 — according to Zhang T, Wang XF, et al. [12]

for targeted migration of fibroblasts due to the release of vascular endothelial growth factor (VEGF), platelet-derived growth factor (PDGF), and TGFβ, contributing to angiogenesis, collagen production, and re-epithelization [12].

Furthermore, the numerical density of fibroblast type cells was significantly increased in the group with covering. This also suggested that the major processes observed in the wound shifted from inflammatory response to connective tissue formation in the group with wound covering.

However, to properly interpret these indicators, it was necessary to analyze their dynamic changes, since preservation of extensive infiltration, especially with macrophages, at the later stages of wound regeneration could be a prerequisite for the development of fibrosis. That is exactly what we saw in the group with no wound covering, where the macrophage numerical density was significantly higher, than in the group with wound covering, on day 7 of the study and did not reach the control values on day 12 of the study. The fibroblast numerical density, on the contrary, was significantly lower in the group with no covering on day 7. On day 12, the fibroblast numerical density increased relative to the intact mucosa and the group with covering. Such a relationship between macrophages and fibroblasts in the group with open wounds indicated a prolonged inflammation that contributed to further development of fibrosis [11]. In the group, where biocompatible piezoelectric membranes was used, the numerical density of the studied cell populations recovered to the control values on day 12 of the study, which was considered a positive prognostic sign.

The TGFβ1 release by the cells is a primary trigger for the wound regeneration initiation. In this regard, we observed increased TGFβ1 expression on day 3 of the study in both experimental groups [12]. However, TGFβ1 expression was significantly higher in the group with no wound covering, than in the group with biocompatible membranes; the expression reached its maximum on day 7 of the study and did not return to the control values on day 12 of the study. This marker is released by a number of cells at the wound defect site:

platelets, macrophages, fibroblasts, keratinocytes, etc. [4]. And this specific marker plays a critically important role in the shift of regeneration stages, since it has an effect on cooperation of macrophages and fibroblasts at the wound site [5]. Furthermore, it is reported that not only different cell types respond differently to TGFβ1, but also the same cells can show contradictory responses depending on the experimental conditions [5].

The TGFβ1 expression increase reported on day 7 of the study mediated preservation of extensive infiltration with the synthetically active fibroblasts and macrophages at the wound site on day 12 of the study in the group with open wound defects. At the same time, their numerical density in the group with covering returned to the control values in the final phase of wound regeneration against the background of lower H-score values for TGFβ1. Moreover, the fibroblast type cells were represented mainly by the synthetically inactive fibrocytes, which indicated termination of connective tissue development at the wound defect site in the group with polymeric membranes. In the group with open wound defects, the synthetically active fibroblasts were mostly found at the wound site on day 12 of the study. Proliferation, migration, and differentiation of fibroblasts were observed under exposure to TGFβ1, while aberrant signal transmission from TGFβ1 was associated with activation of the mechanism underlying the scar tissue formation [12]. The scar tissue formation was related to the abnormal, disturbed wound healing process associated with chronic inflammation [13] occurring against the background of increased TGFβ1 expression, which represented an important phase of chronic wound regeneration [14]. Thus, the TGFβ1 expression increase can be considered an important pro-fibrotic marker [15].

That is why dense fibrous connective tissue constituting the basis for fibrotic changes was formed in the group with open wound defects during interaction between fibroblasts and macrophages under exposure to TGFβ1, which was indicated by the presence of the scar, 4.5 mm in length, and soft tissue loss at the macroscopic level.

The polymeric piezoelectric membranes made of vinylidene fluoride/tetrafluoroethylene copolymer by electrospinning represent the most recent creation of the laboratory of hybrid biomaterials of the Tomsk Polytechnic University. There are no earlier studies focused on assessing the effectiveness of using the analogues with similar physical and chemical properties for the oral mucosal wound defect regeneration in global practice. Based on this study we assume that piezoelectric properties of biocompatible polymeric membranes contributed to the TGF $\beta$ 1 expression decrease, which resulted in inhibition of TGF $\beta$ 1 effects on the activity of fibroblasts and macrophages. Consequently, loose fibrous connective tissue was formed, while dense fibrous tissue formation and, as a result, scarring was reported in the group with open wounds. This hypothesis is confirmed by the data of the comparative study of piezoelectric and dielectric coverings in regeneration of oral mucosal

wounds, during which smaller specific area of scar tissue was reported for the group with piezoelectric covering [7].

## CONCLUSIONS

The study revealed positive effects of biocompatible piezoelectric membranes on prevention of fibrosis during wound regeneration, which was confirmed by the analysis of interplay between the macrophage and fibroblast type cells and expression of the CD68 and TGF $\beta$ 1 prognostic markers. The use of polymeric biocompatible membranes in dental practice will make it possible to reduce the risk of postoperative complications in the form of oral soft tissue deformation in the future. It is planned to further assess the effects of covering membranes on the oral mucosal regeneration in order to improve the membrane properties.

## References

- Nikoloudaki G, Creber K, Hamilton DW. Wound healing and fibrosis: a contrasting role for periostin in skin and the oral mucosa. *Am J Physiol Cell Physiol*. 2020; 318 (6): C1065-C1077. DOI: 10.1152/ajpcell.00035.2020.
- Griffin MF, Fahy EJ, King M, Guardino N, Chen K, Abbas DB, et al. Understanding scarring in the oral mucosa. *Adv Wound Care (New Rochelle)*. 2022; 11 (10): 537–547. DOI: 10.1089/wound.2021.0038.
- Smigiel KS, Parks WC. Macrophages, wound healing, and fibrosis: recent insights. *Curr Rheumatol Rep*. 2018; 20 (4): 17. DOI: 10.1007/s11926-018-0725-5.
- Kim YJ, Carvalho FC, Souza JA, Gonçalves PC, Nogueira AV, Spolidório LC, et al. Topical application of the lectin Artin M accelerates wound healing in rat oral mucosa by enhancing TGF- $\beta$  and VEGF production. *Wound Repair Regen*. 2013; 21 (3): 456–63. DOI: 10.1111/wrr.12041.
- Morikawa M, Derynck R, Miyazono K. TGF- $\beta$  and the TGF- $\beta$  Family: Context-Dependent Roles in Cell and Tissue Physiology. *Cold Spring Harb Perspect Biol*. 2016; 8 (5): a021873. DOI: 10.1101/cshperspect.a021873. PMID: 27141051; PMCID: PMC4852809.
- Kuninaka Y, Ishida Y, Ishigami A, Nosaka M, Matsuki J, Yasuda H, et al. Macrophage polarity and wound age determination. *Sci Rep*. 2022; 12 (1): 20327. DOI: 10.1038/s41598-022-24577-9.
- Chemova UV, Varakuta EY, Konjaeva AD, Leyman AE, Sagdullaeva SA, Plotnikov E, et al. Piezoelectric and dielectric electrospun fluoropolymer membranes for oral mucosa regeneration: a comparative study. *ACS Appl Mater Interfaces*. 2024. DOI: 10.1021/acsami.4c01867.
- Ob utverzhdenii SP 2.2.1.3218-14 «Sanitarno-jepidemiologicheskie trebovaniya k ustrojstvu, oborudovaniju i sodержaniju jeksperimental'nyh biologicheskikh klinik (vivariumov)»: postanovlenie Glavnogo gosudarstvennogo sanitarnogo vracha RF ot 29.09.2014 № 51 [Elektronnyj resurs]. *Spravochno-pravovaja sistema «Konsul'tant Pljus»*. Russian.
- Clause BT. The Wistar Rat as a right choice: establishing mammalian standards and the ideal of a standardized mammal. *J Hist Biol*. 1993; 26 (2): 329–49. DOI: 10.1007/BF01061973.
- McCarty KS Jr, Miller LS, Cox EB, Konrath J, McCarty KS Sr. Estrogen receptor analyses. Correlation of biochemical and immunohistochemical methods using monoclonal antireceptor antibodies. *Arch Pathol Lab Med*. 1985; 109(8): 716–21. PMID: 3893381.
- Xu X, Gu S, Huang X, Ren J, Gu Y, Wei C, et al. The role of macrophages in the formation of hypertrophic scars and keloids. *Burn Trauma*. 2020; 8: tkaa006. DOI: 10.1093/burnst/tkaa006.
- Zhang T, Wang XF, Wang ZC, Lou D, Fang QQ, Hu YY, et al. Current potential therapeutic strategies targeting the TGF- $\beta$ /Smad signaling pathway to attenuate keloid and hypertrophic scar formation. *Biomed Pharmacother*. 2020; 129: 110287. DOI: 10.1016/j.biopha.2020.110287.
- Shi A, Li J, Qiu X, Sabbah M, Boroumand S, Huang TC, et al. TGF- $\beta$  loaded exosome enhances ischemic wound healing in vitro and in vivo. *Theranostics*. 2021; 11 (13): 6616–31. DOI: 10.7150/thno.57701.
- Liarte S, Bernabé-García Á, Nicolás FJ. Role of TGF- $\beta$  in skin chronic wounds: a keratinocyte perspective. *Cells*. 2020; 9 (2): 306. DOI: 10.3390/cells9020306.
- Eslami A, Gallant-Behm CL, Hart DA, Wiebe C, Honardoust D, Gardner H, et al. Expression of integrin  $\alpha$ v $\beta$ 6 and TGF $\beta$  in scarless vs scar-forming wound healing. *J Histochem Cytochem*. 2009; 57 (6): 543–57. DOI: 10.1369/jhc.2009.952572.

## Литература

- Nikoloudaki G, Creber K, Hamilton DW. Wound healing and fibrosis: a contrasting role for periostin in skin and the oral mucosa. *Am J Physiol Cell Physiol*. 2020; 318 (6): C1065-C1077. DOI: 10.1152/ajpcell.00035.2020.
- Griffin MF, Fahy EJ, King M, Guardino N, Chen K, Abbas DB, et al. Understanding scarring in the oral mucosa. *Adv Wound Care (New Rochelle)*. 2022; 11 (10): 537–547. DOI: 10.1089/wound.2021.0038.
- Smigiel KS, Parks WC. Macrophages, wound healing, and fibrosis: recent insights. *Curr Rheumatol Rep*. 2018; 20 (4): 17. DOI: 10.1007/s11926-018-0725-5.
- Kim YJ, Carvalho FC, Souza JA, Gonçalves PC, Nogueira AV, Spolidório LC, et al. Topical application of the lectin Artin M accelerates wound healing in rat oral mucosa by enhancing TGF- $\beta$  and VEGF production. *Wound Repair Regen*. 2013; 21 (3): 456–63. DOI: 10.1111/wrr.12041.
- Morikawa M, Derynck R, Miyazono K. TGF- $\beta$  and the TGF- $\beta$  Family: Context-Dependent Roles in Cell and Tissue Physiology. *Cold Spring Harb Perspect Biol*. 2016; 8 (5): a021873. DOI: 10.1101/cshperspect.a021873. PMID: 27141051; PMCID: PMC4852809.
- Kuninaka Y, Ishida Y, Ishigami A, Nosaka M, Matsuki J, Yasuda H, et al. Macrophage polarity and wound age determination. *Sci Rep*. 2022; 12 (1): 20327. DOI: 10.1038/s41598-022-24577-9.
- Chemova UV, Varakuta EY, Konjaeva AD, Leyman AE, Sagdullaeva SA, Plotnikov E, et al. Piezoelectric and dielectric electrospun fluoropolymer membranes for oral mucosa regeneration: a comparative study. *ACS Appl Mater Interfaces*. 2024. DOI: 10.1021/acsami.4c01867.
- Обутверждении СП 2.2.1.3218-14 «Санитарно-эпидемиологические требования к устройству, оборудованию и содержанию экспериментальных биологических клиник (вивариумов)»: постановление Главного государственного санитарного врача РФ от 29.09.2014 № 51 [Электронный ресурс]. *Справочно-*

- правовая система «Консультант Плюс».
9. Clause BT. The Wistar Rat as a right choice: establishing mammalian standards and the ideal of a standardized mammal. *J Hist Biol.* 1993; 26 (2): 329–49. DOI: 10.1007/BF01061973.
  10. McCarty KS Jr, Miller LS, Cox EB, Konrath J, McCarty KS Sr. Estrogen receptor analyses. Correlation of biochemical and immunohistochemical methods using monoclonal antireceptor antibodies. *Arch Pathol Lab Med.* 1985; 109 (8): 716–21. PMID: 3893381.
  11. Xu X, Gu S, Huang X, Ren J, Gu Y, Wei C, et al. The role of macrophages in the formation of hypertrophic scars and keloids. *Burn Trauma.* 2020; 8: tkaa006. DOI: 10.1093/burnst/tkaa006.
  12. Zhang T, Wang XF, Wang ZC, Lou D, Fang QQ, Hu YY, et al. Current potential therapeutic strategies targeting the TGF- $\beta$ /Smad signaling pathway to attenuate keloid and hypertrophic scar formation. *Biomed Pharmacother.* 2020; 129: 110287. DOI: 10.1016/j.biopha.2020.110287.
  13. Shi A, Li J, Qiu X, Sabbah M, Boroumand S, Huang TC, et al. TGF- $\beta$  loaded exosome enhances ischemic wound healing in vitro and in vivo. *Theranostics.* 2021; 11 (13): 6616–31. DOI: 10.7150/thno.57701.
  14. Liarte S, Bernabé-García Á, Nicolás FJ. Role of TGF- $\beta$  in skin chronic wounds: a keratinocyte perspective. *Cells.* 2020; 9 (2): 306. DOI: 10.3390/cells9020306.
  15. Eslami A, Gallant-Behm CL, Hart DA, Wiebe C, Honardoust D, Gardner H, et al. Expression of integrin alphavbeta6 and TGF $\beta$  in scarless vs scar-forming wound healing. *J Histochem Cytochem.* 2009; 57 (6): 543–57. DOI: 10.1369/jhc.2009.952572.

## DISCLOSING ADOLESCENTS' GYNECOLOGICAL CONCERNS: EXPLORING TRENDS IN ADOLESCENT GYNECOLOGY VISITS AND COMPLAINTS

Uyaniklar OO <sup>✉</sup>, Rahimli Ocakoglu S, Atak Z, Suer E

Department of Obstetrics and Gynecology, Bursa City Hospital, Bursa, Turkey

Adolescence represents a pivotal phase in the transition from childhood to adulthood. Adolescent gynecology is the clinical specialty that focuses on the management of gynecological problems during this period. This study's primary objective is to emphasize the importance of adolescent gynecology by examining the gynecological causes of adolescent presentations and highlighting the differences that warrant consideration in the clinical approach to adolescent patients. The study was designed as a retrospective cohort study in an academic tertiary hospital and included adolescent individuals presenting to the obstetrics and gynecology emergency department or outpatient clinic. The analysis encompassed a range of factors, including age, presenting symptoms, examination findings, ultrasound results, laboratory data, and the necessity for hospital admission. The study cohort comprised 750 adolescent patients, 71.3% seeking gynecological care. Adolescents most frequently presented for menstrual irregularities (57.6%) and secondarily for dysmenorrhea. The results of the gynecological clinical evaluations indicated that 62.9% of the patients had menstrual disorders. Of these, 53.4% had irregular menstrual cycles, 4.5% had prolonged and/or heavy bleeding, and 3% had amenorrhea. Ultrasound imaging revealed the presence of pathological findings in 25.8% of the patients. In conclusion, this study's findings indicate that irregular menstrual cycles are the most common gynecological condition in the adolescent population. The physiological characteristics of adolescents require a distinct approach to diagnosis and treatment compared to adult women, which can significantly impact future fertility and overall reproductive health.

**Keywords:** adolescent pathologies, menstrual irregularity, adolescent gynecology, dysmenorrhea, vaginitis

**Compliance with ethical standards:** the study protocol was approved by the Bursa City Hospital Ethics Committee at the beginning of the study period (approval number: 2022-4/5).

✉ **Correspondence should be addressed:** Ozlem Ozgun Uyaniklar  
Department of Obstetrics and Gynecology, Bursa City Hospital, 16110, Nilüfer, Bursa, Turkey; ozlemuyaniklar@gmail.com

**Received:** 16.06.2024 **Accepted:** 22.08.2024 **Published online:** 31.08.2024

**DOI:** 10.24075/brsmu.2024.035

## ГИНЕКОЛОГИЧЕСКИЕ ПРОБЛЕМЫ У ПОДРОСТКОВ: ТЕНДЕНЦИИ ОБРАЩЕНИЙ К ГИНЕКОЛОГАМ И ЖАЛОБ

О. О. Уйаныклар <sup>✉</sup>, С. Рахимлы Очакоглу, З. Атак, Э. Суэр

Отделение акушерства и гинекологии, Городская больница Бурсы, Бурса, Турция

Подростковый период представляет собой ключевой этап перехода от детства к взрослости. Подростковая гинекология занимается лечением гинекологических проблем, возникающих в этот период. Основной целью работы было подчеркнуть важность подростковой гинекологии, исследовав гинекологические причины обращения подростков за медицинской помощью и особо отметив различия, которые необходимо учитывать при обращении за клинической помощью у таких пациентов. В ретроспективное когортное исследование, проведенное на базе специализированной университетской больницы, были включены лица подросткового возраста, обращавшиеся за экстренной помощью в отделение акушерства и гинекологии или в поликлинику. Был проанализирован целый ряд факторов, в том числе возраст, имеющиеся симптомы, результаты обследования, результаты ультразвукового исследования, лабораторные данные и необходимость госпитализации. Исследованную когорту составили 750 пациентов подросткового возраста, 71,3% из них обращались за гинекологической помощью. Подростки чаще всего обращались к врачу по поводу нарушений менструального цикла (57,6%), второй по значимости причиной была дисменорея. Результаты гинекологического обследования показали, что нарушения менструального цикла имели место у 62,9% пациентов. Из них у 53,4% были нерегулярные менструации, у 4,5% — продолжительные и/или обильные кровотечения, у 3% — аменорея. Ультразвуковое исследование выявило патологические изменения у 25,8% пациентов. Результаты исследования показали, что нарушения менструального цикла представляют собой наиболее широко распространенную в подростковой популяции гинекологическую проблему. Физиологические особенности подростков требуют особого подхода к диагностике и лечению по сравнению со взрослыми женщинами, что может негативно повлиять на будущую фертильность и общее репродуктивное здоровье.

**Ключевые слова:** подростковая патология, нарушения менструального цикла, подростковая гинекология, дисменорея, вагинит

**Соблюдение этических стандартов:** исследование одобрено этическим комитетом Городской больницы Бурсы (протокола № 2022-4/5).

✉ **Для корреспонденции:** Озлем Озгюн Уйаныклар  
Отделение акушерства и гинекологии, Городская больница Бурсы, 16110, Нилюфер, Бурса, Турция; ozlemuyaniklar@gmail.com

**Статья получена:** 16.06.2024 **Статья принята к печати:** 22.08.2024 **Опубликована онлайн:** 31.08.2024

**DOI:** 10.24075/vrgmu.2024.035

Adolescence is a period of change between childhood and adulthood, typically between the ages of 10 and 19 [1]. The gynecological problems experienced by adolescent girls differ from those of adult women. The fundamental differences in gynecological changes during adolescence typically begin with the production of steroid hormones, which facilitate breast development, uterine growth, and the development of pubic hair. Menarche, on the other hand, refers to the onset of cyclic ovarian hormone production, leading to menstrual bleeding [2].

Adolescent gynecology is a specialized field of medicine that focuses on adolescents' reproductive health and gynecological issues. It addresses young girls' unique needs and concerns during the transitional period from childhood to adulthood.

In this field, healthcare providers are trained to provide comprehensive care for adolescents, including preventive care, diagnosis, and treatment of gynecological conditions. They address a wide range of issues such as menstrual problems, contraception, sexually transmitted infections (STIs), pelvic



pain, abnormal bleeding, polycystic ovary syndrome (PCOS), and concerns related to sexual development [3].

Adolescent gynecology also encompasses the management of reproductive health concerns specific to teenagers, including education about healthy sexual practices, Human papillomavirus (HPV) vaccination, counseling on contraception and family planning, and addressing the emotional and psychological aspects of sexual development [4]. The American College of Obstetricians and Gynecologists (ACOG) recommends the initial reproductive health visit between 13 and 15 years [5]. Gaining proficiency in the appropriate methods for the initial examination plays a crucial role in forming a lasting connection with individuals within this age group [4].

Adolescent gynecology is a subspecialty within the field of obstetrics and gynecology.

This study aims to emphasize the significance of adolescent gynecology by analyzing the gynecological reasons for which the adolescent population seeks medical care. Additionally, it aims to highlight the distinctions between adolescent gynecology and adult gynecological approaches.

## METHODS

This is a retrospective cohort study, conducted in a high-volume tertiary hospital. Electronic file records for patients who applied to the Gynecology and Obstetrics clinic between June 2021 and January 2022 were analyzed retrospectively. Patients aged between 10 and 18 years who presented to the Obstetrics and Gynecology Emergency Department or outpatient clinic were included in the study. Patients with missing data in the electronic medical records were excluded from the study. The reason at patient admission was evaluated, whether due to pregnancy or gynecological complaints. Patients presenting due to pregnancy were not included in the analysis. The patient's age, complaints at admission, findings from the gynecological examination if performed, ultrasound findings, laboratory results, and the need for hospitalization were also analyzed.

Age values are expressed as mean  $\pm$  standard deviation. Categorical variables are expressed with  $n$  (%). SPSS (IBM Corp. Released 2012. IBM SPSS Statistics for Windows. Version 21.0. Armonk, NY: IBM Corp.) program was used for statistical analysis.

## RESULTS

In total, 750 adolescent girls were included in this study (Figure). Of the adolescents included in the study, 215 (28.7%) presented to the hospital due to pregnancy, while 535 (71.3%)

sought medical care for gynecological reasons. The complaints reported by the patients at admission are presented in Table 1. The majority of adolescents sought care with complaints of menstrual irregularities ( $n = 309$ ; 57.6%), followed by dysmenorrhea (12.7%), vulvar itching/vaginal discharge (9.5%), pelvic pain (5.6%), and hirsutism (5.6%). Patients presenting with complaints of an adnexal mass (5.2%) consisted of individuals who had previously detected adnexal masses through imaging studies. In addition to the mentioned complaints, acne vulgaris (2.2%), contraception counseling (1%), and galactorrhea (3%) were among the other presenting complaints.

The results of the patient's clinical evaluations are presented in Table 2. When questioning the patients about their menstrual history, it was determined that a total of 337 (62.9%) adolescent girls had menstrual irregularities. Among the patients with menstrual irregularity, 16 patients presented with amenorrhea. While 15 adolescents were describing secondary amenorrhea, one patient had primary amenorrhea. When the patient's hospital records were checked, secondary sex characters at the age of 16 showed normal development. As a result of ultrasonography and MRI, the uterus was not observed, and genetic consultation was requested.

Of the girls who underwent ultrasonography, PCO morphology was detected in 89 cases (16.6%), while normal sonographic findings were observed in 385 cases (71.8%). Unilateral unilocular anechoic cysts larger than 4 cm were found in 35 girls. Among the girls with unilocular anechoic cysts, 4 had cyst sizes ranging from 6 to 8 cm. No cases showed evidence of torsion, and all were followed up in the outpatient clinic. A total of 5 girls (0.9%) were diagnosed with corpus hemorrhagicum or corpus luteum. Among the girls with corpus hemorrhagicum, 3 reported pelvic pain and 2 had irregular bleeding as their presenting complaints. Four girls were diagnosed with mature cystic teratomas, and only 1 girl with a 6.5 cm endometrioma presented with dysmenorrhea.

The laboratory results are also presented in Table 2. Hyperprolactinemia was detected in 31 (5.8%) adolescents in two separate measurements. Patients with elevated CA-125 levels were called for outpatient follow-up due to the presence of accompanying ovarian cysts. None of the patients were suspected of malignancy based on sonographic findings, and among these five cases, the highest CA-125 value was determined to be 166 U/mL.

A total of 4 patients (0.7%) were hospitalized. Two of the hospitalized patients were admitted due to heavy menstrual bleeding. Treatment involved the administration of intravenous tranexamic acid and an estrogen-progesterone combination regimen. In a patient who presented with dysmenorrhea and chronic pelvic pain, an ultrasound evaluation revealed a 5.5 cm

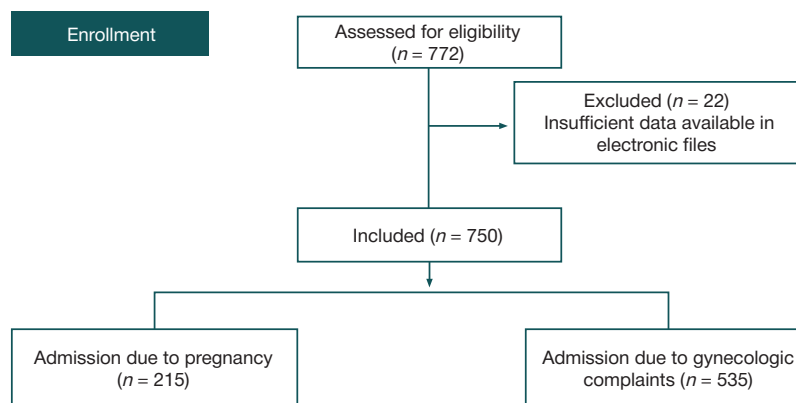


Fig. Flow diagram of patients included in the study

**Table 1.** Complaints at the time of admission

		Frequency (percent)
Admission	Pregnancy	215 (28.7)
	Gynecologic complaints	535 (71.3)
Total		750 (100)
Gynecologic Complaints of Adolescents		
Menstrual irregularity		309 (57.6)
Dysmenorrhea		68 (12.7)
Vulvar pruritus/ vaginal discharge		51 (9.5)
Pelvic pain		30 (5.6)
Hirsutism		30 (5.6)
Adnexal mass		28 (5.2)
Acne vulgaris		12 (2.2)
Contraception counseling		5 (1)
Galactorrhea		3 (0.6)

**Note:** Data are presented as n (%) for nominal variables.

septated cyst in the right ovary and a 3 cm unilocular anechoic cyst in the left ovary. No signs of the acute abdomen were observed during the abdominal examination. The patient's medical history indicated a previous benign ovarian cyst excision surgery performed 5 years ago. Due to the presence of elevated CA-125 levels (594 U/mL) three months ago and the persistence of elevated levels in the current presentation (166 U/mL), a consultation with gynecologic oncology was requested. The patient's Lactate dehydrogenase level was determined to be 110 U/L, and the Alpha-fetoprotein (AFP) level was found to be 3.8 IU/L. The Human epididymis protein 4 (HE4) level was found to be normal three months ago. Considering the newly detected 5.5 cm septated cyst in comparison to previous imaging, it was presumed to be a corpus hemorrhagicum, and analgesics were administered. The fourth hospitalized patient presented to the emergency department with abdominal pain and was admitted following an ultrasound examination that revealed a 4 cm unilocular anechoic cyst and a 3 cm fluid collection in the abdomen. The patient was discharged on the third day of admission with no decrease in hemoglobin/hematocrit values during the hospital follow-up.

## DISCUSSION

In our study, menstrual irregularities were the most frequent reason for adolescents seeking gynecological care (57.6%). Abnormal bleeding is a common complaint in adolescent gynecology [6]. Young girls and their parents may not have enough information about normal bleeding periods, so the age of menarche and the order and duration of menstrual periods should be questioned [2]. Menarche usually occurs within 2–3 years after thelarche (breast budding) [7]. Although there can be variations, the average age of menarche is 12–13[8]. However, due to immaturity in the hypothalamic-pituitary-ovarian axis and anovulation, menstrual cycles can be irregular, but they usually occur every 21–45 days and last for 7 days or less [2,9].

The assessment of heavy menstrual bleeding in adolescents is crucial for the diagnosis of an underlying bleeding disorder [10]. The PALM-COEIN system should be utilized for the classification of heavy menstrual bleeding: Polyp, Adenomyosis, Leiomyoma, Malignancy and hyperplasia, Coagulopathy, Ovulatory dysfunction, Endometrial, Iatrogenic, and Not otherwise classified [11]. However, structural causes are not a very common cause of heavy menstrual bleeding in adolescents [10]. While bleeding disorders occur in approximately 1–2% of

the general population, the prevalence of bleeding disorders is 20% among adolescents experiencing heavy menstrual bleeding [12, 13]. In our study, 24 adolescents (4.5%) were admitted to the hospital due to heavy menstrual bleeding. A total of two adolescents were hospitalized and treated due to heavy menstrual bleeding in our study. Adolescents who are hemodynamically unstable and have heavy bleeding should be hospitalized as in these cases [10]. The monophasic combined oral contraceptive and tranexamic acid combination was administered to both patients by the guidelines [10,14].

The initial management of acute bleeding is medical treatment, which is determined based on the patient's hemodynamic status and the potential etiology of the bleeding. In our study, medical treatment, as applied to the two patients admitted internally, can be implemented as hormonal, non-hormonal, or combination therapy [13]. The primary treatment for acute bleeding is intravenous conjugated estrogen therapy administered every 4–6 hours. Alternatively, monophasic combined oral contraceptives should be administered every 6–8 hours until the bleeding stops. For adolescents who cannot tolerate estrogen, a progestin-only regimen can be applied, such as oral medroxyprogesterone 10–20 mg every 6–12 hours or norethindrone acetate 5–10 mg every 6 hours [15].

Adolescents who have not reached the menarche by 15 years of age or have not menstruated within 3 years of the thelarche should be evaluated for primary amenorrhea. The absence of breast development until 13 years of age should also be evaluated for delayed puberty [16]. Adolescents with more than 3 months between menstrual cycles who were menstruating regularly or absence of menses for more than six months should be evaluated for secondary amenorrhea [17]. In our study, one patient presented with primary amenorrhea. The uterus was not observed as a result of ultrasonography, and Mullerian agenesis was considered as a result of pelvic MRI. Androgen insensitivity syndrome, distal vaginal agenesis, transverse vaginal septum, imperforate hymen, and cervical agenesis should be included in the differential diagnosis of the patient presenting with primary amenorrhea [18]. Additionally, evaluation for renal anomalies is necessary for these patients [18].

Dysmenorrhea is the most common menstrual symptom in the literature among adolescent girls, with a prevalence ranging from 50% to 90% [19]. Furthermore, our study revealed that dysmenorrhea was the most frequent reason for adolescents seeking gynecological care after menstrual irregularities (12.7%). Dysmenorrhea, or painful periods, can significantly

**Table 2.** Menstrual History, Examination, Ultrasonography, and Laboratory Findings

Patients presenting with gynecological complaints	
Age	16.42 ± 1.73
Menstrual Irregularity (Total)	337 (62.9)
Menses at irregular intervals (>45 or <21 days)	286 (53.4)
Prolonged and/or heavy bleeding	24 (4.5)
Intermenstrual or breakthrough bleeding	11 (2.1)
Amenorrhea (primary or secondary)	16 (3)
Sonographic Pathology (Total)	138 (25.8)
Normal sonographic findings	385 (71.8)
PCO morphology	89 (16.6)
Unilateral >4 cm anechoic cyst	35 (6.5)
Corpus hemorrhagicum/ corpus luteum	5 (0.9)
Mature cystic teratoma	4 (0.7)
Bilateral ovarian cyst	3 (0.6)
Endometrioma	1 (0.2)
Intraperitoneal fluid	1 (0.2)
No ultrasonography performed	13 (2.4)
Hyperthyroidism	14 (2.6)
Hypothyroidism	4 (0.7)
Hyperprolactinemia	31 (5.8)
Elevated CA-125 level (35 units/mL)	5 (0.9)
Hospitalization	4 (0.7)
Outpatient management	531(99.3)

**Note:** Data are presented as mean — SD; and *n* (%) for nominal variables. Primary amenorrhea: failure to reach menarche by age 15 years in adolescent girls with otherwise normal secondary sexual development. Secondary amenorrhea: cessation of previously regular menses for 3 months or longer and cessation of previously irregular menses for 6 months or longer. Polycystic ovarian morphology(PCOM):Ovarian volume 10 ml on either ovary (guideline 2018) Hypothyroidism: Elevated TSH with low free T4 or with normal T4. Hyperthyroidism: Suppressed TSH with freeT4 and or T3 elevated

impact the daily activities and quality of life of adolescent girls and it is a common cause of school absenteeism [20]. Primary dysmenorrhea involves painful menstruation without any pelvic pathology. Prostaglandins play a role in the etiology. Secondary dysmenorrhea, on the other hand, refers to painful menstrual periods attributed to pelvic pathology or a medical condition. In adolescents, the most common cause of secondary dysmenorrhea is endometriosis [21]. In our study, however, an endometrioma was detected sonographically in one patient. Within the study population, there are likely more cases of endometriosis; the diagnosis of peritoneal endometriotic lesions can only be established through a laparoscopic intervention. The etiology of secondary dysmenorrhea includes other factors such as adenomyosis, infections, Müllerian anomalies, obstructive tract abnormalities, fibroids, and ovarian cysts [20].

Polycystic ovary syndrome (PCOS) frequently manifests with symptoms during adolescence, primarily characterized by ovulation dysfunction and androgen excess (hyperandrogenism) [22]. Adolescents with the presence of hirsutism or treatment-resistant inflammatory acne, accompanied by menstrual abnormalities (amenorrhea, oligomenorrhea, or excessive menstrual bleeding), acanthosis nigricans, and/or obesity, should be evaluated with consideration of a PCOS diagnosis [22]. Ultrasonographically, the finding of polycystic ovary morphology (PCOM) can also be commonly observed in normal adolescents; therefore, it is not included in the 2015 PCOS diagnostic criteria for adolescents [23]. In our study, a total of 89 adolescents were found to have sonographically detected PCOM; however, it is important to emphasize that this is not a diagnostic criterion for PCOS during adolescence.

Vulvovaginitis is a common gynecologic concern among adolescents and is characterized by discharge, pain, swelling,

itching, and discomfort [24]. The etiology of adolescent vulvovaginitis can be multifactorial, encompassing poor hygiene practices, chemical irritants, infectious agents, and hormonal changes associated with puberty. In adolescents, the most prevalent causes of vaginitis encompass bacterial vaginosis, vulvovaginal candidiasis, and *Trichomonas vaginalis* infection [24]. Within our study cohort, 51 adolescents (9.5%) presented with complaints of vaginal discharge or vulvar itching. Apart from infectious agents, etiological factors include poor hygiene practices, chemical irritants, and feminine hygiene products. In adolescents, obtaining a comprehensive medical history and inquiring about sexual activity is imperative for accurate diagnosis and effective management.

In adolescents, ovarian masses can be incidentally identified during imaging or may give rise to symptoms such as pelvic pain, menstrual irregularities, or findings suggestive of precocious puberty [25]. The majority of ovarian masses encountered in adolescent girls are either physiological ovarian cysts or of a benign nature. In our study, an adolescent presenting with abdominal pain was found to have a 5,5 cm septated cyst and an accompanying 3 cm unilocular anechoic cyst on ultrasonography. The patient was admitted to the hospital, received medical treatment, and underwent evaluation for malignancy.

In the treatment of adnexal masses in adolescents, priority should be given to preserving the ovaries to maintain fertility [26]. Surgical indications include suspicion of malignancy, ovarian torsion, persistent mass, and acute abdominal pain [26]. According to a meta-analysis published in 2020, the reported rate of malignancy is approximately 10–20% of patients who underwent surgical intervention due to ovarian cysts [27]. Germ cell tumors are the most common malignancies of the ovaries in children and adolescents, and AFP,  $\beta$ -hCG, and

lactate dehydrogenase should be tested for the assessment of suspected germ cell tumors [28,29]. The reason for the absence of surgical cases in the patient group included in the study is that patients presenting with abdominal pain or an acute abdominal condition tend to seek treatment in the field of Pediatric Surgery or have their treatment directly coordinated with Pediatric Surgery by the Pediatrics department.

Our study has some strengths and limitations. The retrospective design and single center nature of our study may limit the power of our study. Strengths of the study include conducting it in a high-volume tertiary hospital and enrolling a large number of patients.

## CONCLUSIONS

Adolescent gynecology differs from adult gynecology due to the physiological and psychological specificities of the adolescent

period. Considering the potential psychological impacts of the first gynecological examination on adolescents, understanding appropriate examination techniques is crucial. In our study, adolescents most commonly sought medical attention due to menstrual irregularities. It is important to distinguish normal menstrual patterns encountered during the pubertal period from abnormal menstrual bleeding. Conditions such as PCOS and endometriosis can manifest during adolescence and may have implications for future fertility. Congenital female reproductive tract anomalies can be detected in adolescents, either symptomatically or asymptotically. Accurate diagnosis is crucial for preserving future fertility and has significant psychological and social implications. Our study provides valuable insights into the epidemiology of gynecological issues among adolescents, which can inform healthcare strategies and interventions for this vulnerable population.

## References

1. Adolescent health. World Health Organization n.d. Available from: <https://www.who.int/health-topics/adolescent-health> (accessed June 18, 2023).
2. ACOG Committee Opinion No. 651: Menstruation in girls and adolescents: using the menstrual cycle as a vital sign. *Obstetrics and Gynecology* 2015; 126: e143–6.
3. Snook ML, Nayak S, Lara-Torre E, Sanfilippo JS. Adolescent gynecology: special considerations for special patients gynecologic evaluation of the adolescent. *Clin Obstet Gynecol* 2012; 55: 651–61.
4. Sanfilippo JS, Lara-Torre E. Adolescent gynecology. *Obstetrics and Gynecology* 2009; 113: 935–47. Available from: <https://doi.org/10.1097/AOG.0B013E31819B6303>.
5. The Initial Reproductive Health Visit: ACOG Committee Opinion, Number 811. *Obstetrics and Gynecology* 2020; 136: 70–80. Available from: <https://doi.org/10.1097/AOG.0000000000004094>.
6. Roos EJ, Simms-Cendan J, Cheung C, Laufer D, Grover SR. Pediatric and adolescent gynecology through a global lens. *International Journal Gynecology Obstetrics*. 2022; 156: 189–96. Available from: <https://doi.org/10.1002/ijgo.13723>.
7. Biro FM, Huang B, Crawford PB, Lucky AW, Striegel-Moore R, Barton BA, et al. Pubertal correlates in black and white girls. *J Pediatr*. 2006; 148: 234–40. Available from: <https://doi.org/10.1016/J.JPEDI.2005.10.020>.
8. Chumlea WC, Schubert CM, Roche AF, Kulin HE, Lee PA, Himes JH, et al. Age at menarche and racial comparisons in US girls. *Pediatrics*. 2003; 111: 110–3. Available from: <https://doi.org/10.1542/PEDS.111.1.110>.
9. Sun BZ, Kangaroo T, Adams JM, Sluss PM, Welt CK, Chandler DW, et al. Healthy post-menarchal adolescent girls demonstrate multi-level reproductive axis immaturity. *Journal of Clinical Endocrinology and Metabolism*. 2018; 104: 613–23. Available from: <https://doi.org/10.1210/jc.2018-00595>.
10. Screening and management of bleeding disorders in adolescents with heavy menstrual bleeding: ACOG COMMITTEE OPINION, Number 785. *Obstetrics and Gynecology* 2019; 134: E71–83. Available from: <https://doi.org/10.1097/AOG.0000000000003411>.
11. ACOG committee opinion no. 557: Management of acute abnormal uterine bleeding in nonpregnant reproductive-aged women. *Obstetrics and Gynecology*. 2013; 121: 891–6. Available from: <https://doi.org/10.1097/01.AOG.0000428646.67925.9A>.
12. Venkateswaran L, Dietrich JE. Gynecologic concerns in pubertal females with blood disorders. *J Pediatr Adolesc Gynecol*. 2013; 26: 80–5. Available from: <https://doi.org/10.1016/J.JPAG.2012.07.001>.
13. Haamid F, Sass AE, Dietrich JE. Heavy menstrual bleeding in adolescents. *J Pediatr Adolesc Gynecol*. 2017; 30: 335–40. Available from: <https://doi.org/10.1016/J.JPAG.2017.01.002>.
14. James AH, Kouides PA, Abdul-Kadir R, Dietrich JE, Edlund M, Federici AB, et al. Evaluation and management of acute menorrhagia in women with and without underlying bleeding disorders: consensus from an international expert panel. *Eur J Obstet Gynecol Reprod Biol* 2011; 158: 124–34. Available from: <https://doi.org/10.1016/J.EJOGRB.2011.04.025>.
15. Ely JW, Kennedy CM, Clark EC, Bowdler NC. Abnormal uterine bleeding: a management algorithm. *J Am Board Fam Med* 2006; 19: 590–602. Available from: <https://doi.org/10.3122/JABFM.19.6.590>.
16. Sultan C, Gaspari L, Maimoun L, Kalfa N, Paris F. Disorders of puberty. *Best Pract Res Clin Obstet Gynaecol*. 2018; 48: 62–89. Available from: <https://doi.org/10.1016/J.BPOBGYN.2017.11.004>.
17. Rosenfield RL. Clinical review: Adolescent anovulation: maturational mechanisms and implications. *J Clin Endocrinol Metab*. 2013; 98: 3572–83. Available from: <https://doi.org/10.1210/JC.2013-1770>.
18. Pfeifer SM, Attaran M, Goldstein J, Lindheim SR, Petrozza JC, Rackow BW, et al. ASRM müllerian anomalies classification 2021. *Fertil Steril*. 2021; 116: 1238–52. Available from: <https://doi.org/10.1016/J.FERTNSTERT.2021.09.025>.
19. Al-Jefout M, Nawaiseh N. Continuous Norethisterone Acetate versus Cyclical Drospirenone 3 mg/Ethinyl Estradiol 20 µg for the Management of Primary Dysmenorrhea in Young Adult Women. *J Pediatr Adolesc Gynecol* 2016; 29: 143–7. Available from: <https://doi.org/10.1016/j.jpag.2015.08.009>.
20. ACOG Committee Opinion No. 760: Dysmenorrhea and endometriosis in the adolescent. *Obstetrics and Gynecology* 2018; 132: E249–58. Available from: <https://doi.org/10.1097/AOG.0000000000002978>.
21. Janssen EB, Rijkers ACM, Hoppenbrouwers K, Meuleman C, D'Hooghe TM. Prevalence of endometriosis diagnosed by laparoscopy in adolescents with dysmenorrhea or chronic pelvic pain: a systematic review. *Hum Reprod Update* 2013; 19: 570–82. Available from: <https://doi.org/10.1093/HUMUPD/DMT016>.
22. Ibáñez L, Oberfield SE, Witchel S, Auchus RJ, Chang RJ, Cochner E, et al. An International Consortium Update: pathophysiology, diagnosis, and treatment of polycystic ovarian syndrome in Adolescence. *Horm Res Paediatr* 2017; 88: 371–95. Available from: <https://doi.org/10.1159/000479371>.
23. ACOG Committee Opinion, Number 789; screening and management of the hyperandrogenic adolescent. *Obstetrics and Gynecology*. 2019; 134: E106–14. Available from: <https://doi.org/10.1097/AOG.0000000000003475>.
24. Itriyeva K. Evaluation of vulvovaginitis in the adolescent patient. *Curr Probl Pediatr Adolesc Health Care*. 2020; 50. Available from: <https://doi.org/10.1016/J.CPPEDS.2020.100836>.
25. Heo SH, Kim JW, Shin SS, Jeong SI, Lim HS, Choi YD, et al. Review of ovarian tumors in children and adolescents: radiologic-pathologic correlation. *Radiographics*. 2014; 34: 2039–55. Available from: <https://doi.org/10.1148/RG.347130144>.
26. Eskander R, Berman M, Keder L. Practice Bulletin No. 174: Evaluation and management of adnexal masses. *Obstetrics and Gynecology*. 2016; 128: e210–26. <https://doi.org/10.1097/AOG.0000000000001768>.

27. Qazi SH, Jeelani SM, Dogar SA, Das JK, Saxena AK. Approaches to the management of pediatric ovarian masses in the 21<sup>st</sup> century: Systematic review and meta-analysis. *J Pediatr Surg.* 2020; 55: 357–68. Available from: <https://doi.org/10.1016/J.JPEDIURG.2019.09.003>.
28. Gupta B, Guleria K, Suneja A, Vaid NB, Rajaram S, Wadhwa N. Adolescent ovarian masses: A retrospective analysis. *J Obstet Gynaecol.* 2016; 36: 515–7. Available from: <https://doi.org/10.3109/01443615.2015.1103721>.
29. Papic JC, Finnell SME, Slaven JE, Billmire DF, Rescorla FJ, Leys CM. Predictors of ovarian malignancy in children: overcoming clinical barriers of ovarian preservation. *J Pediatr Surg.* 2014; 49: 144–8. Available from: <https://doi.org/10.1016/J.JPEDIURG.2013.09.068>.

## Литература

- Adolescent health. World Health Organization n.d. Available from: <https://www.who.int/health-topics/adolescent-health> (accessed June 18, 2023).
- ACOG Committee Opinion No. 651: Menstruation in girls and adolescents: using the menstrual cycle as a vital sign. *Obstetrics and Gynecology* 2015; 126: e143–6.
- Snook ML, Nayak S, Lara-Torre E, Sanfilippo JS. Adolescent gynecology: special considerations for special patients gynecologic evaluation of the adolescent. *Clin Obstet Gynecol* 2012; 55: 651–61.
- Sanfilippo JS, Lara-Torre E. Adolescent gynecology. *Obstetrics and Gynecology* 2009; 113: 935–47. Available from: <https://doi.org/10.1097/AOG.0B013E31819B6303>.
- The Initial Reproductive Health Visit: ACOG Committee Opinion, Number 811. *Obstetrics and Gynecology* 2020; 136: 70–80. Available from: <https://doi.org/10.1097/AOG.0000000000004094>.
- Roos EJ, Simms-Cendan J, Cheung C, Laufer D, Grover SR. Pediatric and adolescent gynecology through a global lens. *International Journal Gynecology Obstetrics.* 2022; 156: 189–96. Available from: <https://doi.org/10.1002/ijgo.13723>.
- Biro FM, Huang B, Crawford PB, Lucky AW, Striegel-Moore R, Barton BA, et al. Pubertal correlates in black and white girls. *J Pediatr.* 2006; 148: 234–40. Available from: <https://doi.org/10.1016/J.JPEDI.2005.10.020>.
- Chumlea WC, Schubert CM, Roche AF, Kulin HE, Lee PA, Himes JH, et al. Age at menarche and racial comparisons in US girls. *Pediatrics.* 2003; 111: 110–3. Available from: <https://doi.org/10.1542/PEDS.111.1.110>.
- Sun BZ, Kangaroo T, Adams JM, Sluss PM, Welt CK, Chandler DW, et al. Healthy post-menarchal adolescent girls demonstrate multi-level reproductive axis immaturity. *Journal of Clinical Endocrinology and Metabolism.* 2018; 104: 613–23. Available from: <https://doi.org/10.1210/je.2018-00595>.
- Screening and management of bleeding disorders in adolescents with heavy menstrual bleeding: ACOG COMMITTEE OPINION, Number 785. *Obstetrics and Gynecology* 2019; 134: E71–83. Available from: <https://doi.org/10.1097/AOG.0000000000003411>.
- ACOG committee opinion no. 557: Management of acute abnormal uterine bleeding in nonpregnant reproductive-aged women. *Obstetrics and Gynecology.* 2013; 121: 891–6. Available from: <https://doi.org/10.1097/01.AOG.0000428646.67925.9A>.
- Venkateswaran L, Dietrich JE. Gynecologic concerns in pubertal females with blood disorders. *J Pediatr Adolesc Gynecol.* 2013; 26: 80–5. Available from: <https://doi.org/10.1016/J.JPAG.2012.07.001>.
- Haamid F, Sass AE, Dietrich JE. Heavy menstrual bleeding in adolescents. *J Pediatr Adolesc Gynecol.* 2017; 30: 335–40. Available from: <https://doi.org/10.1016/J.JPAG.2017.01.002>.
- James AH, Kouides PA, Abdul-Kadir R, Dietrich JE, Edlund M, Federici AB, et al. Evaluation and management of acute menorrhagia in women with and without underlying bleeding disorders: consensus from an international expert panel. *Eur J Obstet Gynecol Reprod Biol* 2011; 158: 124–34. Available from: <https://doi.org/10.1016/J.EJOGRB.2011.04.025>.
- Ely JW, Kennedy CM, Clark EC, Bowdler NC. Abnormal uterine bleeding: a management algorithm. *J Am Board Fam Med* 2006; 19: 590–602. Available from: <https://doi.org/10.3122/JABFM.19.6.590>.
- Sultan C, Gaspari L, Maimoun L, Kaifa N, Paris F. Disorders of puberty. *Best Pract Res Clin Obstet Gynaecol.* 2018; 48: 62–89. Available from: <https://doi.org/10.1016/J.BPOBGYN.2017.11.004>.
- Rosenfield RL. Clinical review: Adolescent anovulation: maturational mechanisms and implications. *J Clin Endocrinol Metab.* 2013; 98: 3572–83. Available from: <https://doi.org/10.1210/JC.2013-1770>.
- Pfeifer SM, Attaran M, Goldstein J, Lindheim SR, Petrozza JC, Rackow BW, et al. ASRM müllerian anomalies classification 2021. *Fertil Steril.* 2021; 116: 1238–52. Available from: <https://doi.org/10.1016/J.FERTNSTERT.2021.09.025>.
- Al-Jefout M, Nawaiseh N. Continuous Norethisterone Acetate versus Cyclical Drospirenone 3 mg/Ethinyl Estradiol 20 µg for the Management of Primary Dysmenorrhea in Young Adult Women. *J Pediatr Adolesc Gynecol* 2016; 29: 143–7. Available from: <https://doi.org/10.1016/j.jpag.2015.08.009>.
- ACOG Committee Opinion No. 760: Dysmenorrhea and endometriosis in the adolescent. *Obstetrics and Gynecology* 2018; 132: E249–58. Available from: <https://doi.org/10.1097/AOG.0000000000002978>.
- Janssen EB, Rijkers ACM, Hoppenbrouwers K, Meuleman C, D’Hooghe TM. Prevalence of endometriosis diagnosed by laparoscopy in adolescents with dysmenorrhea or chronic pelvic pain: a systematic review. *Hum Reprod Update* 2013; 19: 570–82. Available from: <https://doi.org/10.1093/HUMUPD/DMT016>.
- Ibáñez L, Oberfield SE, Witchel S, Auchus RJ, Chang RJ, Codner E, et al. An International Consortium Update: pathophysiology, diagnosis, and treatment of polycystic ovarian syndrome in Adolescence. *Horm Res Paediatr* 2017; 88: 371–95. Available from: <https://doi.org/10.1159/000479371>.
- ACOG Committee Opinion, Number 789; screening and management of the hyperandrogenic adolescent. *Obstetrics and Gynecology.* 2019; 134: E106–14. Available from: <https://doi.org/10.1097/AOG.0000000000003475>.
- Itriyeva K. Evaluation of vulvovaginitis in the adolescent patient. *Curr Probl Pediatr Adolesc Health Care.* 2020; 50. Available from: <https://doi.org/10.1016/J.CPPEDS.2020.100836>.
- Heo SH, Kim JW, Shin SS, Jeong SI, Lim HS, Choi YD, et al. Review of ovarian tumors in children and adolescents: radiologic-pathologic correlation. *Radiographics.* 2014; 34: 2039–55. Available from: <https://doi.org/10.1148/RG.347130144>.
- Eskander R, Berman M, Keder L. Practice Bulletin No. 174: Evaluation and management of adnexal masses. *Obstetrics and Gynecology.* 2016; 128: e210–26. <https://doi.org/10.1097/AOG.0000000000001768>.
- Qazi SH, Jeelani SM, Dogar SA, Das JK, Saxena AK. Approaches to the management of pediatric ovarian masses in the 21<sup>st</sup> century: Systematic review and meta-analysis. *J Pediatr Surg.* 2020; 55: 357–68. Available from: <https://doi.org/10.1016/J.JPEDIURG.2019.09.003>.
- Gupta B, Guleria K, Suneja A, Vaid NB, Rajaram S, Wadhwa N. Adolescent ovarian masses: A retrospective analysis. *J Obstet Gynaecol.* 2016; 36: 515–7. Available from: <https://doi.org/10.3109/01443615.2015.1103721>.
- Papic JC, Finnell SME, Slaven JE, Billmire DF, Rescorla FJ, Leys CM. Predictors of ovarian malignancy in children: overcoming clinical barriers of ovarian preservation. *J Pediatr Surg.* 2014; 49: 144–8. Available from: <https://doi.org/10.1016/J.JPEDIURG.2013.09.068>.

## ASSESSMENT OF BLOOD AMINO ACID AND POLYAMINE LEVELS IN PLACENTA-ASSOCIATED PREGNANCY COMPLICATIONS

Gasankbekova AP<sup>1</sup>, Frankevich NA<sup>1</sup>✉, Chagovets VV<sup>1</sup>, Dolgoplova EL<sup>1</sup>, Novoselova AV<sup>1</sup>, Karapetyan TE<sup>1</sup>, Mamedova GE<sup>2</sup>, Frankevich VE<sup>1,3</sup>

<sup>1</sup> Kulakov National Medical Research Center for Obstetrics, Gynecology and Perinatology, Moscow, Russia

<sup>2</sup> Peoples' Friendship University of Russia, Moscow, Russia

<sup>3</sup> Siberian State Medical University, Tomsk, Russia

The features of polyamine and amino acid metabolism play a key role in the cellular processes, and the search for their role as prognostic and diagnostic (assessment of fetal condition severity) markers in obstetrics can contribute to improvement of perinatal outcomes in fetal growth restriction (FGR) syndrome, both isolated and combined with early onset preeclampsia (PE). The study was aimed to determine the features of polyamine and amino acid levels associated with placenta-associated pregnancy complications. Liquid chromatography coupled with mass spectrometry was used to determine blood levels of polyamines and amino acids in 156 pregnant women divided into the following groups: with FGR — 48 pregnant women, with early onset PE — 56 pregnant women, control group — 52 somatically healthy women having no pregnancy complications. As a result, we managed to distinguish significant differences in these metabolites, depending on the obstetric complication (PE or FGR), and to determine correlations of those with a number of clinical data. We revealed a strong negative correlation between the increasing fetal condition decompensation in FGR and the length of the newborn's hospital stay for the PE and FGR groups, as well as between the levels of 1,7-diaminoheptane polyamine ( $r = -0.78$ ,  $CI = -0.92 - -0.37$ ,  $p = 0.002$ ;  $r = -0.76$ ,  $CI = -0.95 - 0.23$ ,  $p = 0.003$ ) and proline amino acid and the increasing fetal condition decompensation in FGR ( $r = -0.56$ ,  $CI = -0.86 - -0.034$ ,  $p = 0.03$ ). Considering the diversity and complexity of metabolic pathways responsible for adaptation in the context of hypoxic damage, the results obtained suggest that regulation of amino acids and polyamines is coordinated. Metabolic pathways of low molecular weight antioxidants, proline and polyamines, are associated with clinical pregnancy outcomes in FGR and early-onset PE.

**Keywords:** intrauterine growth restriction, fetal growth restriction, preeclampsia, metabolomics, newborn, mass spectrometry, biomarkers, polyamines, aminoacids

**Funding:** the study was supported by the RSF grant No. 22-15-00232 "New Noninvasive Diagnostic Approaches for Optimization of Obstetric Tactics, Prediction of Perinatal Outcomes, and Prevention of Abnormal Postnatal Growth in Fetal Growth Restriction Syndrome".

**Author contribution:** Gasankbekova AP — collection and preparation of biological media, manuscript writing; Frankevich NA — clinical data analysis, systematic analysis, manuscript writing; Chagovets VV — metabolomics analysis by mass spectrometry, statistical analysis of the data acquired, manuscript editing; Dolgoplova EL — clinical data analysis, statistical data processing; Novoselova AV — metabolomics analysis by mass spectrometry, mass spectrometry data processing; Karapetyan TE — clinical data analysis, manuscript editing; Mamedova GE — collection and preparation of biological media; Frankevich VE — preparation and control, manuscript editing.

**Compliance with ethical standards:** the study was approved by the Ethics Committee of the Kulakov National Medical Research Center for Obstetrics, Gynecology and Perinatology (protocol No. 11 dated 11 November 2021), the study met the requirements of the Declaration of Helsinki, International Conference on Harmonization (ICF), Good Clinical Practice (GCP), and Federal Law "On the Basics of Protecting Citizens' Health in the Russian Federation"; the informed consent was submitted by all patients.

✉ **Correspondence should be addressed:** Natalia A. Frankevich  
Akademika Oparina, 4, Moscow, 117997, Russia; natasha-lomova@yandex.ru

**Received:** 21.06.2024 **Accepted:** 24.07.2024 **Published online:** 15.08.2024

**DOI:** 10.24075/brsmu.2024.031

## ИЗУЧЕНИЕ УРОВНЯ АМИНОКИСЛОТ И ПОЛИАМИНОВ КРОВИ ПРИ АССОЦИИРОВАННЫХ С ПЛАЦЕНТОЙ ОСЛОЖНЕНИЯХ БЕРЕМЕННОСТИ

А. П. Гасанбекова<sup>1</sup>, Н. А. Франкевич<sup>1</sup>✉, В. В. Чаговец<sup>1</sup>, Е. Л. Дербенцева<sup>1</sup>, А. В. Новоселова<sup>1</sup>, Т. Э. Карапетян<sup>1</sup>, Г. Э. Мамедова<sup>2</sup>, В. Е. Франкевич<sup>1,3</sup>

<sup>1</sup> Национальный медицинский исследовательский центр акушерства, гинекологии и перинатологии имени В. И. Кулакова, Москва, Россия

<sup>2</sup> Российский университет дружбы народов имени Патриса Лумумбы, Москва, Россия

<sup>3</sup> Сибирский государственный медицинский университет, Томск, Россия

Особенности метаболизма полиаминов и аминокислот играют ключевую роль в клеточных процессах, а поиск их роли в качестве прогностических и диагностических (оценка тяжести состояния плода) маркеров в акушерстве может способствовать улучшению перинатальных исходов при синдроме задержки роста плода (ЗРП), как изолированном, так и сочетанном с ранней преэклампсией (ПЭ). Целью исследования было определить особенности уровней полиаминов и аминокислот, сопряженных с плацента-ассоциированными осложнениями беременности. С помощью жидкостной хроматографии с масс-спектрометрическим детектированием были определены уровни полиаминов и аминокислот в крови 156 беременных женщин, разделенных на группы: с ЗРП — 48 беременных, с ранней ПЭ — 56 беременных, в контрольной группе — 52 соматически здоровых женщины с беременностью без осложнений. В результате удалось выделить значимые отличия данных метаболитов, в зависимости от акушерского осложнения (ПЭ или ЗРП) и установить их корреляционную зависимость с рядом клинических данных. Обнаружена сильная обратная корреляционная связь с нарастанием декомпенсации состояния плода при ЗРП и числом койко-дней, проведенных в стационаре новорожденным для групп ПЭ и ЗРП и уровнем полиамина 1,7-диаминогептан ( $r = -0,78$ ,  $CI = -0,92 - -0,37$ ,  $p = 0,002$ ;  $r = -0,76$ ,  $CI = -0,95 - 0,23$ ,  $p = 0,003$ ) и аминокислотой пролин и нарастанием декомпенсации состояния плода при ЗРП ( $r = -0,56$ ,  $CI = -0,86 - -0,034$ ,  $p = 0,03$ ). Учитывая многообразие и сложность метаболических путей, ответственных за адаптацию в условиях гипоксического поражения, на основании полученных результатов, можно предположить, что регуляция аминокислот и полиаминов является координированной. Пути метаболизма низкомолекулярных антиоксидантов — пролина и полиаминов ассоциированы с клиническими исходами беременности при ЗРП и ранней ПЭ.

**Ключевые слова:** задержка внутриутробного развития, ограничение роста плода, преэклампсия, метаболомика, новорожденный, масс-спектрометрия, биомаркеры, полиамины, аминокислоты

**Финансирование:** исследование выполнено при поддержке гранта РНФ № 22-15-00232 «Новые неинвазивные диагностические подходы для оптимизации акушерской тактики, прогнозирования перинатальных исходов и профилактики нарушений постнатального роста при синдроме задержки роста плода».

**Вклад авторов:** А. П. Гасанбекова — сбор и подготовка биологических сред, написание статьи; Н. А. Франкевич — анализ клинических данных, систематический анализ, написание статьи; В. В. Чаговец — проведение метаболомного анализа методом масс-спектрометрии, статистический анализ полученных данных, редактирование статьи; Е. Л. Долгополова — анализ клинических данных, статистическая обработка данных; А. В. Новоселова — проведение метаболомного анализа методом масс-спектрометрии, обработка масс-спектрометрических данных; Т. Э. Карапетян — анализ клинических данных, редактирование рукописи; Г. Э. Мамедова — сбор и подготовка биологических сред; В. Е. Франкевич — подготовка и контроль, редактирование статьи.

**Соблюдение этических стандартов:** исследование одобрено этическим комитетом НЦАГиП имени В. И. Кулакова (протокол № 11 от 11 ноября 2021 г.), проведено в соответствии с требованиями Хельсинкской декларации, Международной конференции по гармонизации (ICF), Стандартами надлежащей клинической практики (GCP), ФЗ «Об основах охраны здоровья граждан в Российской Федерации»; все пациентки подписали добровольное информированное согласие на участие в исследовании.

✉ **Для корреспонденции:** Наталья Анатольевна Франкевич  
ул. Академика Опарина, д. 4, г. Москва, 117997, Россия; natasha-lomova@yandex.ru

**Статья получена:** 21.06.2024 **Статья принята к печати:** 24.07.2024 **Опубликована онлайн:** 15.08.2024

**DOI:** 10.24075/vrgmu.2024.031

Polyamines are polymeric molecules containing several amino groups. These are involved in the broad spectrum of biochemical processes, such as generation of membrane potential, DNA and RNA stabilization, enzyme activation, and ion transport, as well as in regulation of gene expression, protein synthesis; polyamines exert antitoxic activity, have an effect on the body's immune system [1–2].

Since polyamines are derived from amino acids [3], these can be considered an essential component of amino acid metabolism and cell regulation [4]. Polyamine levels can be regulated by changing bioavailability and the concentrations of amino acids essential for synthesis of polyamines [5]. For polyamines to perform their functions in various cells and tissues, these must penetrate cell membranes. This process involves the transport systems, in which amino acids ensure transfer of those through the membrane. Therefore, the link between polyamines and amino acids covers not only polyamine synthesis, but also the effects of polyamines on the cellular processes, including protein regulation and interaction with cell membranes. This is a complex area of research that is of great importance for understanding the cell physiology and biochemistry.

Medical use of polyamines is still evolving, however, there are already several fields, in which these molecules can be used as biomarkers for diagnosis of various disorders: cancer [6, 7], neurodegenerative disorders [8], infectious diseases, and autoimmune disorders [9].

In obstetrics, polyamines are associated with various aspects of pregnancy and childbirth [10], including cell growth and differentiation associated with the development of fetal organs and systems [11–13]. The link between amino acids and polyamines is of high clinical significance. Such an essential amino acid, as arginine, is a precursor of polyamines. Arginine is converted to spermidine polyamine and spermine through the series of biochemical reactions. Cadaverine also can be synthesized from arginine and can take part in regulation of a number of cellular processes. Low levels of arginine, lysine, and aspartic acid can play an important role in the processes resulting in fetal growth restriction (FGR). Arginine, lysine, and aspartic acid are not only involved in protein synthesis, but are important for many biochemical pathways and body functions [14]. Arginine is a precursor of nitric oxide (NO) playing an important role in regulation of vascular function. NO dilates blood vessels and improves blood flow, and this is the key factor ensuring normal growth and development of the fetus. Low arginine levels can decrease NO production and compromise vascular response, thereby limiting fetal nutrient supply [15]. Lysine deficiency can result in the decreased synthesis of certain proteins and affect fetal growth. Furthermore, lysine is involved in the fat and carbohydrate metabolism, and low levels of these amino acids can compromise fetal energy supply. Aspartic acid can affect metabolic pathways of other amino acids, including those associated with fetal growth and development.

Amino acids play a role in regulation of blood pressure and vascular function. The research shows that alterations of maternal amino acid profile can be associated with the development of preeclampsia (PE). For example, high levels of glutamic and aspartic acids are associated with the risk of PE [16].

Determination of amino acid and polyamine levels in mother's body and the fetus can provide important information about the risk of FGR and PE. The research continues, and better understanding of the relationships between amino acids, polyamines, and these obstetric conditions can lead to the development of more effective methods for diagnosis and monitoring of pregnancy, as well as to improvement of treatment and prevention strategies.

The study was aimed to determine the features of polyamine and amino acid levels associated with the placenta-associated pregnancy complications, including FGR (both isolated and combined with early-onset PE), as well as to reveal clinical and laboratory parallels in FGR and PE based on the correlation analysis of the relationship between the levels of important polyamines and amino acids and such clinical parameters, as FGR and PE severity, length of hospital stay in the newborns born to mothers of the FGR and PE groups.

## METHODS

A total of 156 pregnant women, who were admitted to and gave birth in the Kulakov National Medical Research Center for Obstetrics, Gynecology and Perinatology, were included in the study: PE and FGR groups consisted of 56 and 48 patients with the confirmed appropriate diagnoses; the control group included 52 somatically healthy women with no pregnancy complications. Inclusion criteria: pregnant women's age 18–35 years, 24–40 weeks of singleton pregnancy, early-onset preeclampsia and fetal growth restriction. Exclusion criteria: Rh isoimmunization and ABO incompatibility, chromosomal abnormalities, genetic mutations and congenital malformations in the fetus, severe extragenital disorder, chronic kidney disease, large uterine fibroid, acute infectious disease in the mother. Venous blood was collected for analysis.

### Polyamine analysis method

The optimized procedure of blood sample preparation for assessment of polyamine levels includes the following phases: add 1200  $\mu\text{L}$  of methanol to 400  $\mu\text{L}$  of blood plasma, stir for 5 min, centrifuge for 10 min at 13,000 g (Eppendorf MiniSpin centrifuge, Germany), collect 1000  $\mu\text{L}$  of supernatant, dry in nitrogen flow at the temperature of 50  $^{\circ}\text{C}$ , add 600  $\mu\text{L}$  of the 10 mg/mL dansyl chloride solution in the acetonitrile/carbonate buffer with pH = 9.7 (50/50 v/v), stir for 1 min, centrifuge for 1 min at 13,000 g, incubate at 60  $^{\circ}\text{C}$  for 90 min, centrifuge for 1 min at 13,000 g, add 1000  $\mu\text{L}$  of ethyl acetate, stir for 10 min, centrifuge for 10 min at 13,000 g, collect 1000  $\mu\text{L}$  of the top layer, add 1000  $\mu\text{L}$  of ethyl acetate, stir for 10 min, centrifuge for 10 min at 13,000 g; collect 1000  $\mu\text{L}$  of the top layer and combine with the previously collected portion, dry in nitrogen flow at the temperature of 50  $^{\circ}\text{C}$ , add 200  $\mu\text{L}$  of acetonitrile, stir for 5 min, centrifuge for 10 min at 13,000 g; take 170  $\mu\text{L}$  for further analysis.

The analysis of polyamines and amino acids was conducted by liquid chromatography–mass spectrometry (LC–MS) in the system consisting of the ABSciex QTrap 5500 triple quadrupole mass spectrometer (ABSciex; Canada) coupled to electrospray ionization and the Agilent 1260 Infinity liquid chromatography system (Agilent; USA). The Agilent Zorbax Eclipse Plus C18 column (50  $\times$  3 mm, 1.8  $\mu\text{m}$ ; Agilent, USA) was used for separation of the sample. To analyze organic acids, we introduced 20  $\mu\text{L}$  of the sample and used the 0.1% aqueous formic acid solution as eluent A; eluent B was the 0.1% acetonitrile formic acid solution. The flow rate was 650  $\mu\text{L}/\text{min}$ , and the column temperature of 30  $^{\circ}\text{C}$  was maintained. The mobile phase composition changed during the analysis in the following way: 0–0.3 min — 20% of eluent B, by 5.3 min the volume fraction of eluent B increased to 95%, remained the same by 8.3 min, and returned to the value of 20% within 0.1 min. The mass spectrometer settings were as follows: peripheral gas pressure — 1.4 bar, nebulizer gas pressure — 3.4 bar, source temperature — 500  $^{\circ}\text{C}$ , capillary voltage — 4500 V.

Table 1. Clinical characteristics of the studied groups

Parameter	Descriptive statistics if the parameter			Significance of differences in the parameters for pairwise comparison of the group ( $p$ -value)		
	PE ( $n = 56$ )	FGR ( $n = 48$ )	Normal ( $n = 52$ )	PE – Normal	FGR – Normal	PE – FGR
Age	32 ± 5	32 ± 3	31 ± 4	0.654	0.212	0.146
BMI (pregravid)	27 ± 5	20 ± 5	25 ± 3	0.745	0.005	0.003
Gestational age at delivery	35 ± 3	37 ± 2	40 ± 1	< 0.001	< 0.001	0.435
Birth length	45.8 ± 4.5	45.1 ± 2.1	52.1 ± 2.2	0.001	< 0.001	0.378
Birth weight	2132 ± 846.6	1969.7 ± 501.0	3403.7 ± 395.7	< 0.001	< 0.001	0.401
Apgar score 1	7 (7; 8)	8 (8; 8)	8 (8; 8)	< 0.001	0.357	0.06
Apgar score 5	8 (8; 9)	9 (8; 9)	9 (9; 9)	0.02	0.033	0.031

In this study, the following nine polyamines were analyzed: putrescine, ethylenediamine, 1,3-diaminopropane, cadaverine, 1,7-diaminoheptane, cadaverine, N-acetylputrescine, N1-acetylspermine, spermidine; along with 43 amino acids: 1-methylhistidine, 3-aminoisobutyric acid, 3-methylhistidine, argininosuccinic acid, beta-alanine, creatinine, 5-hydroxylysine, homocystine, ethanolamine, gamma-aminobutyric acid, 2-aminoadipic acid, 2-aminobutyric acid, alanine, anserine, arginine, asparagine, aspartic acid, carnosine, citrulline, cystathionine, cystine, glutamic acid, glutamine, glycine, histidine, homocitrulline, isoleucine, leucine, lysine, methionine, norvaline, ornithine, phenylalanine, proline, serine, threonine, tryptophan, tyrosine, valine, O-phosphorylethanolamine, sarcosine, taurine, trans-4-hydroxyproline.

### Statistical analysis

Statistical processing of the experimental data obtained was performed using the R scripts.

Statistical analysis involved the use of the nonparametric Mann-Whitney U test. Quantitative data were described using the median (Me) and  $Q_1$  and  $Q_3$  quartiles in the Me ( $Q_1$ ;  $Q_3$ ) format, along with the mean (M) and standard deviation (SD) in the  $M \pm SD$  format. The threshold significance level  $p$  was considered to be equal to 0.05. When  $p$ -value was below 0.001, it was provided in the  $p < 0.001$  format.

The search for clinical and laboratory parallels in FGR and PE was performed using the Spearman rank correlation test for the polyamine and amino acid levels and clinical indicators. The correlation was considered significant at  $p < 0.05$ .

The logistic regression models were constructed to assess the possibility of classifying patients into groups based on the studied parameters. From all the models constructed we chose four with the largest area under the ROC curve (AUC). Quality of the models constructed was determined by plotting the ROC curve and calculating sensitivity and specificity.

### RESULTS

Pregnant patients were included in the case-control study, as they contacted the Center after being diagnosed with FGR or PE. At the time of inclusion in the study and blood collection, patients of the PE group had moderate PE with stable blood pressure, negligible proteinuria with normal 24-hour diuresis, no fetal disorder based on the Doppler data (fetoplacental blood flow and fetal distress); patients of the FGR group (3rd percentile and below based on fetometry data) showed no Doppler signs of fetal distress. All the patients had no regular labor contractions or threatened preterm labor. At the time of delivery, which happened on average three weeks after

blood collection, one-third of the patients had the diagnosis of severe preeclampsia, and critical disturbances of fetoplacental circulation were found in more than a half of the patients, which was the indication for surgical delivery through cesarean section. In patients of the control group, blood collection was performed at the gestational age similar to that of patients with PE and FGR. Later their course of pregnancy and delivery were monitored and considered to be uncomplicated.

Given the fact, that advanced reproductive age and obesity could become serious confounding factors when assessing blood levels of amino acids and polyamines, the groups were formed so that the age and body weight of patients with PE were matched to that of the control group. Body mass index (BMI) of pregnant women of the FGR group was significantly lower, than that of women of the Normal and Preeclampsia groups ( $p = 0.005$  and  $p = 0.003$ , respectively).

The results of assessing clinical parameters of the studied groups are provided in Table 1.

Due to the need for accelerated delivery for obstetric reasons resulting from the increasing PE severity and progressive intrauterine fetal hypoxia in FGR, the gestational age at delivery in these groups was significantly different from that in the control group ( $p < 0.001$ ). In cases of PE and FGR, the average weight of newborns was 2132.0 g and 1969.7 g.

It should be noted, that the newborns' Apgar scores in the group with PE were significantly lower in the first minute of life ( $p < 0.001$ ), while in the fifth minute there were significant differences in Apgar scores between all groups, which was likely to be associated with impaired adaptation in the early neonatal period in the newborns from the PE and FGR groups, who experienced chronic hypoxia for a long time.

Due to the important role of amino acid in polyamine synthesis and their function in cell metabolism, assessment of amino acid levels in patients of the studied groups was conducted in the first phase of laboratory analysis.

Data analysis made it possible to reveal the decrease in the levels of a number of amino acids relative to the control group in cases of PE and FGR: patients with FGR showed a significant decrease in the levels of alanine ( $p = 0.0136$ ), ornithine ( $p = 0.045$ ), proline ( $p = 0.0044$ ), while patients with PE showed a significant decrease in aspartic acid levels ( $p = 0.0422$ ) (Fig. 1). Low levels (relative units) of arginine, 0.0163 (0.0139, 0.0182), and lysine, 0.0524 (0.0492, 0.056), associated with FGR, can play an important role in FGR syndrome.

Then we determined serum polyamine levels in patients of the studied groups. In the group of patients with PE, we revealed significant differences from the control group for putrescine ( $p = 0.0423$ ) and spermidine ( $p = 0.022$ ); in the FGR group significant differences from the control group were reported for cadaverine ( $p = 0.0282$ ). When comparing the data of the PE



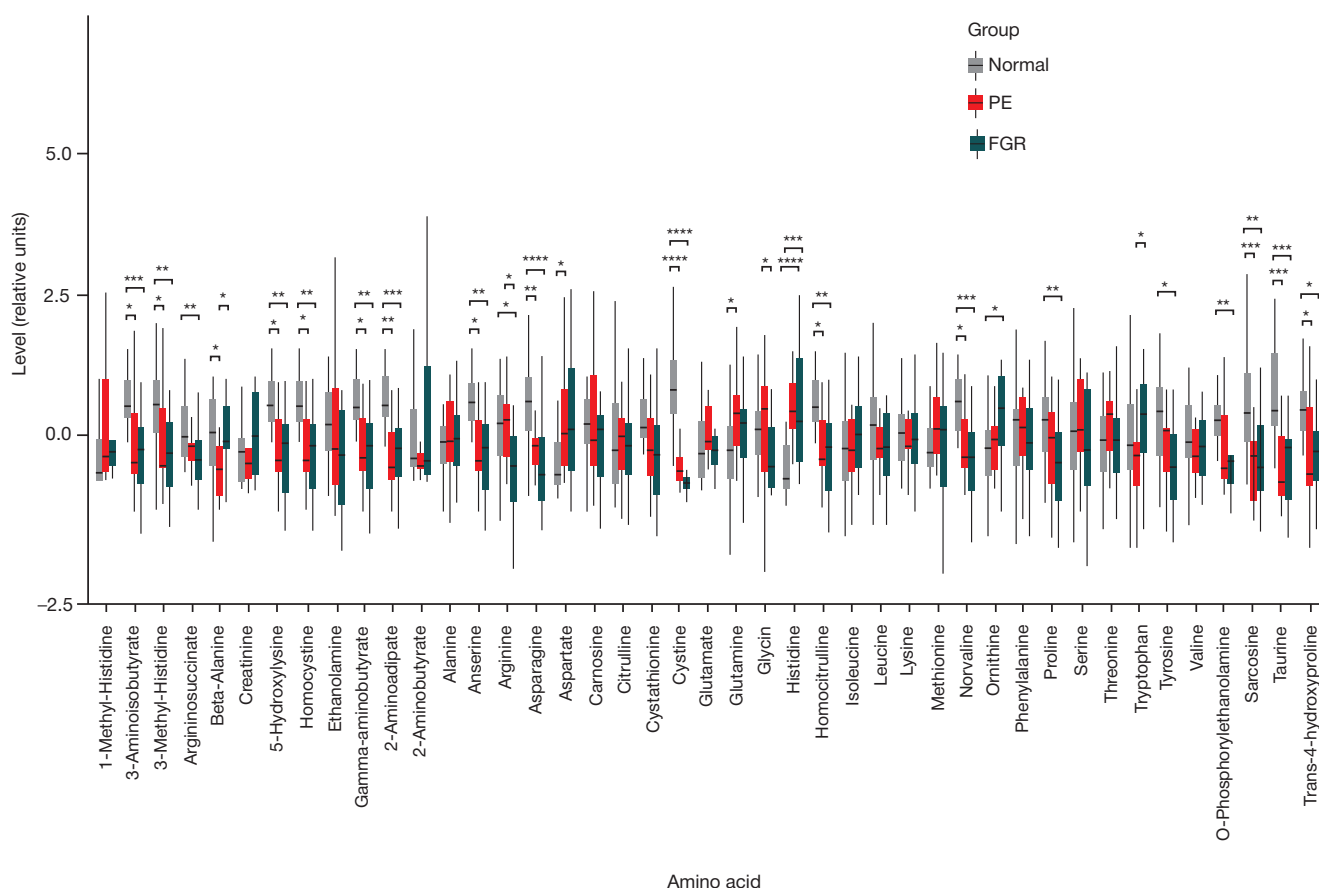


**Fig. 1.** Comparison of plasma amino acid profiles in patients of the groups Normal, PE, and FGR. The first and third quartiles are the margins of the box, while the line in the middle of the box is the median; the ends of whiskers are the difference between the first quartile and the 1.5 interquartile range, the sum of the third quartile and the 1.5 interquartile range

and FGR groups, significant differences were reported for two polyamines: putrescine ( $p = 0.0039$ ) and 1,7-diaminoheptane ( $p = 0.0091$ ) (Fig. 2).

In human body, putrescine is derived from L-ornithine, which involves the ornithine decarboxylase (ODC) enzyme. Spermidine is synthesized from putrescine, which involves two enzymes: spermidine synthase and spermine synthase. These enzymes are the most short-living human enzymes (half-life 5–10 min), which indicates that these are directly involved in protein biosynthesis. Activity of these enzymes can be indirectly estimated based on the spermidine to putrescine ratio (spermidine synthase activity) and spermine to spermidine ratio (spermine synthase activity) (Fig. 3).

The spermidine to putrescine ratio was  $-0.33$  ( $-0.43$ ;  $0.05$ ) in the Normal group of patients,  $-0.21$  ( $-0.29$ ;  $0.25$ ) in the group of patients with PE, and  $-0.34$  ( $-0.44$ ;  $-0.13$ ) in the group of patients with FGR; the spermine to spermidine ratios of these groups were  $0.07$  ( $-0.38$ ;  $0.57$ );  $-0.48$  ( $-0.64$ ;  $-0.08$ );  $-0.33$  ( $-0.65$ ;  $0.52$ ), respectively.

Polyamines are deeply involved in the cellular mechanisms underlying nonspecific stress responses (polyamine stress response). In case of damaging effect on the body, for example when there is nervous tissue ischemia/hypoxia, ODC is activated in the brain, with subsequent increase in polyamine content and triggering of activation of the early response genes (*c-myc*, *c-fos*, etc.) [17].

Considering biological significance of the findings, the search for clinical and laboratory parallels in FGR and PE was of particular interest. For that we performed correlation analysis of the relationship between the levels of important polyamines and amino acids and such clinical indicators, as FGR and PE

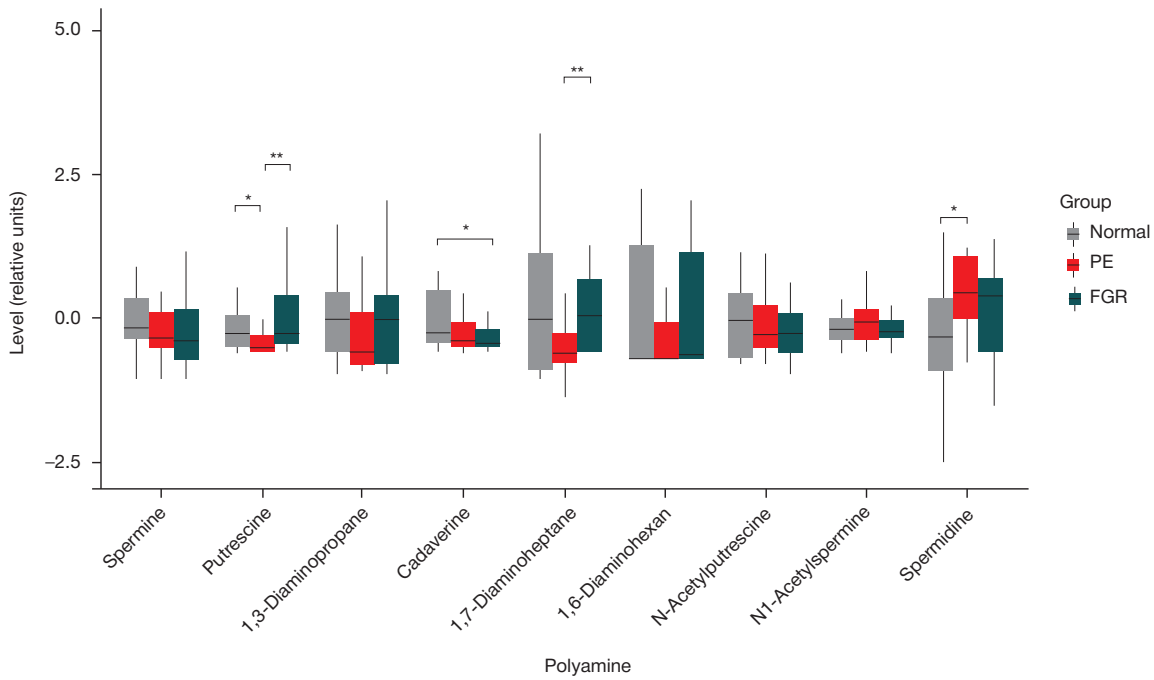
course severity, length of hospital stay in the newborns born to mothers of the FGR and PE groups (Table 2).

Table 2 provides a significant correlation between clinical parameters and plasma levels of amino acids. Plasma levels of trans-4-hydroxyproline showed a significant negative correlation with the fetal condition decompensation in FGR, along with the significant positive correlation with the child's birth weight. Similarly, proline levels showed a significant positive correlation with the child's weight and a significant negative correlation with the fetal condition decompensation in FGR. We also determined that glutamine levels showed a positive correlation with PE severity and a negative correlation with the aspartic acid levels and the length of hospital stay.

Similar analysis was performed for polyamines (Table 2). As for FGR, we revealed a correlation between the severity of this complication and the levels of 1,7-diaminoheptane and cadaverine. Putrescine levels were correlated to PE severity. The length of the newborn's hospital stay in the PE and FGR groups was correlated to the 1,7-diaminoheptane levels.

Of interest are the correlations with proline and 1,7-diaminoheptane revealed. These metabolites show moderate and strong correlations with the clinical data that characterize obstetric outcomes: the child's birth weight and the length of hospital stay, respectively, which makes it possible to consider these as prognostic markers for dynamic assessment of the increasing severity of FGR and early-onset PE.

The mathematical models were constructed in order to ensure primary assessment of the prognostic and diagnostic (assessment of fetal condition severity) capabilities of the above metabolites in terms of assessing the severity of the PE and FGR course and optimization of obstetric tactics for



**Fig. 2.** Comparison of plasma polyamine profiles in patients of the groups Normal, PE, and FGR. The first and third quartiles are the margins of the box, while the line in the middle of the box is the median; the ends of whiskers are the difference between the first quartile and the 1.5 interquartile range, the sum of the third quartile and the 1.5 interquartile range

management of this cohort of pregnant women. Four models including polyamines assessed during the study showed high sensitivity and specificity (Fig. 4).

In the logistic regression model, plasma polyamine levels were independent variables, while the fact that the sample belonged to the PE or FGR group was a dependent variable. The area under the ROC curve for the model was 0.865; sensitivity and specificity were 0.95 and 0.76, respectively. The threshold values for the models constructed were 0.45, 0.3, 0.24, and 0.26.

DISCUSSION

Amino acids are the main building blocks for proteins playing an important role in fetal growth and development. Arginine, lysine, and aspartic acid not only take part in protein synthesis, but are

also important for many biochemical pathways and body functions. Proline has an important function as a component of collagen, the main connective tissue protein. Its effects on the development of placenta and the fetus associated with the enhanced placental transport, angiogenesis, and protein synthesis are well known [18]. The decrease in blood levels of proline observed in pregnant women with FGR and early-onset PE that is directly correlated to the newborn's weight suggests that it can play a role in the pathogenesis of these pregnancy complications. Collagen is an important tissue component of the placental complex, and disruption of its structure in the phase of biosynthesis, secretion or assembly, caused by the proline level decrease, is likely to be one of the existing pathological mechanisms underlying realization of placental insufficiency. There is a report that cervical hydroxyproline concentration decreases in non-pregnant women having a history of cervical incompetence [19].

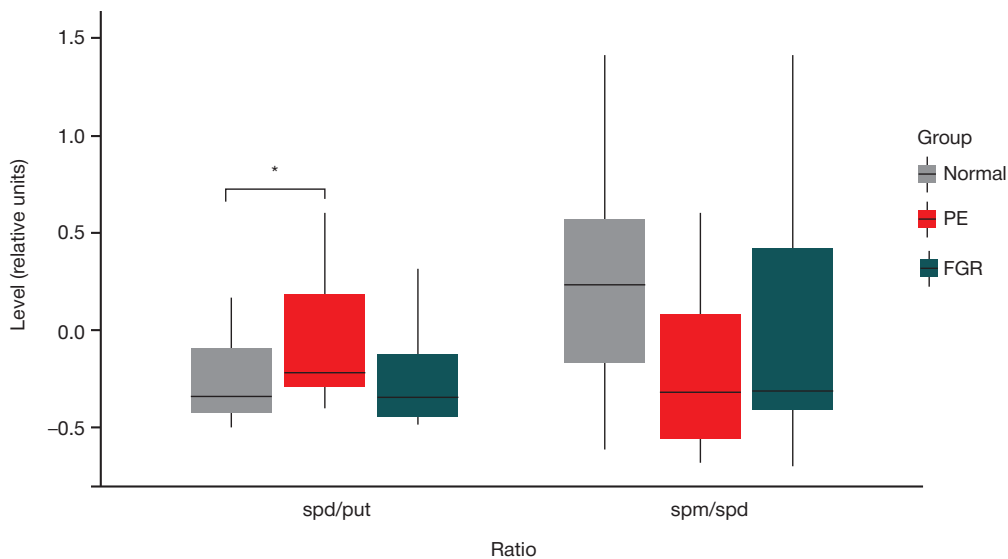


**Fig. 3.** Comparison of physiologically significant ratios of plasma polyamine levels. The first and third quartiles are the margins of the box, while the line in the middle of the box is the median; the ends of whiskers are the difference between the first quartile and the 1.5 interquartile range, the sum of the third quartile and the 1.5 interquartile range. spd/put — spermidine to putrescine ratio (spermidine synthase activity); spm/spd — spermine to spermidine ratio (spermine synthase activity)

**Table 2.** Significant correlation between clinical parameters and the levels of amino acids and polyamines (correlation coefficient, its confidence interval and significance ( $p$ ))

Parameter		R	CI R	$p$
Amino acids				
Fetal condition decompensation in FGR	Proline	-0.56	-0.86 to -0.034	0.03
	Trans-4-hydroxyproline	-0.39	-0.59 to -0.066	0.01
Birth weight	Proline	0.67	0.041 to 0.87	0.02
	Trans-4-hydroxyproline	0.36	0.14 to 0.54	0.002
PE, severity	Glutamine	0.38	0.058 to 0.48	0.01
Length of hospital stay	Aspartic acid	-0.36	-0.5 to -0.088	0.007
Polyamines				
Fetal condition decompensation in FGR	1,7-diaminoheptane	-0.78	-0.92 to -0.37	0.002
	Cadaverine	-0.25	-0.46 to 0.013	0.04
PE, severity	Putrescine	-0.32	-0.52 to 0.083	0.009
Length of newborn's hospital stay	1,7-diaminoheptane	-0.76	-0.95 to 0.23	0.003

Along with the amino acids comprised in proteins, the body has a constant reserve of free amino acids contained in the tissues and various body fluids that are in dynamic equilibrium. During pregnancy free amino acids can serve as inducers of the synthesis of steroid hormones, take part in biosynthesis of glycoproteins, porphyrins, neurotransmitters, polyamines, and nitric oxide.

Metabolism of a number of amino acids results in the synthesis of regulatory polyamines. Polyamines are also found in various body fluids: blood, urine, cerebrospinal fluid, etc. The levels of free polyamines in blood are lower, than in the tissues and urine. However, it is determination of polyamines in blood of pregnant women as a marker of severity of such complications, as PE and FGR, that is of interest for practical medicine.

Assessment of the levels of free amino acids and polyamines can be important for understanding of molecular processes in pregnancy [20].

Our data demonstrate a significant correlation between alteration of blood polyamine levels and placenta-associated

complications of pregnancy. Significant alterations were reported for such polyamines, as spermidine, putrescine, cadaverine, and 1,7-diaminoheptane, in the groups represented by pregnant women with placenta-associated complications. In FGR, the concentration of 1,7-diaminoheptane was significantly increased, against the background of the decrease in individuals with PE. Of particular interest is the fact that this feature observed in patients with FGR was previously reported in our paper on the diagnostic potential of urinary polyamines [21]. The results of our studies resonate with the study of the Chinese researchers, who have considered the effects of N1-guanyl-1,7-diaminoheptane (GC7), the potent deoxyhypusin synthase inhibitor, on proliferation, differentiation, and apoptosis of certain cells [22]. Involvement of diaminoheptanes in expression of cell proliferation proteins and apoptosis of endothelial cells suggests the possibility of using this biomarker for diagnosis of placenta-associated pregnancy complications and prediction of their severity. The increase in blood 1,7-diaminoheptane levels associated with FGR can be

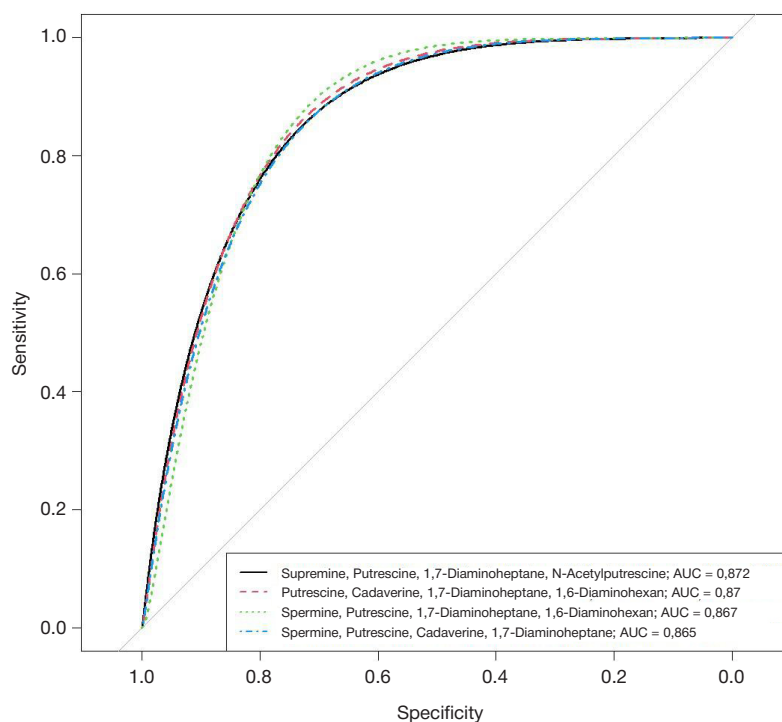


**Fig. 4.** ROC curves of the logistic regression models, in which plasma polyamine levels were independent variables, and the fact that the sample belonged to the PE or FGR group was a dependent variable. The insert shows amino acids, the levels of which a used as independent variables, along with the area under the ROC curve for appropriate logistic regression model

an indirect indicator of the dose-dependent inhibition of cell proliferation and a FGR biomarker, and change depending on the fetal condition severity increase.

Given the diversity and complexity of metabolic pathways responsible for adaptation under conditions of hypoxic damage, it should be expected that their regulation is coordinated. Metabolic pathways of low molecular weight oxidants, proline and polyamines, can be of particular interest in terms of studying regulation of such type.

Normally, homeostasis of proline and polyamines is maintained by the balanced system of their biosynthesis and degradation. The most common precursor in their biosynthesis is glutamate that is a more distant precursor first converted to ornithine or arginine. The resulting amino acids are the direct substrates of two enzymes (ornithine decarboxylase and arginine decarboxylase) catalyzing biosynthesis of putrescine, the precursor of longer polyamines (spermidine and spermine). Despite the determined link between the proline and polyamine synthesis pathways, the question about the possibility of coordinated regulation of metabolism of these low molecular weight compounds, especially in stressful conditions, remains debatable.

Analysis of the blood profile of free amino acids in placenta-associated pregnancy complications was of interest. According to some data, the levels of L-arginine, L-proline, and L-ornithine can reflect perinatal damage to the central nervous system in newborns with intrauterine growth restriction [23]. Significant correlations reported for a number of clinical parameters (fetal

condition decompensation in FGR, PE severity, birth weight, length of stay in the hospital and in the neonatal pathology unit) and such amino acids, as proline and trans-4-hydroxyproline, glutamine and aspartic acid, suggest that these metabolites are involved in protein synthesis, maintenance of ribosome structure and collagen production in FGR, both isolated and combined with early-onset PE.

Considering the fact, that the data were collected in the phase of early clinical manifestations of obstetric syndrome, the possible potential of polyamines for prediction of the course of PE and FGR and the gestational age at delivery is incredibly high. The development of methods for diagnosis and monitoring of polyamine levels in pregnant women is of great interest. Such methods can provide instruments for prediction of the risk of obstetric syndromes and open the window of opportunity for further use of the methods after the in-depth validation and dynamic control depending on the course of FGR and early-onset PE over time.

## CONCLUSIONS

The study of the polyamines' role and correlation with blood levels of free amino acids contributes to the development of methods for diagnosis and prediction of obstetric syndromes, which constitutes an important research area that can result in the emergence of new approaches to assessment and treatment of pregnant women, as well as in improvement of care of the maternal and child health in pregnancy.

## References

- Xuan M, et al. Polyamines: their significance for maintaining health and contributing to diseases. *Cell Communication and Signaling*. 2023; 21 (1): 348.
- Bae D-H, et al. The old and new biochemistry of polyamines. *Biochimica et Biophysica Acta (BBA) — General Subjects*. 2018; 1862 (9): 2053–68.
- Igarashi K, Kashiwagi K. The functional role of polyamines in eukaryotic cells. *Int J Biochem Cell Biol*. 2019; 107: 104–15.
- Zahedi K, Barone S, Soleimani M. Polyamines and Their Metabolism: From the Maintenance of Physiological Homeostasis to the Mediation of Disease. *Medical Sciences*. 2022; 10 (3): 38.
- Abdulhussein AA, Wallace H.M. Polyamines and membrane transporters. *Amino Acids*. 2014; 46 (3): 655–60.
- Damiani E, Wallace HM. Polyamines and Cancer. 2018; 1694: 469–88.
- Holbert CE, Cullen MT, Casero RA Jr, Stewart TM. Polyamines in cancer: integrating organismal metabolism and antitumour immunity. *Nat Rev Cancer*. 2022; 22 (8): 467–80.
- Vrijsen S, Houdou M, Cascalho A, Eggermont J, Vangheluwe P. Polyamines in Parkinson's Disease: Balancing Between Neurotoxicity and Neuroprotection. *Annu Rev Biochem*. 2023; 92: 435–64.
- Proietti E, Rossini S, Grohmann U, Mondanelli G. Polyamines and Kynurenes at the Intersection of Immune Modulation. *Trends Immunol*. 2020; 41 (11): 1037–50.
- Lefèvre PLC, Palin M-F, Murphy BD. Polyamines on the Reproductive Landscape. *Endocr Rev*. 2011; 32 (5): 694–712.
- Aihara S, Torisu K, Uchida Y, Imazu N, Nakano T, Kitazono T. Spermidine from arginine metabolism activates Nrf2 and inhibits kidney fibrosis. *Commun Biol*. 2023; 6 (1): 676.
- Bae DH, Lane DJR, Jansson PJ, Richardson DR. The old and new biochemistry of polyamines. *Biochimica et Biophysica Acta (BBA) — General Subjects*. 2018; 1862 (9): 2053–68.
- Zou D, Zhao Z, Li L, Min Y, Zhang D, Ji A, Jiang C, Wei X, Wu X. A comprehensive review of spermidine: Safety, health effects, absorption and metabolism, food materials evaluation, physical and chemical processing, and bioprocessing. *Compr Rev Food Sci Food Saf*. 2022; 21 (3): 2820–42.
- Cao Y, Liu S, Liu K, Abbasi IHR, Cai C, Yao J. Molecular mechanisms relating to amino acid regulation of protein synthesis. *Nutr Res Rev*. 2019; 32 (2): 183–91.
- Wu G, Meininger CJ, McNeal CJ, Bazer FW, Rhoads JM. Role of L-Arginine in Nitric Oxide Synthesis and Health in Humans. *Adv Exp Med Biol*. 2021; 1332: 167–87.
- Prameswari N, Irwinda R, Wibowo N, Saroyo YB. Maternal Amino Acid Status in Severe Preeclampsia: A Cross-Sectional Study. *Nutrients*. 2022; 14 (5): 1019.
- Berezov TT, Maklecova MG, Fedorova TN. Poli aminy: ih rol' v norme i pri patologii central'noj nervnoj sistemy. *Annaly klinicheskoy i jeksperimental'noj nevrologii*. 2012; 2: 38–48. Russian.
- Wu G, Bazer FW, Burghardt RC, Johnson GA, Kim SW, Knabe DA, Li P, et al. Proline and hydroxyproline metabolism: implications for animal and human nutrition. *Amino Acids*. 2011; 40 (4): 1053–63.
- Petersen LK, Uldbjerg N. Cervical collagen in non-pregnant women with previous cervical incompetence. *Eur J Obstet Gynecol Reprod Biol*. 1996; 67 (1): 41–5.
- Rider JE, Hacker A, Mackintosh CA, Pegg AE, Woster PM, Casero RA Jr. Spermine and spermidine mediate protection against oxidative damage caused by hydrogen peroxide. *Amino Acids*. 2007; 33 (2): 231–40.
- Gasanbekova AP, Frankevich NA, Chagovec VV, Tokareva AO, Kachikovskiy YuN, Novoselova AV, Karapetyan TYe. Rol' poli aminov v neinvazivnoj diagnostike placenta-associirovannyh oslozhnenij beremennosti. *Akusherstvo i ginekologija*. 2024; 2: 52–61. Russian.
- Lee Y, Kim HK, Park HE, Park MH, Joe YA. Effect of N1-guanyl-1,7-diaminoheptane, an inhibitor of deoxyhypusine synthase, on endothelial cell growth, differentiation and apoptosis. *Mol Cell Biochem*. 2002; 237 (1–2): 69–76.
- Krukier II, Avruckaja VV, Narezhnaja EV, Levkovich MA, Kravchenko LV, Nikashina AA, Rozhkov AV, Galusyak AV. Rol' produkcii aminokislot v formirovanii cerebral'nyh porazhenij u novorozhdennyh, rodivshih u materej s placental'noj nedostatochnost'ju i vnutritrobnnoj zaderzhkoj rosta ploda. *Rossijskij vestnik akushera-ginekologa*. 2022; 22 (4): 19. Russian.

## Литература

- Xuan M, et al. Polyamines: their significance for maintaining health and contributing to diseases. *Cell Communication and Signaling*. 2023; 21 (1): 348.
- Bae D-H, et al. The old and new biochemistry of polyamines. *Biochimica et Biophysica Acta (BBA) — General Subjects*. 2018; 1862 (9): 2053–68.
- Igarashi K, Kashiwagi K. The functional role of polyamines in eukaryotic cells. *Int J Biochem Cell Biol*. 2019; 107: 104–15.
- Zahedi K, Barone S, Soleimani M. Polyamines and Their Metabolism: From the Maintenance of Physiological Homeostasis to the Mediation of Disease. *Medical Sciences*. 2022; 10 (3): 38.
- Abdulhussein AA, Wallace H.M. Polyamines and membrane transporters. *Amino Acids*. 2014; 46 (3): 655–60.
- Damiani E, Wallace HM. Polyamines and Cancer. 2018; 1694: 469–88.
- Holbert CE, Cullen MT, Casero RA Jr, Stewart TM. Polyamines in cancer: integrating organismal metabolism and antitumour immunity. *Nat Rev Cancer*. 2022; 22 (8): 467–80.
- Vrijzen S, Houdou M, Cascalho A, Eggermont J, Vangheluwe P. Polyamines in Parkinson's Disease: Balancing Between Neurotoxicity and Neuroprotection. *Annu Rev Biochem*. 2023; 92: 435–64.
- Proietti E, Rossini S, Grohmann U, Mondanelli G. Polyamines and Kynurenines at the Intersection of Immune Modulation. *Trends Immunol*. 2020; 41 (11): 1037–50.
- Lefèvre PLC, Palin M-F, Murphy BD. Polyamines on the Reproductive Landscape. *Endocr Rev*. 2011; 32 (5): 694–712.
- Aihara S, Torisu K, Uchida Y, Imazu N, Nakano T, Kitazono T. Spermidine from arginine metabolism activates Nrf2 and inhibits kidney fibrosis. *Commun Biol*. 2023; 6 (1): 676.
- Bae DH, Lane DJR, Jansson PJ, Richardson DR. The old and new biochemistry of polyamines. *Biochimica et Biophysica Acta (BBA) — General Subjects*. 2018; 1862 (9): 2053–68.
- Zou D, Zhao Z, Li L, Min Y, Zhang D, Ji A, Jiang C, Wei X, Wu X. A comprehensive review of spermidine: Safety, health effects, absorption and metabolism, food materials evaluation, physical and chemical processing, and bioprocessing. *Compr Rev Food Sci Food Saf*. 2022; 21 (3): 2820–42.
- Cao Y, Liu S, Liu K, Abbasi IHR, Cai C, Yao J. Molecular mechanisms relating to amino acid regulation of protein synthesis. *Nutr Res Rev*. 2019; 32 (2): 183–91.
- Wu G, Meininger CJ, McNeal CJ, Bazer FW, Rhoads JM. Role of L-Arginine in Nitric Oxide Synthesis and Health in Humans. *Adv Exp Med Biol*. 2021; 1332: 167–87.
- Prameswari N, Irwinda R, Wibowo N, Saroyo YB. Maternal Amino Acid Status in Severe Preeclampsia: A Cross-Sectional Study. *Nutrients*. 2022; 14 (5): 1019.
- Березов Т. Т., Маклецова Марина Геннадьевна, Федорова Т. Н. Полиамины: их роль в норме и при патологии центральной нервной системы. *Анналы клинической и экспериментальной неврологии*. 2012; 2: 38–48.
- Wu G, Bazer FW, Burghardt RC, Johnson GA, Kim SW, Knabe DA, Li P, et al. Proline and hydroxyproline metabolism: implications for animal and human nutrition. *Amino Acids*. 2011; 40 (4): 1053–63.
- Petersen LK, Ulbjerg N. Cervical collagen in non-pregnant women with previous cervical incompetence. *Eur J Obstet Gynecol Reprod Biol*. 1996; 67 (1): 41–5.
- Rider JE, Hacker A, Mackintosh CA, Pegg AE, Woster PM, Casero RA Jr. Spermine and spermidine mediate protection against oxidative damage caused by hydrogen peroxide. *Amino Acids*. 2007; 33 (2): 231–40.
- Гасанбекова А. П., Франкевич Н. А., Чаговец В. В., Токарева А. О., Качиковски Ю. Н., Новоселова А. В., Карапетян Т. Э. Роль полиаминов в неинвазивной диагностике плаценто-ассоциированных осложнений беременности. *Акушерство и гинекология*. 2024; 2: 52–61.
- Lee Y, Kim HK, Park HE, Park MH, Joe YA. Effect of N1-guanyl-1,7-diaminoheptane, an inhibitor of deoxyhypusine synthase, on endothelial cell growth, differentiation and apoptosis. *Mol Cell Biochem*. 2002; 237 (1–2): 69–76.
- Крукиер И. И., Авруцкая В. В., Нарезная Е. В., Левкович М. А., Кравченко Л. В., Никашина А. А., Рожков А. В., Галусяк А. В. Роль продукции аминокислот в формировании церебральных поражений у новорожденных, родившихся у матерей с плацентарной недостаточностью и внутриутробной задержкой роста плода. *Российский вестник акушера-гинеколога*. 2022; 22 (4): 19.

## DISCRIMINATORY POWER OF MULTIPLEX PCR FOR DETECTION OF MYCOBACTERIAL CO-INFECTION

Smirnova TG<sup>1</sup> ✉, Andreevskaya SN<sup>1</sup>, Ustinova VV<sup>1</sup>, Larionova EE<sup>1</sup>, Kiseleva EA<sup>1</sup>, Chernousova LN<sup>1</sup>, Ergeshov A<sup>1,2</sup><sup>1</sup> Central Tuberculosis Research Institute, Moscow, Russia<sup>2</sup> Yevdokimov Moscow State University of Medicine and Dentistry, Moscow, Russia

The diagnosis of mycobacterial co-infection is one of the pressing public health issues. The study was aimed to determine discriminatory power of multiplex PCR used for species identification when detecting mixed mycobacterial populations. The study involved model samples representing the mixtures of DNA of two mycobacterial species with the ratios of 1 : 1, 1 : 9, 1 : 99, and 1 : 999 and different total DNA concentrations ( $10^3$  gEq/mL to  $10^6$  gEq/mL). The model samples were assessed using the multiplex PCR-based AmpliTube-RV-Differentiation kit (Syntol LLC; Russia). It has been shown that the kit is capable of detecting the mixtures of mycobacterial species with high discriminatory power. The discriminatory power of real-time PCR used for analysis of the mixture of DNA of two mycobacterial species depended on the total DNA content in the sample and varied between 0.1% for high-rate samples (total DNA concentration  $10^6$  gEq/mL) and 50% for low-rate samples (total DNA concentration  $10^3$  gEq/mL) and corresponded to the amount of DNA of the species in the sample of at least  $5 \times 10^2$  gEq/mL. When the amount of DNA of each species in the mixture was at least  $5 \times 10^2$  gEq/mL, the results of PCR test for detection of co-infection did not depend on the mycobacterial species contained in the mixture, which should be taken into account when analyzing PCR results.

**Keywords:** *Mycobacterium tuberculosis* complex, nontuberculous mycobacteria, mycobacterial co-infection, multiplex PCR, mycobacteriosis, tuberculosis

**Funding:** the study was conducted within the framework of the State Assignment of the Central Tuberculosis Research Institute, R&D project No. 122041100246-3 "Interspecific and intraspecific polymorphism of mycobacteria in patients with tuberculosis and mycobacteriosis receiving specific therapy"

**Author contribution:** Smirnova TG — experimental procedure (real-time PCR), data analysis, manuscript draft; Andreevskaya SN — literature review, data interpretation, review of publications on the issue; Ustinova VV — PCR; Larionova EE — data analysis; Kiseleva EA — model sample preparation; Chernousova LN, Ergeshov A — developing the study design; all authors contributed to discussion

✉ **Correspondence should be addressed:** Tatiana G. Smirnova  
Yauza alley, 2, str. 1A, Moscow, 107564, Russia; s\_tatka@mail.ru

**Received:** 21.06.2024 **Accepted:** 16.07.2024 **Published online:** 04.08.2024

**DOI:** 10.24075/brsmu.2024.029

## ДИСКРИМИНИРУЮЩАЯ СПОСОБНОСТЬ МЕТОДА МУЛЬТИПЛЕКСНОЙ ПЦР ПРИ ВЫЯВЛЕНИИ МИКОБАКТЕРИАЛЬНОЙ КОИНФЕКЦИИ

Т. Г. Смирнова<sup>1</sup> ✉, С. Н. Андреевская<sup>1</sup>, В. В. Устинова<sup>1</sup>, Е. Е. Ларионова<sup>1</sup>, Е. А. Киселева<sup>1</sup>, Л. Н. Черноусова<sup>1</sup>, А. Эргешов<sup>1,2</sup><sup>1</sup> Центральный научно-исследовательский институт туберкулеза, Москва, Россия<sup>2</sup> Московский государственный медико-стоматологический университет имени А. И. Евдокимова, Москва, Россия

Диагностика микобактериальной коинфекции — одна из актуальных проблем здравоохранения. Целью исследования было определить дискриминирующую способность метода мультиплексной ПЦР видовой идентификации при выявлении смешанных популяций микобактерий. Исследование выполнено на модельных образцах, представляющих собой смесь ДНК микобактерий двух видов в соотношении 1 : 1, 1 : 9, 1 : 99 и 1 : 999 с разной суммарной концентрацией ДНК (от  $10^3$  ГЭ/мл до  $10^6$  ГЭ/мл). Модельные образцы исследовали набором «Амплитуб-РВ-дифференциация» («Синтол»; Россия), основанном на мультиплексной ПЦР. Показано, что набор способен выявлять смеси видов микобактерий с высокой дискриминирующей способностью. Дискриминирующая способность метода ПЦР в режиме реального времени при анализе смеси ДНК двух видов микобактерий зависела от суммарного содержания ДНК в образце и варьировала от 0,1% для высоконагруженных образцов (суммарная концентрация ДНК  $\times 10^6$  ГЭ/мл) до 50% для низконагруженных образцов (суммарная концентрация ДНК  $\times 10^3$  ГЭ/мл) и соответствовала количеству ДНК вида в смеси не менее  $5 \times 10^2$  ГЭ/мл. При количестве ДНК каждого вида в смеси не менее  $5 \times 10^2$  ГЭ/мл результат ПЦР на выявление коинфекции не зависел от вида микобактерий, входящих в смесь, что необходимо учитывать при анализе результатов ПЦР.

**Ключевые слова:** микобактерии туберкулезного комплекса, нетуберкулезные микобактерии, микобактериальная коинфекция, мультиплексная ПЦР, микобактериоз, туберкулез

**Финансирование:** исследование проведено в рамках выполнения работ по Государственному заданию ФГБНУ "ЦНИИТ" № НИОКТР 122041100246-3 «Межвидовой и внутривидовой полиморфизм микобактерий у больных туберкулезом и микобактериозом на фоне специфической терапии».

**Вклад авторов:** Т. Г. Смирнова — проведение эксперимента (постановка ПЦР в режиме реального времени), анализ полученных данных, подготовка черновика рукописи; С. Н. Андреевская — анализ литературы, интерпретация данных, обзор публикаций по теме статьи; В. В. Устинова — постановка ПЦР; Е. Е. Ларионова — анализ данных; Е. А. Киселева — подготовка модельных образцов; Л. Н. Черноусова, А. Эргешов — разработка дизайна исследования; все авторы участвовали в обсуждении результатов.

✉ **Для корреспонденции:** Татьяна Геннадьевна Смирнова  
Яузская аллея, д. 2, к. 1А, г. Москва, 107564, Россия; s\_tatka@mail.ru

**Статья получена:** 21.06.2024 **Статья принята к печати:** 16.07.2024 **Опубликована онлайн:** 04.08.2024

**DOI:** 10.24075/vrgmu.2024.029

The diseases of mycobacterial etiology, including tuberculosis, constitute a significant challenge to public health. Tuberculosis is the second most common cause of death from infectious diseases [1]. The incidence of tuberculosis in the RF decreases, while the diseases caused by nontuberculous mycobacteria (NTM) become more and more common. The same trend is observed all over the world [2–6]. The researchers believe that

the growing rate of mycobacteriosis is associated with ageing of the global population and increasing rate of congenital and acquired immunodeficiency [4, 7–9].

In some cases, more often in old age and in cases of immunosuppression, the patient can be infected by both *Mycobacterium tuberculosis* complex (MTBC) and NTM or by several species of nontuberculous mycobacteria [2, 10–12]. The

prevalence of mycobacterial co-infection in Russia is 1.16% of all sputum smear-positive patients. The most common combinations of species in the mixed mycobacterial populations are as follows: *M. tuberculosis* + *M. avium*, *M. tuberculosis* + *M. abscessus*, *M. avium* + *M. intracellulare*, *M. avium* + *M. kansasii*, *M. avium* + *M. abscessus* [2].

It is important to diagnose the cases of mixed mycobacterial infection in time, since undetected co-infection by several mycobacterial species inevitably results in treatment failure. The treatment failure results from the fact, that NTM are resistant to the majority of anti-tuberculosis drugs and have species-specific profiles of antibiotic sensitivity [13–15].

Since tuberculosis and mycobacteriosis have similar clinical and radiographic features, these can be differentiated by identification of species in mycobacterial culture by HPLC, mass spectrometry or molecular genetic methods [16–19]. The advantage of molecular genetic diagnosis of tuberculosis and mycobacteriosis is that these methods ensure analysis of both cultures and clinical diagnostic material. In 2021, the Central Tuberculosis Research Institute together with Syntol LLC developed the multiplex PCR-based AmpliTube-NTM-Differentiation test system ensuring differentiation between MTBC and NTM and detection of 12 NTM species (*M. avium*, *M. intracellulare*, *M. xenopi*, *M. chimaera*, *M. kansasii*, *M. gordonae*, *M. lentiflavum*, *M. paragordoniae*, *M. abscessus*, *M. chelonae*, *M. fortuitum*, *M. malmoense*) [20].

According to the purpose, the test system must have a good potential for detection of mycobacterial co-infection, including that caused by several NTM species. Therefore, it seems to be relevant to determine the ability of this kit to detect mixed populations of mycobacteria, depending on the mixture species composition.

The study was aimed to determine discriminatory power of multiplex PCR used for species identification when detecting mixed mycobacterial populations.

## METHODS

### Research object

The model samples represented DNA of mycobacteria most often identified in the mixed populations mixed at various ratios. The model samples were prepared using DNA extracted from the cultures of the following mycobacterial strains from the mycobacterial culture collection of the microbiology department of the Central Tuberculosis Research Institute: *M. tuberculosis* H37Rv (TMC 102), *M. avium*. (ATCC-35719), *M. intracellulare*. (ATCC-25120), *M. kansasii* (ATCC-12478), *M. abscessus* (ATCC-19977).

### Study design

DNA was extracted from the mycobacterial species cultures using the AmpliTube-RV kit (Syntol LLC; Russia). The concentration of DNA of each mycobacterial species

was determined by spectrophotometry (Picopet “Picodrop” spectrophotometer; UK) and adjusted for the number of genomic equivalents. Then we prepared serial dilutions of DNA of each mycobacterial species, which were mixed at the ratios of 1 : 1, 1 : 9, 1 : 99, and 1 : 999; the total DNA concentration of the mixtures was  $10^6$  gEq/mL,  $10^5$  gEq/mL,  $10^4$  gEq/mL, and  $10^3$  gEq/mL. The model samples were assessed using the AmpliTube-NTM-Differentiation kit (Syntol LLC; Russia). Amplification was performed in the CFX96Touch thermal cycler with the optic module (Bio-Rad; USA). Species were identified in accordance with the instructions to the kit based on the presence of fluorescence-enhancement kinetic curves for appropriate signals: kinetic curves in the tube of strip No. 1 reflected accumulation of the amplification products corresponding to specific genome regions of MTBC and/or genome regions specific for all NTM species, while in the tubes No. 2–4 the fluorescence-enhancement kinetic curves corresponded to the presence of the NTM species the kit was targeted at in the DNA sample (Table 1).

Thus, we assessed samples with various DNA load, each of which contained DNA of two mycobacterial species mixed at different ratios (Table 2). Each model sample variant was assessed in 10 replicates.

Discriminatory power of the method was determined based on its detectability limit for two mycobacterial species expressed as the smallest proportion of DNA content of one of the mycobacterial species in a sample found in the mixture in all 10 replicates.

## RESULTS

The results of model DNA sample assessment by multiplex PCR for identification of mycobacterial species are provided in Table 3. Discriminatory power of multiplex PCR used for identification of species depended on the total DNA concentration in the sample. When the total DNA concentration was high ( $10^6$  gEq/mL), the discriminatory power was 0.1; it was 1% at the concentration of  $10^5$  gEq/mL, 10% at the concentration of  $10^4$  gEq/mL, and 50% at the concentration of  $10^3$  gEq/mL. Such pattern was typical for all the studied mycobacterial species and was discernible when differentiating between MTBC and NTM. In model samples of all kinds this smallest proportion of the species corresponded to the mycobacterial species DNA concentration of at least  $5 \times 10^2$  gEq/mL.

The probability of finding each species in the proportion one notch below discriminated (hereinafter, pre-discriminated share) varied between various mycobacterial species contained in the mixture (Table 3). MTBC was most likely to be found in the mixture in the pre-discriminated share ( $1 \times 10^2$  gEq/mL), along with *M. avium* and *M. intracellulare* detected as the second species in 7/10–9/10 replicates, depending on the total DNA content. The probability of finding *M. kansasii* in the pre-discriminated share was slightly lower (5/10–6/10), while the lowest probability was reported for *M. abscessus* (2/10–4/10). The same pattern of the probability of finding mycobacteria in

**Table 1.** The layout of the PCR strip and fluorescence detection channels

№ tube strip	Detection channel			
	FAM	ROX	HEX	Cy5
1	MTBC	NTM	MTBC	–
2	<i>M. avium</i>	<i>M. xenopi</i>	<i>M. intracellulare</i>	<i>M. chimaera</i>
3	<i>M. kansasii</i>	<i>M. gordonae</i>	<i>M. lentiflavum</i>	<i>M. paragordoniae</i>
4	<i>M. abscessus</i>	<i>M. chelonae</i>	<i>M. fortuitum</i>	<i>M. malmoense</i>

Table 2. Characteristics of model DNA samples

Ratio (species 1: species 2)	Concentration of DNA of mycobacterial species in the mixture (gEq/mL) with the total DNA load of the sample:			
	10 <sup>6</sup> gEq/mL	10 <sup>5</sup> gEq/mL	10 <sup>4</sup> gEq/mL	10 <sup>3</sup> gEq/mL
1 : 1	5.00 × 10 <sup>5</sup> / 5.00 × 10 <sup>5</sup>	5.00 × 10 <sup>4</sup> / 5.00 × 10 <sup>4</sup>	5.00 × 10 <sup>3</sup> / 5.00 × 10 <sup>3</sup>	5.00 × 10 <sup>2</sup> / 5.00 × 10 <sup>2</sup>
1 : 9	1.00 × 10 <sup>5</sup> / 9.00 × 10 <sup>5</sup>	1.00 × 10 <sup>4</sup> / 9.00 × 10 <sup>4</sup>	1.00 × 10 <sup>3</sup> / 9.00 × 10 <sup>3</sup>	1.00 × 10 <sup>2</sup> / 9.00 × 10 <sup>2</sup>
1 : 99	1.00 × 10 <sup>4</sup> / 9.90 × 10 <sup>5</sup>	1.00 × 10 <sup>3</sup> / 9.90 × 10 <sup>4</sup>	1.00 × 10 <sup>2</sup> / 9.90 × 10 <sup>3</sup>	1.00 × 10 <sup>1</sup> / 9.90 × 10 <sup>2</sup>
1 : 999	1.00 × 10 <sup>3</sup> / 9.99 × 10 <sup>5</sup>	1.00 × 10 <sup>2</sup> / 9.99 × 10 <sup>4</sup>	1.00 × 10 <sup>1</sup> / 9.99 × 10 <sup>3</sup>	1.00 × 10 <sup>0</sup> / 9.99 × 10 <sup>2</sup>
9 : 1	9.00 × 10 <sup>5</sup> / 1.00 × 10 <sup>5</sup>	9.00 × 10 <sup>4</sup> / 1.00 × 10 <sup>4</sup>	9.00 × 10 <sup>3</sup> / 1.00 × 10 <sup>3</sup>	9.00 × 10 <sup>2</sup> / 1.00 × 10 <sup>2</sup>
99 : 1	9.90 × 10 <sup>5</sup> / 1.00 × 10 <sup>4</sup>	9.90 × 10 <sup>4</sup> / 1.00 × 10 <sup>3</sup>	9.90 × 10 <sup>3</sup> / 1.00 × 10 <sup>2</sup>	9.90 × 10 <sup>2</sup> / 1.00 × 10 <sup>1</sup>
999 : 1	9.99 × 10 <sup>5</sup> / 1.00 × 10 <sup>3</sup>	9.99 × 10 <sup>4</sup> / 1.00 × 10 <sup>2</sup>	9.99 × 10 <sup>3</sup> / 1.00 × 10 <sup>1</sup>	9.99 × 10 <sup>2</sup> / 1.00 × 10 <sup>0</sup>

the mixture in the pre-discriminated share was reported when analyzing the results of differentiating between MTBC and NTM: *M. avium* as NTM in the pre-discriminated share were found in the mixture with *M. tuberculosis* in 8/10–9/10 replicates, with *M. abscessus* in 4/10–5/10 replicates. When the proportion of mycobacterial species was two notches below discriminated (which corresponded to 1.00 × 10<sup>1</sup> gEq/mL), the results of PCR test for this species were negative, and only one dominant species was reported for the mixture.

Thus, it can be concluded that multiplex PCR allows one to detect the mixture of mycobacterial species, if the concentration of DNA of each species is at least 5 × 10<sup>2</sup> gEq/mL. When mycobacterial DNA concentration is lower (1 × 10<sup>2</sup> gEq/mL), sensitivity of the kit used for detection of mixed mycobacterial populations depends on the species composition: the probability of finding MTBC, *M. avium*, and *M. intracellulare* in the mixture is higher, than the probability of finding *M. kansasii* and especially *M. abscessus*.

## DISCUSSION

MTBC and NTM cause human diseases characterized by almost the same clinical and radiographic features [21]. However, the treatment regimens for patients differ radically depending on the causative agent. That is why the need for differential diagnosis of the diseases caused by MTBC and NTM is enshrined in legislation [22, 23]. However, the existing legislation does not take into account the fact that the same patient can be infected with several mycobacterial species and does not define the value of the methods for etiological diagnosis of mycobacterial co-infection.

The molecular genetic methods allowing one to determine the pathogen within 24 h are especially useful for diagnosis of the diseases caused by mycobacteria, in contrast to the culture-based tests, the results of which can be obtained no earlier than in three weeks [24]. There is quite a lot of domestic PCR tests allowing one to detect MTBC and/or differentiate between species of *M. tuberculosis* complex [25]. There are only two kits for detection of NTM registered in the RF: the MTB-Test produced by TestGen (Russia) for detection of MTBC or NTM and the AmpliTube-NTM-Differentiation kit produced by Syntol LLC (Russia) used in our study, which enables both differentiation between MTBC and NTM and identification of NTM species. Therefore, AmpliTube-NTM-Differentiation is the only domestic kit registered in the RF that enables express identification of the species of pathogens causing mycobacterial infections. That is why our study was aimed to estimate the ability of this test to detect mycobacterial co-infection. For that, the model samples representing DNA of various mycobacterial species mixed at various ratios were prepared. It has been

shown that the AmpliTube-NTM-Differentiation kit allows one to detect mycobacterial co-infection, if the concentration of DNA of NTM species in the mixture is at least 5 × 10<sup>2</sup> gEq/mL, of between 0.1 and 50% of species in the mixture depending on the total DNA concentration in the sample.

There is a lack of studies assessing the diagnostic value of molecular genetic methods for detection of mixed infection. Only one study was focused on assessing the GeneXpert methods (Cepheid; USA) and multilocus sequence analysis used for detection of mixed mycobacterial cultures [26]. The authors have shown that GeneXpert can identify MTBC mixed with various NTM species in the proportion of 1% (in the reported study, the detection limit for the species in the mixture is 3000 CFU/mL).

Comparison of discriminatory power of the GeneXpert method and the real-time PCR used in our study has shown that discriminatory power of multiplex PCR used to detect MTBC in the mixed populations is higher than that reported for GeneXpert (5 × 10<sup>2</sup> gEq/mL vs. 3 × 10<sup>3</sup> CFU/mL, respectively). Furthermore, the GeneXpert system detects MTBC only and is unable to detect mixtures of various mycobacteria. In cases of MTBC and NTM co-infection, the GeneXpert test results demonstrate the presence of MTBC only, while in cases when there is a mixture of NTM, the GeneXpert test result is negative.

The earlier reported discriminatory power of the sequencing method [26] depended on the mycobacterial species contained in the mixture. The mixture of MTBC with *M. intracellulare*, *M. kansasii*, *M. abscessus*, and *M. fortuitum* was determined as two species by the sequencing method, when the share of one of two species was at least 1% (3 × 10<sup>3</sup> CFU/mL). When the mixture of MTBC and *M. avium* was assessed by the sequencing method, the presence of *M. avium* in the mixture was determined, if its proportion was at least 10% (3 × 10<sup>4</sup> CFU/mL); when the proportion of *M. avium* was lower than 10%, MTBC only was determined [26]. Therefore, discriminatory power of multiplex PCR is higher, than that of the sequencing method, for the species *M. avium*, *M. intracellulare*, *M. kansasii*, *M. abscessus*. We have not determined discriminatory power of multiplex PCR for the mixture of MTBC + *M. fortuitum*, since, according to our data, the *M. fortuitum* species is not a common cause of mycobacterial diseases and is extremely rare in the mixed populations isolated from patients [2]. The advantage of multiplex PCR over sequencing when used for detection of mycobacterial co-infection is that DNA isolated from mycobacterial cultures is used for sequencing, while DNA isolated directly from the diagnostic material is used for multiplex PCR, which speeds up data acquisition and makes the results independent from the species-specific mycobacterial culture features.



**Table 3.** Results of testing of model samples of the DNA mixture of two mycobacterial species by multiplex PCR

Combination of species (species 1 : species 2)	Ratio	Number of positive PCR results among the tested DNA samples by target detection channels with the total DNA concentration			
		10 <sup>6</sup> gEq/mL	10 <sup>5</sup> gEq/mL	10 <sup>4</sup> gEq/mL	10 <sup>3</sup> gEq/mL
<i>M. tub.</i> : <i>M. avi.</i>	1 : 1	MIX – 10/10	MIX – 10/10	MIX – 10/10	MIX – 10/10
	1 : 9	MIX – 10/10	MIX – 10/10	MIX – 10/10	MIX – 9/10; <i>M. avi.</i> – 1/10
	1 : 99	MIX – 10/10	MIX – 10/10	MIX – 8/10; <i>M. avi.</i> – 2/10	<i>M. avi.</i> – 10/10
	1 : 999	MIX – 10/10	MIX – 9/10; <i>M. avi.</i> – 1/10	<i>M. avi.</i> – 10/10	<i>M. avi.</i> – 10/10
	9 : 1	MIX – 10/10	MIX – 10/10	MIX – 10/10	MIX – 7/10; МБТК – 3/10
	99 : 1	MIX – 10/10	MIX – 10/10	MIX – 7/10; МБТК – 3/10	МБТК – 10/10
	999 : 1	MIX – 10/10	MIX – 8/10; МБТК – 2/10	МБТК – 10/10	МБТК – 10/10
<i>M. tub.</i> : <i>M. abs.</i>	1 : 1	MIX – 10/10	MIX – 10/10	MIX – 10/10	MIX – 10/10
	1 : 9	MIX – 10/10	MIX – 10/10	MIX – 10/10	MIX – 8/10; <i>M. abs.</i> – 2/10
	1 : 99	MIX – 10/10	MIX – 10/10	MIX – 9/10; <i>M. abs.</i> – 1/10	<i>M. abs.</i> – 10/10
	1 : 999	MIX – 10/10	MIX – 8/10; <i>M. abs.</i> – 2/10	<i>M. abs.</i> – 10/10	<i>M. abs.</i> – 10/10
	9 : 1	MIX – 10/10	MIX – 10/10	MIX – 10/10	MIX – 3/10 МБТК – 7/10
	99 : 1	MIX – 10/10	MIX – 10/10	MIX – 3/10; МБТК – 7/10	МБТК – 10/10
	999 : 1	MIX – 10/10	MIX – 4/10; МБТК – 6/10	МБТК – 10/10	МБТК – 10/10
<i>M. avi.</i> : <i>M. int.</i>	1 : 1	MIX – 10/10	MIX – 10/10	MIX – 10/10	MIX – 10/10
	1 : 9	MIX – 10/10	MIX – 10/10	MIX – 10/10	MIX – 7/10; <i>M. int.</i> – 3/10
	1 : 99	MIX – 10/10	MIX – 10/10	MIX – 8/10; <i>M. int.</i> – 2/10	<i>M. int.</i> – 100%
	1 : 999	MIX – 10/10	MIX – 9/10; <i>M. int.</i> – 1/10	<i>M. int.</i> – 10/10	<i>M. int.</i> – 100%
	9 : 01	MIX – 10/10	MIX – 10/10	MIX – 10/10	MIX – 9/10; <i>M. avi.</i> – 1/10
	99 : 1	MIX – 10/10	MIX – 10/10	MIX – 8/10; <i>M. avi.</i> – 2/10	<i>M. avi.</i> – 10/10
	999 : 1	MIX – 10/10	MIX – 8/10; <i>M. avi.</i> – 2/10	<i>M. avi.</i> – 10/10	<i>M. avi.</i> – 10/10
<i>M. avi.</i> : <i>M. kans.</i>	1 : 1	MIX – 10/10	MIX – 10/10	MIX – 10/10	MIX – 10/10
	1 : 9	MIX – 10/10	MIX – 10/10	MIX – 10/10	MIX – 8/10; <i>M. kans.</i> – 2/10
	1 : 99	MIX – 10/10	MIX – 10/10	MIX – 9/10; <i>M. kans.</i> – 1/10	<i>M. kans.</i> – 10/10
	1 : 999	MIX – 10/10	MIX – 8/10; <i>M. kans.</i> – 2/10	<i>M. kans.</i> – 10/10	<i>M. kans.</i> – 10/10
	9 : 1	MIX – 10/10	MIX – 10/10	MIX – 10/10	MIX – 5/10; <i>M. avi.</i> – 5/10
	99 : 1	MIX – 10/10	MIX – 10/10	MIX – 5/10; <i>M. avi.</i> – 5/10	<i>M. avi.</i> – 10/10
	999 : 1	MIX – 10/10	MIX – 6/10; <i>M. avi.</i> – 4/10	<i>M. avi.</i> – 10/10	<i>M. avi.</i> – 10/10
<i>M. avi.</i> : <i>M. abs.</i>	1 : 1	MIX – 10/10	MIX – 10/10	MIX – 10/10	MIX – 10/10
	1 : 9	MIX – 10/10	MIX – 10/10	MIX – 10/10	MIX – 9/10; <i>M. abs.</i> – 1/10
	1 : 99	MIX – 10/10	MIX – 10/10	MIX – 8/10; <i>M. abs.</i> – 2/10	<i>M. abs.</i> – 100%
	1 : 999	MIX – 10/10	MIX – 9/10; <i>M. abs.</i> – 1/10	<i>M. abs.</i> – 10/10	<i>M. abs.</i> – 100%
	9 : 1	MIX – 10/10	MIX – 10/10	MIX – 10/10	MIX – 2/10; <i>M. avi.</i> – 8/10
	99 : 1	MIX – 10/10	MIX – 10/10	MIX – 4/10; <i>M. avi.</i> – 6/10	<i>M. avi.</i> – 10/10
	999 : 1	MIX – 10/10	MIX – 3/10; <i>M. avi.</i> – 7/10	<i>M. avi.</i> – 10/10	<i>M. avi.</i> – 10/10

**Note:** NTM — nontuberculous mycobacteria; MTBC — *Mycobacterium tuberculosis* complex; *M. tub.* — *M. tuberculosis*; *M. avi.* — *M. avium*; *M. int.* — *M. intracellulare*; *M. kans.* — *M. kansasii*; *M. abs.* — *M. abscessus*; MIX — model sample is recognized as the mixture of mycobacterial species; cells with the rate of detecting mycobacterial species in the pre-discriminated share are highlighted in gray.

CONCLUSIONS

The diagnostic value of multiplex PCR used for detection of mixed mycobacterial populations was studied. It was shown that the multiplex PCR-based AmpliTube-NTM-Differentiation kit was capable of detecting mycobacterial mixtures with high discriminatory power. The discriminatory power of real-time PCR used for analysis of the mixture of DNA of two mycobacterial species depended on the total DNA content in the sample and varied between 0.1% for high-rate samples (total DNA concentration 10<sup>6</sup> gEq/mL) and 50% for low-rate samples (total DNA concentration 10<sup>3</sup> gEq/mL), it corresponded to the amount

of DNA of species in the mixture of at least 5 × 10<sup>2</sup> gEq/mL. When the amount of DNA of each species in the mixture was at least 5 × 10<sup>2</sup> gEq/mL, the results of PCR test for co-infection did not depend on the species of mycobacteria contained in the mixture. When the amount of DNA of mycobacterial species in the mixture was below 5 × 10<sup>2</sup> gEq/mL, the PCR results depended on the mycobacterial species: the probability of detecting *M. avium* and *M. abscessus* in the MTBC mixture was higher, than the probability of detecting *M. kansasii*; the lowest probability of being detected in the pre-discriminated share is reported for *M. abscessus*, which should be considered when performing the analysis of PCR results.

## References

- Global tuberculosis report 2023. Geneva: World Health Organization, 2023; 75 p.
- Smirnova TG, Andreevskaya SN, Larionova EE, Chernousova LN, Ergeshov A. Smeshannyye populjatsii mikobakterij u bol'nyh tuberkulezom i mikobakteriozom: chastota vyjavlenija i spektr vidov. *Tuberkulez i social'no-znachimye zabolevanija*. 2023; 2 (42): 19–24. Russian.
- Surkova LK, Zaluckaya OM, Skryagina EM, Nikolenko EN, Jackevich NV, Strinovich AL, i dr. Vydelenie i identifikacija netuberkuleznyh mikobakterij i diagnostika mikobakterioza legkih v Respublike Belarus'. *Klinicheskaja infektologija i parazitologija*. 2020; 9 (2): 161–9. Russian.
- Park SC, Kang MJ, Han CH, Lee SM, Kim CJ, Lee JM, et al. Park SC, Kang MJ, Han CH, Lee SM, Kim CJ, Lee JM, Kang YA. Prevalence, incidence, and mortality of nontuberculous mycobacterial infection in Korea: a nationwide population-based study. *BMC Pulm Med*. 2019; 19 (1): 140.
- Nasiri MJ, Dabiri H, Darban-Sarokhalil D, Hashemi Shahraki A. Prevalence of Non-Tuberculosis Mycobacterial Infections among Tuberculosis Suspects in Iran: Systematic Review and Meta-Analysis. *PLoS One*. 2015; 10 (6): e0129073.
- Brode SK, Daley CL, Marras TK. The epidemiologic relationship between tuberculosis and non-tuberculous mycobacterial disease: a systematic review. *Int J Tuberc Lung Dis*. 2014; 18 (11): 1370–7.
- Henkle E, Winthrop KL. Nontuberculous mycobacteria infections in immunosuppressed hosts. *Clin Chest Med*. 2015; 36 (1): 91–9.
- To K, Cao R, Yegiazaryan A, Owens J, Venketaraman V. General Overview of Nontuberculous Mycobacteria Opportunistic Pathogens: *Mycobacterium avium* and *Mycobacterium abscessus*. *J Clin Med*. 2020; 9 (8): 2541.
- Lin CK, Yang YH, Lu ML, Tsai YH, Hsieh MJ, Lee YC, et al. Incidence of nontuberculous mycobacterial disease and coinfection with tuberculosis in a tuberculosis-endemic region: A population-based retrospective cohort study. *Medicine (Baltimore)*. 2020; 99 (52): e23775.
- Ishiekwene C, Subran M, Ghitan M, Kuhn-Basti M, Chapnick E, Lin YS. Case report on pulmonary disease due to coinfection of *Mycobacterium tuberculosis* and *Mycobacterium abscessus*: Difficulty in diagnosis. *Respir Med Case Rep*. 2017; 20: 123–4.
- Jun HJ, Jeon K, Um SW, Kwon OJ, Lee NY, Koh WJ. Nontuberculous mycobacteria isolated during the treatment of pulmonary tuberculosis. *Respir Med*. 2009; 103 (12): 1936–40.
- Kurahara Y, Tachibana K, Tsuyuguchi K, Suzuki K. Mixed pulmonary infection with three types of nontuberculous mycobacteria. *Intern Med*. 2013; 52 (4): 507–10.
- Andreevskaya SN, Larionova EE, Smirnova TG, Andrievskaya IYu, Kiseleva EA, Chernousova LN. Lekarstvennaja chuvstvitel'nost' medlennorastushhij netuberkuleznyh mikobakterij. *Tuberkulez i bolezni legkih*. 2016; 94 (4): 43–50. Russian.
- Shahraki AH, Heidarieh P, Bostanabad SZ, Khosravi AD, Hashemzadeh M, Khandan S, et al. "Multidrug-resistant tuberculosis" may be nontuberculous mycobacteria. *Eur J Intern Med*. 2015; 26 (4): 279–84.
- Bazzi AM, Abulhamayel Y, Rabaan AA, Al-Tawfiq JA. The impact of the coexistence of *Mycobacterium avium* with *Mycobacterium tuberculosis* on the result of GeneXpert and MGIT susceptibility test. *J Infect Public Health*. 2020; 13 (5): 827–9.
- Makarova MV, Krasnova MA, Moroz AM. Sravnitel'nye dannye primenenija vysokojeffektivnoj zhidkostnoj hromatografii dlja identifikacii mikobakterij, vydelennyh na zhidkoj i plotnoj pitatel'nyh sredah. *Tuberkulez i bolezni legkih*. 2009; 86 (10): 46–48. Russian.
- Shitikov E, Ilina E, Chernousova L, Borovskaya A, Rukin I, Afanas'ev M, et al. Mass spectrometry based methods for the discrimination and typing of mycobacteria. *Infect Genet Evol*. 2012; 12 (4): 838–45.
- Smirnova TG, Andreevskaya SN, Larionova EE, Andrievskaya IYu, Ustinova VV, Chernousova LN. Monitoring vidovogo raznobrazija netuberkuleznyh mikobakterij v rjade oblastej RF s ispol'zovaniem DNK-stripov Genotype *Mycobacterium CM/AS* (Hain Lifescience, Germanija). *Tuberkulez i bolezni legkih*. 2017; 95 (5): 54–59. Russian.
- Starkova DA, Zhuravlev YuV, Vyazovaya AA, Soloveva NS, Kulikova ON, Narvskaya OV. Vidovoe raznobrazие netuberkuleznyh mikobakterij u bol'nyh mikobakteriozom na territorijah Severo-Zapadnogo federal'nogo okruga Rossii. *Tuberkulez i bolezni legkih*. 2019; 97 (6): 16–22. Russian.
- Smirnova T, Ustinova V, Andreevskaya S, Larionova E, Kiseleva E, Chernousova L, et al. Evaluation of a new assay for nontuberculous mycobacteria species identification in diagnostic material and cultures. *Tuberculosis (Edinb)*. 2021; 130: 102124.
- Guntupova LD, Borisov SE, Soloveva IP. Mikobakteriozy vo ftziopul'monologicheskoy praktike: obzor literatury i sobstvennyj opyt. *Prakticheskaja medicina*. 2011; 51 (3): 39–50. Russian.
- Prikaz # 951 MZ RF ot 29.12.2014. Ob utverzhenii metodicheskikh rekomendacij po sovershenstvovaniu diagnostiki i lechenija tuberkuleza organov dyhanija. Russian.
- Sevastyanova YeV, Chernousova LN. Sovremennyye algoritmy mikrobiologicheskoy diagnostiki tuberkuleza. *Tuberkuljoz i bolezni ljogkih*. 2018; 96 (7): 11–17. Russian.
- Ergeshov AE, Chernousova LN, Andreevskaya SN. Novyye tehnologii diagnostiki lekarstvenno-ustojchivogo tuberkuleza. *Vestnik Rossijskoj akademii medicinskih nauk*. 2019; 74 (6): 413–22. Russian.
- Ergeshov AE, Andreevskaya SN, Smirnova TG, Chernousova LN. Tuberkulez s lekarstvennoj ustojchivost'ju vozбудitelja: mehanizmy formirovanija i metody molekularno-geneticheskoy diagnostiki. *Vestnik Rossijskoj akademii medicinskih nauk*. 2023; 78 (6): 609–20. Russian.
- Liang Q, Shang Y, Huo F, Xue Y, Li Y, Dong L, et al. Assessment of current diagnostic algorithm for detection of mixed infection with *Mycobacterium tuberculosis* and nontuberculous mycobacteria. *J Infect Public Health*. 2020; 13 (12): 1967–71.

## Литература

- Global tuberculosis report 2023. Geneva: World Health Organization, 2023; 75 p.
- Смирнова Т. Г., Андреевская С. Н., Ларионова Е. Е., Черноусова Л. Н., Эргешов А. Смешанные популяции микобактерий у больных туберкулезом и микобактериозом: частота выявления и спектр видов. *Туберкулез и социально-значимые заболевания*. 2023; 2 (42): 19–24.
- Суркова Л. К., Залущая О. М., Скрягина Е. М., Николенко Е. Н., Яцкевич Н. В., Стринович А. Л. и др. Выделение и идентификация нетуберкулезных микобактерий и диагностика микобактериоза легких в Республике Беларусь. *Клиническая инфектология и паразитология*. 2020; 9 (2): 161–9.
- Park SC, Kang MJ, Han CH, Lee SM, Kim CJ, Lee JM, et al. Park SC, Kang MJ, Han CH, Lee SM, Kim CJ, Lee JM, Kang YA. Prevalence, incidence, and mortality of nontuberculous mycobacterial infection in Korea: a nationwide population-based study. *BMC Pulm Med*. 2019; 19 (1): 140.
- Nasiri MJ, Dabiri H, Darban-Sarokhalil D, Hashemi Shahraki A. Prevalence of Non-Tuberculosis Mycobacterial Infections among Tuberculosis Suspects in Iran: Systematic Review and Meta-Analysis. *PLoS One*. 2015; 10 (6): e0129073.
- Brode SK, Daley CL, Marras TK. The epidemiologic relationship between tuberculosis and non-tuberculous mycobacterial disease: a systematic review. *Int J Tuberc Lung Dis*. 2014; 18 (11): 1370–7.
- Henkle E, Winthrop KL. Nontuberculous mycobacteria infections in immunosuppressed hosts. *Clin Chest Med*. 2015; 36 (1): 91–9.
- To K, Cao R, Yegiazaryan A, Owens J, Venketaraman V. General Overview of Nontuberculous Mycobacteria Opportunistic Pathogens: *Mycobacterium avium* and *Mycobacterium*

- abscessus. *J Clin Med*. 2020; 9 (8): 2541.
9. Lin CK, Yang YH, Lu ML, Tsai YH, Hsieh MJ, Lee YC, et al. Incidence of nontuberculous mycobacterial disease and coinfection with tuberculosis in a tuberculosis-endemic region: A population-based retrospective cohort study. *Medicine (Baltimore)*. 2020; 99 (52): e23775.
  10. Ishiekwene C, Subran M, Ghitan M, Kuhn-Basti M, Chapnick E, Lin YS. Case report on pulmonary disease due to coinfection of *Mycobacterium tuberculosis* and *Mycobacterium abscessus*: Difficulty in diagnosis. *Respir Med Case Rep*. 2017; 20: 123–4.
  11. Jun HJ, Jeon K, Um SW, Kwon OJ, Lee NY, Koh WJ. Nontuberculous mycobacteria isolated during the treatment of pulmonary tuberculosis. *Respir Med*. 2009; 103 (12): 1936–40.
  12. Kurahara Y, Tachibana K, Tsuyuguchi K, Suzuki K. Mixed pulmonary infection with three types of nontuberculous mycobacteria. *Intern Med*. 2013; 52 (4): 507–10.
  13. Андреевская С. Н., Ларионова Е. Е., Смирнова Т. Г., Андриевская И. Ю., Киселева Е. А., Черноусова Л. Н. Лекарственная чувствительность медленнорастущих нетуберкулезных микобактерий. *Туберкулез и болезни легких*. 2016; 94 (4): 43–50.
  14. Shahraki AH, Heidarieh P, Bostanabad SZ, Khosravi AD, Hashemzadeh M, Khandan S, et al. "Multidrug-resistant tuberculosis" may be nontuberculous mycobacteria. *Eur J Intern Med*. 2015; 26 (4): 279–84.
  15. Bazzi AM, Abulhamayel Y, Rabaan AA, Al-Tawfiq JA. The impact of the coexistence of *mycobacterium avium* with *mycobacterium tuberculosis* on the result of GeneXpert and MGIT susceptibility test. *J Infect Public Health*. 2020; 13 (5): 827–9.
  16. Макарова М. В., Краснова М. А., Мороз А. М. Сравнительные данные применения высокоэффективной жидкостной хроматографии для идентификации микобактерий, выделенных на жидкой и плотной питательных средах. *Туберкулез и болезни легких*. 2009; 86 (10): 46–48.
  17. Shitikov E, Ilina E, Chernousova L, Borovskaya A, Rukin I, Afanas'ev M, et al. Mass spectrometry based methods for the discrimination and typing of mycobacteria. *Infect Genet Evol*. 2012; 12 (4): 838–45.
  18. Смирнова Т. Г., Андреевская С. Н., Ларионова Е. Е., Андриевская И. Ю., Устинова В. В., Черноусова Л. Н. Мониторинг видового разнообразия нетуберкулезных микобактерий в ряде областей РФ с использованием ДНК-стрипов Genotype *Mycobacterium* CM/AS (Hain Lifescience, Германия). *Туберкулез и болезни легких*. 2017; 95 (5): 54–59.
  19. Старкова Д. А., Журавлев Ю. В., Вязовая А. А., Соловьева Н. С., Куликова О. Н., Нарвская О. В. Видовое разнообразие нетуберкулезных микобактерий у больных микобактериозом на территориях Северо-Западного федерального округа России. *Туберкулез и болезни легких*. 2019; 97 (6): 16–22.
  20. Smirnova T, Ustinova V, Andreevskaya S, Larionova E, Kiseleva E, Chernousova L, et al. Evaluation of a new assay for nontuberculous mycobacteria species identification in diagnostic material and cultures. *Tuberculosis (Edinb)*. 2021; 130: 102124.
  21. Гунтупова Л. Д., Борисов С. Е., Соловьева И. П. Микобактериозы во фтизиопульмонологической практике: обзор литературы и собственный опыт. *Практическая медицина*. 2011; 51 (3): 39–50.
  22. Приказ № 951 МЗ РФ от 29.12.2014. Об утверждении методических рекомендаций по совершенствованию диагностики и лечения туберкулеза органов дыхания.
  23. Севастьянова Э. В., Черноусова Л. Н. Современные алгоритмы микробиологической диагностики туберкулеза. *Туберкулез и болезни легких*. 2018; 96 (7): 11–17.
  24. Эргешов А. Э., Черноусова Л. Н., Андреевская С. Н. Новые технологии диагностики лекарственно-устойчивого туберкулеза. *Вестник Российской академии медицинских наук*. 2019; 74 (6): 413–22.
  25. Эргешов А. Э., Андреевская С. Н., Смирнова Т. Г., Черноусова Л. Н. Туберкулез с лекарственной устойчивостью возбудителя: механизмы формирования и методы молекулярно-генетической диагностики. *Вестник Российской академии медицинских наук*. 2023; 78 (6): 609–20.
  26. Liang Q, Shang Y, Huo F, Xue Y, Li Y, Dong L, et al. Assessment of current diagnostic algorithm for detection of mixed infection with *Mycobacterium tuberculosis* and nontuberculous mycobacteria. *J Infect Public Health*. 2020; 13 (12): 1967–71.

## EFFECTIVENESS OF ENRICHING DRUG TREATMENT WITH SYSTEMIC OZONE THERAPY IN PATIENTS WITH POST-COVID ASTHENIC SYNDROME

Soldatenko AA<sup>1</sup>, Gumenyuk LN<sup>2</sup>✉, Berdieva DM<sup>2</sup>, Ponomarchuk EI<sup>2</sup>

<sup>1</sup> Rein-LTD LLC, Avicenna Clinic, Simferopol, Russia

<sup>2</sup> Georgievsky Medical Academy, Vernadsky Crimean Federal University, Simferopol, Russia

Post-COVID asthenic syndrome (PCAS) is still the subject of active study. The study was aimed to assess the effects of systemic ozone therapy used to complement drug therapy on plasma levels of TNF $\alpha$ , IL1 $\beta$ , IL6 and parameters of mental status in patients with PCAS. Two randomized groups of patients with PCAS ( $n = 140$ , age 18–45) were assessed and treated: patients of the index group ( $n = 70$ ) received systemic ozone therapy in addition to drug therapy; patients of the comparison group ( $n = 70$ ) received drug therapy without systemic ozone therapy. Plasma levels of TNF $\alpha$ , IL1 $\beta$ , IL6 were measured and the patients' mental status was assessed using the MFI-20, MoCa, ISI, HARS, and CGI-S scores before and after treatment. After the end of therapy (on day 30) the TNF $\alpha$ , IL1 $\beta$ , IL6 levels reported for the index group showed no significant differences from the values reported for the control group ( $p > 0.05$ ) and were lower, than the values of the comparison group by 39% ( $p = 0.003$ ), 33.3% ( $p = 0.022$ ), and 36.1% ( $p = 0.012$ ), respectively. The changes in mental status were also more pronounced in the index group, than in the comparison group: the average final MFI-20 score was lower by 36.7% ( $p = 0.001$ ), ISI by 50.5% ( $p < 0.001$ ), HARS score by 45.8% ( $p = 0.001$ ), while MoCa score was higher by 10.9% ( $p = 0.046$ ), respectively. In the index group, the number of patients with "no disease" based on CGI-S was 94.2%, while in the comparison group it was 62.9% ( $p = 0.001$ ). In our study adding systemic ozone therapy to drug therapy in patients with PCAS allowed us to achieve normalization of the TNF $\alpha$ , IL1 $\beta$ , IL6 levels and complete reduction of PCAS clinical manifestations in 94.2% of cases. Thus, the use of systemic ozone therapy can be considered as one of the effective and pathogenetically substantiated strategies for combination treatment of patients with PCAS in outpatient settings.

**Keywords:** post-COVID asthenic syndrome, systemic ozone therapy, TNF $\alpha$ , IL1 $\beta$ , IL6

**Author contribution:** Soldatenko AA — study concept and design, data acquisition; Gumenyuk LN — data analysis and interpretation, manuscript writing; Berdieva DM — data acquisition; Ponomarchuk EI — data analysis and interpretation.

**Compliance with ethical standards:** the study was approved by the Ethics Committee of the S.I. Georgievsky Medical Academy, V.I. Vernadsky Crimean Federal University (protocol No. 10 dated 16 October 2021), planned and conducted in accordance with the Declaration of Helsinki. The informed consent was submitted by all individuals included in the study.

✉ **Correspondence should be addressed:** Lesya N. Gumenyuk  
Bulvar Lenina, 5/7, Simferopol, 295006, Republic of Crimea; lesya\_gumenyuk@mail.ru

**Received:** 02.07.2024 **Accepted:** 21.07.2024 **Published online:** 27.08.2024

**DOI:** 10.24075/brsmu.2024.034

## ЭФФЕКТИВНОСТЬ ДОБАВЛЕНИЯ СИСТЕМНОЙ ОЗОНОТЕРАПИИ К ФАРМАКОЛОГИЧЕСКОМУ ЛЕЧЕНИЮ У ПАЦИЕНТОВ С ПОСТКОВИДНЫМ АСТЕНИЧЕСКИМ СИНДРОМОМ

А. А. Солдатенко<sup>1</sup>, Л. Н. Гуменюк<sup>2</sup>✉, Д. М. Бердиева<sup>2</sup>, Э. И. Пономарчук<sup>2</sup>

<sup>1</sup> «ООО Рейн-ЛТД» Клиника Авиценна, Симферополь, Россия

<sup>2</sup> Медицинский институт имени С. И. Георгиевского (структурное подразделение Крымского федерального университета имени В. И. Вернадского), Симферополь, Россия

Постковидный астенический синдром (ПКАС) остается предметом активного изучения. Целью исследования было оценить влияние применения системной озонотерапии в дополнение к фармакотерапии на показатели в плазме крови TNF $\alpha$ , IL1 $\beta$ , IL6 и параметры психического статуса у пациентов с ПКАС. Обследовано и пролечено две рандомизированных группы пациентов с ПКАС ( $n = 140$ , возраст 18–45): пациентам основной группы ( $n = 70$ ) дополнительно к фармакотерапии проводили системную озонотерапию; пациентам группы сравнения ( $n = 70$ ) проводили только фармакотерапию. До и после лечения в плазме крови измеряли уровни TNF $\alpha$ , IL1 $\beta$ , IL6 и оценивали психический статус пациентов по шкалам MFI-20, MoCa, ISI, HARS и CGI-S. По завершении терапии (на 30-й день) в основной группе уровни TNF $\alpha$ , IL1 $\beta$ , IL6 не имели статистически значимых различий с показателями в контрольной группе ( $p > 0,05$ ) и были ниже значений группы сравнения на 39% ( $p = 0,003$ ), 33,3% ( $p = 0,022$ ) и 36,1% ( $p = 0,012$ ) соответственно. Изменения показателей психического статуса также более выражены в основной группе, чем в группе сравнения: средние итоговые баллы MFI-20 ниже на 36,7% ( $p = 0,001$ ), ISI — на 50,5% ( $p < 0,001$ ), HARS — на 45,8% ( $p = 0,001$ ), MoCa — выше на 10,9% ( $p = 0,046$ ) соответственно. В основной группе число пациентов с «отсутствием заболевания» по CGI-S — 94,2%, в группе сравнения — 62,9% ( $p = 0,001$ ). В выполненном нами исследовании добавление системной озонотерапии к фармакотерапии у пациентов с ПКАС позволило добиться нормализации уровней TNF $\alpha$ , IL1 $\beta$ , IL6 и полной редукции клинических проявлений ПКАС в 94,2% случаев. Таким образом, применение системной озонотерапии можно рассматривать в качестве одной из эффективных и патогенетически обоснованных стратегий комплексного лечения пациентов с ПКАС в амбулаторных условиях.

**Ключевые слова:** постковидный астенический синдром, системная озонотерапия, TNF $\alpha$ , IL1 $\beta$ , IL6

**Вклад авторов:** А. А. Солдатенко — замысел и дизайн исследования, сбор данных; Л. Н. Гуменюк — анализ и интерпретация данных, написание статьи; Д. М. Бердиева — сбор данных; Э. И. Пономарчук — анализ и интерпретация данных.

**Соблюдение этических стандартов:** исследование одобрено этическим комитетом Медицинского института имени С. И. Георгиевского ФГАОУ ВО «Крымский федеральный университет им. В. И. Вернадского» (протокол № 10 от 16 октября 2021 г.), спланировано и проведено в соответствии с принципами Хельсинкской декларации. Все лица, включенные в исследование, подписали добровольное информированное согласие.

✉ **Для корреспонденции:** Леся Николаевна Гуменюк  
бульвар Ленина, 5/7, г. Симферополь, 295006, Республика Крым; lesya\_gumenyuk@mail.ru

**Статья получена:** 02.07.2024 **Статья принята к печати:** 21.07.2024 **Опубликована онлайн:** 27.08.2024

**DOI:** 10.24075/vrgmu.2024.034

Post-COVID asthenic syndrome (PCAS), the leading positions in the structure of which are occupied by chronic fatigue, cognitive dysfunction, sleep disorders, and anxiety [1], is still the subject of active study.

According to the literature data, 40–70% of patients, regardless of their age and past COVID-19 severity, suffer from PCAS [2, 3], which is strongly associated with the significant decline in daily functioning (by 64%), professional and social activity (by 70%) [4], and quality of life (by 92.4%) [5]; up to 20% of patients are unable to return to work a year after the acute phase of the infection [6]. Such statistics show high social significance of PCAS.

It has been proven that PCAS is a multifactorial disorder with the complex and poorly understood pathogenesis. In the light of current knowledge, systemic inflammation, the key role in the development of which is played by aberrant cytokine expression, is one of the major links of the disease process associated with PCAS [7]. Tumor necrosis factor (TNF $\alpha$ ) and pro-inflammatory interleukins IL1 $\beta$ , IL6 are considered to be the most important. Plasma levels of these mediators that are increased in patients with PCAS are associated with the severity of clinical manifestations [8, 9]. These data make it possible to consider TNF $\alpha$ , IL1 $\beta$ , and IL6 as potential targets for PCAS therapy and the dynamic changes in these indicators as markers of treatment efficacy [10, 11].

Drug therapy involving the use of drugs of various classes (including antidepressants, tranquilizers, nootropic, neurovascular, and neurometabolic agents, vitamin and mineral supplements, adaptogens) is considered to be a decisive treatment strategy in patients with PCAS [12–14]. Unfortunately, it is currently obvious that these are not always effective both against PCAS symptoms and for the control over the patient's condition and quality of life when used as monotherapy [15]. That is why combinations of several drug classes are often used [16]. It should be emphasized that combination therapy shows higher clinical efficacy [15], however, the use of combination therapy is limited due to potential risk of multiple organ dysfunction and other severe adverse events (such as vertigo, nausea, sleep disorders) and the decrease in patient's adherence to treatment. That is why the use of physical treatment methods capable of enriching monopharmacotherapy of PCAS, increasing treatment efficacy, and preventing polypharmacy becomes relevant [17].

Considering the main mechanisms and clinical manifestations of PCAS, the use of systemic ozone therapy having a potent, broad spectrum of anti-inflammatory effects can be of great interest [18–20]. Furthermore, systemic ozone therapy has multimodal immunomodulatory, antioxidant, metabolic, neuroprotective, and anxiolytic effects [21–24], which is also important for treatment of patients with PCAS. Systemic ozone therapy is well tolerated; there is credible evidence of its efficacy in patients with COVID-19 [25–27]. Thus, in elderly patients (over 60) admitted to the intensive care using due to severe COVID-19, the decrease in C-reactive protein (CRP) levels by 48.2% and IL6 levels by 86.2% was revealed as early as after nine days of using systemic ozone therapy involving five procedures performed daily as part of standard treatment [25]. Some small-scale studies conducted in the specialized hospital settings or under conditions of health resort treatment report the efficacy of ozone therapy as part of the combination treatment regimen for such post-COVID syndrome manifestations, as bilateral polysegmental pneumonia [28], decreased exercise tolerance, sleep disorder, and chronic fatigue [29]. Important results of the studies were as follows: significantly decreased C-reactive protein

(CRP) levels [28, 29], IL6 levels back to normal, restoration of functional status and quality of life (QOL) in 94.6% of patients [29]. These data suggest potential efficacy of systemic ozone therapy as part of PCAS combination treatment. However, to date there is no evidence obtained in randomized controlled trials that would show the effectiveness of complementing drug treatment of PCAS, associated with chronic fatigue, cognitive dysfunction, sleep disorders, and anxiety, with systemic ozone therapy, in outpatient settings.

The study was aimed to assess the effects of systemic ozone therapy used to complement drug therapy on plasma levels of TNF $\alpha$ , IL1 $\beta$ , IL6 and parameters of mental status in patients with PCAS.

## METHODS

Assessment and outpatient treatment of 140 patients (77 females and 63 males) aged 18–45 years (average age 34.2 [32.3; 36.2] years) with asthenic syndrome within the framework of the condition meeting the criteria for U 09.9 Post COVID-19 condition, unspecified (ICD-10) was performed at the Simferopol City Clinical Hospital No. 7 in 2022–2023.

Inclusion criteria: age 18–45 years; body mass index 18.5–24.9 kg/m<sup>2</sup>; history of serologically verified COVID-19; emergence or noticeable progression of the asthenic syndrome symptoms (chronic fatigue, cognitive dysfunction, sleep disorders, anxiety) persisting for 3–12 months after having COVID-19, which cannot be explained by the fact of having another disorder (other than past coronavirus infection); final MFI-20 score  $\geq$  30, MoCa score  $\leq$  26, ISI  $\geq$  8, ESS score  $\geq$  11, HARS score  $\geq$  8; no contraindications to systemic ozone therapy.

Exclusion criteria: body mass index  $<$  18.5 and  $\geq$  25 kg/m<sup>2</sup>; history of mental disorders, including cognitive dysfunction, sleep disorders, mood disorders, and taking psychotropic drugs; history of disorders associated with the use of alcohol or other psychoactive substances; focal neurologic signs (based on the neurological assessment data); structural disorders of the brain (based on magnetic resonance imaging data); increased intracranial pressure; chronic infectious, inflammatory, endocrine, autoimmune, thrombophilic disorders, cancer; taking antibiotics, antiviral, vascular, metabolic, nootropic, anabolic, diuretic, or antioxidant agents, oral contraceptives within 3 months before the beginning of the study; previous drug therapy, psychotherapy or rehabilitation due to PCAS; smoking; refusal to take part in the study.

Patients were randomized into two groups based on the treatment method. The index group consisted of 70 patients (43 females and 27 males, average age 34.3 [32.5; 36.3] years), who received systemic ozone therapy in addition to drug therapy. The comparison group included 70 patients (44 females and 26 males, average age 33.7 [31.9; 35.9] years), who received drug therapy without systemic ozone therapy.

The drug based on the succinic acid complex with trimethylhydrazinium (Biokhimik JSC; Russia) was recommended to patients of both groups as a model of monopharmacotherapy to be used in accordance with the scheme proposed by the manufacturer: orally, 2 capsules twice a day (daily dose 2000 mg) for 30 days. The drug was selected based on the officially approved indications for use in PCAS associated with the increased fatigue, sleep disorders, emotional lability, and cognitive dysfunction [30], as well as on the fact that the drug was effective against PCAS [31]. All patients agreed to pay for the prescribed drug. Patients of the index group received extra systemic ozone therapy in the form of intravenous administration of 200 mL of the ozonized 0.9%

Table 1. Characteristics of patients with PCAS

Indicator	Index group (n = 70)	Comparison group (n = 70)	$P_{1-2}$
	1	2	
Average age, years (median [25%; 75%])	34.3 [32.5; 36.3]	33.7 [31.9; 35.9]	0.781
Females/males	43 (61.4) / 27 (38.6)	44 (62.9) / 26 (37.1)	0.771
Body mass index, kg/m <sup>2</sup> (median [25%; 75%])	20.3 [18.3; 22.6]	21.0 [18.6; 22.7]	0.874
Mild COVID-19 (n, %)	43 (61.4)	44 (62.9)	0.884
Moderate COVID-19 (n, %)	20 (28.5)	20 (28.5)	1
Severe COVID-19 (n, %)	7 (10.0)	6 (8.6)	0.075
Time prior to the onset of PCAS symptoms after the acute COVID-19, months (median [25%; 75%])	4.9 [3.0; 5.7]	4.4 [3.3; 5.1]	0.893
MFI-20 AFS (median [25%; 75%])	81.9 [77.7; 84.9]	81.3 [78.1; 83.9]	0.801
MoCa AFS (median [25%; 75%])	24.2 [24.0; 25.7]	24.1 [24.0; 25.4]	0.881
ISI AFS (median [25%; 75%])	18.2 [16.3; 19.2]	17.7 [16.0; 18.8]	0.867
HARS AFS (median [25%; 75%])	21.3 [19.2; 22.9]	20.9 [18.7; 22.7]	0.891
CGI-S severe disorder (n, %)	41 (58.6)	39 (55.7)	0.072
CGI-S moderate disorder (n, %)	29 (41.4)	31(44.3)	0.07

Note: AFS — average final score.

sodium chloride solution (daily, course of 10 procedures, the first three procedures involving the ozone concentration of 2.0 mg/L, with subsequent ozone concentration increase to 3.0–4.0 mg/L) since the first day of prescribed drug therapy. All patients of the index group and comparison group successfully completed the trial.

A total of 50 generally healthy volunteers, unvaccinated and having no history of COVID-19, were assessed as controls. This group included both females and males aged 18–45 years with the body mass index of 18.5–24.9 kg/m<sup>2</sup>, final MFI-20 scores <30, MoCa scores >26, ISI <8, and HARS scores <8. The non-inclusion criteria for the control group were identical to that for the group of patients with PCAS. The control group was matched by gender (32 females and 18 males), age (33.9 [32.3; 36.6] years, and body mass index (19.3 [18.8; 23.4] kg/m<sup>2</sup>) to the group of patients with PCAS.

All the patients underwent clinical and psychopathological assessment that included collecting patient complaints, assessment of life history and history of the disorder, and assessment of mental status, including using the following methods: Multidimensional Fatigue Inventory (MFI-20) [32], Montreal Cognitive Assessment (MoCa) [33], Insomnia Severity Index (ISI) [34], Hamilton Anxiety Rating Scale (HARS) [35], Clinical Global Impression Scale (CGI), specifically the CGI-S Improvement subscale [36] (before treatment and after 30 days of treatment). Furthermore, any possible adverse event (AE) was recorded.

Assessment of plasma TNF $\alpha$ , IL1 $\beta$ , and IL6 levels by enzyme-linked immunoassay (ELISA) using the tests systems by Vector-Best (Russia) was performed in all healthy volunteers in the control group (once) and patients with PCAS (before treatment and after 30 days of treatment). Blood was collected from the cubital vein in the morning (7.00–9.00) in the fasting state (after the 8–12 h fasting).

Statistical processing of the results was performed using the STATISTICA 8.0 software package (StatSoft.Inc.; USA). Quantitative parameters were presented as the median (Me) with the interquartile range [25th; 75th percentiles (%)], while qualitative parameters were presented as the share and absolute number of values. The Mann-Whitney U test was used for comparative analysis of quantitative parameters, while comparative analysis of qualitative parameters involved the use

of the chi-squared test ( $\chi^2$ ). Spearman's rank correlation was used for correlation analysis. The differences were considered significant at  $p < 0.05$ .

## RESULTS

The main characteristics of patients with PCAS are provided in Table 1. The groups of patients were matched by all parameters.

Initially, patients of the index group and comparison group showed a comparable significant increase in plasma levels of TNF $\alpha$ , IL1 $\beta$ , and IL6 relative to the control group. After the end of therapy (on day 30) the TNF $\alpha$ , IL1 $\beta$ , and IL6 levels significantly decreased ( $p < 0.05$ ) in both groups, however, the differences in the decrease were very large. In the index group, the TNF $\alpha$ , IL1 $\beta$ , and IL6 levels showed no significant differences from the values of the control group ( $p > 0.05$ ) and were lower, than the values of the comparison group, by 39% ( $p = 0.003$ ), 33.3% ( $p = 0.022$ ), and 36.1% ( $p = 0.012$ ), respectively (Table 2).

The dynamic changes in the mental status parameters associated with treatment of patients with PCAS are provided in Table 3. The findings suggest that after the end of therapy (on day 30) the changes were significant ( $p < 0.05$ ) and more pronounced in the index group. The average difference in the changes between the index group and the comparison group based on the average final MFI-20 score was 36.7% ( $p = 0.001$ ), MoCa — 10.9% ( $p = 0.046$ ), ISI — 50.5% ( $p < 0.001$ ), HARS — 45.8% ( $p = 0.001$ ). In the index group, the number of patients with “no disease” based on CGI-S subscale was 66 (94.2%), while in the comparison group it was 44 (62.9%) ( $p = 0.001$ ).

No adverse events were reported for patients of the index group and comparison group during the study.

## DISCUSSION

As noted above, the levels of pro-inflammatory cytokines TNF $\alpha$ , IL1 $\beta$ , and IL6 in blood plasma are significantly increased in PCAS [37]; these cytokines cause activation of macrophages and microglial cells after crossing the blood-brain barrier at the damaged sites or sites with increased permeability [38]. This causes cell morphology transformation and initiation of the IBA1 antigen expression. The result is secretion of de novo cytokines (especially IL1 $\beta$  and TNF $\alpha$ ) in the brain and neuroinflammation

**Table 2.** Dynamic changes in the plasma TNF $\alpha$ , IL1 $\beta$ , IL6 levels during treatment of patients with PCAS (median [25%; 75%])

Indicator	Control	Index group (n = 70)		Comparison group (n = 70)		$\Delta_{3-5} / p_{3-5}$
		Before treatment	After treatment	Before treatment	After treatment	
	1	2	3	4	5	
TNF $\alpha$ , pg/mL	5.2 [2.8; 7.6]	14.9 [9.1; 15.2]	6.1 [3.6; 8.2]	15.2 [8.8; 15.7]	10.0 [7.4; 12.3]	39.0% / 0.003
		$\Delta_{3-2}$ -59.1%, $p_{3-2} < 0.001$		$\Delta_{5-4}$ -34.2%, $p_{5-4} = 0.002$		
		$p_{2-1} < 0.001$ , $p_{3-1} = 0.074$		$p_{4-1} < 0.001$ , $p_{5-1} = 0.001$		
IL1 $\beta$ , pg/mL	2.9 [1.5; 4.1]	8.1 [6.6; 10.3]	3.6 [2.5; 4.8]	8.0 [6.4; 10.1]	5.4 [4.7; 7.3]	33.3% / 0.022
		$\Delta_{3-2}$ -55.6%, $p_{3-2} = 0.001$		$\Delta_{5-4}$ -32.5%, $p_{5-4} = 0.021$		
		$p_{2-1} < 0.001$ , $p_{3-1} = 0.079$		$p_{4-1} < 0.001$ , $p_{5-1} = 0.033$		
IL6, pg/mL	3.8 [2.0; 5.6]	9.9 [6.7; 12.4]	3.9 [2.7; 6.2]	9.6 [6.4; 13.0]	6.1 [5.5; 9.3]	36.1% / 0.012
		$\Delta_{3-2}$ -60.6%, $p_{3-2} < 0.001$		$\Delta_{5-4}$ -36.5%, $p_{5-4} = 0.016$		
		$p_{2-1} < 0.001$ , $p_{3-1} = 0.082$		$p_{4-1} < 0.001$ , $p_{5-1} = 0.026$		

**Note:**  $p$  — significance of differences between the groups compared,  $\Delta$  — difference of changes.

[39]. At the same time, neuroinflammation is recognized as the most important mechanism, through which cytokines that change molecular and epigenetic processes eventually cause cell plasticity disturbances, nervous tissue dysfunction [40], and clinical manifestations of PCAS [41, 42]. The broad spectrum of the systemic ozone therapy anti-inflammatory effects is well understood and rather complex. Systemic ozone therapy inhibits transcription activity of the intracellular NF- $\kappa$ B signaling pathway, which results in suppression of the release of a number of inflammatory mediators involved in inflammatory response, such as IL1 $\beta$ , IL6, and TNF $\alpha$  [18]. Furthermore, the activity of the nuclear factor-erythroid-2-related factor 2 (Nrf2) is intensively suppressed [43], which is manifested in the increased activity of the antioxidant enzymes (superoxide dismutase, glutathione peroxidase, catalase) [44, 45] involved in inhibition of inflammation through their influence on the cytokine expression [46]. Moreover, systemic ozone therapy inhibits the p38MAPK and ERK1/ERK2 signaling, thereby reducing TNF $\alpha$  and IL1 $\beta$  production by monocytes [47]. Multiple studies have proven that the systemic ozone therapy effects are consistent, safe, and show high therapeutic potential in many disorders, the common pathogenetic link of which is inflammation, including COVID-19 [25–27]. To date, only three studies have been published (one observational and two randomized controlled trials (RCT)), the authors of which assessed efficacy and safety of systemic ozone therapy used as monotherapy or as part of combination treatment in patients with post-COVID syndrome.

Thus, in one observational study 100 patients (average age  $55.2 \pm 12.72$  years) with PCAS symptoms received systemic ozone therapy: 2–3 procedures per week (course of 6–9 procedure) [48]. Complete reduction of asthenic symptoms and significant (60%) decrease in the symptom severity (based on the Fatigue Severity Scale scores) was reported in 40% of patients by the end of the follow-up period.

In another study, efficacy and safety of the systemic ozone therapy inclusion in the combination treatment (rehabilitation exercises, physical therapy: low-frequency magnetic therapy and iontophoresis with KI, CaCl $_2$ ) of the hospitalized patients aged 29–78 years with post-COVID bilateral polysegmental pneumonia in the second phase of rehabilitation were assessed in the RCT [28]. Significantly better results based on CRP, D-dimer, overall assessment of clinical status, and achieved improvement of the quality of life were reported for the group of patients, who received systemic ozone therapy.

Efficacy of systemic ozone therapy added to the standard resort treatment complex was also assessed in the RCT involving examination of 140 patients (males — 44.3%,

females — 55.7%, average age 49.2 [46.5; 52.3] years) with post-COVID syndrome, who still experienced chronic fatigue, depressed mood, shortness of breath, exercise intolerance 7 months after having the novel coronavirus infection [29]. Patients were randomized into two groups: group 1 ( $n = 70$ ) underwent systemic ozone therapy in the form of intravenous drop infusions of the ozonized saline solution with the ozone concentration of 2.0 mg/L, course of 10 procedures, one procedure per day + resort treatment complex (climate therapy, rehabilitation exercises, full body massage with the focus on the chest, pelotherapy with the Saki Lake mud, hyaluronic acid inhalations); patients of group 2 ( $n = 70$ ) received the same resort treatment complex without systemic ozone therapy. The resort treatment duration was 14 days. The study showed that inclusion of systemic ozone therapy ensured a significant decrease in the malondialdehyde levels (3.3-fold,  $p < 0.001$ ), increase in the glutathione peroxidase activity (1.7-fold,  $p = 0.003$ ), normalization of the IL6 levels, which were accompanied by significant improvement of the clinical status and quality of life in 94.6% of patients (vs. 62.3% in group 2). It is important to note that the results of the above studies show both efficacy and good safety profile of systemic ozone therapy in patients with post-COVID syndrome [29, 49].

In this study, the results of using systemic ozone therapy to complement drug therapy in patients with PCAS, associated with chronic fatigue, cognitive dysfunction, sleep disorders, and anxiety, in outpatient settings are presented.

Reliance on the systemic ozone therapy efficacy was considered to be associated with the broad spectrum of its anti-inflammatory effects, which was fully confirmed in our study. After the end of therapy (on day 30) the levels of TNF $\alpha$  decreased by 59.1% — from 14.9 [9.1; 15.2] pg/mL to 6.1 [3.6; 8.2] pg/mL, IL1 $\beta$  by 55.6% — from 8.1 [6.6; 10.3] pg/mL to 3.6 [2.5; 4.8] pg/mL, i.e. were completely back to normal and more than 30% lower compared to the comparison group ( $p = 0.003$  and  $p = 0.022$ , respectively). The IL6 levels were also significantly lower (by 36.5%), than in the comparison group ( $p = 0.012$ ). Apparently, this can be considered as one manifestation of the systemic ozone therapy anti-inflammatory effect in patients with PCAS. Our findings demonstrate the anti-inflammatory effect and benefits of adding systemic ozone therapy to drug therapy for adjustment of the TNF $\alpha$ , IL1 $\beta$ , and IL6 level changes in patients with PCAS. Since elevated levels of these cytokines are strongly associated with the PCAS clinical manifestation severity and outcome [8, 9], the above data make it possible to consider adding systemic ozone therapy not only effective, but also maximally pathogenetically substantiated.

**Table 3.** Dynamic changes in the mental status parameters during treatment of patients with PCAS

Indicator	Index group (n = 70)		Comparison group (n = 70)		$\Delta_{4-2} / p_{4-2}$
	Before treatment	After treatment	Before treatment	After treatment	
	1	2	3	4	
MFI-20 AFS (median [25%; 75%])	81.9 [77.7; 84; 9]	20.5 [18.1; 22.3]	81.6 [78.3; 84; 6]	32.4 [29.0; 34.2]	36.7% / 0.001
	$\Delta_{2-1} -74.7\%$ , $p_{2-1} < 0.001$		$\Delta_{4-3} -60.3\%$ , $p_{4-3} < 0.001$		
MoCa AFS (median [25%; 75%])	24.2 [24.0; 25.7]	28.5 [27.3; 29.5]	24.5 [24.2; 25.6]	25.7 [25.1; 26.2]	10.9% / 0.046
	$\Delta_{2-1} +17.1\%$ , $p_{2-1} = 0.041$		$\Delta_{4-3} +4.9\%$ , $p_{4-3} = 0.072$		
ISI AFS (median [25%; 75%])	18.2 [16.3; 19.2]	5.0 [3.7; 7.5]	17.7 [16.0; 18.5]	10.1 [9.3; 11.7]	50.5% / <0.001
	$\Delta_{2-1} -81.3\%$ , $p_{2-1} < 0.001$		$\Delta_{4-3} -42.9\%$ , $p_{4-3} = 0.001$		
HARS AFS (median [25%; 75%])	21.3 [19.2; 22.9]	5.8 [4.3; 6.8]	20.7 [18.8; 23.1]	10.7 [9.5; 12.1]	45.8 / 0.001
	$\Delta_{2-1} -72.8\%$ , $p_{2-1} < 0.001$		$\Delta_{4-3} -48.3\%$ , $p_{4-3} < 0.001$		
CGI-S no disease (n, %)	0	66 (94.2)	0	44 (62.9)	49.8% / 0.001
	$p_{2-1} < 0.001$		$p_{4-3} < 0.001$		
CGI-S mild disorder (n, %)	0	4 (5.8)	0	19 (27.1)	78.6% / 0.001
	$p_{2-1} = 0.072$		$p_{4-3} < 0.001$		
CGI-S severe disorder (n, %)	41 (58.6)	0	39 (55.7)	0	5.0% / 0.893
	$p_{2-1} = 0.001$		$p_{4-3} = 0.001$		
CGI-S moderate disorder (n, %)	29 (41.4)	0	31 (44.3)	0	7.0% / 0.887
	$p_{2-1} = 0.001$		$p_{2-1} = 0.001$		

**Note:** AFS — average final score,  $\Delta$  — difference of changes.

As a result, after the end of therapy (on day 30) we managed to achieve significant clinical status improvement in the form of significant steady decrease in the severity of all PCAS symptoms in patients with PCAS from the ozone therapy group, which was confirmed by the dynamic changes in the MFI-20, MoCa, ISI, and HARS scores. In particular, after the end of therapy (on day 30) the total MFI-20 chronic fatigue severity score significantly decreased (by 74.7%) from the median score of 81.9 “severe” to 20.5 “no symptoms of chronic fatigue”; ISI — from the median score of 18.2 “moderate insomnia” to 5.0 “normal” (the average decrease in the indicator was 81.3%); HARS — from the median score of 21.3 “moderate anxiety severity” to 5.8 “no anxiety” (the average decrease in the indicator was 72.8%). The total MoCa cognitive status score increased by 17.1% from the median score of 24.2 “cognitive impairment” to 28.5 “normal cognition”. All the indicators achieved were significantly superior to the indicators of the comparison group ( $p = 0.001$ ).

Finally, after the end of therapy (on day 30) the number of patients with “no disease”, i.e. complete reduction of PCAS clinical manifestations based on CGI, in the systemic ozone therapy group was 94.2%, and there were much more such

patients, than in the comparison group ( $p = 0.001$ ). These data are consistent with the results of assessing other efficacy parameters and confirm clinical benefits of adding systemic ozone therapy to drug therapy in patients with PCAS.

In our study, tolerability of the systemic ozone therapy added to drug treatment in patients with PCAS was good (no adverse events were reported), which was in line with the data of the earlier studies [28, 29].

Thus, according to the findings, the use of systemic ozone therapy to complement drug therapy is highly effective and safe in patients with PCAS.

## CONCLUSIONS

In our study, adding systemic ozone therapy to drug treatment in patients with PCAS made it possible to achieve normalization of the TNF $\alpha$ , IL1 $\beta$ , and IL6 levels and complete reduction of PCAS clinical manifestations in 94.2% of cases. The use of systemic ozone therapy can be considered as one effective and pathogenetically substantiated strategy for combination treatment of patients with PCAS in outpatient settings.

## References

- Buttery S, Philip KEJ, Williams P, Fallas A, West B, Cumella A, et al. Patient symptoms and experience following COVID-19: results from a UK-wide survey. *BMJ Open Respir Res.* 2021; 8 (1): e001075. DOI: 10.1136/bmjresp-2021-001075.
- Chen C, Hauptert SR, Zimmermann L, Shi X, Fritsche LG, Mukherjee B. Global Prevalence of Post COVID-19 Condition or Long COVID: A Meta-Analysis and Systematic Review. *J Infect Dis.* 2022; 226: 1593–607. DOI: 10.1093/infdis/jiac136
- Seang S, Itani O, Monsel G, Abdi B, Marcelin AG, Valantin MA, et al. Long COVID-19 symptoms: Clinical characteristics and recovery rate among non-severe outpatients over a six-month follow-up. *Infect Dis Now.* 2022; 52: 165–9. DOI: 10.1016/j.idnow.2022.02.005.
- Boutou AK, Asimakos A, Kortianou E, Vogiatzis I, Tzouveleki A. Long COVID-19 pulmonary sequelae and management considerations. *J Personal Med.* 2021; 11 (9): 838. DOI: 10.3390/jpm11090838.
- Vélez-Santamaría R, Fernández-Solana J, Méndez-López F, Domínguez-García M, González-Bernal JJ, Magallón-Botaya R, et al. Functionality, physical activity, fatigue and quality of life in patients with acute COVID-19 and Long COVID infection. *Sci Rep.* 2023; 14: 13 (1): 19907. DOI: 10.1038/s41598-023-47218-1.
- Rooney S, Webster A, Paul L. Systematic Review of Changes and Recovery in Physical Function and Fitness after Severe Acute Respiratory Syndrome-Related Coronavirus Infection: Implications for COVID-19 Rehabilitation. *Phys Ther.* 2020; 100: 1717–29. DOI: 10.1093/ptj/pzaa129.
- Schultheiß C, Willscher E, Paschold L, Gottschick C, Klee B, Glasauer S,



- et al. From online data collection to identification of disease mechanisms: the IL1 $\beta$ , IL6 and TNF $\alpha$  cytokine triad is associated with post-acute sequelae of COVID-19 in a digital research cohort. SSRN Electron J [Internet]. 2021. DOI: 10.2139/ssrn.3963839.
8. Salamanna F, Veronesi F, Martini L, Landini MP, Fini M. Post-COVID-19 syndrome: the persistent symptoms at the post-viral stage of the disease: a systematic review of the current data. *Frontiers in medicine*. 2021; 8: 392. DOI: 10.3389/fmed.2021.653516.
  9. Liu Z, Lv Z, Zhou X, Shi J, Hong S, Huang H, Lv L. Efficacy of traditional Chinese exercises in patients with post-COVID-19 chronic fatigue syndrome: A protocol for systematic review and meta-analysis. *Medicine (Baltimore)*. 2022; 18: 101 (46): e31450. DOI: 10.1097/MD.00000000000031450.
  10. Kappelmann N, Dantzer R, Khandaker GM. Interleukin-6 as potential mediator of long-term neuropsychiatric symptoms of COVID19. *Psychoneuroendocrinology*. 2021; 131: 105295. DOI: 10.1016/j.psyneuen.2021.105295.
  11. Yin JX, Agbana YL, Sun ZS, Fei SW, Zhao HQ, Zhou XN, et al. Increased interleukin-6 is associated with long COVID-19: a systematic review and meta-analysis. *Infect Dis Poverty*. 2023; 12 (1): 43. DOI: 10.1186/s40249-023-01086-z.
  12. Zaharov DV, Buryak YU. Postkovidnye kognitivnye rasstrojstva. Sovremennyj vzglyad na problemu, patogenezu i terapiyu. *Obozrenie psikiatrii i medicinskoj psihologii im. V. M. Bekhtereva*. 2021; 55 (4): 97–105. Russian.
  13. Hasanova DR, Zhitkova YU, Vaskaeva GR. Postkovidnyj sindrom: obzor znaniy o patogeneze, neiropsihiatricheskikh proyavleniyah i perspektivah lecheniya. *Nevrologiya, neiropsihiatriya, psihosomatika*. 2021; 13 (3): 93–98. Russian.
  14. Ahmedzhanova LT, Ostroumova TM, Soloha OA. Vedenie pacientov s bolevymi sindromami na fone COVID-19. *Nevrologiya, neiropsihiatriya, psihosomatika*. 2021; 13 (5): 96–101. Russian.
  15. Haibullina DH, Maksimov YuN. Astenicheskiy postkovidnyj sindrom. *Zhurnal nevrologii i psikiatrii im. S. S. Korsakova*. 2023; 123 (3): 61–69. DOI: 10.17116/inevro202312303161. Russian.
  16. Naumov KM, Andreeva GO, Bazhenov DA. Differencirovannyj podhod k korrekcii vegetativnyh narushenij pri postkovidnom sindrome. *Izvestiya Rossijskoj Voenno-medicinskoj akademii*. 2021; 40 (S4): 88–91. Russian.
  17. Bahareva ON, Baharev SA, Konov KYu, Vanteev DA, Lyagushin RS. Nevrologicheskie proyavleniya postkovidnogo sindroma i vozmozhnosti rehabilitacii. *Lazernaya medicina*. 2021; 25 (1): 16–20. Russian.
  18. AlMogbel AA, Albarak MI, AlNumair SF. Ozone Therapy in the Management and Prevention of Caries. *Cureus*. 2023; 15 (4): e37510. DOI: 10.7759/cureus.37510.
  19. Bette M, Cors E, Kresse C, Schütz B. Therapeutic treatment of superoxide dismutase 1 (G93A) amyotrophic lateral sclerosis model mice with medical ozone decelerates trigeminal motor neuron degeneration, attenuates microglial proliferation, and preserves monocyte levels in mesenteric lymph nodes. *Int J Mol Sci*. 2022; 23: 3403. DOI: 10.3390/ijms23063403.
  20. Wang Z, Zhang A, Meng W, Wang T, Li D, Liu Z, Liu H. Ozone protects the rat lung from ischemia-reperfusion injury by attenuating NLRP3-mediated inflammation, enhancing Nrf2 antioxidant activity and inhibiting apoptosis. *Eur J Pharmacol*. 2018; 835: 82–93. DOI: 10.1016/j.ejphar.2018.07.059.
  21. Sallustio F, Cardinale G, Voccola S, Picerno A, Porcaro P, Gesualdo L. Ozone eliminates novel coronavirus Sars-CoV-2 in mucosal samples. *New Microbes New Infect*. 2021; 43: 100927. DOI: 10.1016/j.nmni.2021.100927.
  22. Zheng Z, Dong M, Hu K. A preliminary evaluation on the efficacy of ozone therapy in the treatment of COVID-19. *J Med Virol*. 2020; 92: 2348–50. DOI: 10.1002/jmv.26040.
  23. Díaz-Soto MT, Pérez AF, Vaillant JD, Mallok A, Viebahn-hänsler R, Menéndez C, et al. Ozone Therapy Ameliorates Nervous System Disorders and Oxidative Stress in Patients During Ethanol Withdrawal - A Pilot Study. *Ozone: Science & Engineering*. 2012; 34 (6): 432–37. DOI: 10.1080/01919512.2012.717858.
  24. Rudnev IE, Proshchenko IV, Maksimova NE. Ozonoterapiya pri trevoznyh i depressivnyh rasstrojstvah s panicheskimi atakami. *Verhnevolzhskij medicinskij zhurnal*. 2018; 17 (4): 18–21. Russian.
  25. Franzini M, Valdenassi L, Ricevuti G, Chirumbolo S, Depfenhart M, Bertossi D, Tirelli U. Oxygen-ozone (O2–O3) immunocellular therapy for patients with COVID-19 Preliminary evidence reported. *Int Immunopharmacol*. 2020; 88: 106879. DOI: 10.1016/j.intimp.2020.106879.
  26. Shah M, Captain J, Vaidya V, Kulkarni A, Valsangkar K, Nair PMK, Ganu G. Safety and efficacy of ozone therapy in mild to moderate COVID-19 patients: A phase 1/11 randomized control trial (SEOT study). *Int Immunopharmacol*. 2021; 91: 107301. DOI: 10.1016/j.intimp.2020.107301.
  27. Fernandez-Cuadros ME, Albaladejo-Florin MJ, Alava-Rabasa S, Usandizaga-Elio I, Martinez-Quintanilla Jimenez D, Pena-Lora D, et al. Effect of Rectal ozone (O3) in severe COVID-19 pneumonia: preliminary results. *SN Compr Clin Med*. 2020; 2: 1328–36. DOI: 10.1007/s42399-020-00374-1.
  28. Cvetkova AV, Koneva ES, Kostenko AA, Bisheva DR, Sidiyakina IV, Konev SM, i dr. Rol' sistemoj ozonoterapii v rehabilitacii pacientov, perenesshih COVID-19. *Voprosy kurortologii, fizioterapii i lechebnoj fizicheskoj kul'tury*. 2022; 99 (4–2): 22–29. DOI: 10.17116/kurort20229904222. Russian.
  29. Gumenyuk LN, Ternovaya AI, Parshikova VO, Hudyakova AS, Dzheparov EF. Effektivnost' primeneniya ozonoterapii u pacientov s postkovidnym sindromom na etape sanatorno-kurortnogo lecheniya. *Medicina. Sociologiya. Filosofiya. Prikladnye issledovaniya*. 2023; 3: 59–65. Russian.
  30. Tanashyan MM, Kuznecova PI, Raskurazhev AA, Zaslavskaya KYa. Struktura postkovidnogo astenicheskogo sindroma. *Perspektivy korrekcii. Terapevticheskiy arhiv*. 2023; 95 (5): 418–24. DOI: 10.26442/00403660.2023.05.202224. Russian.
  31. Tanashyan MM, Raskurazhev AA, Kuznecova PI, Belyj PA, Zaslavskaya KYa. Perspektivy i vozmozhnosti terapii pacientov s astenicheskim sindromom posle perenesennoj novoj koronavirusnoj infekcii COVID-19. *Terapevticheskij arhiv*. 2022; 94 (11): 1285–93. DOI: 10.26442/00403660.2022.11.201981. Russian.
  32. Smets EMA, Garssen B, Bonke B, De Haes JCJM. The multidimensional fatigue inventory (MFI) psychometric qualities of an instrument to assess fatigue. *Journal of Psychosomatic Research*. 1995; 39 (5): 315–25.
  33. Kopecek M, Stepankova H, Lukavsky J, Ripova D, Nikolai T, Bezdicek O. Montreal Cognitive Assessment (MoCA): Normative Data for Old and Very Old Czech Adults// *Applied Neuropsychology: Adult*. 2016; 1–7. DOI: 10.1080/23279095.2015.1065261.
  34. Buysse DJ, Reynolds CF 3rd, Monk TH, Berman SR, Kupfer DJ. The Pittsburgh Sleep Quality Index: a new instrument for psychiatric practice and research. *Psychiatry Res*. 1989; 28 (2): 193–213. DOI: 10.1016/0165-1781(89)90047-4.
  35. Hamilton M. The assessment of anxiety states by rating. *Br J Med Psychol*. 1959; 32: 50–55. DOI: 10.1111/j.2044-8341.1959.tb00467.x.
  36. Busner J, Targum SD. The clinical global impressions scale: applying a research tool in clinical practice. *Psychiatry (Edmont)*. 2007; 4 (7): 28–37.
  37. Alonso-Domínguez J, Gallego-Rodríguez M, Martínez-Barros I, Calderón-Cruz B, Leiro-Fernández V, Pérez-González A, Poveda E. High Levels of IL1 $\beta$ , TNF $\alpha$  and MIP-1 $\alpha$  One Month after the Onset of the Acute SARS-CoV-2 Infection, Predictors of Post COVID-19 in Hospitalized Patients. *Microorganisms*. 2023; 26: 11 (10): 2396. DOI: 10.3390/microorganisms11102396.
  38. Majolo F, Silva GL, Vieira L, Anli C, Timmers LF, Laufer S, Goettert MI. Neuropsychiatric disorders and COVID-19: what we know so far. *Pharmaceuticals*. 2021; 14 (9): 933. DOI: 10.3390/ph14090933.
  39. Ganong WF. Circumventricular organs: definition and role in the regulation of endocrine and autonomic function. *Clin Exp Pharmacol Physiol*. 2000; 27: 422–7. DOI: 10.1046/j.1440-1681.2000.03259.x.
  40. Evrensel A, Ünsalver BÖ, Ceylan ME. Neuroinflammation, Gut-Brain Axis and Depression. *Psychiatry Investig*. 2020; 17 (1): 2–8. DOI: 10.30773/pi.2019.08.09.
  41. Tang Y, Liu J, Zhang D, Xu Z, Ji J, Wen C. Cytokine Storm in COVID-19: The Current Evidence and Treatment Strategies. *Front Immunol*. 2020; 11: 1708. DOI: 10.3389/fimmu.2020.01708.

## Литература

- Buttery S, Philip KEJ, Williams P, Fallas A, West B, Cumella A, et al. Patient symptoms and experience following COVID-19: results from a UK-wide survey. *BMJ Open Respir Res.* 2021; 8 (1): e001075. DOI: 10.1136/bmjresp-2021-001075.
- Chen C, Hauptert SR, Zimmermann L, Shi X, Fritsche LG, Mukherjee B. Global Prevalence of Post COVID-19 Condition or Long COVID: A Meta-Analysis and Systematic Review. *J Infect Dis.* 2022; 226: 1593–607. DOI: 10.1093/infdis/jiac136
- Seang S, Itani O, Monsel G, Abdi B, Marcelin AG, Valantin MA, et al. Long COVID-19 symptoms: Clinical characteristics and recovery rate among non-severe outpatients over a six-month follow-up. *Infect Dis Now.* 2022; 52: 165–9. DOI: 10.1016/j.idnow.2022.02.005.
- Boutou AK, Asimakos A, Kortianou E, Vogiatzis I, Zouvelekis A. Long COVID-19 pulmonary sequelae and management considerations. *J Personal Med.* 2021; 11 (9): 838. DOI: 10.3390/jpm11090838.
- Vélez-Santamaría R, Fernández-Solana J, Méndez-López F, Domínguez-García M, González-Bernal JJ, Magallón-Botaya R, et al. Functionality, physical activity, fatigue and quality of life in patients with acute COVID-19 and Long COVID infection. *Sci Rep.* 2023; 14: 13 (1): 19907. DOI: 10.1038/s41598-023-47218-1.
- Rooney S, Webster A, Paul L. Systematic Review of Changes and Recovery in Physical Function and Fitness after Severe Acute Respiratory Syndrome-Related Coronavirus Infection: Implications for COVID-19 Rehabilitation. *Phys Ther.* 2020; 100: 1717–29. DOI: 10.1093/ptj/pzaa129.
- Schultheiß C, Willscher E, Paschold L, Gottschick C, Klee B, Glasauer S, et al. From online data collection to identification of disease mechanisms: the IL1 $\beta$ , IL6 and TNF $\alpha$  cytokine triad is associated with post-acute sequelae of COVID-19 in a digital research cohort. *SSRN Electron J [Internet].* 2021. DOI: 10.2139/ssrn.3963839.
- Salamanna F, Veronesi F, Martini L, Landini MP, Fini M. Post-COVID-19 syndrome: the persistent symptoms at the post-viral stage of the disease: a systematic review of the current data. *Frontiers in medicine.* 2021; 8: 392. DOI: 10.3389/fmed.2021.653516.
- Liu Z, Lv Z, Zhou X, Shi J, Hong S, Huang H, Lv L. Efficacy of traditional Chinese exercises in patients with post-COVID-19 chronic fatigue syndrome: A protocol for systematic review and meta-analysis. *Medicine (Baltimore).* 2022; 18: 101 (46): e31450. DOI: 10.1097/MD.00000000000031450.
- Kappellmann N, Dantzer R, Khandaker GM. Interleukin-6 as potential mediator of long-term neuropsychiatric symptoms of COVID19. *Psychoneuroendocrinology.* 2021; 131: 105295. DOI: 10.1016/j.psyneuen.2021.105295.
- Yin JX, Agbana YL, Sun ZS, Fei SW, Zhao HQ, Zhou XN, et al. Increased interleukin-6 is associated with long COVID-19: a systematic review and meta-analysis. *Infect Dis Poverty.* 2023; 12 (1): 43. DOI: 10.1186/s40249-023-01086-z.
- Захаров Д. В., Буряк Ю. В. Постковидные когнитивные расстройства. Современный взгляд на проблему, патогенез и терапию. *Обзорные психиатрии и медицинской психологии им. В. М. Бехтерева.* 2021; 55 (4): 97–105.
- Хасанова Д. Р., Житкова Ю. В., Васкаева Г. Р. Постковидный синдром: обзор знаний о патогенезе, нейропсихиатрических проявлениях и перспективах лечения. *Неврология, нейропсихиатрия, психосоматика.* 2021; 13 (3): 93–98.
- Ахмеджанова Л. Т., Остроумова Т. М., Солоха О. А. Ведение пациентов с болевыми синдромами на фоне COVID-19. *Неврология, нейропсихиатрия, психосоматика.* 2021; 13 (5): 96–101.
- Хайбуллина Д. Х., Максимов Ю. Н. Астенический постковидный синдром. *Журнал неврологии и психиатрии им. С. С. Корсакова.* 2023; 123 (3): 61–69. DOI: 10.17116/jnevro202312303161.
- Наумов К. М., Андреева Г. О., Баженов Д. А. Дифференцированный подход к коррекции вегетативных нарушений при постковидном синдроме. *Известия Российской Военно-медицинской академии.* 2021; 40 (S4): 88–91.
- Бахарева О. Н., Бахарев С. А., Конов К. Ю., Вантеев Д. А., Лягушин Р. С. Неврологические проявления постковидного синдрома и возможности реабилитации. *Лазерная медицина.* 2021; 25 (1): 16–20.
- AlMogbel AA, Albarak MI, AlNumair SF. Ozone Therapy in the Management and Prevention of Caries. *Cureus.* 2023; 15 (4): e37510. DOI: 10.7759/cureus.37510.
- Bette M, Cors E, Kresse C, Schütz B. Therapeutic treatment of superoxide dismutase 1 (G93A) amyotrophic lateral sclerosis model mice with medical ozone decelerates trigeminal motor neuron degeneration, attenuates microglial proliferation, and preserves monocyte levels in mesenteric lymph nodes. *Int J Mol Sci.* 2022; 23: 3403. DOI: 10.3390/ijms23063403.
- Wang Z, Zhang A, Meng W, Wang T, Li D, Liu Z, Liu H. Ozone protects the rat lung from ischemia-reperfusion injury by attenuating NLRP3-mediated inflammation, enhancing Nrf2 antioxidant activity and inhibiting apoptosis. *Eur J Pharmacol.* 2018; 835: 82–93. DOI: 10.1016/j.ejphar.2018.07.059.
- Sallustio F, Cardinale G, Voccola S, Picerno A, Porcaro P, Gesualdo L. Ozone eliminates novel coronavirus Sars-CoV-2 in mucosal samples. *New Microbes New Infect.* 2021; 43: 100927. DOI: 10.1016/j.nmni.2021.100927.
- Zheng Z, Dong M, Hu K. A preliminary evaluation on the efficacy of ozone therapy in the treatment of COVID-19. *J Med Virol.* 2020; 92: 2348–50. DOI: 10.1002/jmv.26040.
- Díaz-Soto MT, Pérez AF, Vaillant JD, Mallok A, Viebahn-hänsler R, Menéndez C, et al. Ozone Therapy Ameliorates Nervous System Disorders and Oxidative Stress in Patients During Ethanol Withdrawal - A Pilot Study. *Ozone: Science & Engineering.* 2012; 34 (6): 432–37. DOI: 10.1080/01919512.2012.717858.
- Руднев И. Е., Проценко И. В., Максимова Н. Е. Озонотерапия при тревожных и депрессивных расстройствах с паническими атаками. *Верхневолжский медицинский журнал.* 2018; 17 (4): 18–21.
- Franzini M, Valdenassi L, Ricevuti G, Chirumbolo S, Deptenhardt M, Bertossi D, Tirelli U. Oxygen-ozone (O<sub>2</sub>-O<sub>3</sub>) immunocutaneous therapy for patients with COVID-19 Preliminary evidence reported. *Int Immunopharmacol.* 2020; 88: 106879. DOI: 10.1016/j.intimp.2020.106879.
- Shah M, Captain J, Vaidya V, Kulkarni A, Valsangkar K, Nair PMK, Ganu G. Safety and efficacy of ozone therapy in mild to moderate COVID-19 patients: A phase 1/11 randomized control trial (SEOT study). *Int Immunopharmacol.* 2021; 91: 107301. DOI: 10.1016/j.intimp.2020.107301.
- Fernandez-Cuadros ME, Albaladejo-Florin MJ, Alava-Rabasa S, Usandizaga-Elio I, Martinez-Quintanilla Jimenez D, Pena-Lora D, et al. Effect of Rectal ozone (O<sub>3</sub>) in severe COVID-19 pneumonia: preliminary results. *SN Compr Clin Med.* 2020; 2: 1328–36. DOI: 10.1007/s42399-020-00374-1.
- Цветкова А. В., Конева Е. С., Костенко А. А., Бишева Д. Р., Сидякина И. В., Конев С. М., и др. Роль системной озонотерапии в реабилитации пациентов, перенесших COVID-19. *Вопросы курортологии, физиотерапии и лечебной физической культуры.* 2022; 99 (4–2): 22–29. DOI: 10.17116/kurort20229904222.
- Гуменюк Л. Н., Терновая А. И., Паршикова В. О., Худякова А. С., Джепаров Э. Ф. Эффективность применения озонотерапии у пациентов с постковидным синдромом на этапе санаторно-курортного лечения. *Медицина. Социология. Философия. Прикладные исследования.* 2023; 3: 59–65.
- Танашян М. М., Кузнецова П. И., Раскуражев А. А., Заславская К. Я. Структура постковидного астенического синдрома. *Перспективы коррекции. Терапевтический архив.* 2023; 95 (5): 418–24. DOI: 10.26442/00403660.2023.05.202224.
- Танашян М. М., Раскуражев А. А., Кузнецова П. И., Бельий П. А., Заславская К. Я. Перспективы и возможности терапии пациентов с астеническим синдромом после перенесенной новой коронавирусной инфекции COVID-19. *Терапевтический архив.* 2022; 94 (11): 1285–93. DOI: 10.26442/00403660.2022.11.201981.
- Smets EMA, Garssen B, Bonke B, De Haes JCJM. The multidimensional fatigue inventory (MFI) psychometric qualities of an instrument to assess fatigue. *Journal of Psychosomatic Research.* 1995; 39 (5): 315–25.
- Korecek M, Stepankova H, Lukavsky J, Ripova D, Nikolai T, Bezdicek O. Montreal Cognitive Assessment (MoCA): Normative Data for Old and Very Old Czech Adults// *Applied Neuropsychology:*

- Adult. 2016; 1–7. DOI: 10.1080/23279095.2015.1065261.
34. Buysse DJ, Reynolds CF 3rd, Monk TH, Berman SR, Kupfer DJ. The Pittsburgh Sleep Quality Index: a new instrument for psychiatric practice and research. *Psychiatry Res.* 1989; 28 (2): 193–213. DOI: 10.1016/0165-1781(89)90047-4.
  35. Hamilton M. The assessment of anxiety states by rating. *Br J Med Psychol.* 1959; 32: 50–55. DOI: 10.1111/j.2044-8341.1959.tb00467.x.
  36. Busner J, Targum SD. The clinical global impressions scale: applying a research tool in clinical practice. *Psychiatry (Edgmtont).* 2007; 4 (7): 28–37.
  37. Alonso-Domínguez J, Gallego-Rodríguez M, Martínez-Barros I, Calderón-Cruz B, Leiro-Fernández V, Pérez-González A, Poveda E. High Levels of IL1 $\beta$ , TNF $\alpha$  and MIP-1 $\alpha$  One Month after the Onset of the Acute SARS-CoV-2 Infection, Predictors of Post COVID-19 in Hospitalized Patients. *Microorganisms.* 2023; 26: 11 (10): 2396. DOI: 10.3390/microorganisms11102396.
  38. Majolo F, Silva GL, Vieira L, Anli C, Timmers LF, Laufer S, Goettert MI. Neuropsychiatric disorders and COVID-19: what we know so far. *Pharmaceuticals.* 2021; 14 (9): 933. DOI: 10.3390/ph14090933.
  39. Ganong WF. Circumventricular organs: definition and role in the regulation of endocrine and autonomic function. *Clin Exp Pharmacol Physiol.* 2000; 27: 422–7. DOI: 10.1046/j.1440-1681.2000.03259.x.
  40. Evrensel A, Ünsalver BÖ, Ceylan ME. Neuroinflammation, Gut-Brain Axis and Depression. *Psychiatry Investig.* 2020; 17 (1): 2–8. DOI: 10.30773/pi.2019.08.09.
  41. Tang Y, Liu J, Zhang D, Xu Z, Ji J, Wen C. Cytokine Storm in COVID-19: The Current Evidence and Treatment Strategies. *Front Immunol.* 2020; 11: 1708. DOI: 10.3389/fimmu.2020.01708.
  42. Hojo S, Uchida M, Tanaka K, Hasebe R, Tanaka Y, Murakami M, Hirano T. How COVID-19 induces cytokine storm with high mortality. *Inflamm Regen.* 2020; 40: 37. DOI: 10.1186/s41232-020-00146-3.
  43. Scassellati C, Galoforo AC, Bonvicini C, Esposito C, Ricevuti G. Ozone: a natural bioactive molecule with antioxidant property as potential new strategy in aging and in neurodegenerative disorders. *Ageing Res Rev.* 2020; 63: 101138. DOI: 10.1016/j.arr.2020.101138.
  44. Kim AN, Jeon W-K, Lee JJ, Kim B-C. Up-regulation of heme oxygenase-1 expression through CaMKII-ERK1/2-Nrf2 signaling mediates the anti-inflammatory effect of bisdemethoxycurcumin in LPS-stimulated macrophages. *Free Radic Biol Med.* 2010; 49 (3): 323–33. DOI: 10.1016/j.freeradbiomed.2010.04.015.
  45. Ahmed SM, Luo L, Namani A, Wang XJ, Tang X. Nrf2 signaling pathway: pivotal roles in inflammation. *BBA–Mol Basis Dis.* 2017; 1863 (2): 585–97. DOI: 10.1016/j.bbadis.2016.11.005.
  46. Ahmed SM, Luo L, Namani A, Wang XJ, Tang X. Nrf2 signaling pathway: Pivotal roles in inflammation. *Biochim Biophys Acta Mol Basis Dis.* 2017; 1863 (2): 585–97. DOI: 10.1016/j.bbadis.2016.11.005.
  47. Cenci A, Macchia I, La Sorsa V, Sbarigia C, Di Donna V, Pietraforte D. Mechanisms of Action of Ozone Therapy in Emerging Viral Diseases: Immunomodulatory Effects and Therapeutic Advantages With Reference to SARS-CoV-2. *Front Microbiol.* 2022; 21 (13): 871645. DOI: 10.3389/fmicb.2022.871645.
  48. Tirelli U, Franzini M, Valdenassi L, Pisconti S, Taibi R, Torrisi C, et al. Fatigue in post-acute sequelae of SARS-CoV2 (PASC) treated with oxygen-ozoneautohemotherapy - preliminary results on 100 patients. *Eur Rev Med Pharmacol Sci.* 2021; 25 (18): 5871–5. DOI: 10.26355/eurrev\_202109.

## ASSOCIATION OF LOCAL BIOIMPEDANCE ANALYSIS OF THE ABDOMINAL REGION WITH MORPHOLOGICAL AND BIOCHEMICAL TRAITS

Bondareva EA<sup>1</sup>✉, Leonov GE<sup>1</sup>, Parfenteva OI<sup>1</sup>, Arutiunian AA<sup>2</sup>, Bevziuk NA<sup>2</sup>, Kovaleva ON<sup>2</sup>, Gadzhiakhmedova AN<sup>1</sup>, Shemyakov SE<sup>2</sup>, Kulemin NA<sup>1</sup>

<sup>1</sup> Lopukhin Federal Research and Clinical Center of Physical-Chemical Medicine of the Federal Medical Biological Agency, Moscow, Russia

<sup>2</sup> Pirogov Russian National Research Medical University, Moscow, Russia

Quantification of the subcutaneous and visceral fat depot in the abdominal region is a promising method to assess individual risk of cardiometabolic disorders and estimate the efficacy of certain drugs. The local bioimpedance analysis (BIA) represent a new promising method for separate quantification of two fat depots in the abdominal region. The method combines high accuracy, low cost, and noninvasiveness. The study was aimed to analyze the relationships between the impedance estimates obtained in the local BIA lead and the complex of anthropometric and biochemical characteristics in males and females. A total of 147 females and 42 males aged 18–73 years were assessed. To estimate subcutaneous fat, we used the local BIA lead (ABC-02 Medass) in accordance with the earlier proposed electrode placement scheme. Local impedance ( $Z_{50_{sc}}$ , Ohm) was recorded using the ABC-02 Medass software. The correlation analysis revealed significant correlations of  $Z_{50_{sc}}$  with the waist-to-height ratio, insulin concentration, body fat percentage, and HOMA-IR. Markers of the risk of cardiometabolic diseases (abdominal obesity, insulin resistance, and body fat percentage) are associated with the increased  $Z_{50_{sc}}$  values. The results of ROC analysis with the insulin resistance index (AUC 0.79 [0.72; 0.84],  $p < 0.000$ ) make it possible to consider  $Z_{50_{sc}}$  a promising marker of the risk of cardiometabolic diseases. The differences between subgroups are confirmed by both statistical significance and large effect size.

**Keywords:** subcutaneous fat, local BIA, abdominal obesity, waist circumference, normal-weight obesity

**Funding:** the study was supported by the Russian Science Foundation (RSF grant No. 22-75-10122).

**Author contribution:** Bondareva EA — study design, statistical analysis, manuscript writing; Leonov GE — conducting BIA; Parfenteva OI, Gadzhiakhmedova AN — ultrasound scan, statistical analysis; Arutiunian AA, Kovaleva ON, Bevziuk NA — anthropometric measurements, BIA, ultrasound scan; Shemyakov SE — literature review, manuscript writing; Kulemin NA — manuscript writing.

**Compliance with ethical standards:** the study was approved by the Ethics Committee of the Lopukhin Federal Research and Clinical Center of Physical-Chemical Medicine of FMBA of Russia (protocol No. 2022/12/06 dated 06 December 2022). All the examined individuals submitted the informed consent to participation in the study.

✉ **Correspondence should be addressed:** Elvira A. Bondareva  
Malaya Pirogovskaya, 1a, Moscow, 119453, Russia; bondareva.e@gmail.com

**Received:** 31.05.2024 **Accepted:** 21.07.2024 **Published online:** 07.08.2024

**DOI:** 10.24075/brsmu.2024.030

## СВЯЗЬ ЛОКАЛЬНОЙ БИОИМПЕДАНСОМЕТРИИ В АБДОМИНАЛЬНОЙ ОБЛАСТИ С ЕЕ МОРФОЛОГИЧЕСКИМИ И БИОХИМИЧЕСКИМИ ПРИЗНАКАМИ

Э. А. Бондарева<sup>1</sup>✉, Г. Е. Леонов<sup>1</sup>, О. И. Парфентьева<sup>1</sup>, А. А. Арутюнян<sup>2</sup>, Н. А. Бевзюк<sup>2</sup>, О. Н. Ковалева<sup>2</sup>, А. Н. Гаджихмедова<sup>1</sup>, С. Е. Шемяков<sup>2</sup>, Н. А. Кулемин<sup>1</sup>

<sup>1</sup> Федеральный научно-клинический центр физико-химической медицины имени Ю. М. Лопухина Федерального медико-биологического агентства, Москва, Россия

<sup>2</sup> Российский национальный исследовательский медицинский университет имени Н. И. Пирогова, Москва, Россия

Количественное определение подкожного и висцерального депо жира в абдоминальной области является перспективным методом оценки индивидуальных рисков развития cardiometabolic заболеваний и оценки эффективности некоторых лекарственных препаратов. Локальные отведения биоимпедансометрии (БИА) — новый перспективный метод раздельной количественной оценки двух депо жира в области живота. Он сочетает высокую точность, невысокую себестоимость и неинвазивность. Целью работы было провести анализ связей импедансных оценок, полученных в локальном отведении БИА с комплексом антропометрических и биохимических характеристик у мужчин и женщин. Обследованы 147 женщин и 42 мужчины в возрасте 18–73 лет. Для оценки подкожного жира использовали локальное отведение БИА (ABC-02 «Медасс») по предложенной ранее схеме расположения электродов. При помощи программного обеспечения ABC-02 «Медасс» фиксировали локальный импеданс —  $Z_{50_{sc}}$ , Ом. Корреляционный анализ выявил значимые связи  $Z_{50_{sc}}$  с индексом талия/рост, концентрацией инсулина, процентом жировой массы тела и HOMA-IR. Маркеры риска cardiometabolic заболеваний (абдоминальное ожирение, инсулинорезистентность и доля жировой массы) связаны с повышенными значениями  $Z_{50_{sc}}$ . Результаты ROC-анализа с индексом инсулинорезистентности (AUC 0,79 [0,72; 0,84],  $p < 0,000$ ) позволяют рассматривать  $Z_{50_{sc}}$  в качестве перспективного маркера риска cardiometabolic заболеваний. Различия между подгруппами подтверждаются не только уровнем статистической значимости, но и значительным размером эффекта.

**Ключевые слова:** подкожное жиротложение, локальный БИА, абдоминальное ожирение, обхват талии, скрытое ожирение

**Финансирование:** научное исследование проведено при поддержке Российского научного фонда (грант РНФ № 22-75-10122).

**Вклад авторов:** Э. А. Бондарева — дизайн исследования, статистический анализ, написание статьи; Г. Е. Леонов — проведение БИА; О. И. Парфентьева, А. Н. Гаджихмедова — проведение УЗИ-сканирования, статистический анализ; А. А. Арутюнян, О. Н. Ковалева, Н. А. Бевзюк — проведение антропометрических измерений, БИА, УЗИ-сканирования; С. Е. Шемяков — анализ литературы, написание статьи; Н. А. Кулемин — написание статьи.

**Соблюдение этических стандартов:** исследование одобрено этическим комитетом ФГБУ ФНКЦ ФХМ имени Ю. М. Лопухина ФМБА России (протокол № 2022/12/06 от 06 декабря 2022 г.). Все обследованные подписали добровольное информированное согласие на участие в исследовании.

✉ **Для корреспонденции:** Эльвира Александровна Бондарева  
ул. Малая Пироговская, д. 1а, г. Москва, 119453, Россия; bondareva.e@gmail.com

**Статья получена:** 31.05.2024 **Статья принята к печати:** 21.07.2024 **Опубликована онлайн:** 07.08.2024

**DOI:** 10.24075/vrgmu.2024.030

It is well known that the pattern of fat depot distribution (body fat topography) is an independent factor associated with the severity of cardiovascular disorders, risk of metabolic diseases, and overall mortality [1]. Timely assessment of body fat topography will make it possible to determine the groups at risk of metabolic and cardiovascular disorders associated with abdominal (central) obesity, regardless of body mass index (BMI) and body fat percentage (PBF) [1]. In turn, abdominal fat is formed from the depot of subcutaneous and visceral fat. Simple anthropometric traits and indices, such as waist circumference (WC), waist-to-hip ratio (WHR), and waist-to-height ratio (WHtR), are used to estimate the abdominal fat quantity. However, these estimates showed low sensitivity at the individual level and turned out to be ineffective for separate quantitative assessment of subcutaneous and visceral fat [2]. Computed tomography (CT) and magnetic resonance imaging (MRI) are the reference methods for assessment of these components. However, these methods cannot be used for the large-scale screening of the population due to high cost, radiation exposure, and high demands on the personnel qualification. Moreover, the methods cannot be used outside the specialized medical institutions and/or research centers [3]. The method for quantitative assessment of abdominal fat, devoid of the shortcomings of CT and MRI and ensuring comparable accuracy and sensitivity, is in demand in medicine, in prediction of the risk associated with the specific features of fat accumulation in the abdominal region.

Bioimpedance analysis (BIA) of body composition is widely used in the world's medical practice to assess body fat mass and lean body mass, as well as to assess body's water compartments [4]. However, conventional (hand–leg) schemes allow one to obtain the integrated body composition estimates only and do not allow to judge on the fat depot distribution or to assess subcutaneous and visceral fat in the abdominal region separately. Furthermore, the contribution of the trunk to the impedance estimate does not exceed 5–10%, when the conventional electrode placement scheme is used. This means that the integrated body composition indicators are calculated based mainly on the limb impedance estimates [4, 5].

It has been shown that quantitative assessment of subcutaneous fat thickness can be performed by transimpedance measurement between two pairs of electrodes mounted directly above the region, the researcher is interested in [5]. Several electrode placement schemes for the abdominal region have been also presented. The analysis of consistency between the subcutaneous fat thickness quantitative assessment by MRI and the local impedance value in the broad morphological range has shown strong correlation between these two values ( $r^2 = 0.984$ ) [6].

Two studies focused on assessing local BIA leads have been published in Russia [7, 8]. Our study was aimed to analyze the relationships between the impedance characteristics obtained from the local leads in the abdominal region and the complex of morphological and biochemical traits of adult males and females. We study the relationships between local BIA leads and the complex of anthropometric traits and indices characterizing the amount of fat and its topography and complement the estimates obtained by the data on the carbohydrate metabolism markers and sonographic estimates of subcutaneous fat thickness in the abdominal region.

## METHODS

A total of 189 conditionally healthy volunteers (147 females aged 18–67 years and 42 males aged 20–73 years) were

assessed. Examination was performed in the outpatient clinic of the Lopukhin Federal Research and Clinical Center of Physical-Chemical Medicine of FMBA of Russia between January 2022 and April 2023. Ethnicity, physical activity level, and the number of the diseases diagnosed were determined during the questionnaire survey. The vast majority of the assessed individuals specified their ethnicity as Russian (at least one parent was Russian). Inclusion criteria: the legal age males and females diagnosed with no chronic or acute disorders at the time of examination, who had passed all the stages of examination (questionnaire survey, anthropometric measurements, blood biochemistry test), were included in the study. Exclusion criteria: age under 18 years, pregnancy and lactation, pacemaker installed, metal implants in the trunk and/or limbs.

The assessment program included measuring standing height (SH) with the laser anthropometer (KAFA; Russia), body weight (BW) (Seca; Germany), waist (WC) and hip (HC) circumference with the non-elastic measuring tape. BIA was performed using the ABC-02 Medas system (Medas; Russia) with the probing current frequency of 50 kHz in two leads

1. Using the standard tetrapolar scheme “wrist — ankle joint” on the right side of the body with the F3001 placement (FIAB; Italy) and the subject in supine position.

2. To estimate subcutaneous fat in the abdominal region, the source electrodes were placed at a distance of 12 cm, and the measurement electrodes were placed at a distance of 7 cm to the left and right of the umbilicus when the subject was standing [6] (Fig. 1A).

The ABC01-0362 software was used to determine active and reactive resistance (R, Ohm — for the integrated scheme; Rsc, Ohm — for the local scheme) and appropriate impedance values ( $Z_{50}$  and  $Z_{50_{sc}}$ ). The integrated lead values were used to determine absolute and relative body fat mass (FM and PBF, respectively) and lean body mass (LM).

The BodyMetrix BX2000 ultrasound scanner (IntelaMetrix; USA) was used to determine subcutaneous fat thickness (mm) in two points of the abdominal region of each subject: near the umbilicus (SFL1) and above the iliac crest (SFL2), which corresponded to the suprailiac skinfold (Fig. 1B) [9]. The Mediagel medium viscosity ultrasound gel (Geltek; Russia) was used as the contact medium.

Anthropometric traits were used to calculate the following indices: BMI — body mass index, WHR — waist-to-hip ratio, WHtR — waist-to-height ratio [10]. Nutritional status (underweight, normal weight, overweight or obesity) was determined based on BMI in accordance with the WHO criteria. Furthermore, obesity was diagnosed based on the  $PBF \geq 30\%$  for females and  $\geq 25\%$  for males. Central obesity was assessed based on  $WHtR \geq 0.5$  [10].

Blood biochemistry test was performed to estimate the carbohydrate metabolism parameters (insulin, fasting glucose, and glycated hemoglobin levels). These data were used to calculate the HOMA (Homeostasis model assessment) indices: HOMA-IR, HOMA-%B, HOMA-%S. Furthermore, HOMA2-IR, HOMA2-%B, and HOMA2-%S values were calculated using the online calculator (<https://www2.dtu.ox.ac.uk/homacalculator/>). HOMA-IR > 2.7 was considered to indicate insulin resistance.

## Statistical analysis

Parameters of the studied traits' distribution position, variation, and shape were assessed using the PAST tool (<https://www.nhm.uio.no/english/research/resources/past/>). The Shapiro–Wilk, Anderson–Darling, Lilliefors, and Jarque–Bera tests were used to test consistency of the data with normal distribution.

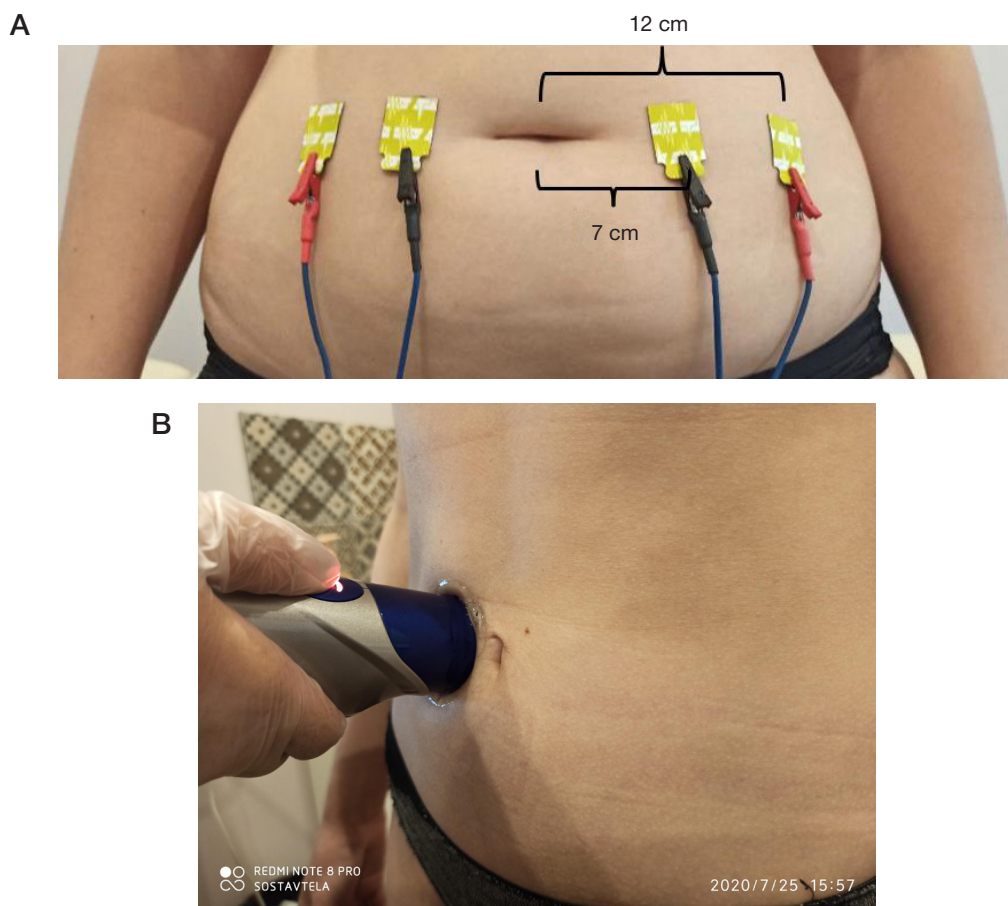


**Fig. 1. A.** Electrode placement scheme in the local BIA lead (ABC-02 Medas) for assessment of subcutaneous fat in the abdominal region. **B.** Measuring the subcutaneous fat thickness near the umbilicus with the BodyMetrix BX2000 ultrasound scanner

The Monte Carlo algorithm was implemented in the calculation procedures for all tests, except the Shapiro–Wilk test. When performing statistical comparison, we did not limit ourselves to calculating  $p$ -values, but assessed the Cohen's standardized effect size ( $d_c$ ) for pairwise comparison and the  $\epsilon^2$  measurement for the Kruskal–Wallis test. The effect sizes, the lower limits of 95% confidence intervals (CI) of which exceeded  $d_c = 1$ , were accepted as noteworthy [11].

The Welch's  $t$ -test, Mann–Whitney U test, and Kruskal–Wallis test were used to assess the differences between groups. The Benjamini–Hochberg procedure was applied when performing multiple comparisons. The analysis of differences between groups and the correlation analysis were performed using Past and JASP (JASP Team (2024). JASP (Version 0.18.3) [Computer software]), as well as the following software packages: “ggpubr” (Kassambara A (2023). `ggpubr: 'ggplot2' Based Publication Ready Plots`. R package version 0.6.0, <<https://CRAN.R-project.org/package=ggpubr>>) and “rstatix” (Kassambara A (2023). `rstatix: Pipe-Friendly Framework for Basic Statistical Tests`. R package version 0.7.2, <<https://CRAN.R-project.org/package=rstatix>>) in R (R Core Team (2023). `R: A Language and Environment for Statistical Computing`. R Foundation for Statistical Computing, Vienna, Austria. <<https://www.R-project.org/>>). The 95% CI was calculated for all the assessed statistics. The ROC analysis was performed using EasyROC (<http://biosoft.erciyes.edu.tr/app/easyROC>).

## RESULTS

The subgroups of males and females did not differ in age, BMI, WHtR, absolute body fat mass,  $Z50_{sc}$ , subcutaneous fat

thickness in the abdominal region, biochemical parameters, and HOMA2 indices. The traits, for which significant differences ( $p < 0.001$ ) between the subgroups of males and females have been reported, are provided in Table 1.

According to the data provided (Table 1), no sexual dimorphism is reported for the values of subcutaneous fat thickness in the abdominal region and local impedance of the abdominal region. In the context of sex-related differences in WC and WHR, the lack of sexual dimorphism in the SFL1, SFL2, and  $Z50_{sc}$  values can indicate differences in the amount of visceral fat and the possibility of visceral fat quantification by local BIA methods. That is why the examination should be complemented by the local lead in the sagittal area of the abdomen. The correlation analysis of the complex of studied traits (Fig. 2) revealed significant correlations of  $Z50_{sc}$  with WHtR (0.739 [0.667; 0.797]), body weight (0.609 [0.510; 0.691]), waist circumference (0.700 [0.510; 0.766]), BMI (0.731 [0.657; 0.791]), FM and body fat percentage (0.724 [0.648; 0.786] and 0.662 [0.573; 0.735]), subcutaneous fat thickness in the abdominal region (0.692 [0.608; 0.761] and 0.743 [0.671; 0.802]), insulin concentration (0.541 [0.428; 0.637]), HOMA2-IR (0.539 [0.425; 0.636]), and HOMA2-%S (−0.539 [−0.636; −0.425]).

A broad spectrum of morphological traits represented in the studied sample makes it possible to conduct comparative analysis of  $Z50_{sc}$  values in various subgroups: by the nutritional status determined based on BMI, by the fact of having obesity determined based on the PBF value, as well as by the fact of having abdominal obesity determined based on the WHtR value (Table 2).

The increased values of the traits associated with the risk of cardiometabolic disorders (abdominal obesity, insulin

**Table 1.** Traits, for which significant sex-related differences were reported

Trait	Sex	Mean (SD)	Effect size [95% CI]
WHR	F	0.764 (0.091)	-1.221 [-1.602; -0.834]
	M	0.860 (0.063)	
Height, cm	F	167.1 (7.6)	-1.871 [-2.302; -1.433]
	M	179.4 (5.3)	
Body weight, kg	F	69.7 (15.6)	-1.023 [-1.407; -0.632]
	M	86.6 (17.4)	
Waist circumference, cm	F	77.8 (13.2)	-0.823 [-1.190; -0.450]
	M	88.6 (13.1)	
Body fat percentage (%)	F	30.6 (8.7)	0.910 [0.533; 1.282]
	M	22.9 (8.2)	
Lean body mass, kg	F	47.3 (6.1)	-2.719 [-3.315; -2.114]
	M	65.6 (7.3)	

resistance, and body fat percentage) are correlated to the higher local impedance values. The differences between subgroups are confirmed not only by the significance level, but also by the large effect size (Table 2).

Then ROC analysis was performed for these traits in order to assess the possibility of using  $Z50_{sc}$  as a diagnostic criterion for abdominal obesity, body fat percentage, and insulin resistance (Fig. 3). The highest AUC values are reported for the WHtR index. The AUC value reported for HOMA-IR is lower, however, it is significantly different from the “don’t care” value (AUC = 0.5), which suggests the need for further study of  $Z50_{sc}$  involving the groups diagnosed with prediabetes and type 2 diabetes mellitus.

Thus, higher values of the traits associated with the increased fat accumulation and the risk of comorbidities correspond to the high local impedance values (Fig. 3). The AUC values suggest that  $Z50_{sc}$  can be potentially used as a diagnostic test, while certain  $Z50_{sc}$  threshold values can constitute an additional noninvasive express method for assessment of cardiometabolic risk in the future.

The combination of BMI and PBF can confirm the diagnosis of obesity and select individuals with normal-weight obesity [12] and individuals with the increased BMI (excess body weight), but normal fat percentage. Fig. 4 presents  $Z50_{sc}$  values in the subgroups with increasing body weight and body

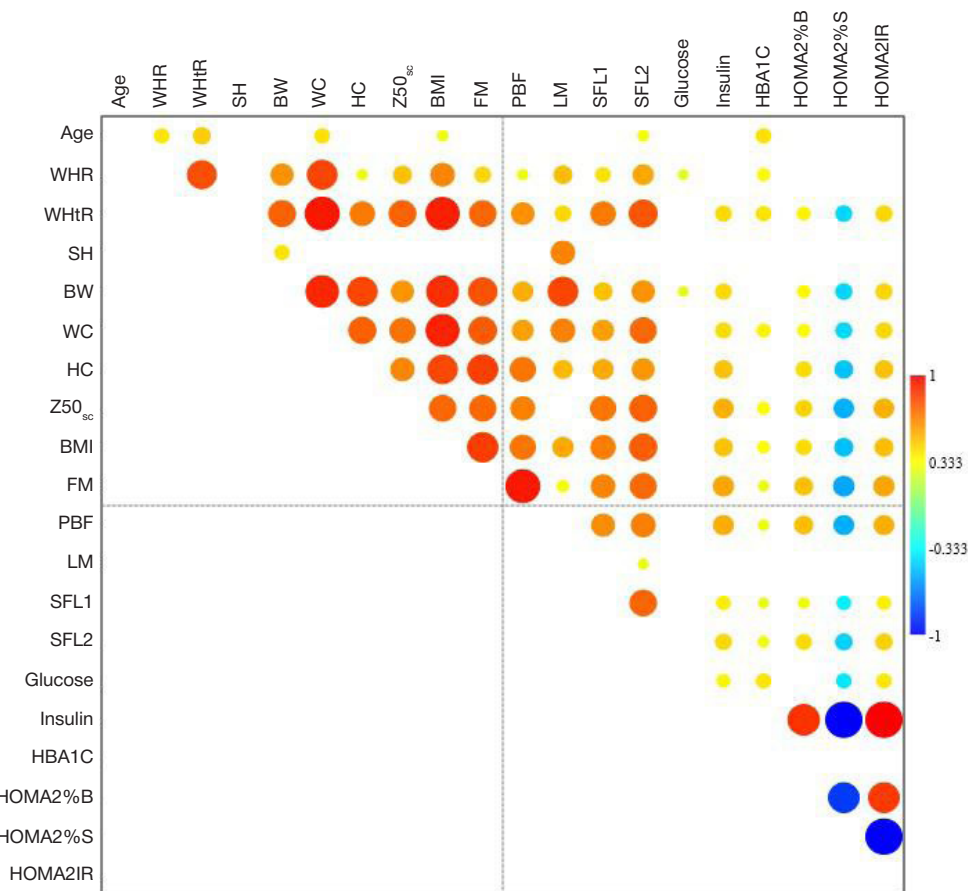


**Fig. 2.** Correlations of the complex of studied traits. SH — standing height, BW — body weight, WC — waist circumference, HC — hip circumference, SFL1 — subcutaneous fat thickness near the umbilicus, SFL2 — subcutaneous fat thickness in the suprailiac skinfold region. The statistically significant correlations only are shown

**Table 2.** Comparative analysis of  $Z50_{sc}$  in various subgroups of the assessed sample

Trait	Subgroup	$Z50_{sc}$	Effect size [95% CI]	$p$ -value
Sex	F	51.6 (23.1)	-0.112 [-0.455; 0.232]	0.525
	M	54.2 (25.8)		
WHtR	<0.5	41.1 (14.1)	2.252 [1.77; 2.73]	< 0.001
	≥0.5	79.9 (19.9)		
HOMA-IR	Normal	44.7 (19.1)	-1.718 [-2.007; -1.521]	< 0.001
	IR	69.6 (24.7)		
PBF	Normal	38.6 (13.6)	-1.654 [-1.984; -1.320]	< 0.001
	Obesity	68.8 (22.8)		
BMI	Normal	39.6 (13.1)	0.533 [0.44; 0.62]	< 0.001
	Overweight	59.0 (18.8)		
	Obesity	82.2 (20.3)		

**Note:** the  $\epsilon^2$  measure was used as the effect size for BMI,  $d_c$  was used as the effect size for other parameters; IR — insulin resistance (HOMA-IR > 2.7)

fat percentage: underweight (UW) — BMI < 18.5 kg/m<sup>2</sup>; normal body weight and PBF (NWN0) — BMI within the range of 18.5–24.9 kg/m<sup>2</sup> and PBF < 25% for males and < 30% for females; normal-weight obesity (NW\_O) — BMI within the range of 18.5–24.9 kg/m<sup>2</sup> and PBF ≥ 25% for males and ≥ 30% for females; excess body weight based on BMI and normal PBF (OWN0) — BMI within the range of 25.0–29.9 and PBF < 25% for males and < 30% for females; excess body weight based on BMI and obesity based on PBF (OWO) — BMI within the range of 25.0–29.9 and PBF ≥ 25% for males and ≥ 30% for females; obesity based on BMI and PBF (OB) — BMI > 29.9 and PBF ≥ 25% for males and ≥ 30% for females.

The findings suggest that local impedance estimates in the abdominal region increase with increasing BMI and PBF. We revealed significant differences between subgroups with normal body weight and the subgroup with normal-weight obesity (NWN0 vs. NW\_O;  $p = 0.029$ ), along with the lack of significant differences between the subgroups with normal-weight obesity and excess body weight and obesity (NW\_O vs. OWO;  $p = 0.097$ ), as well as between the NWN0 and OWN0 subgroups ( $p = 0.118$ ). The subgroup with obesity (OB) significantly differs from other groups ( $p < 0.005$ ). There are no differences in the waist circumference, subcutaneous fat thickness near the umbilicus, and WHtR between NWN0 and NW\_O, however, there are significant differences in SFL2 between these subgroups ( $p = 0.015$ ).

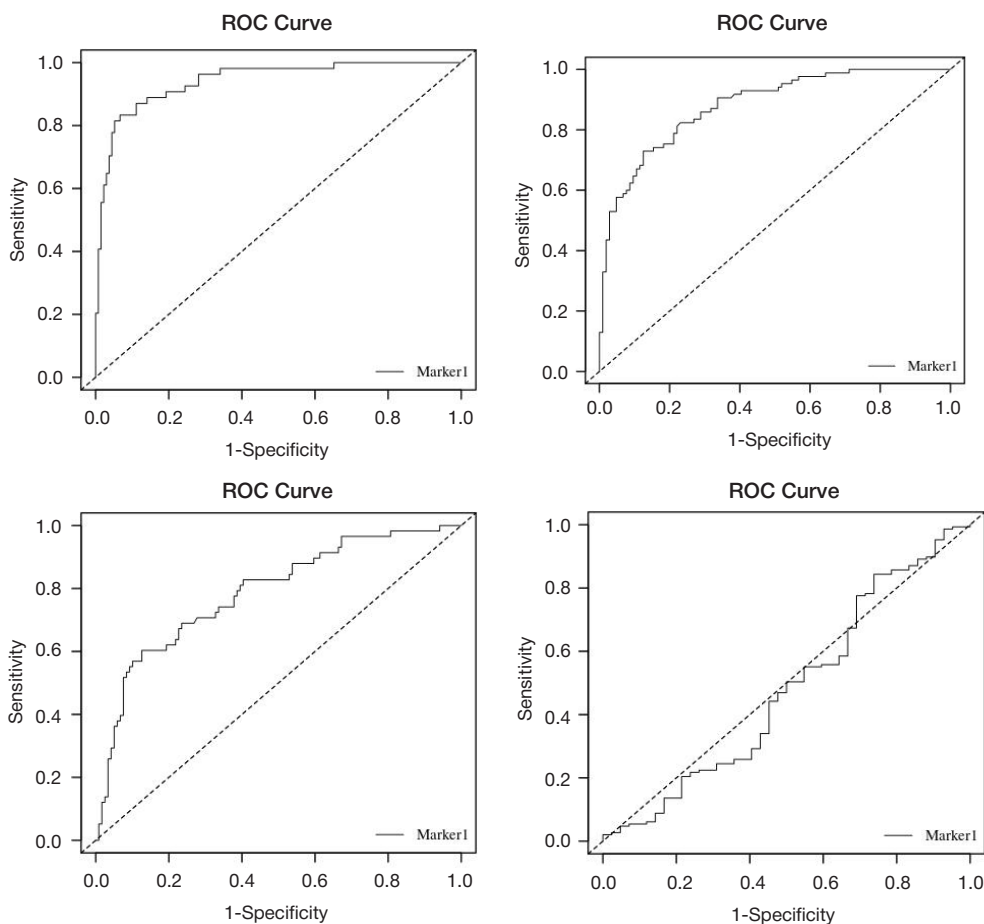


**Fig. 3.** ROC analysis of the values of local impedance in the abdominal region ( $Z50_{sc}$ ) in the subgroups by sex, fact of having abdominal obesity, fact of having obesity based on body fat percentage, and the fact of having insulin resistance based on the HOMA-IR index



## DISCUSSION

The search for the best characteristics describing individual obesity phenotype has shifted from anthropometric measurements to separate assessment of body fat mass and lean body mass and nowadays to quantitative assessment of various fat depots and the features of fat distribution [13, 14]. There are incomparably more studies focused on assessing the possibility of visceral fat quantification by BIA, than that focused on subcutaneous fat in the abdominal region [15].

In our study we conducted analysis of the correlation of impedance in the abdominal region determined using the Russian bioimpedance analyzer (ABC-02 Medas) with subcutaneous fat thickness in the abdominal region and the biochemical carbohydrate metabolism markers. The results obtained confirm a close relationship between the estimates obtained in the local BIA lead and the complex of morphological and metabolic traits characterizing subcutaneous fat accumulation in the abdominal region. It should be noted that foreign manufacturers of bioimpedance equipment produce serial products (Y-scope InBody, Korea and Maltron BioScan 920-II, UK) allowing one to quantify subcutaneous and visceral fat in the local leads. However, manufacturers have not published the estimation equations. That is why, in our opinion, investigation of the capabilities of domestic BIA, widely used in the medical and research institutions of the RF, for estimation of subcutaneous and visceral fat using local schemes, is particularly relevant.

No sexual dimorphism is reported for  $Z50_{sc}$ , in contrast to WC and PBF. Coefficients of  $Z50_{sc}$  correlation with WHtR, BW, WC, BMI, SFL1, and SFL2 are higher, than that for PBF determined using the integrated BIA scheme. However, it should be noted that the 95% CI of the correlation coefficients of  $Z50_{sc}$ , PBF and WC for almost all pairs of traits overlap, which suggests that there are no significant differences between these correlational pairs in the studied sample (Fig. 5). The correlations of  $Z50_{sc}$  and PBF with insulin levels were stronger, than the correlation of insulin with WC, however, local assessment has no advantage over the PBF calculated using the conventional scheme.

The correlation estimates obtained in the study for the pairs  $Z50_{sc}$ -PBF and  $Z50_{sc}$ -WC are close to the estimates obtained in the earlier study [7]. While the estimates obtained for the group of Altai people turned out to be lower for the pair  $Z50_{sc}$ -WC and similar for the pairs  $Z50_{sc}$ -WHtR and  $Z50_{sc}$ -PBF [8].

The ROC analysis results (Fig. 3; HOMA-IR) suggest that  $Z50_{sc}$  can be used as the additional criterion for assessment of insulin resistance in adults, however, it is necessary to increase the sample size and include individuals with confirmed cardiometabolic disorders in the group. It is also necessary to assess the  $Z50_{sc}$  diagnostic value in the groups formed based on sex. Quantitative assessment of abdominal fat is also important in terms of studying the white adipose tissue remodeling, for both assessment of the development of metabolic disorders associated with obesity and estimation of the efficacy of a number of drugs [13, 16]. The relationship between two quantitative characteristics of subcutaneous fat (local BIA and subcutaneous fat thickness determined by ultrasonography) makes it possible to develop the equation for calculation of subcutaneous fat thickness or cross-sectional area based on the ABC-02 Medass local lead indicators. With appropriate verification by reference methods, such equations can replace CT and MRI in the large-scale screening studies [6, 16].

The estimates obtained in local BIA leads (impedance, active and reactive resistance) can be used to develop various

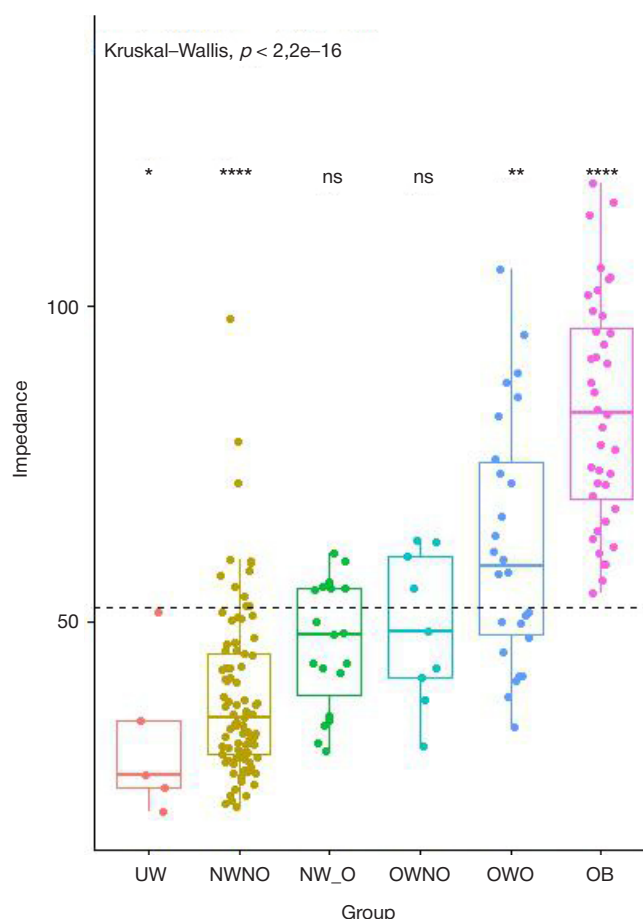


**Fig. 4.** Distribution of  $Z50_{sc}$  values in subgroups of the surveyed sample formed in ascending order of BMI and PBF. UW — underweight; NWNNO — normal body weight and PBF; NW\_O — obesity with normal body weight; OWNO — excess body weight based on BMI and normal PBF value; OWO — excess body weight based on BMI and obesity based on PBF; OB — obesity based on BMI and PBF. Dashed horizontal line — average  $Z50_{sc}$  value for the surveyed sample. \* —  $p < 0.05$ ; \*\* —  $p < 0.01$ ; \*\*\*\* —  $p < 0.0001$ ; ns —  $p \geq 0.05$

indices, such as indices derived from active resistance [8, 17]. We have also analyzed the subcutaneous fat index ( $Rsc^*WC, m^2$ ). SFI was proposed earlier [7] by analogy with the visceral fat index reported in the earlier study [17]. To date, these indices have not been validated as the criteria for assessment of the risk of comorbidities in obesity. The correlations of SFI with WHtR (0.87 [0.71; 0.90]), WC (0.87 [0.81; 0.91]) and WHR (0.66 [0.59; 0.73]) are higher, than the correlation of  $Z50_{sc}$  with these indices (0.74 [0.67; 0.80], 0.70 [0.62; 0.77], and 0.49 [0.38; 0.59], respectively). The correlation of  $Z50_{sc}$  with SFI is 0.95 [0.92; 0.97]. In general, SFI has shown no fundamental differences from  $Z50_{sc}$ , except for significant differences between subgroups of females and males (36.2 (29.5) vs. 47.9 (35.3) Ohm/m<sup>2</sup>;  $p = 0.021$ ). The SFI correlation estimates are consistent with the earlier reported data [7], however, the median values and SFI correlations with morphological traits turned out to be significantly lower in the group of ethnic Altaians [8].

It is interesting that among all studied traits only  $Z50_{sc}$  and SFL2 make it possible to distinguish people with normal-weight obesity from the group with the same BMI having normal body fat percentage. Furthermore, groups with high body fat percentage and different BMI show no differences in  $Z50_{sc}$ , while significant differences in WC, WHtR, and SFL1 are reported for these groups. Similarly, the subgroups having no obesity based on PBF, but different BMI, show no differences in  $Z50_{sc}$ . This is due to the fact that  $Z50_{sc}$  to the greater extent

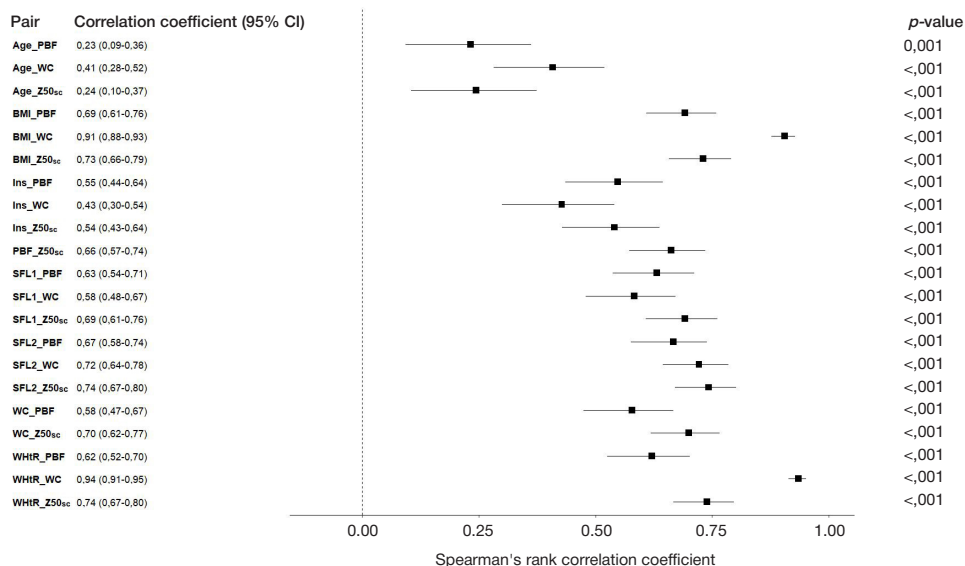


**Fig. 5.** Spearman's rank correlation coefficients and their 95% CI for the pairs of studied traits. PBF — body fat percentage, WC — waist circumference, Z50<sub>sc</sub> — impedance in the local lead, BMI — body mass index, Ins — insulin ( $\mu$ U/mL), SFL1 — subcutaneous fat thickness near the umbilicus, SFL2 — subcutaneous fat thickness above the iliac crest, WHtR — waist-to-height ratio

reflects the fat component, while WC and WHtR serve as the surrogate estimates of abdominal fat, and high values of these traits can be associated with the development of skeletal muscles in physically active people. Or, alternatively, normal WC and WHtR values result from the muscle tissue replacement with fat together with the preserved low waist circumference, as in normal-weight obesity. In general, the pattern of local impedance assessment in the abdominal region in these groups corresponds to PBF determined in the integrated scheme, but the correlation of Z50<sub>sc</sub> with PBF in the combined sample of males and females is 0.662 [0.573; 0.735], i.e. it is not high.

The study limitations include small size of the group of underweight adults ( $BMI < 18.5 \text{ kg/m}^2$ ), as well as the group of individuals with low fat percentage and well developed skeletal muscles.

## CONCLUSIONS

The study has shown the correlation of the Z50<sub>sc</sub> trait obtained in the local BIA lead using domestic bioimpedance equipment with the complex of anthropometric and biochemical traits in males and females. In general, high Z50<sub>sc</sub> values correspond to the more pronounced fat deposition and its abdominal

topography. Correlations of Z50<sub>sc</sub> with subcutaneous fat thickness in the abdominal region make it possible to develop equation for recalculation of Z50<sub>sc</sub> into subcutaneous fat thickness in the abdominal region (cross-sectional area of subcutaneous fat). The results of the ROC analysis of Z50<sub>sc</sub> with the HOMA-IR index make it possible to consider the local BIA lead as a simple noninvasive criterion for assessment of carbohydrate metabolism disorders associated with excess fat accumulation in the abdomen in the future. However, further research focused on determining quantitative characteristics of such test for assessment of the Z50<sub>sc</sub> diagnostic value is required: assessment of the threshold value, sensitivity and specificity. The quantitative estimates of fat depots are used to develop the criteria (for example, adjusted for BMI and sex) for differential assessment of the risk of comorbidities [18]. In prospect there is a possibility of developing equations for quantitative assessment of the subcutaneous and visceral fat depot area based on the data obtained in the local BIA leads and the indices based on these data. Such estimates can become the new additional diagnostic criteria for assessment of individual risk of cardiometabolic disorders or personalized approach to treatment of those depending on the patients' sex and age.

## References

- Alser M, Elrayess MA. From an Apple to a Pear: Moving Fat around for Reversing Insulin Resistance. *Int J Environ Res Public Health*. 2022; 19 (21): 14251. DOI: 10.3390/ijerph192114251.
- Zhu K, Walsh JP, Murray K, Hunter M, Hui J, Hung J. DXA-Derived vs Standard Anthropometric Measures for Predicting Cardiometabolic Risk in Middle-Aged Australian Men and Women. *J Clin Densitom*. 2022; 25 (3): 299–307. DOI: 10.1016/j.jocd.2022.01.006.
- Lee MH, Zea R, Garrett JW, Summers RM, Pickhardt PJ. Ab-based abdominal CT measurements of orthotopic and ectopic fat predict mortality and cardiometabolic disease risk in adults. *Eur Radiol*. 2024; 12. DOI: 10.1007/s00330-024-10935-w.
- Catapano A, Trinchese G, Cimmino F, Petrella L, D'Angelo M, Di Maio G, et al. Impedance Analysis to Evaluate Nutritional Status in Physiological and Pathological Conditions. *Nutrients*. 2023;15 (10): 2264. DOI: 10.3390/nu15102264.
- Gonzalez CA, Zuniga O, Padilla LE. Detection of animal tissue thickness using simple vertical electric sounding (VES). *Physiol Measmt* 1997; 18: 85–91.
- Scharfetter H, Schlager T, Stollberger R, Felsberger R, Hutten H, Hinghofer-Szalkay H. Assessing abdominal fatness with local bioimpedance analysis: basics and experimental findings. *Int J Obes Relat Metab Disord*. 2001; 25 (4): 502–11. DOI: 10.1038/sj.ijo.0801556.
- Soloveva AE, Gil-Ordones Ye, Gonzales-Korra KH, Rudnev SG. Primeniye lokal'noj impedansometrii dlja ocerki podkozhnogo i visceral'nogo zhirootlozheniya v abdominal'noj oblasti u studentov vuzov. *Morfologija*. 2019; 156 (4): 85–90. Russian.
- Rokkina AN, Pravednikova AYe. Shidlovskij YuV, Popova EV, Zadorozhnaja LV, Homjakova IA. Indeksy podkozhnogo i visceral'nogo zhirootlozheniya i ih svyaz' s kompleksom jendogennyh i jekzogenykh faktorov v gruppe vzroslogo naselenija Respubliki

- Altaj. Vestnik Moskovskogo universiteta. Serija 16. Biologija. 2021; 76 (1): 33–40. Russian.
9. Bondareva EA, Parfenteva OI, Troshina EA, Ershova EV, Mazurina NV, Komshilova KA, et al. Agreement between bioimpedance analysis and ultrasound scanning in body composition assessment. *Am J Hum Biol.* 2024; 36 (4): e24001. DOI: 10.1002/ajhb.24001.
  10. Sadeghi E, Khodadadiyan A, Hosseini SA, Hosseini SM, Aminorroaya A, Amini M, et al. Novel anthropometric indices for predicting type 2 diabetes mellitus. *BMC Public Health.* 2024; 24 (1): 1033. DOI: 10.1186/s12889-024-18541-7.
  11. Solla F, Tran A, Bertoncelli D, Musoff C, Bertoncelli CM. Why a P-Value is Not Enough. *Clin Spine Surg.* 2018; 31 (9): 385–88. DOI: 10.1097/BSD.0000000000000695.
  12. De Lorenzo A, Martinoli R, Vaia F, Di Renzo L. Normal weight obese (NWO) women: an evaluation of a candidate new syndrome. *Nutr Metab Cardiovasc Dis.* 2006; 16 (8): 513–23. DOI: 10.1016/j.numecd.2005.10.010.
  13. Zhao JY, Zhou LJ, Ma KL, Hao R, Li M. MHO or MUO? White adipose tissue remodeling. *Obes Rev.* 2024; 25 (4): e13691. DOI:10.1111/obr.13691
  14. Piché ME, Tchernof A, Després JP. Obesity phenotypes, diabetes, and cardiovascular diseases. *Circ Res.* 2020; 126 (11): 1477–500.
  15. Lai CL, Lu HK, Huang AC, Chu LP, Chuang HY, Hsieh KC. Bioimpedance analysis combined with sagittal abdominal diameter for abdominal subcutaneous fat measurement. *Front Nutr.* 2022; 9: 952929. DOI: 10.3389/fnut.2022.952929.
  16. Gastaldelli A, Cusi K, Fernández Landó L, Bray R, Brouwers B, Rodríguez Á. Effect of tirzepatide versus insulin degludec on liver fat content and abdominal adipose tissue in people with type 2 diabetes (SURPASS-3 MRI): a substudy of the randomised, open-label, parallel-group, phase 3 SURPASS-3 trial. *Lancet Diabetes Endocrinol.* 2022; 10 (6): 393–406.
  17. Watson S, Blundell HL, Evans WD, Griffiths H, Newcombe RG, Rees DA. Can abdominal bioelectrical impedance refine the determination of visceral fat from waist circumference? *Physiol Meas.* 2009; 30 (7): N53–8. DOI: 10.1088/0967-3334/30/7/N01.
  18. Agrawal S, Klarqvist MDR, Diamant N, Stanley TL, Ellinor PT, Mehta NN, et al. BMI-adjusted adipose tissue volumes exhibit depot-specific and divergent associations with cardiometabolic diseases. *Nat Commun.* 2023; 14 (1): 266. DOI: 10.1038/s41467-022-35704-5.

## Литература

1. Alser M, Elrayess MA. From an Apple to a Pear: Moving Fat around for Reversing Insulin Resistance. *Int J Environ Res Public Health.* 2022; 19 (21): 14251. DOI: 10.3390/ijerph192114251.
2. Zhu K, Walsh JP, Murray K, Hunter M, Hui J, Hung J. DXA-Derived vs Standard Anthropometric Measures for Predicting Cardiometabolic Risk in Middle-Aged Australian Men and Women. *J Clin Densitom.* 2022; 25 (3): 299–307. DOI: 10.1016/j.jocd.2022.01.006.
3. Lee MH, Zea R, Garrett JW, Summers RM, Pickhardt PJ. AI-based abdominal CT measurements of orthotopic and ectopic fat predict mortality and cardiometabolic disease risk in adults. *Eur Radiol.* 2024; 12. DOI: 10.1007/s00330-024-10935-w.
4. Catapano A, Trinchese G, Cimmino F, Petrella L, D'Angelo M, Di Maio G, et al. Impedance Analysis to Evaluate Nutritional Status in Physiological and Pathological Conditions. *Nutrients.* 2023; 15 (10): 2264. DOI: 10.3390/nu15102264.
5. Gonzalez CA, Zuniga O, Padilla LE. Detection of animal tissue thickness using simple vertical electric sounding (VES). *Physiol Measmt* 1997; 18: 85–91.
6. Scharfetter H, Schlager T, Stollberger R, Felsberger R, Hutten H, Hinghofer-Szalkay H. Assessing abdominal fatness with local bioimpedance analysis: basics and experimental findings. *Int J Obes Relat Metab Disord.* 2001; 25 (4): 502–11. DOI: 10.1038/sj.jjo.0801556.
7. Соловьева А. Е., Гиль-Ордонес Э., Гонзалес-Корреа К. Х., Руднев С. Г. Применение локальной импедансометрии для оценки подкожного и висцерального жиросотложения в абдоминальной области у студентов вуза. *Морфология.* 2019; 156 (4): 85–90.
8. Роккина А. Н., Праведникова А. Э., Шидловский Ю. В., Попова Е. В., Задорожная Л. В., Хомякова И.А. Индексы подкожного и висцерального жиросотложения и их связь с комплексом эндогенных и экзогенных факторов в группе взрослого населения Республики Алтай. *Вестник Московского университета. Серия 16. Биология.* 2021; 76 (1): 33–40.
9. Bondareva EA, Parfenteva OI, Troshina EA, Ershova EV, Mazurina NV, Komshilova KA, et al. Agreement between bioimpedance analysis and ultrasound scanning in body composition assessment. *Am J Hum Biol.* 2024; 36 (4): e24001. DOI: 10.1002/ajhb.24001.
10. Sadeghi E, Khodadadiyan A, Hosseini SA, Hosseini SM, Aminorroaya A, Amini M, et al. Novel anthropometric indices for predicting type 2 diabetes mellitus. *BMC Public Health.* 2024; 24 (1): 1033. DOI: 10.1186/s12889-024-18541-7.
11. Solla F, Tran A, Bertoncelli D, Musoff C, Bertoncelli CM. Why a P-Value is Not Enough. *Clin Spine Surg.* 2018; 31 (9): 385–88. DOI: 10.1097/BSD.0000000000000695.
12. De Lorenzo A, Martinoli R, Vaia F, Di Renzo L. Normal weight obese (NWO) women: an evaluation of a candidate new syndrome. *Nutr Metab Cardiovasc Dis.* 2006; 16 (8): 513–23. DOI: 10.1016/j.numecd.2005.10.010.
13. Zhao JY, Zhou LJ, Ma KL, Hao R, Li M. MHO or MUO? White adipose tissue remodeling. *Obes Rev.* 2024; 25 (4): e13691. DOI:10.1111/obr.13691
14. Piché ME, Tchernof A, Després JP. Obesity phenotypes, diabetes, and cardiovascular diseases. *Circ Res.* 2020; 126 (11): 1477–500.
15. Lai CL, Lu HK, Huang AC, Chu LP, Chuang HY, Hsieh KC. Bioimpedance analysis combined with sagittal abdominal diameter for abdominal subcutaneous fat measurement. *Front Nutr.* 2022; 9: 952929. DOI: 10.3389/fnut.2022.952929.
16. Gastaldelli A, Cusi K, Fernández Landó L, Bray R, Brouwers B, Rodríguez Á. Effect of tirzepatide versus insulin degludec on liver fat content and abdominal adipose tissue in people with type 2 diabetes (SURPASS-3 MRI): a substudy of the randomised, open-label, parallel-group, phase 3 SURPASS-3 trial. *Lancet Diabetes Endocrinol.* 2022; 10 (6): 393–406.
17. Watson S, Blundell HL, Evans WD, Griffiths H, Newcombe RG, Rees DA. Can abdominal bioelectrical impedance refine the determination of visceral fat from waist circumference? *Physiol Meas.* 2009; 30 (7): N53–8. DOI: 10.1088/0967-3334/30/7/N01.
18. Agrawal S, Klarqvist MDR, Diamant N, Stanley TL, Ellinor PT, Mehta NN, et al. BMI-adjusted adipose tissue volumes exhibit depot-specific and divergent associations with cardiometabolic diseases. *Nat Commun.* 2023; 14 (1): 266. DOI: 10.1038/s41467-022-35704-5.

## STRUCTURE OF TIME PERSPECTIVE IN COMBATANTS WITH AMPUTATED LIMBS

Nikishina VB, Petrash EA <sup>✉</sup>, Yunina-Pakulova NYu, Lukyanov ES

Pirogov Russian National Research Medical University, Moscow, Russia

The relevance of the reported study results from the need to clearly define the target of psychological impact in combatants with amputated limbs. The time perspective being an integral characteristic ensures the life experience integrity: all life events are intertwined within the boundaries of the past, present and future. The study was aimed to assess the time perspective structure in combatants with amputated limbs. The sample consisted of 78 males aged 20–53 years, who had combat experience and underwent treatment or rehabilitation after getting injured. The study involved the use of the Mississippi Scale for Combat-Related Post-Traumatic Stress Disorder, Zimbardo Time Perspective Inventory, method for event-based reconstruction of a person's time perspective by V.B. Nikishina and E.A. Petrash, SR-45 method by P.I. Yunatskevich, infantilism inventory by A.A. Seregin. The factor structure of time perspective in combatants with amputated upper limbs includes the factor of non-reflexive future, factor of limited time perspective, and the situational and behavioral risk factor. In cases of amputated lower limbs, the situational future factor, past orientation factor, and situational and behavioral risk factor are represented. In cases of no amputated limbs, the combatants' time perspective structure includes the factor of reflexive future perspective, factor of limited present fatalistic, and past orientation factor.

**Keywords:** time perspective, amputation of limbs, post-traumatic stress disorder, combat experience

**Funding:** the study was conducted within the framework of the State Assignment of the Ministry of Health of the Russian Federation No. 122051700017-2.

**Author contribution:** the authors contributed to manuscript writing equally.

**Compliance with ethical standards:** the study was approved by the Ethics Committee of the Pirogov Russian National Research Medical University (protocol No. 57 dated 21 September 2023); the informed consent to examination was submitted by all subjects.

✉ **Correspondence should be addressed:** Ekaterina A. Petrash  
Ostrovytyanova, 1, Moscow, 117997, Russia; petrash@mail.ru

**Received:** 24.06.2024 **Accepted:** 28.06.2024 **Published online:** 31.07.2024

**DOI:** 10.24075/brsmu.2024.028

## СТРУКТУРА ВРЕМЕННОЙ ПЕРСПЕКТИВЫ УЧАСТНИКОВ БОЕВЫХ ДЕЙСТВИЙ С АМПУТАЦИЕЙ КОНЕЧНОСТЕЙ

В. Б. Никишина, Е. А. Петраш <sup>✉</sup>, Н. Ю. Юнина-Пакулова, Е. С. Лукьянов

Российский национальный исследовательский медицинский университет имени Н. И. Пирогова, Москва, Россия

Актуальность предлагаемого исследования обусловлена необходимостью четкого определения мишени психологического воздействия у участников боевых действий с ампутацией конечностей. Временная перспектива, являясь интегральной характеристикой, обеспечивает целостность жизненного опыта: все события жизни в границах прошлого, настоящего и будущего взаимосвязаны. Целью исследования было оценить структуру временной перспективы участников боевых действий с ампутацией конечностей. Объем выборки составил 78 мужчин 20–53 лет, имеющих опыт участия в боевых действиях и находящихся на лечении либо реабилитации после ранений. В работе использовали Миссисипскую шкалу для оценки посттравматических реакций, опросник временной перспективы Ф. Зимбардо, методику событийной реконструкции временной перспективы личности Никишиной В. Б. и Петраш Е. А., методику СР-45 П. И. Юнацкевича, опросник уровня инфантилизма А. А. Серегина. Факторная структура временной перспективы участников боевых действий с ампутацией верхних конечностей включает в себя фактор неререфлексивного будущего, фактор ограниченности временной перспективы и фактор ситуативно-поведенческих рисков. При ампутации нижних конечностей представлены фактор ситуативного будущего, фактор ориентированности на прошлое, а также фактор ситуативно-поведенческих рисков. При отсутствии ампутации конечностей в структуре временной перспективы участников боевых действий представлены фактор перспективы рефлексивного будущего, фактор ограниченно-фаталистического настоящего, а также фактор направленности в прошлое.

**Ключевые слова:** временная перспектива, ампутация конечностей, посттравматическое стрессовое расстройство, опыт участия в боевых действиях

**Финансирование:** работа выполнена в рамках государственного задания Министерства здравоохранения Российской Федерации №122051700017-2.

**Вклад авторов:** всеми авторами был внесен равнозначный вклад в подготовку рукописи статьи.

**Соблюдение этических стандартов:** исследование одобрено этическим комитетом РНИМУ им. Н. И. Пирогова (протокол № 57 от 21 сентября 2023 г.); все участники подписали добровольное информированное согласие на обследование.

✉ **Для корреспонденции:** Екатерина Анатольевна Петраш  
ул. Островитянова, д. 1, г. Москва, 117997, Россия; petrash@mail.ru

**Статья получена:** 24.06.2024 **Статья принята к печати:** 28.06.2024 **Опубликована онлайн:** 31.07.2024

**DOI:** 10.24075/vrgmu.2024.028

The relevance of assessing the structure of time perspective in combatants with amputated limbs results from the need to search for targets of psychological impact. Chronological narrowing of the time perspective and event (substantial) scantiness characterize manifestations of post-traumatic stress disorder [1–3]. The study of the time perspective structural organization transformation as a target for psychological impact will make it possible to change the combatants' emotional and behavioral status, thereby decreasing the intensity of the traumatic event flashbacks.

In combatants, stressful influences include both combat experience itself and acquisition of various physical injuries and

disabilities. A number of authors report that the person's time perspective changes under the long-term exposure to stressful factors, including those leading to post-traumatic stress disorder (PTSD): chronological boundaries change, along with the correlation between the past–present–future parameters and emotional assessment of the time perspective content [4–10].

When constructing the sequence of ideas, we proceeded from the assumption that the time perspective that is substantially characterized by assessing events as traumatic is implemented considering the emotional and behavioral status manifesting in the PTSD severity, degree of personal maturity or infantilism (considered to be the opposite of personal maturity),

and suicidal tendencies at the level of behavior. Therefore, different people can assess the same events differently: what for one is a stressful factor, for another is a usual, ordinary event (one of many other events).

The study was aimed to assess the structure of time perspective in combatants with amputated limbs.

## METHODS

The study involved 78 male subjects aged 20–53 years ( $31.16 \pm 4.28$  years), who underwent treatment and rehabilitation (early stage — preparation for prosthetics) after the mine blast injuries and gunshot wounds resulting from participation in hostilities. Inclusion criteria: wounds resulting from participation in hostilities (mine blast injuries and gunshot wounds without any severe damage to the internal organs); normative cognitive status assessed using the Mini-Mental State Examination (MMSE) scale [11]. The subjects, whose scores corresponded to 28–30 points, were included in the study. Exclusion criteria: female gender, impaired cognitive status (MMSE score below 28), severe damage to the internal organs due to injuries. The experimental group included 42 individuals with traumatic amputation (26 individuals with the lower limb amputated at the level of the foot/lower leg and 16 individuals with the upper limb amputated at the level of the hand/forearm), who had not proceeded to the prosthetics stage. The control group consisted of 36 combatants with the mine blast and gunshot soft tissue injuries and no amputated limbs.

The study was conducted using the following methods: Mississippi Scale for Combat-Related Post-Traumatic Stress Disorder (Mississippi Scale — MS, Keane et al., adapted by N. V. Tarabrina) — military version; Zimbardo Time Perspective Inventory; method for event-based reconstruction of a person's time perspective by V. B. Nikishina and E. A. Petrash; method to reveal suicidal tendencies (SR-45) by P. I. Yunatskevich; infantilism inventory by A. A. Seregin [7, 12–17].

The study consisted of three sequential phases. In the first phase, we assessed significance of differences in the time perspective and event space parameters of combatants by groups considering the fact of amputation. The objective of the second phase was to assess the combatants' emotional and behavioral status considering the fact of limb amputation.

Emotional and behavioral status was studied in terms of the PTSD manifestation severity parameters, degree of infantilism, and suicidal tendencies. These parameters were assessed in the groups of combatants having/not having amputated limbs considering the type of amputation (upper or lower limb amputation). In the third phase, we assessed the time perspective factor structure with the emotional and behavioral status indicators by groups of subjects.

Statistical processing was performed by statistical methods for comparison (nonparametric Mann–Whitney  $U$  test used in accordance with the limitations). Multivariate statistics were also calculated: factor analysis with varimax rotation ( $p < 0.05$ ) was performed for the studied parameters.

The study was aimed to assess the structure of time perspective in combatants with amputated limbs.

## RESULTS

In the first phase, we assessed significance of differences in the time perspective parameters of combatants in the groups having/not having amputated limbs. It was found that the time perspective was characterized by predominance of future and past positive orientation (Fig. 1).

Considering the general future orientation, we can conclude that the combatants' behavior is determined by aspirations for the future goals and rewards, regardless of the fact of having/not having amputated limbs. However, the chronological boundaries of that future are determined by the current period of hospitalization and subsequent rehabilitation that is also carried out at the specialized institution (period of up to 1–3 months). Past positive is characterized by positive reconstruction of the past, but only before the beginning of participation in hostilities. Furthermore, combatants having the history of amputation report lower past positive values compared to combatants with no amputated limbs ( $p = 0.026^*$ ). Significant differences are also reported for such parameters, as past negative ( $p = 0.024^*$ ) and present fatalistic ( $p = 0.023^*$ ). These indicators are significantly higher in the group of combatants having no history of amputation, which suggests higher degree of the time perspective differentiation and structuredness.

Assessment of the time perspective indicators in combatants considering the type of amputation (upper/lower

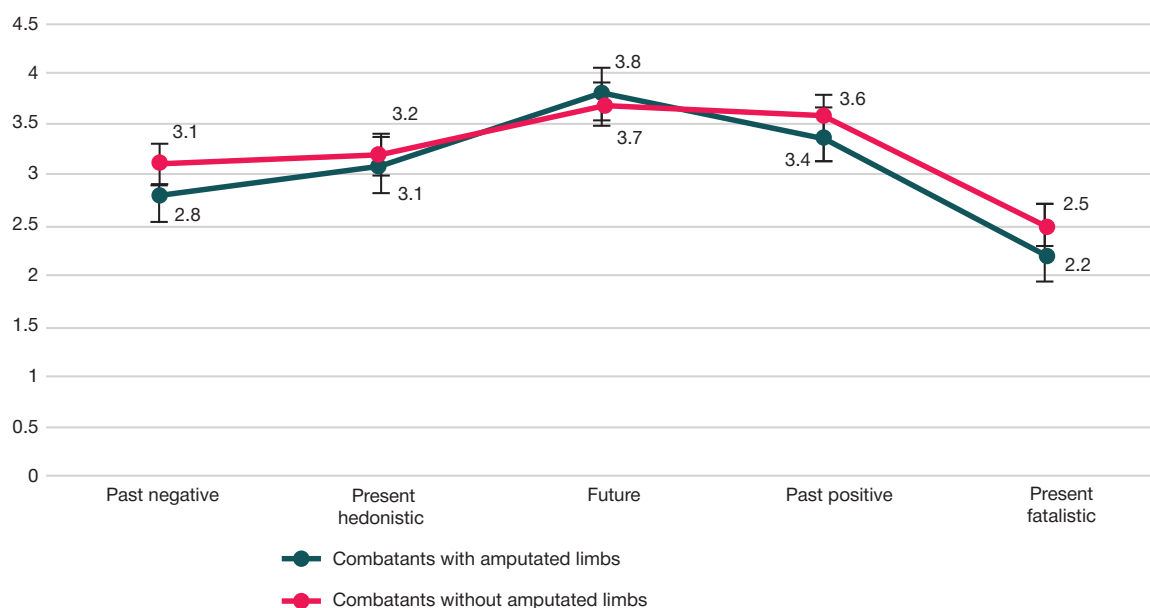


Fig. 1. Profiles of the combatants' time perspective parameter average values considering the fact of limb amputation

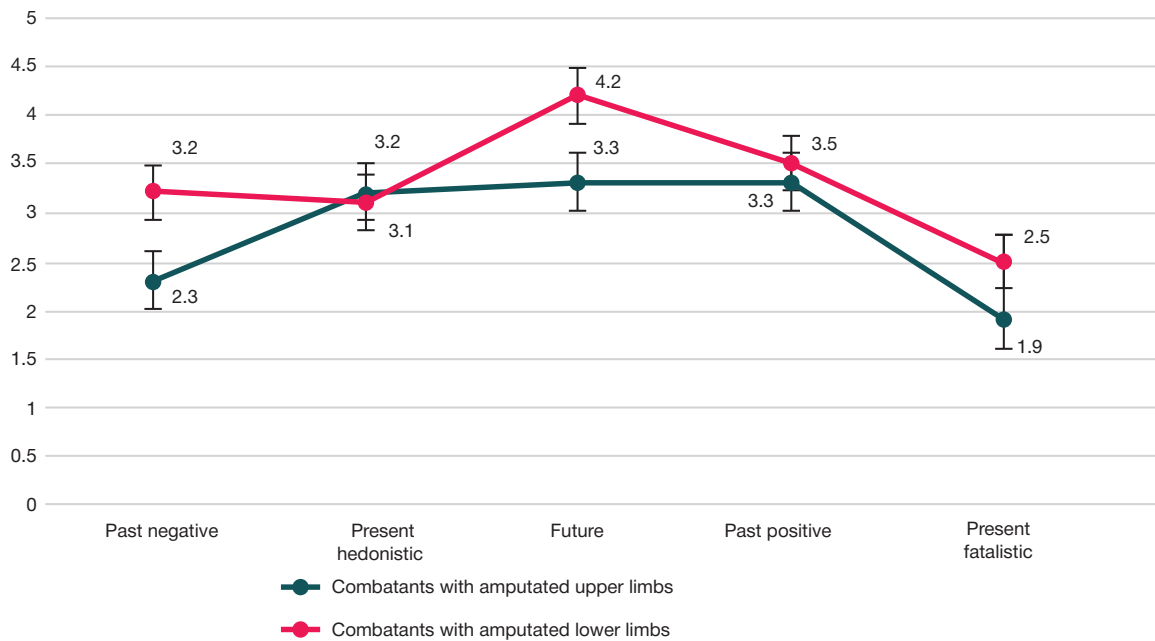


Fig. 2. Profiles of the combatants' time perspective parameter average values in the groups with the upper and lower limb amputation

limb amputation) has revealed significant predominance of such indicators, as past negative, future, and present fatalistic in combatants with amputated lower limbs compared to combatants with amputated upper limbs. In cases of upper limb amputation, the time perspective is characterized by lower scores of indicators with their good balance, while in cases of lower limb amputation the patients are future-oriented (the future is rather short-term, not extending beyond the phase of treatment and rehabilitation), they show predominance of negative assessment of the past (related not only to the traumatic event, but also to negative perception of neutral events) and present fatalistic (Fig. 2).

Assessment of the time perspective event fullness via the event space size has shown that the number of the past ( $p = 0.031^*$ ) and future ( $p = 0.033^*$ ) events is significantly higher in combatants with the mine blast and gunshot soft tissue injuries and no amputated limbs, than in combatants with amputated limbs. There are no significant differences in the number of present-day events.

Regardless of the presence of the fact of having/not having amputated limbs in the event space structure, the maximum number of events belongs to the past, with the minimum

number of events belonging to the present. Assessing the total number of events, we can conclude that the total number of events (belonging to the past, present and future) is lower in combatants with amputated limbs. This suggests significant narrowing of the event space surrounding the events with post-traumatic effects that accumulate the system of relationships between the events and disrupt personal time perspective in combatants (Fig. 3).

Assessment of the event space integration in combatants considering the fact of amputation has revealed a significant excess of the number of relationships between events in the group of combatants with amputated limbs within the coordinates of the past ( $p = 0.034^*$ ), present ( $p = 0.031^*$ ), and future ( $p = 0.027^*$ ). The findings suggest the combatants' fixation on the obviously traumatic event. Furthermore, the entire time perspective flows through the system of relationships of the traumatic event (designated as the fact of participating in hostilities, getting wounded, amputation and all the things related to this situation by the subjects) in both groups.

Assessment of the time perspective event fullness in combatants with amputated upper and lower limbs has revealed that in cases of lower limb amputation the

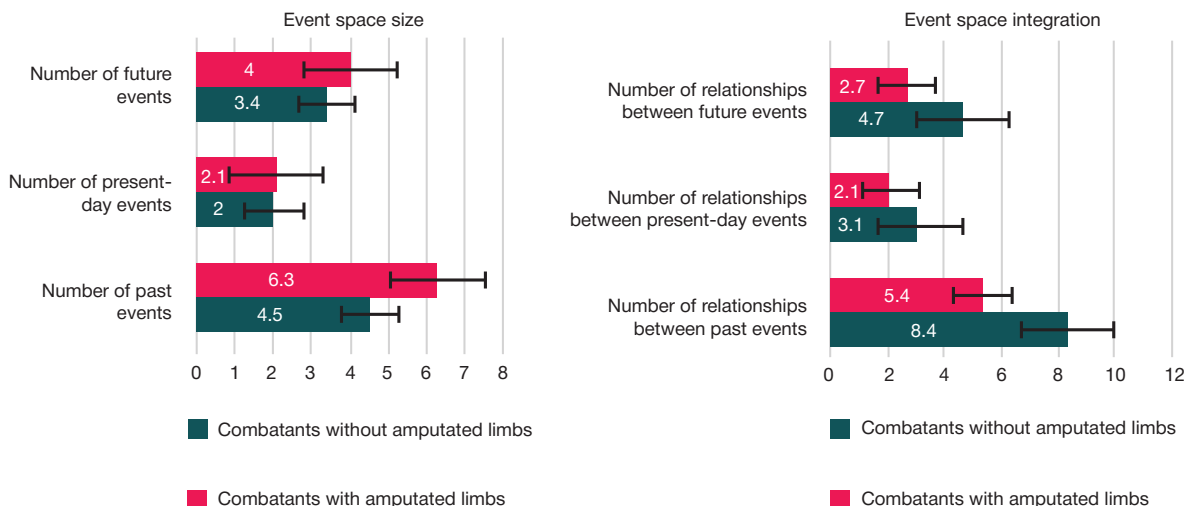


Fig. 3. Event space size and integration in combatants considering the fact of limb amputation

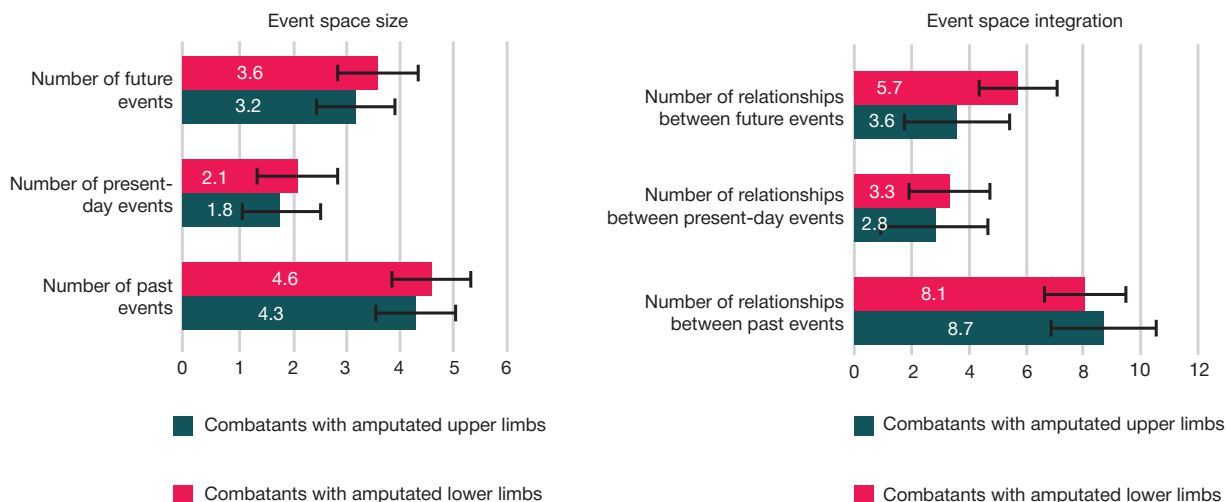


Fig. 4. Event space size and integration in combatants with amputated upper and lower limbs

number of the past ( $p = 0.022^*$ ), present-day ( $p = 0.023^*$ ), and future ( $p = 0.022^*$ ) events is significantly higher than that in combatants with amputated upper limbs. Assessment of the number of relationships within the boundaries of the present ( $p = 0.026^*$ ) and future ( $p = 0.024^*$ ) has revealed a larger number of relationships in combatants with amputated lower limbs compared to combatants with amputated upper limbs. Furthermore, in combatants with amputated lower limbs, the larger number of past events is involved in the smaller number of relationships ( $p = 0.046^*$ ) relative to combatants with amputated upper limbs (Fig. 4).

When solving the problem of assessing severity of PTSD manifestations in combatants, it has been revealed that severity of PTSD manifestations is significantly higher in combatants with amputated limbs, than in combatants with no amputated limbs, however, it is within the medium range with the trend toward high severity ( $98.4 \pm 2.86$ ) in both groups, which characterizes the adjustment disorder. Furthermore, assessment of the significance of differences in the group of combatants with amputated upper and lower limbs has revealed that in cases of upper limb amputation the severity of PTSD manifestations ( $92.2 \pm 2.31$ ) manifesting in the adjustment disorder is significantly higher than in cases of lower limb amputation ( $88.3 \pm 2.57$ ). The findings result from the fact that self-care skills are significantly impaired after amputation of the upper limbs, the feeling of helplessness and hopelessness increases (according to the subjects). The adjustment disorder is less severe in cases of lower limb amputation, since limitations are related mainly to movement in space that can be compensated using mobility aids.

Considering infantilism as a complex personality trait manifested in immaturity of the emotional and volitional sphere, low achievement motivation, lack of independence in decision-making and actions, subjugate, disorganized behavior, orientation towards hedonic values, as well as low ability to reflect and undeveloped coping behavior, the medium degree of total infantilism has been revealed in both groups, regardless of the fact of having/not having amputated limbs. Assessment of the significance of differences has shown that the total infantilism level is higher in combatants with amputated limbs ( $p = 0.021^*$ ), than in combatants with no amputated limbs (Fig. 5). Assessment of the significance of differences in the total infantilism level in the groups of combatants with amputated upper and lower limbs has revealed no significant differences ( $p = 0.129$ ).

The total infantilism level being an integrative indicator includes a number of indicators allowing one to determine, which personal manifestations are characterized by immaturity (what level of personal manifestations produces the signs of infantilism: emotional and volitional, axiological, motivational or behavioral).

Consideration of infantilism parameters in combatants has revealed that personal immaturity manifests itself at the axiological and motivational-behavioral levels in both groups of subjects (Fig. 6).

Combatants with no amputated limbs having the medium infantilism level characterized by situational emotional control experience difficulties with planning ways to achieve their goals, when they have life goals; they are characterized by the pronounced parasitic attitude and shifting responsibility to

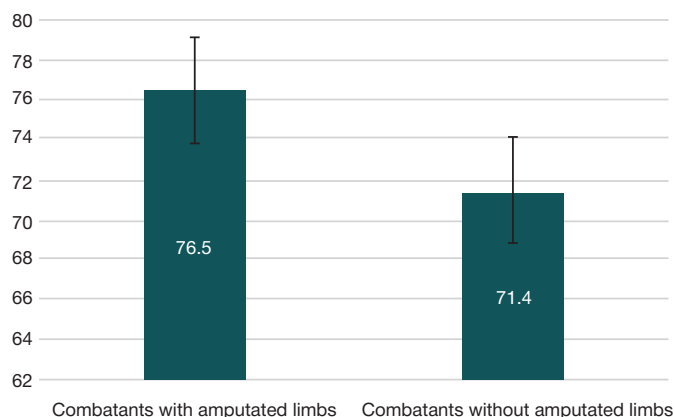


Fig. 5. Average values of total infantilism level in combatants considering the fact of limb amputation

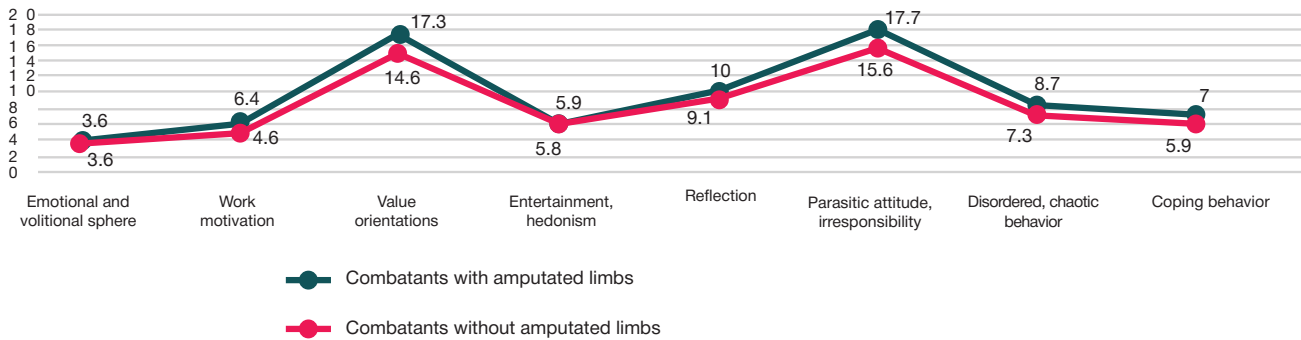


Fig. 6. Average severity of infantilism manifestations in combatants considering the fact of limb amputation

others. Such attitude corresponds to avoidance behavior in difficult and uncertain situations. In combatants with amputated limbs (both upper and lower) with medium total infantilism level, value orientation ( $p = 0.022^*$ ), work motivation ( $p = 0.021^*$ ), parasitic attitude ( $p = 0.019^*$ ), and chaotic behavior ( $p = 0.043^*$ ) are significantly higher, than in combatants with no amputated limbs. The findings are natural, since traumatic amputation is an objective factor that disturbs behavior.

No statistically significant differences in infantilism indicator scores have been revealed in the experimental group (when comparing infantilism indicators in combatants with amputated lower and upper limbs).

In the next phase, we assessed the combatants' suicidal tendencies. As a result, significant differences in the strength of suicidal tendencies between the experimental and control groups ( $p = 0.024^*$ ), as well as in the experimental group ( $p = 0.038^*$ ) have been revealed. It has been found, that combatants with the suicidal tendency levels below average are characterized by the probability of situational emergence of the risk of suicide, regardless of the fact of having/not having amputated limbs: suicide can happen only in the context of long-term stressful impact or in case of reactive mental disorder (Fig. 7).

Combatants with amputated limbs are characterized by the stronger situational suicidal tendencies compared to combatants without limb amputation. Situational suicidal tendencies are stronger in combatants with amputated upper limbs, than in combatants with amputated lower limbs.

During the next phase we implemented the procedure of the studied parameter factorization by groups of subjects.

The time perspective factor structure of combatants with amputated upper limbs includes three factors with the highest factor loadings: factor of future non-reflexive (including future orientation — 0.736 in terms of shifting responsibility — 0.729),

factor of time perspective limitation (characterized by past negative — 0.691, the content of which includes stressful experience — 0.704), and the situational behavioral risk factor (including situational suicidal tendencies — 0.726 with fatalistic assessment of the present — 0.808) (Fig. 8).

The time perspective factor structure of combatants with amputated lower limbs consists of three factors, including the factor of situational future (characterizing the limited nature of the future events — 0.709 with the situational emotional control — 0.806), past orientation factor (including event fullness of the past — 0.725 realized through avoidance behavior — 0.748), and the situational behavioral risk factor (including situational suicidal tendencies — 0.734; present fatalistic — 0.731; PTSD manifestations — 0.764).

The time perspective factor structure of combatants with no amputated limbs also includes three factors with the highest factor loadings: factor of future reflexive perspective (future orientation — 0.752 with negative assessment of the past — 0.702 and shifting responsibility attitude — 0.729), factor of limited present fatalistic (with fatalistic present-day events — 0.801 that are considered stressful), and the past orientation factor (with positive assessment of the past — 0.736 in terms of shifting responsibility — 0.705).

DISCUSSION

The features of the combatants' time perspective factor structure identified during the study are consistent with the data acquired in the earlier studies [4, 5, 9, 12], according to which the authors clearly see the time perspective inconsistency, orientation towards past events, and narrowing of chronological boundaries of the past, present, and future. The factors determining the time perspective structural organization

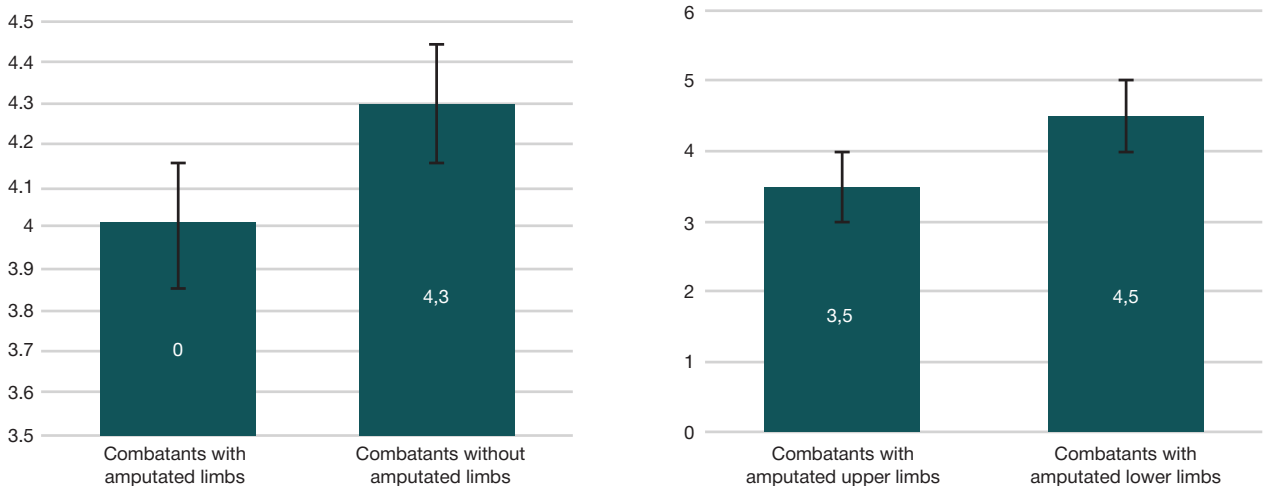


Fig. 7. Bar charts of the average values of suicidal tendency strength in combatants considering the fact of limb amputation



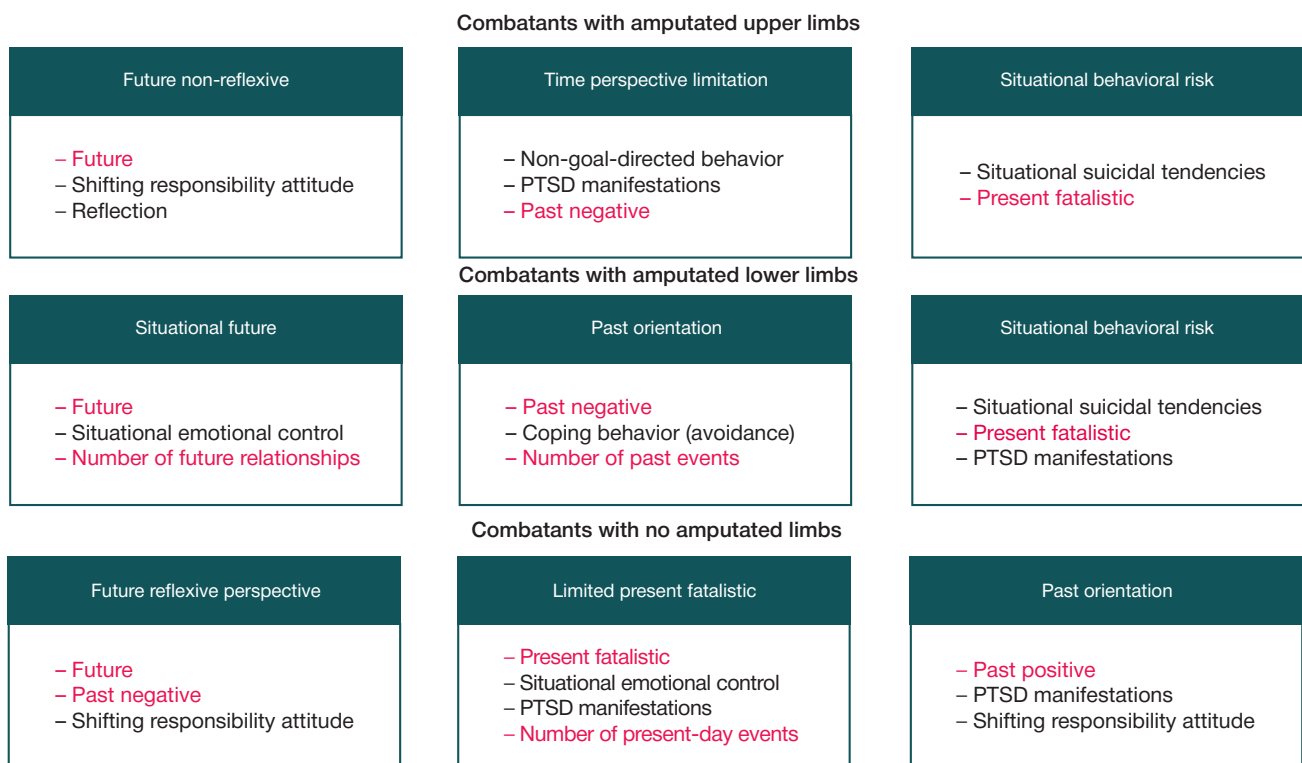


Fig. 8. Time perspective factor structure in combatants considering the fact of limb amputation

in combatants are, on the one hand, traumatic events (either combat experience, or combat experience combined with the acquired physical defect in the form of limb amputation), and on the other hand, the level of personal maturity (or rather, on the contrary, the degree of infantilism), as well as suicidal tendencies. According to the findings, a pattern has been identified confirming our hypothesis that the more severe the PTSD manifestations, the higher the degree of infantilism (which is observed in the group of combatants with traumatic amputation of the limbs), the more inconsistent the time perspective is.

Inconsistency of the time perspective structural organization in combatants with amputated upper limbs seems to be the most challenging, since it is this group, where manifestations of destructive emotional and behavioral status are more severe (more severe PTSD manifestations and stronger suicidal tendencies), which significantly limits the future perspective and future planning. They tend to shift responsibility for future events while the present, which, in turn, results from the past (stressful) events, is fatalistic. In cases of lower limb amputation, the combatants' time perspective structural organization is similar to the earlier reported, however, it has some specific features. The event-related limitation of the future with selective situational emotional control is ensured mainly by the past events (each event of the future results from the past events with traumatic content). Furthermore, event fullness of the past is realized through avoidance behavior: traumatic events are not designated as traumatic; these are more often assessed as negative.

The time perspective structural organization of combatants with no amputated limbs is also characterized by chronological and event (substantial) limitation of the future, along with fatalistic nature of the present and positively assessed past. In this case, traumatic events represent the content of present fatalistic: these events have not yet been transferred to the chronological past. This fact significantly limits the possibilities of forward planning and prediction of the future perspective.

## CONCLUSIONS

The study of the time perspective structural organization in combatants has revealed fatalistic nature of the present along with future orientation in the group of males having a history of limb amputation and in the group of males with the mine blast and gunshot soft tissue injuries and no amputated limbs. Furthermore, the future chronologically reduced to 1–3 months is characterized by the lack of life goals, imprecise and chaotic ways to achieve the goals, as well as by developing the attitude with the lack of responsibility and avoidance behavior in the situations, when coping is required. Inconsistency of the combatants' time perspective structural organization is more pronounced in the groups with amputated limbs (both upper and lower), than in the group of combatants with no amputated limbs. The time perspective inconsistency associated with amputation of the limbs (both lower and upper) results from more severe PTSD manifestations. Dissociation being one of the key PTSD manifestations also manifests itself at the level of time perspective, clearly delimiting events of the past, present, and future. The medium degree of infantilism reported for this group of subjects manifests itself in developing a pronounced parasitic attitude in the context of the future, as well as in the chaotic behavior and situational suicidal tendencies (as one of manifestations of coping behavior in the form of avoidance). Combatants with no amputated limbs assess their past as negative, limiting it to the events related to their combat experience and subsequent injury. The present limited by the duration of current moment (not exceeding 24 h) is characterized by avoidance behavior based on the hedonic values. No suicidal tendencies are reported. Retrospective assessment of the past disordered in terms of motivation represents an obstacle on the way to shaping the promising future involving sorting the goals, as well as methods and means to achieve the goals.

## References

- Ivanov AL, Rubcov VV, Zhumatij NV, Davletshina MV. Psihologicheskie posledstviya uchastija voennosluzhashhih v boevykh dejstvijah v Chechenskoj respublike i ih mediko-psihologo-social'naja korrekcija. Konsultativnaja psihologija i psihoterapija. 2003; 11 (4): 146–62. Russian.
- Karajani AG. Psihologicheskaja rehabilitacija uchastnikov boevykh dejstvij. M., 2003; 80 s. Russian.
- Kvasova OG. Transformacija vremennoj perspektivy lichnosti v jekstremal'noj situacii. Prikladnaja psihologija kak resurs social'no-jekonomicheskogo razvitija Rossii v uslovijah preodolenija global'nogo krizisa. M., 2010; s. 125–127. Russian.
- Avdentova VB. Izmenenie vremennoj perspektivy u vzroslogo cheloveka v stressovykh situacijah. Universum: psihologija i obrazovanie. 2023; 1 (103): 20–23. Russian.
- Akimova AR. Sravnitel'nyj analiz stressoustojchivosti lichnosti s razlichnym tipom samoreguljacii vo vremennoj perspektive. Psihologija. Istoriko-kriticheskie obzory i sovremennye issledovanija. 2017; 6 (2A): 68–76. Russian.
- Golovaha EI. Psihologicheskoe vremja lichnosti. Kiev: Naukova dumka, 1984; 207 s. Russian.
- Zimbardo F, Boyd Dzh. Paradoks vremeni. SPb.: Rech', 2010; 352 s. Russian.
- Zudova EA. Vzaimosvjaz' psihologicheskoi travmy i vremennoj perspektivy lichnosti. Innovacionnaja nauka. 2024; 1–2: 181–6. Russian.
- Rudenko SV. Dinamika vremennoj perspektivy v uslovijah nestabil'noj voenno-politicheskoj situacii. Vestnik Doneckogo nacional'nogo universiteta. Serija D: Filologija i psihologija. 2023; 1: 99–106. Russian.
- Janickij MS, Seryj AV, Balabashuk RO. Hronotopicheskie harakteristiki obraza mira osuzhdennykh, nahodjashhihsja v mestah lishenija svobody. Psihopedagogika v pravoohranitel'nykh organah. 2022; 27 (3-90): 298–306. Russian.
- Folstein MF, Folstein SE, McHugh PR. Mini-mental state. A practical method for grading the cognitive state of patients for the clinician. Journal of psychiatric research. 1975; 12 (3): 189–98. DOI:10.1016/0022-3956(75)90026-6.
- Nikishina VB, Petrash EA, Kuznecova AA. Aprobacija metodiki sobytijnoj rekonstrukcii vremennoj perspektivy lichnosti. Voprosy psihologii. 2015; 2: 140–8. Russian.
- Nikishina VB, Petrash EA. Struktura sobytijnogo prostranstva lichnosti na raznykh jetapah vozrastnogo razvitija. Voprosy psihologii. 2017; 3: 28–39. Russian.
- Tarabrina NV, redaktor. Psihologija posttravmaticheskogo stressa. Prakticheskoe rukovodstvo v 2 chastjah. M., 2007. Russian.
- Tarabrina NV. Praktikum po psihologii posttravmaticheskogo stressa. SPb.: Piter, 2001; 272 s. Russian.
- Junackevich PI. Osnovy psihologo-pedagogicheskoi diagnostiki i korrekcii suicidal'nogo povedenija. SPb.: VIKА im. Mozhajskogo, 1998; 160 s. Russian.
- Keane NM, Caddell JM, Taylor KL. Mississippi Scale for Combat-Related PTSD: Three Studies in Reliability and Validity. J Consulting and Clinical Psychology. 1988; 56 (1).

## Литература

- Иванов А. Л., Рубцов В. В., Жуматий Н. В., Давлетшина М. В. Психологические последствия участия военнослужащих в боевых действиях в Чеченской республике и их медико-психолого-социальная коррекция. Консультативная психология и психотерапия. 2003; 11 (4): 146–62.
- Караяни А. Г. Психологическая реабилитация участников боевых действий. М., 2003; 80 с.
- Квасова О. Г. Трансформация временной перспективы личности в экстремальной ситуации. Прикладная психология как ресурс социально-экономического развития России в условиях преодоления глобального кризиса. М., 2010; с. 125–127.
- Авдентова В. Б. Изменение временной перспективы у взрослого человека в стрессовых ситуациях. Universum: психология и образование. 2023; 1 (103): 20–23.
- Акимова А. Р. Сравнительный анализ стрессоустойчивости личности с различным типом саморегуляции во временной перспективе. Психология. Историко-критические обзоры и современные исследования. 2017; 6 (2A): 68–76.
- Головаха Е. И. Психологическое время личности. Киев: Наукова думка, 1984; 207 с.
- Зимбардо Ф., Бойд Дж. Парадокс времени. СПб.: Речь, 2010; 352 с.
- Зудова Е. А. Взаимосвязь психологической травмы и временной перспективы личности. Инновационная наука. 2024; 1–2: 181–6.
- Руденко С. В. Динамика временной перспективы в условиях нестабильной военно-политической ситуации. Вестник Донецкого национального университета. Серия Д: Филология и психология. 2023; 1: 99–106.
- Яницкий М. С., Серый А. В., Балабашук Р. О. Хронотопические характеристики образа мира осужденных, находящихся в местах лишения свободы. Психопедagogика в правоохранительных органах. 2022; 27 (3-90): 298–306.
- Folstein MF, Folstein SE, McHugh PR. Mini-mental state. A practical method for grading the cognitive state of patients for the clinician. Journal of psychiatric research. 1975; 12 (3): 189–98. DOI:10.1016/0022-3956(75)90026-6.
- Никишина В. Б., Петраш Е. А., Кузнецова А. А. Аprobация методики событийной реконструкции временной перспективы личности. Вопросы психологии. 2015; 2: 140–8.
- Никишина В. Б., Петраш Е. А. Структура событийного пространства личности на разных этапах возрастного развития. Вопросы психологии. 2017; 3: 28–39.
- Тарабрина Н. В., редактор. Психология посттравматического стресса. Практическое руководство в 2 частях. М., 2007.
- Тарабрина Н. В. Практикум по психологии посттравматического стресса. СПб.: Питер, 2001; 272 с.
- Юнацкевич П. И. Основы психолого-педагогической диагностики и коррекции суицидального поведения. СПб.: ВИКА им. Можайского, 1998; 160 с.
- Keane NM, Caddell JM, Taylor KL. Mississippi Scale for Combat-Related PTSD: Three Studies in Reliability and Validity. J Consulting and Clinical Psychology. 1988; 56 (1).

## ESTIMATION OF DIFFUSION CHAMBER BIOCOMPATIBILITY IN THE EXPERIMENTAL MODEL OF IMPLANTATION IN THE NEUROVASCULAR BUNDLE

Marzol EA<sup>✉</sup>, Dvornichenko MV, Mitryaikin NS, Aparshev NA

Siberian State Medical University, Tomsk, Russia

Polycaprolactone as a material used when constructing nanocomposite structures is sufficiently studied in terms of therapeutic effect and safety of use. However, its biocompatibility in the form of three-dimensional carrier macrochambers is still a matter of debate due to changes in the way the 3D printing is done. The study was aimed to determine biocompatibility of the diffusion chamber made of polycaprolactone after implantation in the rat femoral neurovascular bundle. The study involved mature male Wistar rats. Animals of group 1 (experimental,  $n = 4$ ) underwent implantation of the polycaprolactone diffusion chamber in the femoral neurovascular bundle. Group 2 (control,  $n = 3$ ) included intact rats. Macroscopic assessment revealed no abnormalities at the site of implantation and in the target organs. Tissue microscopy revealed no systemic response; the number of binucleated hepatocytes was 1.05%. The stromal-parenchymal relationship values were as follows: liver — 1/33.20, adrenal glands — 1/19.53, kidney — 1/23.65, spleen — 1/26.52. On day 40, hemogram showed the increase in lymphocyte counts by 4%, the decrease in segmented neutrophil counts by 17% and monocyte counts by 17%. These findings confirm safety of using the polycaprolactone diffusion chamber and its biocompatibility when installed in the large neurovascular bundle. However, the effects of polycaprolactone degradation products require more extensive study over the longer periods of biointegration.

**Keywords:** diffusion chambers, polycaprolactone, biocompatibility, cell technologies, systemic reaction, microfluidic technologies

**Funding:** the study was supported by the RSF (research project No. 23-25-00346).

**Author contribution:** Marzol EA, Dvornichenko MV — developing concept and design; Marzol EA, Aparshev NA, Mitryaikin NS — data analysis and interpretation; Marzol EA, Mitryaikin NS, Dvornichenko MV — substantiation of manuscript or verification of critical intellectual content; Dvornichenko MV — final approval of manuscript before publishing.

**Compliance with ethical standards:** the study was approved by the Ethics Committee of the Siberian State Medical University (protocol No. CDI-005 dated 5 February 2022). Animals were handled in accordance with the Directive 2010/63/EU of the European Parliament and the Council on the protection of animals used for scientific purposes dated 22 September 2010, rules and regulations of the European Community (86/609/EEC), Declaration of Helsinki, and orders of the Ministry of Health of the USSR (No. 742 dated 13 November 1984 and No. 48 dated 23 January 1985).

✉ **Correspondence should be addressed:** Ekaterina A. Marzol  
Kartashova, 29b, kv. 78, Tomsk, 634 041; Katya4803@mail.ru

**Received:** 27.06.2024 **Accepted:** 21.07.2024 **Published online:** 19.08.2024

**DOI:** 10.24075/brsmu.2024.032

## ОЦЕНКА БИОСОВМЕСТИМОСТИ ДИФФУЗИОННЫХ КАМЕР В ЭКСПЕРИМЕНТАЛЬНОЙ МОДЕЛИ ИМПЛАНТАЦИИ НА СОСУДИСТО-НЕРВНОМ ПУЧКЕ

Е. А. Марзоль<sup>✉</sup>, М. В. Дворниченко, Н. С. Митряйкин, Н. А. Апаршев

Сибирский государственный медицинский университет, Томск, Россия

Поликапролактон как материал при создании нанокомпозитных структур достаточно изучен с позиции терапевтического эффекта и безопасности применения. Однако его биосовместимость в виде объемных макрокамер-носителей остается предметом дискуссии ввиду изменения способа 3D-печати. Целью работы было определить биосовместимость диффузионной камеры из поликапролактона при ее имплантации на бедренный сосудисто-нервный пучок крысы. Исследование проводили на половозрелых крысах-самцах линии Wistar. Животным группы 1 (экспериментальная,  $n = 4$ ) проводили имплантацию диффузионной камеры из поликапролактона на бедренный сосудисто-нервный пучок. В группу 2 (контрольная,  $n = 3$ ) вошли интактные крысы. В ходе макроскопической оценки не было выявлено патологических изменений на месте имплантации и в органах-мишенях. При микроскопии тканей не выявлено системной реакции, количество двуядерных гепатоцитов составило 1,05%. Показатели стромально-паренхиматозного отношения составили: печень — 1/33,20, надпочечники — 1/19,53, почки — 1/23,65, селезенка — 1/26,52. На 40-е сутки картина крови включала в себя повышение числа лимфоцитов на 4%, уменьшение сегментоядерных нейтрофилов на 17% и моноцитов на те же 17%. Эти результаты подтверждают безопасность использования диффузионной камеры из поликапролактона и ее биосовместимость при постановке на крупные сосудисто-нервные пучки, однако влияние продуктов биодegradации поликапролактона требует более широкого исследования при более длительных сроках биоинтеграции.

**Ключевые слова:** диффузионная камера, поликапролактон, биосовместимость, клеточные технологии, системная реакция, микрофлюидные технологии

**Финансирование:** исследование выполнено при финансовой поддержке РФФИ в рамках научного проекта №23-25-00346.

**Вклад авторов:** Е. А. Марзоль, М. В. Дворниченко — разработка концепции и дизайна; Е. А. Марзоль, Н. А. Апаршев, Н. С. Митряйкин — анализ и интерпретация данных; Е. А. Марзоль, Н. С. Митряйкин, М. В. Дворниченко — обоснование рукописи или проверка критически важного интеллектуального содержания; М. В. Дворниченко — утверждение рукописи.

**Соблюдение этических стандартов:** исследование одобрено этическим комитетом Сибирского государственного медицинского университета (протокол № ЦДИ-005 от 5 февраля 2022 г.). Все манипуляции с животными проводили в соответствии с директивой Европейского Парламента № 2010/63/EU от 22.09.2010 «О защите животных, используемых для научных целей», с соблюдением правил и норм Европейского общества (86/609/EEC), Хельсинкской декларации и приказов Министерства здравоохранения СССР (№ 742 от 13.11.1984 и № 48 от 23.01.1985).

✉ **Для корреспонденции:** Екатерина Александровна Марзоль  
ул. Карташова, 29б, кв. 78, г. Томск, 634 041; Katya4803@mail.ru

**Статья получена:** 27.06.2024 **Статья принята к печати:** 21.07.2024 **Опубликована онлайн:** 19.08.2024

**DOI:** 10.24075/vrgmu.2024.032

Materials showing maximum biocompatibility after implantation, including polycaprolactone, polyvinylpyrrolidone, polyglycolic acid, etc., are currently used in tissue modeling [1–2]. In this row polycaprolactone (PCL), a synthetic polymer belonging to the class of aliphatic polyesters that was synthesized in early 1930s, is the most promising for bioengineered constructs [3]. Its specific physical-chemical and mechanic properties, viscoelasticity, and ease of molding resulted in production of products of various shapes for biomedical sphere: from suturing to replacement of organs and tissues using 3D printing, particularly, 3D printing of isolation (diffusion) chambers for implantation of cellular material. To date, the nanocomposite modifications and additive technologies to fabricate polycaprolactone scaffolds for regenerative medicine have been studied in terms of both therapeutic efficacy and safety of use [4]. However, forming three-dimensional hollow carrier macrochambers for cellular material (diffusion chambers), allowing one to some extent isolate the chamber content from the recipient organism environment and not losing sufficient adhesion properties, from polycaprolactone requires modification of 3D printing conditions, which results in alteration of the material fibers' density and architecture and, therefore, changes its physical-chemical properties and biocompatibility degree [5–6]. It has been proven that PCL shows low bioresorption counter to moderate biodegradation, which can be adjusted by changing the volume of the structure formed, polarization, or additional administration of anti-inflammatory cytokines [7–8]. The PCL degradation parameters depend on molecular weight, polymer shape, and implantation localization, specifically on the degree of vascularization. According to this, both complete elimination of products yielding carbon dioxide, caproic acid, and water and breakdown to intermediate polymer crystals, 6-hydroxycarboxylic acid, amorphous colloids being the components of macrophage endosomes are possible [9]. The studies of such constructs are most often conducted at the level of foreign body reaction (FBR) considering local tissue alterations, immune response morphology *in situ*, and resorptive potential within a short period of time, which makes it possible to partially exponentially estimate the terms of possible implantation, half-life, and possible consequences for the host [1, 10–11]. However, this approach does not allow us to claim with confidence that morphofunctional alterations, including the increase in osmotic pressure relative to the surrounding tissues, pH shift to the acidic side, low-grade productive inflammation and undulating oxidative stress associated with uneven autocatalytic cleavage of the low molecular weight fragments, are just local [12–14].

Under conditions of the diffusion chamber installation in the neurovascular bundle (NVB) the direct transfer of PCL crystals and breakdown products into bloodstream by macrophages is the bioresorption criterion [15–16], which in combination with the material physical-chemical properties can change both qualitative characteristics of the blood vessel and cellular makeup of the capsule, possibly leading to the more acute oxidative stress in the host at both local (at the construct installation site) [17] and systemic [18] levels.

Thus, there is a need to study the effects of polycaprolactone biodegradation products and general significance of implantation at the local and systemic morphofunctional levels, which can be achieved under conditions of using a diffusion chamber in the rat femoral NVB *in vivo* [19].

The study was aimed to determine biocompatibility of the polycaprolactone diffusion chamber, when implanted in the rat femoral neurovascular bundle.

## METHODS

A diffusion chamber (DC) was designed using the Blender open-source software and made of polycaprolactone (Natural works Ingeo 40-43d NatureWorks LLC) by Fused Filament Fabrication involving filaments obtained by electrospinning using the CreatBot Duo 3D printer (CreatBot 3D Printer; China). The chamber consisted of two parts connected with the latches to form a hollow capsule with grooves in the end walls (Fig. 1), which made it possible to fix the chamber on the NVB. The chamber material represented a biodegradable polyester (PCL 100%) that was allowed for medical use and had low melting point (59–64 °C).

The DC was sterilized with the 100% ethylene oxide vapor at 37 °C for 9 h in the 3M Steri-Vac Sterilizer/Aerator (3M; USA) in accordance with the guidelines (GOST ISO 11135-2017).

Wistar rats with the body weight of 280–300 g kept under standard vivarium conditions without antibiotic therapy at the laboratory of biological models of the Siberian State Medical University (Tomsk) were used as experimental models. The animals were divided into two groups for the experiment: the experimental group 1 ( $n = 4$ ) included animals with the DC implanted in the femoral NVB; the control group 2 ( $n = 3$ ) included intact rats. DCs were implanted to experimental animals under isoflurane anesthesia. Atropine in a dose of 0.2 mg/kg was administered intramuscularly 15 min before surgery in order to prevent intraoperative complications. Surgical approach began from the 2–3 cm incision, deep in the inguinal fold, in the inward direction from the femoral artery pulsation (Fig. 1).

The animals were euthanized through CO<sub>2</sub> inhalation 40 days after the end of the experiment. Macroscopic (visual) assessment of the implantation site was performed on days 3, 7, 12, as well as 40 days after the beginning of the experiment during necropsy; assessment was performed based on blood filling of blood vessels, incapsulation, and visual signs of inflammation (presence of hyperemia, edema, infiltration) in points, where score 0 meant no sign, score 1 meant mild degree, score 2 meant moderate degree.

To assess the recipient's reactive response, we collected the tail vein blood smears before implantation and on day 40 after implantation. Blood smears were Romanovsky–Giemsa stained. Histological specimens of the target organs (liver,

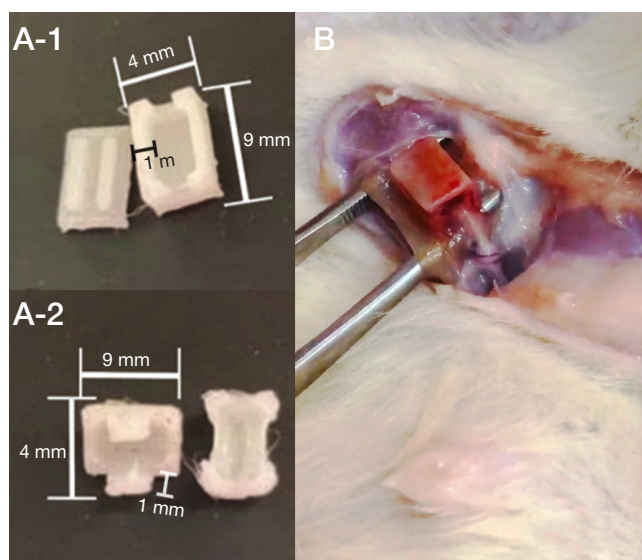


Fig. 1. A-1, A-2. Parameters of the experimental of the PCL DC (length — 9 mm, width — 4 mm, thickness — 1 mm). B. Surgical site of the DC (PCL) implantation

**Table 1.** Macroscopic parameters of polycaprolactone diffusion chambers implanted in the femoral neurovascular bundles of the Wistar rats

Study groups	Inflammation	Hyperemic implantation site	Chamber incapsulation
Experimental group	0	1	1,5
<i>n</i> = 4	(0–0)	(1–1.5)	(1–1.5)
Control group	0	0	–
<i>n</i> = 3	(0–0)	(0–1)	

spleen, kidney, adrenal glands) were prepared after necropsy by the standard method involving hematoxylin and eosin staining [20]. Microscopy was performed using the Karl Zeiss Observer D1 light microscope (Carl Zeiss; Germany).

Morphometry aimed to estimate possible reactive changes of the organs was performed based on the images acquired with the Zeiss AxioCam ICc5 digital camera for light microscopy (Carl Zeiss; Germany). It was based on the stromal–parenchymal relationship: stromal components (blood vessels, interstitial tissue, septal areas, capsule)/parenchyma, as well as on determination of the percentage of binucleated hepatocytes per 100 cells. Hematogram was assessed based on the white blood cell differential. A total of 10 fields of view per group were assessed to calculate the parameters. Statistical processing was performed using the Statistica 10.0, IBM software (TIBCO Software; USA). Statistical hypotheses were tested for the trait distribution normality using the Shapiro–Wilk test for small ( $n < 30$ ) samples. Descriptive and nonparametric statistics were used to process the results obtained. The studied parameters were described as the median (Me), 25% ( $Q_1$ ) and 75% ( $Q_3$ ) quartiles. The Mann–Whitney  $U$  test and the median test were used when comparing independent samples; the Friedman test was used for pairwise comparison. The differences were considered significant at  $p < 0.05$ .

## RESULTS

Behavior, appearance, and haircoat of rats in the experimental group were the same as that of control animals throughout the period of experimental modeling of the DC implantation in the NVB. No local postoperative complications were revealed; the operated limb mobility was preserved and remained unchanged.

The studied biocompatibility parameters are provided in Table 1.

The anatomic and topographic state of the studied internal organs (kidney, adrenal glands, spleen, liver) of animals in the experimental group showed no differences from the control group.

Macroscopic assessment of the organs of animals in the experimental group revealed no typical lesions or alterations (normally colored organs with the even surface, intact, not enlarged, showing no signs of atrophy, fibrosis, scarring, the capsule was preserved, not thickened) compared with the organs of control animals.

Microscopic examination of the liver in rats of the control group (Fig. 2) showed the following: the non-thickened Glisson's fibrous capsule, lobules of irregular hexagonal shape were visible at low magnification, the boundaries between the lobules were unclear due to underdeveloped connective tissue, the triad structure was preserved. No lesions or alterations were revealed.

At high magnification, the lobules consisted of the radially arranged hepatic cords representing the anastomosing strands of hepatocytes. The liver sinusoids lined with endothelial cells were located between the cords. The portal tract consisting of

the interlobular artery, the vein (the vein was 3–4 times larger in diameter, than the artery), bile duct lined with a single layer of cuboidal epithelium with the large, dark, round nuclei and surrounded by the connective tissue envelope, and the interlobular lymphatic vessel was visible in close vicinity to the lobule. Hepatocytes were mostly mononuclear, with the clearly visible basophilic nuclei and homogeneous dark red cytoplasm. The relative binucleated hepatocyte counts per 100 cells in the fields of view were 1.05% (1.02%; 1.11%), i.e. less than 10%.

Interstitial tissue was visible showing no infiltration, proliferation or signs of fibrosis. Blood vessels were represented by the central veins located in the center of the hepatic lobules, sublobular veins having a significantly larger lumen, gathering veins located between the lobules, portal tract (sporadic lymphocytes, monocytes, and histiocytes were found), sinusoids. The lumen was the same in the visible field, the walls were unchanged, there were no cell infiltration or signs of extravasation.

Microscopic examination of the adrenal glands in rats of the experimental group (Fig. 3) showed the following: the non-thickened fibrous capsule, and the boundary between the cortex and medulla were visible at low magnification. The cortex consisted of the zona glomerulosa, zona fasciculata, and zona reticularis. The medulla contained the darker and larger cells. No lesions or alterations were revealed.

At high magnification, the zona glomerulosa was represented by small monomorphic cells with the evenly stained oxyphilic cytoplasm and the eccentrically located nuclei, forming the racemose patterns. Sporadic larger cells with polymorphic nuclei were visible. The zona fasciculata was larger, the cortical plateau consisted of branching divergent sinusoids, between which the cords of oxyphilic, vacuolated, mostly large cells with hyperchromatic nuclei were located. The boundary between the zona fasciculata and zona reticularis was determined by the connective tissue layer. The zona reticularis was represented by small blood vessels, intensely colored round and angulate cells with small hyperchromatic nuclei.

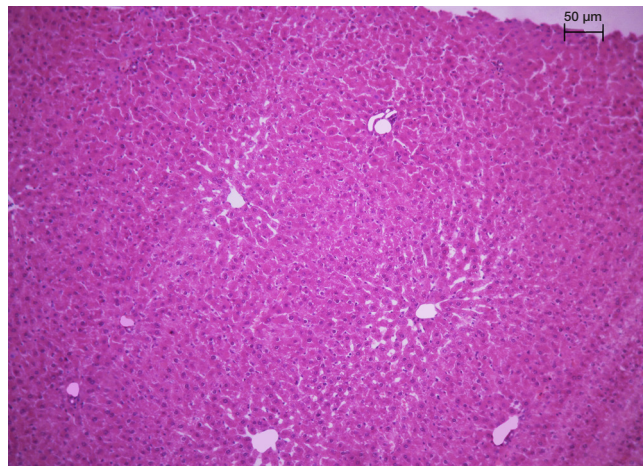


**Fig. 2.** Microscopic slices of the liver of Wistar rats of the experimental group (with the implanted PCL DC). Hematoxylin and eosin; 10× magnification

The medulla was visible as the vascular network, large parenchymal cells forming dense cords, large light nucleus, vacuolated cytoplasm; punctate granulation was revealed. Wide efferent gathering veins and sinusoid capillaries surrounded by the chromaffin cells with basophilic cytoplasm were determined.

Interstitial tissue was visible showing no infiltration or proliferation. The lumen was the same in the visible field, the walls were unchanged, there were no cell infiltration or signs of extravasation.

Microscopic examination of the spleen in rats of the experimental group (Fig. 4) showed the following: the non-thickened fibrous capsule, from which the ill-defined trabeculae anastomosing with each other radiated, was visible at low magnification. The boundary between the white and red pulp was preserved. The white pulp constituted 1/5 of the organ, it was diffusely distributed, mainly subcapsularly. The red pulp constituted the remaining part of the organ (without the capsule and trabeculae), it consisted of the splenic capillaries and splenic cords. No lesions or alterations were revealed.

At high magnification, the oxiphilic capsule composition was as follows: mesothelium, dense fibrous tissue, and smooth muscle cells. The oxiphilic trabeculae consisted of collagen fibers and smooth muscle cells. There was the splenic pulp with the reticular tissue framework between the trabeculae. The splenic white pulp was represented by the lymphoid tissue of the lymphoid nodules (lymphocyte clusters) and periarteriolar lymphoid sheaths (composition: reticular cells, lymphocytes, macrophages, plasma cells), surrounding the arteries at the exit from the trabeculae. Lymphocytes, macrophages, reticular cells were visible in the lymphoid nodule crowns, while lymphocytes at various stages of proliferation and differentiation, plasma cells, macrophages were visible in the germinal center. The mantle zone (cluster of memory B cells and proplasmocytes) surrounded the periarteriolar and reactive areas. The nodule marginal zone was surrounded by the sinusoid capillaries. The main components of the red pulp were reticular tissue with blood cells (erythrocytes, granular and non-granular leukocytes) and sinusoids anastomosing with each other.

Interstitial tissue was visible showing no infiltration or proliferation. Blood vessels were represented by the trabecular veins, trabecular arteries, pulp arteries (around which T cells accumulated), central arteries located eccentrically on the periphery of the follicle, venous sinuses and capillaries. The lumen was the same in the visible field, the walls were unchanged, there were no cell infiltration or signs of extravasation.

Microscopic examination of the rat kidney in the experimental group also showed that the organ had a typical structure: the non-thickened fibrous capsule was visible at low magnification, the boundary between the renal cortex and medulla was preserved. The renal cortex included the renal corpuscles, the system of convoluted tubules radially converging to the medulla consisting of the straight tubules. No lesions or alterations were revealed.

At high magnification, the renal corpuscle was represented by the glomerule of capillaries, non-thickened external capsule, the parietal and visceral layers of which fitted tightly together; the Bowman's space was almost invisible. The histological slice showed proximal convoluted tubules, the single-layer cubic epithelium of which showed oxiphilic staining, basophilic nuclei. The lumens of these tubules were narrow and free. Distal tubules with the wide lumen were lined with the columnar epithelium having opalescent cytoplasm, no rim was visible, a dense spot was visible in the surroundings. The medulla was represented by the straight tubules and the collecting ducts.

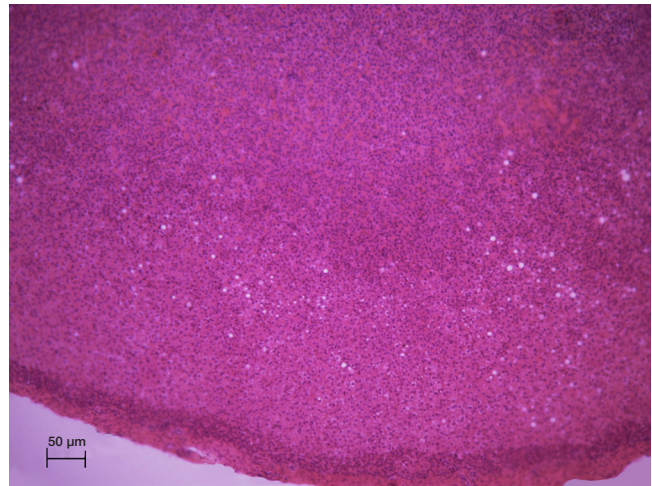


Fig. 3. Microscopic slices of the adrenal glands of Wistar rats of the experimental group (with the implanted PCL DC). Hematoxylin and eosin; 10× magnification

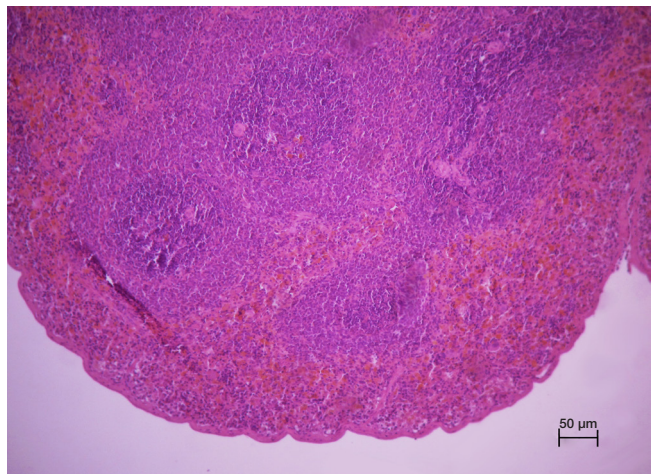


Fig. 4. Microscopic slices of the spleen of Wistar rats of the experimental group (with the implanted PCL DC). Hematoxylin and eosin; 10× magnification

The straight tubules with the narrow lumen were represented by the single-layer cuboidal brush border epithelium. The collecting ducts with the free lumen consisted of the single-layer cuboidal epithelium showing paler oxiphilic staining, the nuclei were located closer to the lumen. No lesions or alterations were revealed.

Interstitial tissue was visible showing no infiltration, it occupied an interstitial position relative to the parenchyma, there was no proliferation. Blood vessels were represented by the subcapsular veins, afferent arteries, interlobular arteries and veins in the cortex and arcuate arteries and veins in the medulla. The lumen was the same in the visible field, the walls were unchanged, there were no cell infiltration or signs of extravasation.

Descriptive assessment of the morphometric parameter, the stromal–parenchymal relationship, in the control group of animals showed no significant differences from the experimental group. The following values of the studied parameter were obtained when assessing the adrenal gland histological specimen: control — 1/21.21 (1/21.27; 1/23.13), experiment — 1/19.53 (1/17.85; 1/20.56); calculation for the microscopic slices of rat liver showed that the value of the parameter reported for the control group was 1/33.85 (1/31.69; 1/39.05), while in the experimental group it was 1/33.20 (1/33.14; 1/34.67); the value of the studied ratio for the histological specimens of the spleen in the control group was 1/24.36 (1/20.58; 1/25.61),

**Table 2.** White blood cell differential before implantation of the polycaprolactone diffusion chambers in the femoral neurovascular bundles of the Wistar rats and on day 40 after implantation

	Immature neutrophils	Band neutrophils	Segmented neutrophils	Eosinophils	Basophils	Monocytes	Lymphocytes
Before implantation of DC (PCL)	0%	3%	5%	0%	1%	9%	82%
	0	4%	11%	1%	0	6%	78%
	0	7%	5%	0	0	4%	84%
	0	5%	10%	0	0	8%	77%
	0	9%	14%	0	1%	8%	68%
	0	1%	14%	0	0	7%	78%
	0	3%	13%	0	1%	4%	79%
	0	1%	8%	1%	2%	6%	82%
	0	5%	18%	0	2%	6%	69%
	0	5%	12%	0	0	7%	76%
	0	5%	12%	1%	1%	6%	75%
On day 40	0	3%	5%	0	0	6%	86%
	0	1%	7%	0	2%	5%	85%
	0	8%	8%	0	0	4%	80%
	0	4%	10%	0	1%	3%	82%
	0	5%	9%	1%	1%	7%	77%
	0	4%	12%	0	0	6%	78%
	0	5%	13%	1%	0	5%	76%
	0	6%	9%	0	1%	3%	81%
	0	4%	12%	1%	0	6%	77%
	0	3%	11%	0	0	3%	83%
	0	2%	10%	0	1%	4%	83%

while in the experimental group it was 1/26.52 (1/24.39; 1/28.86); in turn, the morphometric indicator for histological specimens of the kidney was as follows: control — 1/21.87 (1/17.33; 1/28.50), experiment — 1/23.65 (1/21.78; 1/26.93).

Calculation of the white blood cell differential revealed the following characteristics: prior to implantation, lymphocyte counts were 78.00 (75.50; 80.50); monocyte counts were 6.00 (6.00; 7.50); segmented neutrophil counts were 12.00 (9.00; 13.50), which exceeded the stab form counts — 5.00 (3.00; 5.00); eosinophil counts — 0.00 (0.00; 0.50) and basophil counts — 1.00 (0.00; 1.00) were relatively low.

On day 40 after implantation the rat white blood cell differential showed a slight increase in lymphocyte counts to 81.00 (77.50; 83.00), a non-significant decrease in segmented neutrophil counts — 10.00 (8.50; 11.50), a decrease in the percentage of monocytes — 5.00 (3.50; 6.00) ( $p < 0.05$ ).

The granulocyte and agranulocyte counts of the laboratory animals reported before and after the experiment are provided in Table 2.

## DISCUSSION

Detection of macroscopic changes is possible, when the effects of the chamber and the products of its degradation are large, which indicates a rapidly developing adaptation to the foreign body [21]. The results of macroscopic assessment (appearance, slice, and capsule) of the white rat target organs, in which polycaprolactone degradation products can accumulate, reported for the experimental group have revealed no visible alterations, which suggests no effect of the PCL DC on the gross specimen structure.

The microscopic assessment data (structure and staining of the major histological structures, the lack of abnormal

regenerative and degenerative cell forms) have not allowed us to identify alterations of the organ histoarchitectonics. Histological specimens obtained from laboratory animals of the experimental group are characterized by the typical structure without any alternative, dystrophic or necrotic changes.

The schemes of possible pathogenic changes of the studied organs (kidney, liver, spleen) resulting from the DC (PCL) implantation in the rat femoral NVB are provided in Fig. 5 [21–24], 6 [21, 25].

Thus, the alleged adrenal gland tissue pathogenesis is characterized by the septic or toxic (PCL biodegradation) damage to the tissue of the gland, abnormal increase in cortisol production, increased release of aldosterone into the bloodstream independently of the renin-angiotensin-aldosterone system, which occurs due to adrenal hyperplasia and eventually leads to hypernatremia, hypokalemia, hypertension, and metabolic acidosis [21, 26–27].

Calculation of the stromal–parenchymal relationship for the studied Wistar rat organs performed when comparing the control group and the experimental group verified no enlargement of the connective tissue component and hypo- or hyperplasia of the cellular structure of the histological specimens' parenchymal tissue. This criterion is promising for assessment of the dynamic changes in the organ morphological structure. Furthermore, its convenience lies in the universal characteristics of the tissue pool condition, which is important in cirrhotic changes of the liver, hyper- and hypofunction of both adrenal glands and the spleen, as well as for assessment of dystrophic and atrophic changes of the renal tubules and corpuscles [28].

The increase in the binucleated hepatocyte counts verifies damage to the liver parenchyma, which suggests the association of the material toxicity degree and the possibility

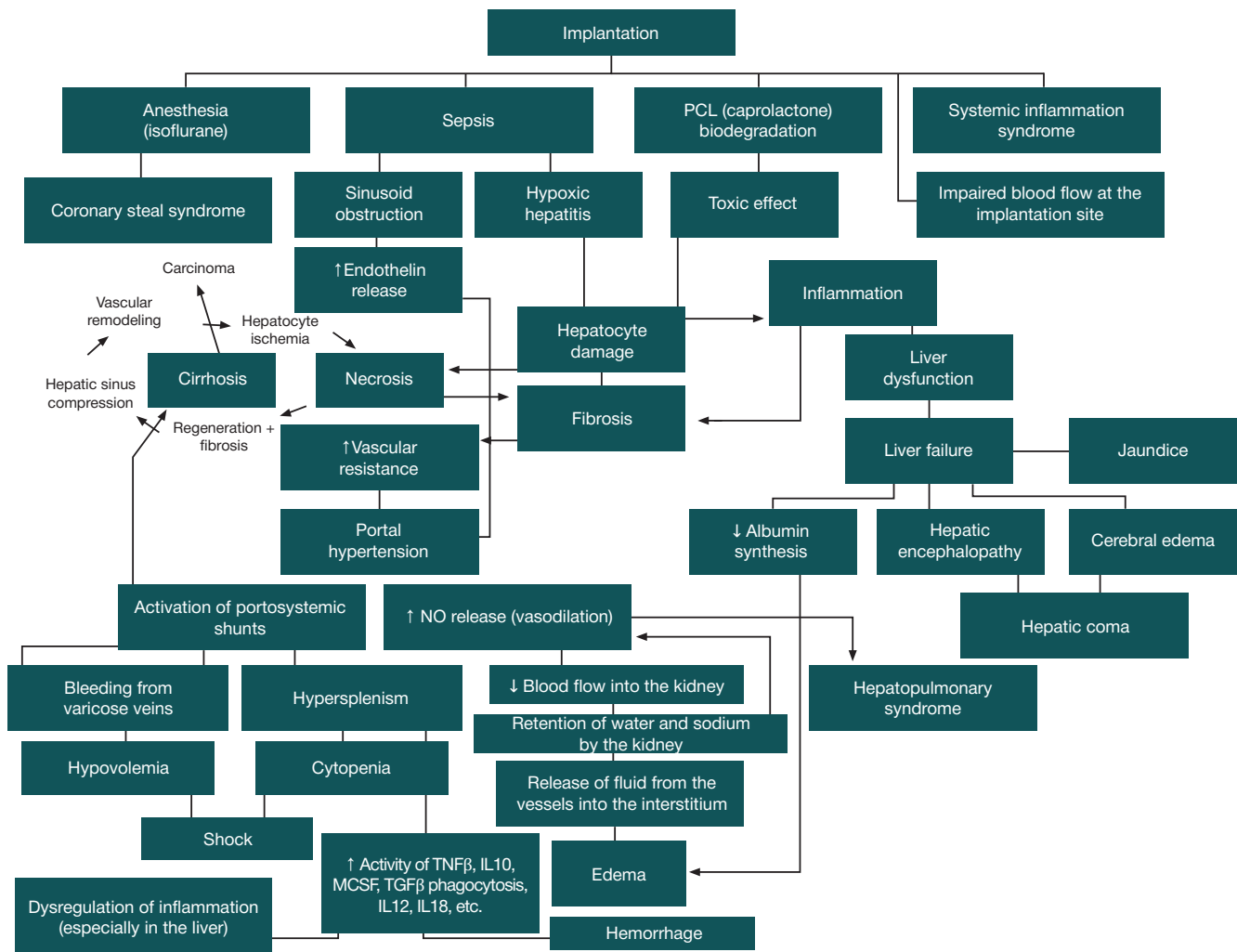


Fig. 5. Possible pathogenic changes of the liver and spleen following implantation of the PCL DC to Wistar rats [21–24]

of hepatocyte self-renewal under conditions of further longer implantation [28]. The findings also suggest that there is no active regenerative cell proliferation in the organ parenchyma.

Systemic inflammation is assessed by determining the cytokine levels [29] and peripheral blood leukogram pattern. The hemogram acquired before implantation and on day 40 after implantation is characterized by redistribution of the functionally unequal cells within the limits of physiological norm [30].

Thus, there is no chance of systemic low-grade chronic inflammation after the PCL DC implantation in the femoral NVB, which is confirmed by the use of such constructs in reconstructive surgery (arteriovenous shunts, flaps) [16], oncology (neoplastic process modeling) [19], and endocrinology (model of the pancreas).

Furthermore, it should be noted that PCL needs to be further studied at the molecular level, and the PCL study should be focused on assessing the impact of the chamber physical parameters (pore size, elasticity (including longitudinal)) on communication with the chamber microenvironment (proliferation of fibroblasts, endothelial cell growth, possible arterial hyaline or calcification both inside the chamber and throughout the blood vessel length) and the material degradation process: rate, nature of the products obtained, main ways to neutralize and eliminate from the body. For reasons of clarity, further experiments should involve SPF animals and longer terms of implantation in order

to clarify possible vascular remodeling considering the blood flow dynamics, determination of the most functional vasa vasorum, and the development of delayed post-implantation complications (thrombogenesis).

## CONCLUSIONS

According to the findings, the polycaprolactone diffusion chamber installed in the femoral NVB had no adverse effect on both implantation site and the target organs. The macro- and microscopic structure of the organs of laboratory animals in the experimental group was determined as normal structure with no alterations: no atypia, signs of inflammation or progressive degeneration of the tissues were found. Calculation of the stromal–parenchymal relationship showed that there were no abnormalities of regenerative nature: signs of fibrosis, excess angiogenesis or parenchymal expansion.

The white blood cell differential indicators determined before the experiment and on day 40 after it suggest no abnormal systemic changes in the laboratory animal body following the diffusion chamber implantation in the femoral NVB. With such a time frame, fluctuations have shown no significant differences from the pre-implantation period, which indicates sufficient isolation of the material from the body's internal environment.

The DC (PCL) used can be considered a safe engineered construct when implanted in large blood vessels,



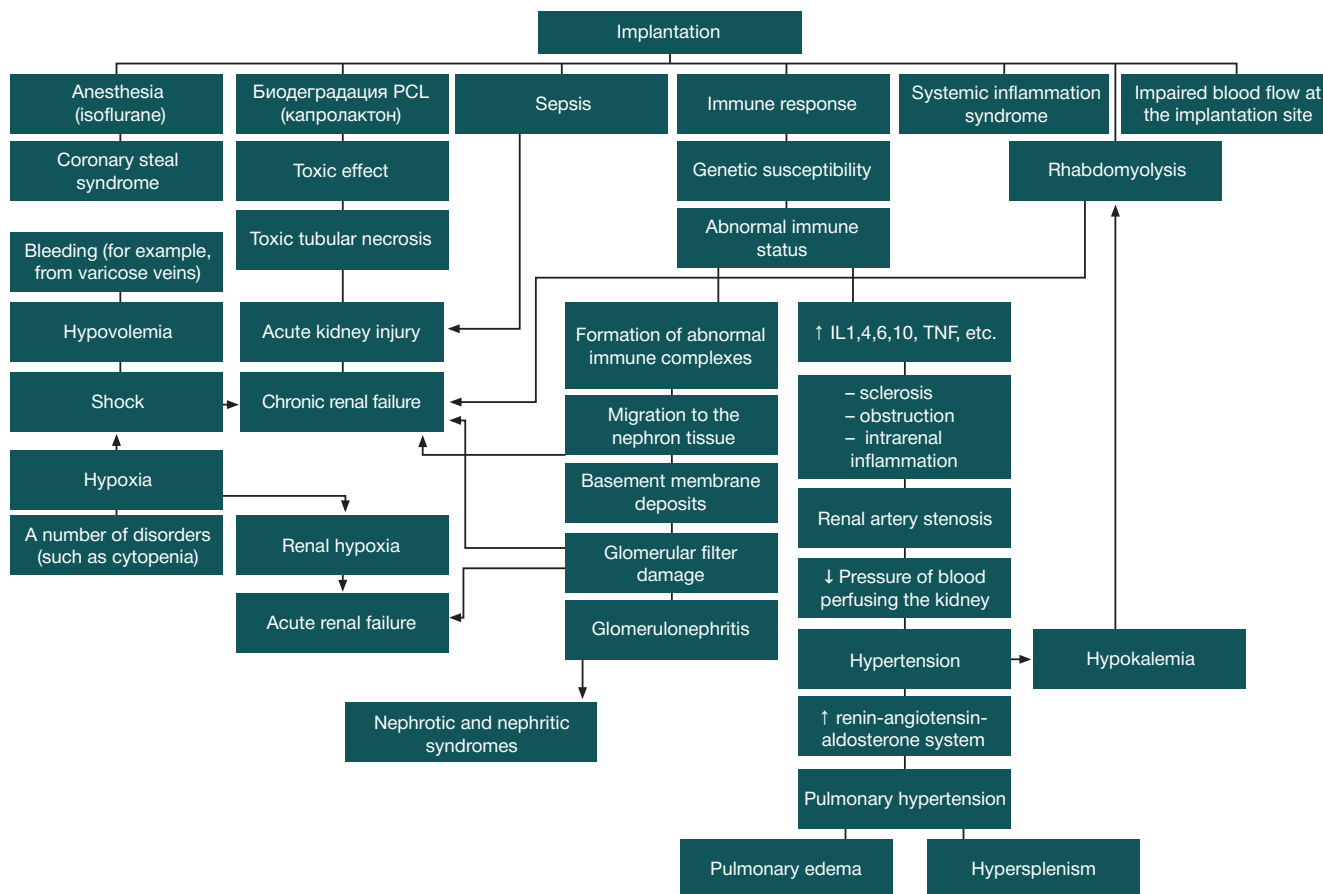


Fig. 6. Possible pathogenic changes of the kidney following implantation of the PCL DC to Wistar rats [21, 25]

specifically femoral NVB, in terms of its biocompatibility. It is important to note that assessment of the effects of the polycaprolactone biodegradation products is still relevant

when choosing the research object, which requires further investigation of the PCL systemic effects during the longer biointegration period.

## References

- Abtahi S, Chen X, Shahabi S, Nasiri N. Resorbable membranes for guided bone regeneration: critical features, potentials, and limitations. *ACS Mater Au*. 2023; 3 (5): 394–417. PMID: 38089090; PMCID: PMC10510521.
- Tan RP, Chan AHP, Wei S, Santos M, Lee BSL, Filipe EC, et al. Bioactive materials facilitating targeted local modulation of inflammation. *JACC Basic Transl Sci*. 2019; 4 (1): 56–71. PMID: 30847420; PMCID: PMC6390730.
- Chen Tingting, Cai Tongjiang, Jin Qiao, Ji Jian. Design and fabrication of functional polycaprolactone. *E-Polymers*. 2015; 15 (1): 3–13.
- Mkhabela Vuyiswa, Sinha Ray Suprakas. Poly( $\epsilon$ -caprolactone) nanocomposite scaffolds for tissue engineering: A brief overview. *Journal of nanoscience and nanotechnology*. 2014; 14 (1): 535–45.
- Liu Fengyuan, Vyas Cian, Poologasundarampillai Gowsihan, Pape Ian, Hinduja Srichand, Mirihanage Wajira, Bartolo Paulo. Structural evolution of PCL during melt extrusion 3D printing. *Macromolecular Materials and Engineering*. 2017; 303 (2): 1700494.
- Lebedeva AI, Maraeva EV. Osnovnye tendencii sozdaniya kompozitnykh 3d-skaffoldov na osnove polikaprolaktona i gidroksiapatita. *Nauka nastojashhego i budushhego*. 2021; (1): 98–101. Russian.
- Kazanceva EA. Konstruirovaniye i ocenka jeffektivnosti sistem kontroliruemoj dostavki sel'skhozajstvennykh preparatov razlichnogo dejstvija [dissertacija]. Krasnojarsk, 2018. Russian.
- Homenjuk S. V. Morfologija regeneratorynykh processov pri implantacii kollagenovogo materiala s adsorbirovannymi mul'tipotentnymi stromal'nymi kletkami [dissertacija]. Novosibirsk, 2023. Russian.
- Emily Archer, Marissa Torretti, Samy Madbouly. Biodegradable polycaprolactone (PCL) based polymer and composites. *Physical Sciences Reviews*. 2021; (8): 4391–414. Available from: <https://doi.org/10.1515/psr-2020-0074>.
- Xiang Z, Guan X, Ma Z, Shi Q, Panteleev M, Ataulkhanov FI. Bioactive engineered scaffolds based on PCL-PEG-PCL and tumor cell-derived exosomes to minimize the foreign body reaction. *Biomater Biosyst*. 2022; 6 (7): 100055. DOI: 10.1016/j.bbiosy.2022.100055. PMID: 36824486; PMCID: PMC9934494.
- Luo L, He Y, Chang Q, Xie G, Zhan W, Wang X, et al. Polycaprolactone nanofibrous mesh reduces foreign body reaction and induces adipose flap expansion in tissue engineering chamber. *Int J Nanomedicine*. 2016; 12 (11): 6471–83. DOI: 10.2147/IJN.S114295. PMID: 27980405; PMCID: PMC5147407.
- Fairag R, Li L, Ramirez-GarciaLuna JL, Taylor MS, Gaerke B, Weber MH, et al. A composite lactide-mineral 3D-printed scaffold for bone repair and regeneration. *Front Cell Dev Biol*. 2021; 7 (9): 654518. DOI: 10.3389/fcell.2021.654518. PMID: 34307346; PMCID: PMC8299729.
- Prabhath A, Vernekar VN, Vasu V, Badon M, Avochinou JE, Asandei AD, et al. Kinetic degradation and biocompatibility evaluation of polycaprolactone-based biologics delivery matrices for regenerative engineering of the rotator cuff. *J Biomed Mater Res A*. 2021; 109 (11): 2137–53. DOI: 10.1002/jbm.a.37200. Epub 2021 May 11. PMID: 33974735; PMCID: PMC8440380.
- Duda S, Dreyer L, Behrens P, Wienecke S, Chakradeo T,

- Glasmacher B, et al. Outer electrospun polycaprolactone shell induces massive foreign body reaction and impairs axonal regeneration through 3D multichannel chitosan nerve guides. *Biomed Res Int.* 2014; 2014: 835269. DOI: 10.1155/2014/835269. Epub 2014 Apr 9. PMID: 24818158; PMCID: PMC4000981.
15. Bereshhenko VV, Nadyrov JeA, Lyzikov AN, Petrenjov DR, Kondrachuk AN. Tkanevye reakcii podkozhnoj kletchatki v otvet na implantaciju polipropilenovogo jendoproteza, modifirovannogo rastvorom polikaprolaktona metodom jelektrospinninga. *Problemy zdorov'ja i jekologii.* 2020; 1: 65–71. Russian.
  16. Cygankov JuM, Sergeev AA, Zhorzholiani ShT, Shepelev AD, Krashennikov SV, Tenchurin TH, i dr. Vlijanie biomehanicheskoj sovместimosti i trombogennosti novogo sinteticheskogo sosudistogo proteza na ego integraciju v arterial'noe ruslo (jeksperimental'noe issledovanie). *Nauki o zhizni.* 2021; (500): 466–9. DOI: 10.31857/S2686738921050309. Russian.
  17. Mishanin AI, Panina AN, Bol'basov EN, Tverdohlebov SI, Golovkin AS. Biosovместimost' skaffoldov iz smesej i sopolimerov polikaprolaktona i polimolochnoj kisloty v testah s mezenhimal'nymi stvolovymi kletkami. *Transljacionnaja medicina.* 2021; 8 (5): 38–49. DOI: 10.18705/2311-4495-2021-8-5-38-49. Russian.
  18. Pankajakshan D, Krishnan VK, Krishnan LK. Vascular tissue generation in response to signaling molecules integrated with a novel poly(epsilon-caprolactone)-fibrin hybrid scaffold. *J Tissue Eng Regen Med.* 2007; 1 (5): 389–97. DOI: 10.1002/term.48. PMID: 18038433.
  19. Ivanov AN, Chibrikova JuA, Saveleva MS, Rogozhina AS, Norkin IA. Ocenka biosovместimosti polikaprolaktonovyh skaffoldov, obespechivajushhih adresnuju dostavku shhelochnoj fosfatazy. *Citologija.* 2020; 62 (12): 903–12. DOI 10.31857/S0041377120120032. Russian.
  20. Bogdanov LA, Kutihin AG. Optimizacija okrashivaniya jelementov sistemy krovoobrashhenija i gepatolienal'noj sistemy gematoksilinom i jeozinom. *Fundamental'naja i klinicheskaja medicina.* 2019; 4 (4): 70–77. Russian.
  21. Novickij VV, Urazova OI. *Patofizilogija. M.: Izd-vo «GJeOTAR-Media», 2022; T. 2: 592 s.* Russian.
  22. Chunpeng Nie Yan Yu. Cirrhosis: pathogenesis and complications, 2022. Calgary: The Calgary guide to understanding disease; c2024 [cited 2024 March 22]. Available from: <https://calgaryguide.ucalgary.ca/cirrhosis-pathogenesis-and-complications/>.
  23. Yunfu Lv, Wan Yee Lau, Yejuan Li, Jie Deng, Xiaoyu Han, Xiaoguang Gong, et al. Hypersplenism: History and current status. *Exp Ther Med.* 2016; 12 (4): 2377–82. DOI: 10.3892/etm.2016.3683.
  24. Yasuko Iwakiri. Pathophysiology of portal hypertension. *Clin Liver Dis.* 2014; 18 (2): 281–91. DOI: 10.1016/j.cld.2013.12.001.
  25. Dane Richard, Robin Bessemer. Nephritic syndrome: pathogenesis and clinical finding, 2016. Calgary: The Calgary guide to understanding disease; c2024 [cited 2024 March 22]. Available from: <https://calgaryguide.ucalgary.ca/nephritic-syndrome-pathogenesis-and-clinical-findings/>.
  26. Kyle Moxham. Primary aldosteronism: pathogenesis and clinical findings, 2021. Calgary: The Calgary guide to understanding disease; c2024 [cited 2024 March 23]. Available from: <https://calgaryguide.ucalgary.ca/primary-aldosteronism-pathogenesis-and-clinical-findings/>.
  27. Samin Dolatabadi, Yan Yu. Hypercortisolemia (Cushing's syndrome): clinical findings, 2021. Calgary: The Calgary guide to understanding disease; c2024 [cited 2024 March 23]. Available from: <https://calgaryguide.ucalgary.ca/hypercortisolemia-cushings-syndrome-clinical-findings/>.
  28. Tan L, Xu X, Song J, Luo F, Qian Z. Synthesis, characterization, and acute oral toxicity evaluation of pH-sensitive hydrogel based on MPEG, poly(epsilon-caprolactone), and itaconic acid. *Biomed Res Int.* 2013; 2013: 239838. DOI: 10.1155/2013/239838. Epub 2013 Nov 30. PMID: 24364030; PMCID: PMC3864077.
  29. Galashina EA, Chibrikova JuA, Ivanov AN, Gladkova EV, Norkin IA. Biohimicheskie parametry intensivnosti sistemoj vospalitel'noj reakcii v ocenke biosovместimosti skaffoldov na osnove polikaprolaktona i vaterita. *Vestnik medicinskogo instituta «Reaviz».* 2020; 2: 98–103. Russian.
  30. Kosjakova GP, Muslimov AA, Lysenko AI. Vzaimodejstvie immunnnoj i nervnoj sistem pri primenenii PCI-skaffoldov v cheljustno-licevoj hirurgii. *Medicinskij akademicheskij zhurnal.* 2019; 19 (1): 82–84. Russian.

## Литература

1. Abtahi S, Chen X, Shahabi S, Nasiri N. Resorbable membranes for guided bone regeneration: critical features, potentials, and limitations. *ACS Mater Au.* 2023; 3 (5): 394–417. PMID: 38089090; PMCID: PMC10510521.
2. Tan RP, Chan AHP, Wei S, Santos M, Lee BSL, Filipe EC, et al. Bioactive materials facilitating targeted local modulation of inflammation. *JACC Basic Transl Sci.* 2019; 4 (1): 56–71. PMID: 30847420; PMCID: PMC6390730.
3. Chen Tingting, Cai Tongjiang, Jin Qiao, Ji Jian. Design and fabrication of functional polycaprolactone. *E-Polymers.* 2015; 15 (1): 3–13.
4. Mkhabela Vuyiswa, Sinha Ray Suprakas. Poly(epsilon-caprolactone) nanocomposite scaffolds for tissue engineering: A brief overview. *Journal of nanoscience and nanotechnology.* 2014; 14 (1): 535–45.
5. Liu Fengyuan, Vyas Cian, Poologasundarampillai Gowsihan, Pape Ian, Hinduja Srichand, Mirihanage Wajira, Bartolo Paulo. Structural evolution of PCL during melt extrusion 3D printing. *Macromolecular Materials and Engineering.* 2017; 303 (2): 1700494.
6. Лебедева А. И., Мараева Е. В. Основные тенденции создания композитных 3d-скаффолдов на основе поликапролактона и гидроксиапатита. *Наука настоящего и будущего.* 2021; (1): 98–101.
7. Казанцева Е. А. Конструирование и оценка эффективности систем контролируемой доставки сельскохозяйственных препаратов различного действия [диссертация]. Красноярск, 2018.
8. Хоменюк С. В. Морфология регенераторных процессов при имплантации коллагенового материала с адсорбированными мультипотентными стромальными клетками [диссертация]. Новосибирск, 2023.
9. Emily Archer, Marissa Torretti, Samy Madbouly. Biodegradable polycaprolactone (PCL) based polymer and composites. *Physical Sciences Reviews.* 2021; (8): 4391–414. Available from: <https://doi.org/10.1515/psr-2020-0074>.
10. Xiang Z, Guan X, Ma Z, Shi Q, Panteleev M, Ataulkhanov FI. Bioactive engineered scaffolds based on PCL-PEG-PCL and tumor cell-derived exosomes to minimize the foreign body reaction. *Biomater Biosyst.* 2022; 6 (7): 100055. DOI: 10.1016/j.bbiosy.2022.100055. PMID: 36824486; PMCID: PMC9934494.
11. Luo L, He Y, Chang Q, Xie G, Zhan W, Wang X, et al. Polycaprolactone nanofibrous mesh reduces foreign body reaction and induces adipose flap expansion in tissue engineering chamber. *Int J Nanomedicine.* 2016; 12 (11): 6471–83. DOI: 10.2147/IJN.S114295. PMID: 27980405; PMCID: PMC5147407.
12. Fairag R, Li L, Ramirez-GarciaLuna JL, Taylor MS, Gaerke B, Weber MH, et al. A composite lactide-mineral 3D-printed scaffold for bone repair and regeneration. *Front Cell Dev Biol.* 2021; 7 (9): 654518. DOI: 10.3389/fcell.2021.654518. PMID: 34307346; PMCID: PMC8299729.
13. Prabhat A, Vernekar VN, Vasu V, Badon M, Avochinou JE, Asandei AD, et al. Kinetic degradation and biocompatibility evaluation of polycaprolactone-based biologics delivery matrices for regenerative engineering of the rotator cuff. *J Biomed Mater Res A.* 2021; 109 (11): 2137–53. DOI: 10.1002/jbm.a.37200. Epub 2021 May 11. PMID: 33974735; PMCID: PMC8440380.
14. Duda S, Dreyer L, Behrens P, Wienecke S, Chakradeo T, Glasmacher B, et al. Outer electrospun polycaprolactone shell induces massive foreign body reaction and impairs axonal regeneration through 3D multichannel chitosan nerve guides. *Biomed Res Int.* 2014; 2014: 835269. DOI: 10.1155/2014/835269. Epub 2014 Apr 9. PMID: 24818158; PMCID: PMC4000981.
15. Берещенко В. В., Надыров Э. А., Лызикив А. Н., Петренёв Д. Р., Кондрачук А. Н. Тканевые реакции подкожной клетчатки

- в ответ на имплантацию полипропиленового эндопротеза, модифицированного раствором поликапролактона методом электроспиннинга. *Проблемы здоровья и экологии*. 2020; 1: 65–71.
16. Цыганков Ю. М., Сергеев А. А., Жоржوليани Ш. Т., Шепелев А. Д., Крашенинников С. В., Тенчурин Т. Х. и др. Влияние биомеханической совместимости и тромбогенности нового синтетического сосудистого протеза на его интеграцию в артериальное русло (экспериментальное исследование). *Науки о жизни*. 2021; (500): 466–9. DOI: 10.31857/S2686738921050309.
  17. Мишанин А. И., Панина А. Н., Большасов Е. Н., Твердохлебов С. И., Головкин А. С. Биосовместимость скаффолдов из смесей и сополимеров поликапролактона и полимолочной кислоты в тестах с мезенхимальными стволовыми клетками. *Трансляционная медицина*. 2021; 8 (5): 38–49. DOI: 10.18705/2311-4495-2021-8-5-38-49.
  18. Pankajakshan D, Krishnan VK, Krishnan LK. Vascular tissue generation in response to signaling molecules integrated with a novel poly(epsilon-caprolactone)-fibrin hybrid scaffold. *J Tissue Eng Regen Med*. 2007; 1 (5): 389–97. DOI: 10.1002/term.48. PMID: 18038433.
  19. Иванов А. Н., Чибрикова Ю. А., Савельева М. С., Рогожина А. С., Норкин И. А. Оценка биосовместимости поликапролактоновых скаффолдов, обеспечивающих адресную доставку щелочной фосфатазы. *Цитология*. 2020; 62 (12): 903–12. DOI 10.31857/S0041377120120032.
  20. Богданов Л. А., Кутихин А. Г. Оптимизация окрашивания элементов системы кровообращения и гепатолиенальной системы гематоксилином и эозином. *Фундаментальная и клиническая медицина*. 2019; 4 (4): 70–77.
  21. Новицкий В. В., Уразова О. И. *Патофизиология*. М.: Изд-во «ГЭОТАР-Медиа», 2022; Т. 2: 592 с.
  22. Chunpeng Nie Yan Yu. Cirrhosis: pathogenesis and complications, 2022. Calgary: The Calgary guide to understanding disease; c2024 [cited 2024 March 22]. Available from: <https://calgaryguide.ucalgary.ca/cirrhosis-pathogenesis-and-complications/>.
  23. Yunfu Lv, Wan Yee Lau, Yejuan Li, Jie Deng, Xiaoyu Han, Xiaoguang Gong, et al. Hypersplenism: History and current status. *Exp Ther Med*. 2016; 12 (4): 2377–82. DOI: 10.3892/etm.2016.3683.
  24. Yasuko Iwakiri. Pathophysiology of portal hypertension. *Clin Liver Dis*. 2014; 18 (2): 281–91. DOI: 10.1016/j.cld.2013.12.001.
  25. Dane Richard, Robin Bessemer. *Nephritic syndrome: pathogenesis and clinical finding*, 2016. Calgary: The Calgary guide to understanding disease; c2024 [cited 2024 March 22]. Available from: <https://calgaryguide.ucalgary.ca/nephritic-syndrome-pathogenesis-and-clinical-findings/>.
  26. Kyle Moxham. *Primary aldosteronism: pathogenesis and clinical findings*, 2021. Calgary: The Calgary guide to understanding disease; c2024 [cited 2024 March 23]. Available from: <https://calgaryguide.ucalgary.ca/primary-aldosteronism-pathogenesis-and-clinical-findings/>.
  27. Samin Dolatabadi, Yan Yu. *Hypercortisolemia (Cushing's syndrome): clinical findings*, 2021. Calgary: The Calgary guide to understanding disease; c2024 [cited 2024 March 23]. Available from: <https://calgaryguide.ucalgary.ca/hypercortisolemia-cushings-syndrome-clinical-findings/>.
  28. Tan L, Xu X, Song J, Luo F, Qian Z. Synthesis, characterization, and acute oral toxicity evaluation of pH-sensitive hydrogel based on MPEG, poly(epsilon-caprolactone), and itaconic acid. *Biomed Res Int*. 2013; 2013: 239838. DOI: 10.1155/2013/239838. Epub 2013 Nov 30. PMID: 24364030; PMCID: PMC3864077.
  29. Галашина Е. А., Чибрикова Ю. А., Иванов А. Н., Гладкова Е. В., Норкин И. А. Биохимические параметры интенсивности системной воспалительной реакции в оценке биосовместимости скаффолдов на основе поликапролактона и ватерита. *Вестник медицинского института «Реавиз»*. 2020; 2: 98–103.
  30. Косякова Г. П., Муслимов А. А., Лысенко А. И. Взаимодействие иммунной и нервной систем при применении PCL-скаффолдов в челюстно-лицевой хирургии. *Медицинский академический журнал*. 2019; 19 (1): 82–84.